QUADRATIC DIFFERENTIAL SYSTEMS WITH A WEAK FOCUS OF FIRST ORDER AND A FINITE SADDLE-NODE

JOAN C. ARTÉS
Departament de Matemàtiques, Universitat Autònoma de Barcelona, 08193 Bellaterra, Barcelona, Spain
E–mail: artes@mat.uab.cat
CARLES TRULLÀS
Departament de Matemàtiques, Universitat Autònoma de Barcelona, 08193 Bellaterra, Barcelona, Spain
E–mail: carlestrullasfernandez10@gmail.com

Planar quadratic differential systems occur in many areas of applied mathematics. Although more than one thousand papers were written on these systems, a complete understanding of this class is still missing. Classical problems, and in particular, Hilbert's 16th problem, are still open for this class. One of the goals of recent researchers is the topological classification of quadratic systems. As this attempt is not possible in the whole class due to the large number of parameters (twelve, but, after affine transformations and time rescaling, we arrive at families with five parameters, which is still a large number), many subclasses are considered and studied. Specific characteristics are taken into account and this implies a decrease in the number of parameters, which makes possible the study.
In this article we perform a global study (modulo islands) of the class $\overline{\mathbf{Qwf1sn}}$ which is the closure within real quadratic differential systems, of the family **Qwf1sn** of all such systems which have a weak focus of first order and a finite saddle-node. The bifurcation diagram for this class, done in the adequate parameter space which is the 3-dimensional real projective space $\mathbb{RP}^3$, is quite rich in its complexity since yields 399 subsets with 192 topologically distinct phase portraits for $\overline{\mathbf{Qwf1sn}}$, 146 of which have a representative in **Qwf1sn**. It can be shown that some of these parts have at least two limit cycles.
The phase portraits are always represented in the Poincaré disc. The bifurcation set is formed by an algebraic set of bifurcations of singularities, finite or infinite and by a set of bifurcations which we suspect to be analytic corresponding to global separatrices which have connections, or double limit cycles. Algebraic invariants were needed to construct the algebraic part of the bifurcation set, symbolic computations to deal with some quite complex invariants and numerical calculations to determine the position of the analytic bifurcation set of connections.

Keywords: Quadratic differential systems; finite saddle-node; weak focus of first order; limit cycle; phase portraits; bifurcation diagram; algebraic invariants.

1. Introduction

The objective of this section is double: On the one hand, we present an overview of an actual research project which has as objective obtaining all the phase portraits of quadratic differential systems, modulo limit cycles. On the other hand, we introduce the study realized in this article, whose main objective is to contribute to the research project explained in Section 1.1.

1.1. The study of quadratic differential systems modulo limit cycles

We consider here differential systems of the form

$$\begin{cases} \dot{x} = P(x,y) \\ \dot{y} = Q(x,y) \end{cases} \tag{1}$$

where $P, Q \in \mathbb{R}[x,y]$, i.e. P, Q are polynomials in x, y over $\mathbb{R}$. We call degree of the system (1) the integer $m = \max(\deg P, \deg Q)$ and we say that (1) is a *polynomial differential system of degree* m. In particular, the polynomial differential systems of degree 1 (resp. 2) are called *linear systems* (resp. *quadratic systems*). We denote here by **QS** the whole class of quadratic systems.

The family of linear systems was completely studied by Laplace in 1812, not only in the planar case, but for any dimension. In fact, the solutions can be explicitly computed. In [Perko, 2000] you can find a modern version of the previous results.

After the complete resolution of linear differential systems, it seemed natural to address the classification of the family **QS**. Because, unlike the linear case, the solutions of a quadratic system cannot always be explicitly computed, we need a concept that allows us to compare the behavior of two different quadratic systems in order to be able to classify the family **QS**. This concept, of course, is the *topological equivalence* between phase portraits (see [Dumortier *et al.*, 2006]), where we recall that the phase portraits are always drawn in the Poincaré disc (see Appendix B.2). In this situation, the objective is to classify the family **QS** under the equivalence relation given by the topological equivalence, i.e. we must obtain a representative of each equivalence class.

Despite the above reductions, the classification of the family **QS** under the topological equivalence is, at least by now, impossible. The main problem, undoubtedly, are the *limit cycles*. It is well known that a quadratic system can have up to two *eyes of limit cycles*, each one of which is surrounding a unique singularity being a focus (see **(ix)** and **(xi)** in Appendix B.1). However, we cannot assure which is the maximum number of limit cycles that a quadratic system can have, despite there exists a conjecture which says: *"The maximum number of limit cycles that* $S \in \boldsymbol{QS}$ *can have is four, and in case of having four they must appear in configuration* $(3,1)$*"*. In fact, not even the individual finiteness of limit cycles in polynomial systems is fully demonstrated. Indeed, despite approximately thirty years ago Ilyashenko and Ecalle presented independent proofs for a result which imply as a particular case that a polynomial differential system must have a finite number of limit cycles (see [Ilyashenko, 1991, Ecalle, 1990]), no other specialist on dynamical systems has checked these proofs up to now and hence they cannot be fully accepted for the moment. However, for $n = 2$, it is proved (and checked by the mathematical community) that a quadratic system must have a finite number of limit cycles (see [Bamon, 1986]).

In conclusion, if we denote as $H(n)$ the maximum number of limit cycles that a polynomial differential system of degree n can have (known as *Hilbert's numbers*), then the existence of $H(n)$ is only proved for $n = 1$ ($H(1) = 0$). It is also known that $H(2) \geq 4$. Regarding the individual finiteness of limit cycles, it is only proved for $n \leq 2$.

All the previous questions regarding limit cycles grouped together are the famous so-called *Hilbert's 16th problem* (we invite the reader to see Section 1.2 of [Artés *et al.*, 2021a] for more details).

Since the study of limit cycles is in general a very difficult problem, it is advisable to separate the study of limit cycles and consider the problem of giving the complete set of phase portraits of quadratic differential systems modulo limit cycles. Consider a quadratic system S, and let $TP(S)$ be its topological phase portrait on the Poincaré disc. We define below the notion of *phase portrait modulo limit cycles* of a quadratic system S.

We first consider a quadratic system S without limit cycles. In this case the phase portrait modulo limit cycles of S is just $TP(S)$. If S has limit cycles, we introduce an equivalence relation

on the phase space of $TP(S)$ as follows: Any point outside the two eyes of limit cycles is equivalent only to itself, and any two points inside an eye of limit cycles or on the largest limit cycle of the corresponding eye are equivalent. This equivalence relation yields a quotient topological space from the phase space, call it $TP(S)/\sim$ and a quotient map $TP(S) \to TP(S)/\sim$ transferring the oriented orbits of $TP(S)$ onto oriented orbits on $TP(S)/\sim$. The topological object obtained in this way is called the *phase portrait modulo limit cycles* of the quadratic system S. The notion of topological equivalence between phase portraits modulo limit cycles is clearly easy to define. Two phase portraits modulo limit cycles of systems S and S' are *topologically equivalent modulo limit cycles* if there is a homeomorphism $f : TP(S)/\sim \to TP(S')/\sim$ that carries oriented orbits to oriented orbits, conserving or reversing the orientation.

Remark 1.1. In case the polynomial systems were of higher degree, the equivalence modulo limit cycles should be redefined so as to cover other possibilities such as having several singularities inside the limit cycles, or even several nests of limit cycles inside a bigger one.

In this situation, the objective is to study the whole class **QS** under the topological equivalence modulo limit cycles (which of course is an equivalence relation), that is, we must present a phase portrait for each equivalence class.

Remark 1.2. The topological equivalence modulo limit cycles is only a tool created in order to justify that we can do a complete classification of quadratic systems tearing apart the Hilbert's 16th problem about limit cycles. However, if some day the previous problem is solved, mathematicians will then have to go through all the equivalence classes modulo limit cycles and find all the possible combinations of limit cycles in any case in order to be able to classify the whole family **QS** under the topological equivalence.

A systematic way to study the whole family **QS** modulo limit cycles, is to divide it by means of working from the lower degrees of degeneracy to the highest ones.

Definition 1.3. A system $S \in \mathbf{QS}$ is said to be *structurally stable modulo limit cycles* (or *structurally unstable of codimension* 0 *modulo limit cycles*) if it possesses a neighborhood in the space $\mathbb{R}^{12}$ of coefficients of quadratic differential systems such that for any system S' in this neighborhood, S and S' are topologically equivalent modulo limit cycles.

Definition 1.4. Let $k \in \mathbb{N}$. A system $S \in \mathbf{QS}$ is said to be *structurally unstable of codimension k modulo limit cycles* if it possesses a neighborhood in the space $\mathbb{R}^{12}$ of coefficients of quadratic differential systems satisfying that: (1) Any system S' in this neighborhood is either structurally unstable of codimension $j < k$ modulo limit cycles or topologically equivalent modulo limit cycles to S; (2) Exists at least one perturbation moving S to a system which is structurally unstable of codimension $k-1$ modulo limit cycles.

Remark 1.5. Definition 1.4 is correct for $k = 0, 1, 2$. However, for $k \geq 3$, we need to demand some extra technical conditions. We point out that Artés and collaborators are already working on refining Definition 1.4 (see [Artés *et al.*, 2023]).

Remark 1.6. Notice that, weak foci and multiple limit cycles are objects of codimension at least one when working with the usual topological equivalence. However, when working modulo limit cycles, they become objects of codimension zero.

Notation 1.1. By simplicity, we denote by Σ_i^2 the subset of **QS** formed by all the quadratic systems which are structurally unstable of codimension i modulo limit cycles.

Remark 1.7. As observed in [Artés *et al.*, 2021d], when applying Defs. 1.3 and 1.4, to phase portraits with centers, it would say that some phase portraits with centers would belong to Σ_i^2 for i as low as two, while geometrically they occupy a much smaller region in $\mathbb{R}^{12}$. So, the best way to avoid inconsistencies in the definitions is to tear apart the phase portraits with centers, that we know they are in number exactly 31 (see [Vulpe, 1983]), and just work with systems without centers.

From article [Artés *et al.*, 1998] we know that $S \in \Sigma_0^2 \iff$ all the singularities of S (finite and

infinite) are elemental without being a center and S does not present any saddle connection.

The study of the whole family Σ_0^2 under the topological equivalence modulo limit cycles was fully completed by Artés, Kooij and Llibre in article [Artés *et al.*, 1998], who obtained 44 phase portraits. For this result they mainly used topological and combinatorial methods. First they used such tools to make a list of possibilities for such phase portraits. Then for each one of these possibilities, they needed to produce examples showing that the corresponding phase portrait modulo limit cycles can be realized in the quadratic class. In the case that such examples turned out to be impossible to find, they proved (mainly using the bound of the number of contact points of orbits with straight lines, see item **(i)** in Appendix B.1) that the corresponding possibility cannot actually occur.

In book [Artés *et al.*, 2018], Artés, Llibre and Rezende classified the family Σ_1^2 under the topological equivalence modulo limit cycles.

According to Thm. 2.2 in [Artés *et al.*, 2018], we know that $S \in \Sigma_1^2$ if and only if all objects of S are stable except one that is either a saddle-node of multiplicity two (finite or infinite), a separatrix from one saddle point to another, or a separatrix forming a loop for a saddle. All the phase portraits corresponding to the family Σ_1^2 are split into four groups according to the possession of a structurally unstable element mentioned before:

- (A) possessing a finite semi-elemental saddle-node $\overline{sn}_{(2)}$.
- (B) possessing an infinite semi-elemental saddle-node $\binom{\overline{0}}{2}SN$.
- (C) possessing an infinite semi-elemental saddle-node $\binom{\overline{1}}{1}SN$.
- (D) possessing a separatrix connection between saddles.

Furthermore, the set (D) is split into five subsets according to the type of connection: (a) finite-finite (heteroclinic orbit), (b) loop (homoclinic orbit), (c) finite-infinite, (d) infinite-infinite between symmetric points, and (e) infinite-infinite between adjacent points.

The study of Σ_1^2 was done in approximately 20 years and finally it was obtained at least 204 (and at most 211) topologically distinct phase portraits for Σ_1^2 (modulo limit cycles). Two recent studies [Artés, 2023, Artés *et al.*, 2021e] have shown two mistakes in [Artés *et al.*, 2018] and have reduced the number of cases to 202 (and a most 209).

This work was also mainly topological and combinatorial. The compilation of all possible phase portraits was relatively easy, but the location of examples for each one of them, or proofs of their impossibility, was not so easy. The study of many new families of quadratic systems (obtained mainly thanks to polynomial invariants) was needed to obtain a wide collection of realizable phase portraits, and so reduce the number of those that needed to be proven impossible. The proofs to show the impossibility of some phase portraits in Σ_1^2 proceed by showing that at least one of the phase portraits that appear in perturbations of the unstable element, is not realizable in Σ_0^2. Also the bound of contact points continued to be an important tool to use, as in the case of Σ_0^2.

Once studied the families Σ_0^2 and Σ_1^2 (modulo limit cycles), the next step is to study the family Σ_2^2, also modulo limit cycles. According to article [Artés *et al.*, 2021d], we have that:

Theorem 1.8. *A quadratic system belongs to Σ_2^2 if and only if all its objects are stable except for the presence of two unstable objects of codimension one or one of codimension two.*

As a consequence of Thm. 1.8, combining the classes of the family Σ_1^2 one to each other, we obtain 10 classes for the family Σ_2^2, where three of them splits into 5 subsets and one of them splits into 15 subsets, depending on the type of connection (a), (b), (c), (d) or (e). The previous classes are presented in Tables 1.1 and 1.2.

	(A)	(B)	(C)	(D)
(A)	(AA)	-	-	-
(B)	(AB)	(BB)	-	-
(C)	(AC)	(BC)	(CC)	-
(D)	(AD) (5 cases)	(BD) (5 cases)	(CD) (5 cases)	See Table 1.2

Table 1.1: Sets of family Σ_2^2 considered from combinations of the different classes in family Σ_1^2.

For a more precise definition of the subsets $(JK) \subset \Sigma_2^2$, $J, K \in \{A, B, C, D\}$, we refer the reader to [Artés *et al.*, 2021d].

	(a)	(b)	(c)	(d)	(e)
(a)	(aa)	-	-	-	-
(b)	(ab)	(bb)	-	-	-
(c)	(ac)	(bc)	(cc)	-	-
(d)	(ad)	(bd)	(cd)	(dd)	-
(e)	(ae)	(be)	(ce)	(de)	(ee)

Table 1.2: Sets in class $(DD) \subset \Sigma_2^2$ (see Table 1.1).

The approach is the same as used when studying families Σ_0^2 and Σ_1^2: In order to study a certain family $(JK) \subset \Sigma_2^2$, one must start by looking for all the potential topological phase portraits contained in such family, and then try to realize all of them or show that some of them are impossible. In order to "attack" the realization problem, its crucial to study the bifurcation diagram (constructed via comitants and invariants for quadratic systems as used by the Sibirsky's School) of some "strategic" families from which we could get examples of our topological potential phase portraits, thus proving its realization. In fact, as we explain in Sect. 1.2, the study developed in this article belongs to this last type.

The study of the families $(AA), (AB)$ and (AC) is completely finished (see [Artés *et al.*, 2021e, Artés *et al.*, 2021d]). The family (BB) it is not needed to be studied. Indeed, as described in [Artés *et al.*, 2021d], (BB) it is formed by all the quadratic systems having all its objects stable except for the presence of an infinite triple saddle $\binom{\overline{0}}{3}S$ or an infinite triple node $\binom{\overline{0}}{3}N$. This case is irrelevant to the production of new phase portraits since all the possible phase portraits that may produce are topologically equivalent to a structurally stable one. The families (AD), (BC), (CC), (BD) and (CD) either they are already under study or they have not yet been initiated but it is well known how to approach them. The (DD) family, which consists of all quadratic systems having all its objects stable except for the presence of two separatix connections between saddles (see [Artés *et al.*, 2021d]), will undoubtedly be the most problematic. While it is true that generating all the potential topological portraits should not be too complicated, finding examples to prove the realization of the phase portraits will be a major problem since there is no normal form in which generically the systems have two saddle connections, from which we could study its bifurcation diagram in order to obtain concrete examples in (DD).

Remark 1.9. In order to complete the study of the whole class **QS**, it is well known that: (1) The higher codimension k that we will need in order to cover all the family **QS** is finite; (2) The codimension two family will be the hardest to achieve, since families corresponding to higher codimension either have already been studied or would be easier to do. Thus, following this procedure we will be able to classify the whole class **QS** modulo limit cycles.

1.2. Objectives and relevance of this article

The main goal of this article is to perform the complete study of the class of all quadratic differential systems possessing a weak focus of first order $f^{(1)}$ and a finite saddle-node (see Sect. 3.1 for a precise definition). We denote the previous class as **Qwf1sn**. A first important observation is the following one: Let $S \in$ **Qwf1sn**. Then S has a unique finite saddle-node, which must be semi-elemental and of multiplicity 2 (denoted as $\overline{sn}_{(2)}$, see [Artés *et al.*, 2021a]). The previous result will be proved in detail in Lemma 3.2 (see Sect. 3.1).

Whenever one wants to study a specific family of differential systems sharing a common property, it is necessary to select one (or several) normal form which contains all the phase portraits sharing the desired property. However, except in some trivial cases, it is impossible that the normal form does not contain other phase portraits, normally more degenerate than the cases under study. These other phase portraits are very important to understand the bifurcations that take place inside the chosen normal form. This is why we always study not just the family of systems that have the desired property, but the closure of the normal form which contains that family. That is, we study all the parameter space of the selected normal form, whether if it leads to the desired property or not. However, it is possible that a different normal form could have been chosen and in that case, the generic elements of the family under study should be the same, but the elements in the border might not be. That is, some phase portraits in the border of one normal form could be common or not, with elements in the border of the second normal form.

As we will demonstrate in detail in Sect. 3.1, any $S \in$ **Qwf1sn** can be transformed by means of

affine changes and a time rescaling to a system of the form (5) for certain values $(l, g, m, h) \in \mathbb{R}^4 \setminus \{0\}$. However, the reciprocal is not true, i.e. not any system of the form (5) belongs to **Qwf1sn** (see Remark 3.5). Hence, according to our previous considerations we must study the systems (5) for all values of the parameters. We call $\overline{\textbf{Qwf1sn}}$ (closure of **Qwf1sn**) the set of all systems (5) for $(l, g, m, h) \in \mathbb{R}^4$. Thus, our objective is to study the family $\overline{\textbf{Qwf1sn}}$ under the normal form (5).

The principal aim of this article is to contribute to the research project explained in Sect. 1.1, in addition to the interest that the study has by itself.

The family $(AD) \subset \Sigma_2^2$, consisting in all the quadratic systems whose objects are stable except for the presence of a finite saddle-node $\overline{sn}_{(2)}$ plus a separatrix connection (see [Artés, 2023]), is being studied by Artés. He has obtained all the potential phase portraits and now he is finding examples to demonstrate the realization of the maximum possible number of phase portraits. Despite the systems in $\overline{\textbf{Qwf1sn}}$ not necessarily present a connection between saddles, they generically have a finite saddle-node $\overline{sn}_{(2)}$. In addition, there is a subset in our parameter space whose associated systems belong to the family $(AD) \subset \Sigma_2^2$ (see Theorem 2.11). These phase portraits are needed by Artés in order to complete the realization problem of the family $(AD) \subset \Sigma_2^2$ (see Sect. 2).

The systems in family $\overline{\textbf{Qwf1sn}}$ contained in the three-dimensional regions of our parameter space belong to $(A) \subset \Sigma_1^2$ (see Theorem 2.6), as will become clear in Sects. 3, 4. The intersection between the families Σ_1^2 and $\overline{\textbf{Qwf1sn}}$ allows us to detect some possible mistakes in one of the two studies.

The study of the class $\overline{\textbf{Qwf1sn}}$ we have developed in this article follows the same pattern as articles [Artés *et al.*, 2006, Artés *et al.*, 2021b, Artés *et al.*, 2021c]. In many papers of this last type, where the bifurcation diagrams of families of phase portraits have been studied, it is quite common that the authors have missed one or several phase portraits. This may happen either because they have not interpreted correctly some of the bifurcation parts, or they have missed the existence of some nonalgebraic bifurcation, or there may exist some small "islands". All previous phenomena are described in Sect. 5. It is clear that previous "pathologies" are unavoidable, but it is not a problem. Indeed, the studies of families via bifurcation diagram help us in the problem of finding examples of realization, but in any case it is expected to assure that we have not left any phase portrait. The objective is to present a coherent bifurcation diagram in terms of continuity.

This article is organized as follows. In Sect. 2 we present the results that we have obtained.

In Sect. 3 we describe the normal form for the family of quadratic systems having a weak focus of first order $f^{(1)}$ and a finite semi-elemental saddle-node of type $\overline{sn}_{(2)}$. In addition, we also explain how we treat our parameter space.

In Sect. 4 we briefly mention some algebraic and geometric concepts, which are fully explained in [Artés *et al.*, 2021a], involving comitants and invariants for quadratic systems as used by the Sibirsky's School. Moreover, using the mentioned concepts as tools, we construct the bifurcation surfaces for the class $\overline{\textbf{Qwf1sn}}$.

In Sect. 5 we discuss about the possible existence of "islands" and other phenomena in the bifurcation diagram.

In Sect. 6 we introduce a global invariant denoted by $\mathcal{I}$, which classifies completely, up to topological equivalence, the phase portraits that we have obtained for the systems in the class $\overline{\textbf{Qwf1sn}}$. Indeed, Theorem 6.13 shows clearly that they are uniquely determined (up to topological equivalence) by the values of the invariant $\mathcal{I}$.

In Sect. 7 we present some tables grouping all the regions having the same topological phase portrait.

In Appendix A we present some additional material that is useful when studying the bifurcation diagram in Sect. 4.

In Appendix B we group some basic results in qualitative theory related with this study. These results will be used during this article when necessary.

Finally, in `https://mat.uab.cat/~artes/articles/qwf1sn/qwf1sn.html` you can find additional useful material. During the article we will indicate which documents the reader can find there.

2. Statement of the obtained results

The objective of this section is to present the results we have obtained in this article. For the normal

form (5) defined in Sect. 3, the class $\overline{\mathbf{Qwf1sn}}$ is partitioned into 399 parts: 75 three–dimensional ones, 169 two–dimensional ones, 124 one–dimensional ones and 31 points. As we will explain in detail in Sect. 4, the partition is obtained by considering all the bifurcation manifolds of singularities, one related to the presence of invariant straight lines, one related to connections of separatrices and one related to the presence of one double limit cycle. Moreover, the study is done modulo "islands" (see Sect. 5.1 for details).

2.1. The main theorem

We start recalling that the phase portraits that we present in this section are drawn in the Poincaré disc (see Appendix B.2 for a precise definition). Strictly speaking, we have not listed the phase portraits since these would be impossible to draw, containing *all* oriented phase curves. Instead we have listed the *completed separatrix skeleton* (see Appendix B.3 for a precise definition). However, the completed separatrix skeleton suffices. Indeed, it can be proved that two systems S, S' are topologically equivalent $\iff$ their completed separatrix skeletons are topologically equivalent (see Thm. B.3 for details).

We now introduce the concept of *graphic*, which plays an important role when generating limit cycles, as will become clear during this article:

Definition 2.1. A *nondegenerate graphic* is a subset of the Poincaré disc formed by singular points p_i, $i = 1, \ldots, m+1$, where $m \geq 1$ and $p_{m+1} = p_1$, and orbits s_j, $j \in \{1, \ldots, m\}$ connecting them, such that for each orbit s_j the $\alpha-$limit set of s_j is p_j, the $\omega-$limit set of s_j is p_{j+1}. If $m = 1$ it is also called a *loop* or *homoclinic orbit*.

Definition 2.2. A *degenerate graphic* is a subset of the Poincaré disc formed by the following three items: (1) Singular points p_i, $i = 1, \ldots, m+1$, with $m \geq 1$, $p_{m+1} = p_1$; (2) Orbits s_j, $j \in S$, where S is a strict subset of $\{1, \ldots, m\}$ (S could be $\emptyset$) such that for each orbit s_j the $\alpha-$limit set of s_j is p_j, the $\omega-$limit set of s_j is p_{j+1}; (3) Arcs of curves s_k, $k \in \{1, \ldots, m\} \setminus S$, which connect p_k with p_{k+1} and which are filled with singular points.

Before giving the obtained result, we point out that we cannot have a global result about the number of limit cycles that a phase portrait may have. But we can assure that, in some places of the bifurcation diagram, the corresponding phase portraits have a specific number of limit cycles or a larger quantity with identical parity (taking into account the multiplicity of limit cycles). More precisely, as we may find an "island" (see Sect. 5.1 for more details) inside the parameter space for which in its border there exists a double limit cycle and inside the island there are two more limit cycles, all the claims regarding limit cycles always must be formulated with respect to the minimum number of limit cycles (proved to exist), but always having the possibility of the existence of "more" limit cycles, keeping the parity.

Theorem 2.3. *We have found a total of* 192 *topologically distinct phase portraits for the closure of the family of quadratic systems having a weak focus of first order and a finite saddle-node (class* $\overline{\boldsymbol{Qwf1sn}}$*). All these phase portraits are shown in Figs. 2.1 to 2.6. Also the following statements hold:*

(a) We have found 146 *topologically distinct phase portraits in* $\boldsymbol{Qwf1sn}$*, and they are in parts:* V_i *for* i=1 . . . 13, 15 . . . 28, 30 . . . 34, 37, 39, 42, 43, 46, 47, 53, 54, 56, 59, 66, 68, 72, 75; $1S_i$ *for* i=1 . . . 10, 12 . . . 15; $4S_i$ *for* i=1 . . . 4, 7, 8, 12; $5S_i$ *for* i=1 . . . 8, 10, 11, 14 . . . 16, 18 . . . 23, 28 . . . 31; $7S_i$ *for* i=1 . . . 17, 19, 23, 24, 26, 28, 29; $10S_1$, $10S_2$; $1.4L_i$ *for* i=1 . . . 3; $1.5L_i$ *for* i=1 . . . 8; $1.7L_i$ *for* i=1 . . . 3; $1.10L_1$; $4.5L_i$ *for* i=1, 2, 4, 5; $5.7L_i$ *for* i=1 . . . 5, 7, 8; $7.7L_1$; P_i *for* i=2, 9, 10, 16.

(b) We have also found a topological equivalent version in $\overline{\boldsymbol{Qwf1sn}} \setminus \boldsymbol{Qwf1sn}$ *of some of the previous* 146 *phase portraits. They are listed in Tables 7.1-7.9 in Section 7.*

Moreover, the 46 *phase portraits corresponding to parts $2S_i$ for* i=1 . . . 4; $9S_i$ *for* i=1, 3 . . . 6; $11S_i$ *for* i=3 . . . 5, 9, 12, 14; $1.8L_1$; $1.9L_i$ *for* i=1, 2; $1.11L_i$ *for* i=1 . . . 3; $2.5L_i$ *for* i=1 . . . 3; $3.8L_i$ *for* i=1, 3, 7, 9; $4.8L_i$ *for* i=1, 4 . . . 6; $5.9L_i$ *for* i=1, 2; $5.11L_i$ *for* i=1, 3; $7.9L_1$; $7.11L_i$ *for* i=1, 2, 5; $9.11L_1$ *and* P_i *for* i=5, 15, 19, 23, 28 *belong to* $\overline{\boldsymbol{Qwf1sn}} \setminus \boldsymbol{Qwf1sn}$ *and cannot have a topological equivalent version in* $\boldsymbol{Qwf1sn}$*.*

(c) We have found 28 *topologically distinct phase*

portraits possessing exactly one simple limit cycle (or an odd number of them taking into account their multiplicities). They are in parts V_9, V_{12}, V_{16}, V_{17}, V_{18}, V_{23}, V_{26}, V_{34}, V_{42}, V_{46}, V_{53}, V_{56}, V_{72}, $1S_8$, $1S_9$, $5S_7$, $5S_{14}$, $5S_{18}$, $7S_5$, $7S_6$, $7S_{10}$, $7S_{23}$, $7S_{24}$, $11S_3$, $11S_{12}$, $11S_{14}$, $1.7L_2$, $5.11L_1$.

(d) We have found 3 *phase portraits with exactly two simple limit cycles (or an even number of them taking into account their multiplicity) surrounding the same focus, and they are in the parts* V_{25}, V_{27}, $1S_{10}$.

(e) We have found 3 *phase portraits possessing one double limit cycle (and no signs of other limit cycles), and they are in the parts* $10S_1$, $10S_2$, $1.10L_1$.

(f) We have found a total of 27 *phase portraits with exactly one nondegenerate graphic surrounding a focus. These phase portraits are in the parts* V_{43}, V_{47}, $5S_{15}$, $5S_{16}$, $5S_{19}$, $7S_2$, $7S_4$, $7S_5$, $7S_7$, $7S_9$, $7S_{10}$, $7S_{13}$, $7S_{15}$, $7S_{16}$, $7S_{17}$, $7S_{19}$, $1.7L_1$, $1.7L_2$, $5.7L_2$, $5.7L_3$, $5.7L_4$, $5.7L_5$, $5.11L_3$, $7.7L_1$, $7.11L_1$, $7.11L_5$, P_{19}.

(g) We have found a total of 3 *phase portraits possessing exactly one nondegenerate graphic and one simple limit cycle, both surrounding the same focus, and they are in the parts* $7S_5$, $7S_{10}$, $1.7L_2$.

(h) We have found a total of 5 *phase portraits possessing an infinite family of nondegenerate graphics and without singularities inside the graphics. They are in parts* $1.5L_3$, $4.8L_4$, $4.8L_5$, $4.8L_6$, P_{23}.

(i) We have found exactly 10 *topologically hase portraits possessing at least one nondegenerate graphic surrounding a center, and they are in parts* $3.8L_1$, $3.8L_3$, $3.8L_7$, $3.8L_9$, $4.8L_1$, $4.8L_4$, $4.8L_5$, $4.8L_6$, P_5 *and* P_{23} *(see Thm. 2.7).*

(j) We have found one phase portrait, namely $1.8L_1$, *possessing an infinite number of degenerate graphics, some of them surroundig a center and the rest without singularities inside. In fact, the system* $1.8L_1$ *corresponds to* Vul_{29} *(see Theorem 2.7).*

(k) We have found one phase portrait, namely $4S_7$, *possessing exactly two nondegenerate graphics, each one of them surrounding a single focus (one is the origin, which is of first order, and the other is strong).*

Proof of Theorem 2.3. The bifurcation diagram described in Sect. 4, plus Tables 6.1 to 6.3 (from Sect. 6) of the geometrical invariants distinguishing the 192 phase portraits, plus Tables 7.1 to 7.9 giving the equivalences with the remaining phase portraits lead to the proof of Thm. 2.3. ■

Corollary 2.4. *For the class* $\overline{\boldsymbol{Qwf1sn}}$, *Table 2.1 compares the number of phase portraits possessing some geometrical features between the family* ***Qwf1sn*** *and its border. We have also added in each row the total number of topological distinct phase portraits found which have the particular geometrical feature. We recall that a topological phase portrait can appear in both columns due to the reasons we have mentioned in Thm. 2.3 (b), and hence, the value in the last column is not necessarily the sum of those in the second and third columns.*

Table 2.1: Comparison between the family **Qwf1sn** and its border (the number represent the absolute value in each subclass).

	Qwf1sn	Border of **Qwf1sn**	Total top. distinct
Distinct phase portraits	146	68	192
Phase portraits with exactly one simple limit cycle	24	7	28
Phase portraits with exactly two simple limit cycles	3	0	3
Phase portraits with exactly one double limit cycle	3	0	3
Phase portraits with exactly one nondegenerate graphic	23	11	31
Phase portraits with exactly two nondegenerate graphics	1	1	2
Phase portraits with an infinite number of nondegenerate graphics	1	4	5
Phase portraits with an infinite number of degenerate graphics	0	1	1

From the 146 topologically distinct phase portraits of the family **Qwf1sn** we have found, 46 occur in three-dimensional parts, 69 in two-dimensional parts, 27 in one-dimensional parts and 4 occur in a zero-dimensional part.

For the border of **Qwf1sn**, from its 68 topologically different phase portraits we have found (as we have specified in Table 2.1), 27 occur in two–dimensional parts, 35 in one–dimensional parts and 6 occur in zero-dimensional parts.

We point out that when we say that a phase portrait occurs in a n–dimensional part we mean that the highest dimension of a part where it occurs is n, since there is the possibility that the same

phase portrait appears in a lower dimensional region bordering the n dimensional one. All these situations are described in Tables 7.1-7.9 in Sect. 7.

In Figs. 2.1 to 2.6 we have drawn all the limit cycles (and loops) possessing a convex shape (see item **(v)** in Appendix B.1). The limit cycle is colored in red if it is simple and it is colored in dark green if it is double. In addition, all the graphics (see Defs. 2.1 and 2.2) are colored in blue. On the other hand, we have illustrated all the singular points with a small black disc. We have also drawn with thicker curves the separatrices and also the lines filled up with singularities. Finally, we have added some thinner orbits to avoid confusion in some required specific cases.

Moreover, we label the phase portraits according to the parts of the bifurcation diagram (see Sect. 4) where they appear. Here we call *volumes* (V) the three–dimensional ones, *surfaces* (S) the two–dimensional ones, *curves* (L) the one–dimensional ones, and *points* (P) the zero–dimensional ones. These labels could be different for two topologically equivalent phase portraits occurring in distinct parts. An example of this situation occurs when we have phase portraits in two-dimensional or one-dimensional parts, coinciding with some phase portraits situated on their border (either because a focus has become a node, or because an invariant line not yielding a connection of separatrices has appeared, or because a finite singularity has become weak, among others). We recall again that all these situations have been detailed described in Tables 7.1-7.9 in Section 7.

Finally, we recall that we use the same pattern in order to indicate the elements (V), (S), (L) and (P) in the bifurcation diagram studied in Sect. 4.

2.2. Comparison with studied families

Once finished the study of a new family, it is fundamental to compare it with those families which have been already studied. This allows us to find possible mistakes and to correct them if necessary, either in the new family that we are studying or in the already studied ones.

Theorem 2.5. *We have found* 10 *topologically distinct phase portraits (*7 *modulo limit cycles) in* $\overline{\boldsymbol{Qwf1sn}} \setminus \boldsymbol{Qwf1sn}$ *which are topologically equivalent to a phase portrait of the class* Σ_0^2*. They are described in Table 2.2.*

$\overline{\mathbf{Qwf1sn}} \setminus \mathbf{Qwf1sn}$	Σ_0^2	$\overline{\mathbf{Qwf1sn}} \setminus \mathbf{Qwf1sn}$	Σ_0^2
$2S_1$	$\mathbb{S}^2_{2,1}$	$2S_2 \equiv 11S_{14}$	$\mathbb{S}^2_{11,2}$
$2S_3 \equiv 11S_{12}$	$\mathbb{S}^2_{4,1}$	$2S_4 \equiv 11S_3$	$\mathbb{S}^2_{9,3}$
$11S_4$	$\mathbb{S}^2_{9,2}$	$11S_5$	$\mathbb{S}^2_{9,1}$
$11S_9$	$\mathbb{S}^2_{11,1}$		

Table 2.2: Phase portraits in $\overline{\mathbf{Qwf1sn}} \setminus \mathbf{Qwf1sn}$ belonging to the class Σ_0^2. The symbol $\equiv$ means that two phase portraits are topologically equivalent modulo limit cycles (see Sect. 1.1). The notation $\mathbb{S}^2_{j,k}$ correspond to the one used in [Artés *et al.*, 1998].

Theorem 2.6. *We have found* 48 *topologically distinct phase portraits (*31 *modulo limit cycles) in* $\boldsymbol{Qwf1sn}$ *belonging to the class* $(A) \subset \Sigma_1^2$*. They are described in Table 2.8.*

As we have already mentioned in Sect.1.1, all quadratic systems having a center are completely studied by Vulpe (see [Vulpe, 1983]). There are exactly 31 and they are denoted as Vul_i for $i = 2, \ldots, 32$ (the name Vul_1 is reserved for the linear center). We also recall that if a quadratic system has a center then it cannot have limit cycles. In addition, there is only one quadratic system with center (which is Vul_{30}) having a (strong) focus. Furthermore, $Vul_i \notin \mathbf{Qwf1sn}$ for all i.

$\overline{\mathbf{Qwf1sn}} \setminus \mathbf{Qwf1sn}$	Center	$\overline{\mathbf{Qwf1sn}} \setminus \mathbf{Qwf1sn}$	Center
$1.8L_1$	Vul_{29}	$3.8L_1$	Vul_7
$3.8L_3$	Vul_{19}	$3.8L_7$	Vul_{20}
$3.8L_9$	Vul_2	$4.8L_1$	Vul_{31}
$4.8L_4$	Vul_{22}	$4.8L_5$	Vul_{24}
$4.8L_6$	Vul_{23}	P_5	Vul_{13}
P_{23}	Vul_{14}		

Table 2.3: Systems with centers in $\overline{\mathbf{Qwf1sn}} \setminus \mathbf{Qwf1sn}$.

Theorem 2.7. *We have found* 11 *topologically distinct phase portraits with centers in* $\overline{\boldsymbol{Qwf1sn}} \setminus \boldsymbol{Qwf1sn}$*. They are described in the Table 2.3:*

$\overline{\textbf{Qwf1sn}} \setminus \textbf{Qwf1sn}$	$(AA) \subset \Sigma_2^2$	$\overline{\textbf{Qwf1sn}} \setminus \textbf{Qwf1sn}$	$(AA) \subset \Sigma_2^2$
$9S_1$	$\mathbb{U}^2_{AA,3}$	$9S_3$	$\mathbb{U}^2_{AA,2}$
$9S_4$	$\mathbb{U}^2_{AA,4}$	$9S_5$	$\mathbb{U}^2_{AA,15}$
$9S_6$	$\mathbb{U}^2_{AA,11}$		

Table 2.4: Phase portraits in the class $\overline{\textbf{Qwf1sn}} \setminus \textbf{Qwf1sn}$ belonging to the class $(AA) \subset \Sigma_2^2$. The notation $\mathbb{U}^2_{AA,j}$ correspond to the one introduced in [Artés *et al.*, 2021e].

Theorem 2.8. *We have found* 5 *topologically distinct phase portraits in the class* $\overline{\boldsymbol{Qwf1sn}} \setminus \boldsymbol{Qwf1sn}$ *belonging to the class* $(AA) \subset \Sigma_2^2$. *They are described in the Table 2.4:*

Theorem 2.9. *We have found* 14 *topologically distinct phase portraits (*11 *modulo limit cycles) in* ***Qwf1sn*** *belonging to the class* $(AC) \subset \Sigma_2^2$. *They are listed in Table 2.5.*

Theorem 2.10. *We have found* 23 *topologically distinct phase portraits (*20 *modulo limit cycles) in* ***Qwf1sn*** *belonging to the class* $(AB) \subset \Sigma_2^2$. *They are listed in Table 2.6.*

Qwf1sn	$(AC) \subset \Sigma_2^2$	**Qwf1sn**	$(AC) \subset \Sigma_2^2$
$1S_1$	$\mathbb{U}^2_{AC,2}$	$1S_2$	$\mathbb{U}^2_{AC,18}$
$1S_3$	$\mathbb{U}^2_{AC,23}$	$1S_4$	$\mathbb{U}^2_{AC,24}$
$1S_5$	$\mathbb{U}^2_{AC,26}$	$1S_6 \equiv 1S_9$	$\mathbb{U}^2_{AC,38}$
$1S_7 \equiv 1S_8, 1S_{10}$	$\mathbb{U}^2_{AC,20}$	$1S_{12}$	$\mathbb{U}^2_{AC,30}$
$1S_{13}$	$\mathbb{U}^2_{AC,3}$	$1S_{14}$	$\mathbb{U}^2_{AC,25}$
$1S_{15}$	$\mathbb{U}^2_{AC,1}$		

Table 2.5: Phase portraits in **Qwf1sn** belonging to the class $(AC) \subset \Sigma_2^2$. The symbol $\equiv$ means that two or three phase portraits are topologically equivalent modulo limit cycles (see Sect. 1.1). The notation $\mathbb{U}^2_{AC,j}$ correspond to the one used in [Artés *et al.*, 2021d].

Qwf1sn	$(AB) \subset \Sigma_2^2$	**Qwf1sn**	$(AB) \subset \Sigma_2^2$
$5S_1$	$\mathbb{U}^2_{AB,10}$	$5S_2$	$\mathbb{U}^2_{AB,9}$
$5S_3$	$\mathbb{U}^2_{AB,16}$	$5S_4 \equiv 5S_{14}, 5S_{18}$	$\mathbb{U}^2_{AB,65}$
$5S_5$	$\mathbb{U}^2_{AB,19}$	$5S_6$	$\mathbb{U}^2_{AB,22}$
$5S_7 \equiv 5S_8$	$\mathbb{U}^2_{AB,37}$	$5S_{10}$	$\mathbb{U}^2_{AB,30}$
$5S_{11}$	$\mathbb{U}^2_{AB,64}$	$5S_{15}$	$\mathbb{U}^2_{AB,71}$
$5S_{16}$	$\mathbb{U}^2_{AB,69}$	$5S_{19}$	$\mathbb{U}^2_{AB,54}$
$5S_{20}$	$\mathbb{U}^2_{AB,55}$	$5S_{21}$	$\mathbb{U}^2_{AB,14}$
$5S_{22}$	$\mathbb{U}^2_{AB,12}$	$5S_{23}$	$\mathbb{U}^2_{AB,11}$
$5S_{28}$	$\mathbb{U}^2_{AB,59}$	$5S_{29}$	$\mathbb{U}^2_{AB,66}$
$5S_{30}$	$\mathbb{U}^2_{AB,18}$	$5S_{31}$	$\mathbb{U}^2_{AB,70}$

Table 2.6: Phase portraits in **Qwf1sn** belonging to the class $(AB) \subset \Sigma_2^2$. The symbol $\equiv$ means that two or three phase portraits are topologically equivalent modulo limit cycles (see Sect. 1.1). The notation $\mathbb{U}^2_{AB,j}$ correspond to the one used in [Artés *et al.*, 2021d].

As we have already mentioned, one of the reasons for which this article is relevant is because it gives us concrete examples which are used in order to attack the realization problem for the family $(AD) \subset \Sigma_2^2$. Artés has already produced all the potential topological phase portraits for the family (AD) (the article is not published yet), many of which have a representative in the family **Qwf1sn**, as described in the following result.

Theorem 2.11. *We have found* 30 *topologically distinct phase portraits (*25 *modulo limit cycles) in the family* ***Qwf1sn*** *belonging to the class* $(AD) \subset \Sigma_2^2$. *All of them are described in Table 2.7.*

The production of this study has coincided in time with the study of the class $(AD) \subset \Sigma_2^2$ done by Artés (already at a preprint level, see [Artés, 2023]). Artés found time ago all the potential phase portraits of class (AD) and he had finally found 76 topologically distinct phase portraits modulo limit cycles, and there remained some which would have ended in a conjecture about its impossibility. But Artés decided to delay its publication until the completion of this study since there was the possibility that some of the conjectured impossible could appear here. As it has finally happened. Phase portrait $7S_{13}$ coincides with phase portrait $\mathbb{U}^2_{AD,77}$ (which initially was conjectured as impossible) which is the dual of $\mathbb{U}^2_{AD,8}$. In fact, phase portrait $\mathbb{U}^2_{AD,8}$ does not appear in **Qwf1sn** but its dual does. Artés obtains $\mathbb{U}^2_{AD,8}$ by bifurcation from class (AB). So both possibilities are realizable. Unluckily, no more of the conjectured impossible phase portraits has appeared here. In particular, neither $\mathbb{U}^2_{AD,9}$ nor its still unfound dual $\mathbb{U}^{2,I}_{AD,9}$ appear here.

We point out that, as will become clear in the subsequent sections, the study developed in this article is complete modulo "islands" (see Sect. 5). In particular, we cannot guarantee that we have not left any phase portrait. What we can guarantee is that the bifurcation diagram obtained in Sect. 4 is coherent and that with a very high percentage of certainty, is complete (and in case of being incomplete, at most remain to be detected some small isolated islands which have never been detected before in any of the previous studies of this typology). In view of the previous observations and the obtained results, we conjecture the following.

Conjecture 2.1. *A system $S \in$ **Qwf1sn** can have at most two limit cycles (taking into account multiplicities), and in case of having two then both must surround the unique $f^{(1)}$.*

Qwf1sn	$(AD) \subset \Sigma_2^2$	**Qwf1sn**	$(AD) \subset \Sigma_2^2$	**Qwf1sn**	$(AD) \subset \Sigma_2^2$	**Qwf1sn**	$(AD) \subset \Sigma_2^2$
$4S_1$	$\mathbb{U}^2_{AD,3}$	$4S_2$	$\mathbb{U}^2_{AD,41}$	$4S_3$	$\mathbb{U}^2_{AD,61}$	$4S_4$	$\mathbb{U}^2_{AD,27}$
$4S_7$	$\mathbb{U}^2_{AD,14}$	$4S_8$	$\mathbb{U}^2_{AD,31}$	$4S_{12}$	$\mathbb{U}^2_{AD,13}$	$7S_1$	$\mathbb{U}^2_{AD,1}$
$7S_2$	$\mathbb{U}^2_{AD,10}$	$7S_3$	$\mathbb{U}^2_{AD,43}$	$7S_4$	$\mathbb{U}^2_{AD,59}$	$7S_5 \equiv 7S_7$	$\mathbb{U}^2_{AD,55}$
$7S_6 \equiv 7S_8$	$\mathbb{U}^2_{AD,68}$	$7S_9 \equiv 7S_{10}$	$\mathbb{U}^2_{AD,40}$	$7S_{11} \equiv 7S_{23}$	$\mathbb{U}^2_{AD,4}$	$7S_{12} \equiv 7S_{24}$	$\mathbb{U}^2_{AD,6}$
$7S_{13}$	$\mathbb{U}^2_{AD,77}$	$7S_{14}$	$\mathbb{U}^2_{AD,5}$	$7S_{15}$	$\mathbb{U}^2_{AD,25}$	$7S_{16}$	$\mathbb{U}^2_{AD,34}$
$7S_{17}$	$\mathbb{U}^2_{AD,12}$	$7S_{19}$	$\mathbb{U}^2_{AD,36}$	$7S_{26}$	$\mathbb{U}^2_{AD,2}$	$7S_{28}$	$\mathbb{U}^2_{AD,75}$
$7S_{29}$	$\mathbb{U}^2_{AD,33}$						

Table 2.7: Phase portraits in **Qwf1sn** belonging to the class $(AD) \subset \Sigma_2^2$. The symbol $\equiv$ means that two or three phase portraits are topologically equivalent modulo limit cycles (see Sect. 1.1). The notation $\mathbb{U}^2_{AD,j}$ is the one used by Artés in [Artés, 2023].

Qwf1sn	$(A) \subset \Sigma_1^2$	**Qwf1sn**	$(A) \subset \Sigma_1^2$	**Qwf1sn**	$(A) \subset \Sigma_1^2$	**Qwf1sn**	$(A) \subset \Sigma_1^2$	**Qwf1sn**	$(A) \subset \Sigma_1^2$
V_1	$\mathbb{U}^1_{A,4}$	V_2	$\mathbb{U}^1_{A,3}$	V_3	$\mathbb{U}^1_{A,23}$	V_4	$\mathbb{U}^1_{A,28}$	$V_5 \equiv V_{42}, V_{53}$	$\mathbb{U}^1_{A,66}$
V_6	$\mathbb{U}^1_{A,31}$	V_7	$\mathbb{U}^1_{A,2}$	V_8	$\mathbb{U}^1_{A,5}$	$V_9 \equiv V_{10}$	$\mathbb{U}^1_{A,6}$	V_{11}	$\mathbb{U}^1_{A,34}$
$V_{12} \equiv V_{13}$	$\mathbb{U}^1_{A,46}$	$V_{15} \equiv V_{18}, V_{25}, 10S_1$	$\mathbb{U}^1_{A,26}$	$V_{16} \equiv V_{19}$	$\mathbb{U}^1_{A,40}$	$V_{17} \equiv V_{20}$	$\mathbb{U}^1_{A,54}$	$V_{21} \equiv V_{26}$	$\mathbb{U}^1_{A,68}$
$V_{22} \equiv V_{23}, V_{27}, 10S_2$	$\mathbb{U}^1_{A,67}$	V_{24}	$\mathbb{U}^1_{A,69}$	V_{28}	$\mathbb{U}^1_{A,39}$	V_{30}	$\mathbb{U}^1_{A,65}$	V_{31}	$\mathbb{U}^1_{A,11}$
$V_{32} \equiv V_{72}$	$\mathbb{U}^1_{A,7}$	$V_{33} \equiv V_{34}$	$\mathbb{U}^1_{A,8}$	V_{37}	$\mathbb{U}^1_{A,9}$	$V_{39} \equiv V_{46}, V_{56}$	$\mathbb{U}^1_{A,12}$	V_{43}	$\mathbb{U}^1_{A,70}$
V_{47}	$\mathbb{U}^1_{A,13}$	V_{54}	$\mathbb{U}^1_{A,57}$	V_{59}	$\mathbb{U}^1_{A,58}$	V_{66}	$\mathbb{U}^1_{A,24}$	V_{68}	$\mathbb{U}^1_{A,61}$
V_{75}	$\mathbb{U}^1_{A,30}$								

Table 2.8: Phase portraits in **Qwf1sn** belonging to the class $(A) \subset \Sigma_1^2$. The symbol $\equiv$ means that two or three phase portraits are topologically equivalent modulo limit cycles (see Sect. 1.1). The notation $\mathbb{U}^1_{A,j}$ correspond to the one used in [Artés *et al.*, 2018].

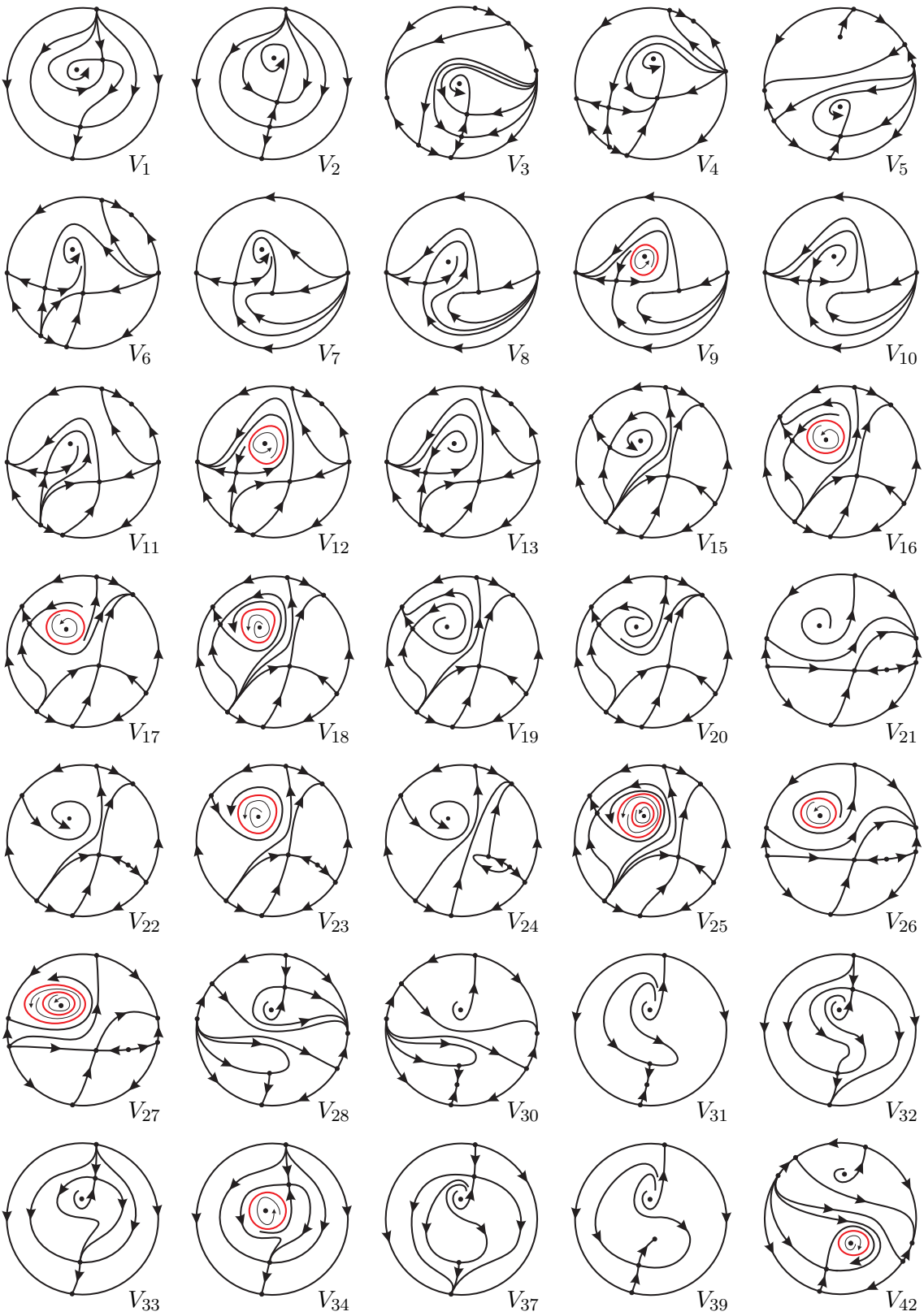

Fig. 2.1: Phase portraits for quadratic vector fields with a finite saddle-node and a weak focus of first order.

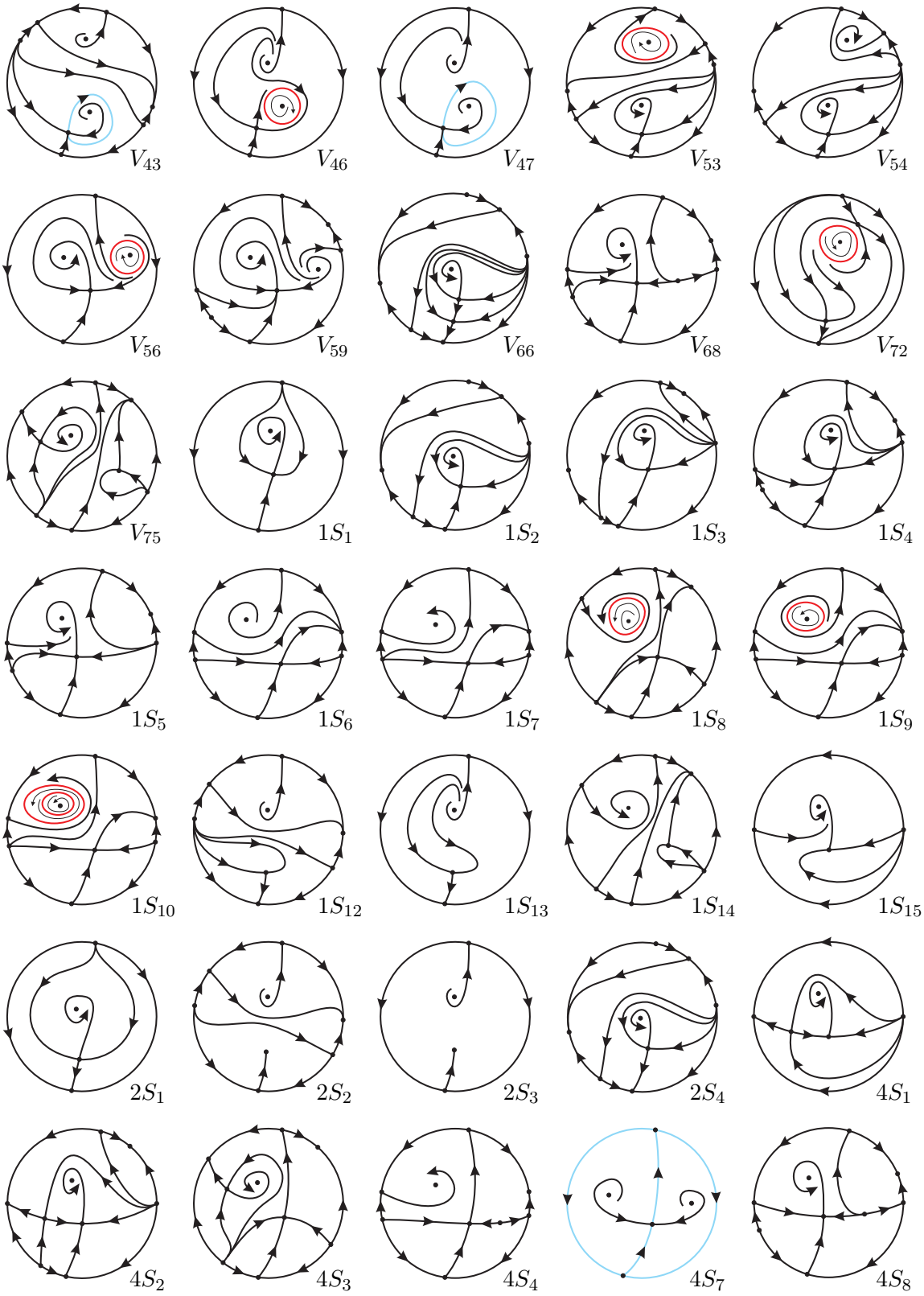

Fig. 2.2: Continuation of Figure 2.1.

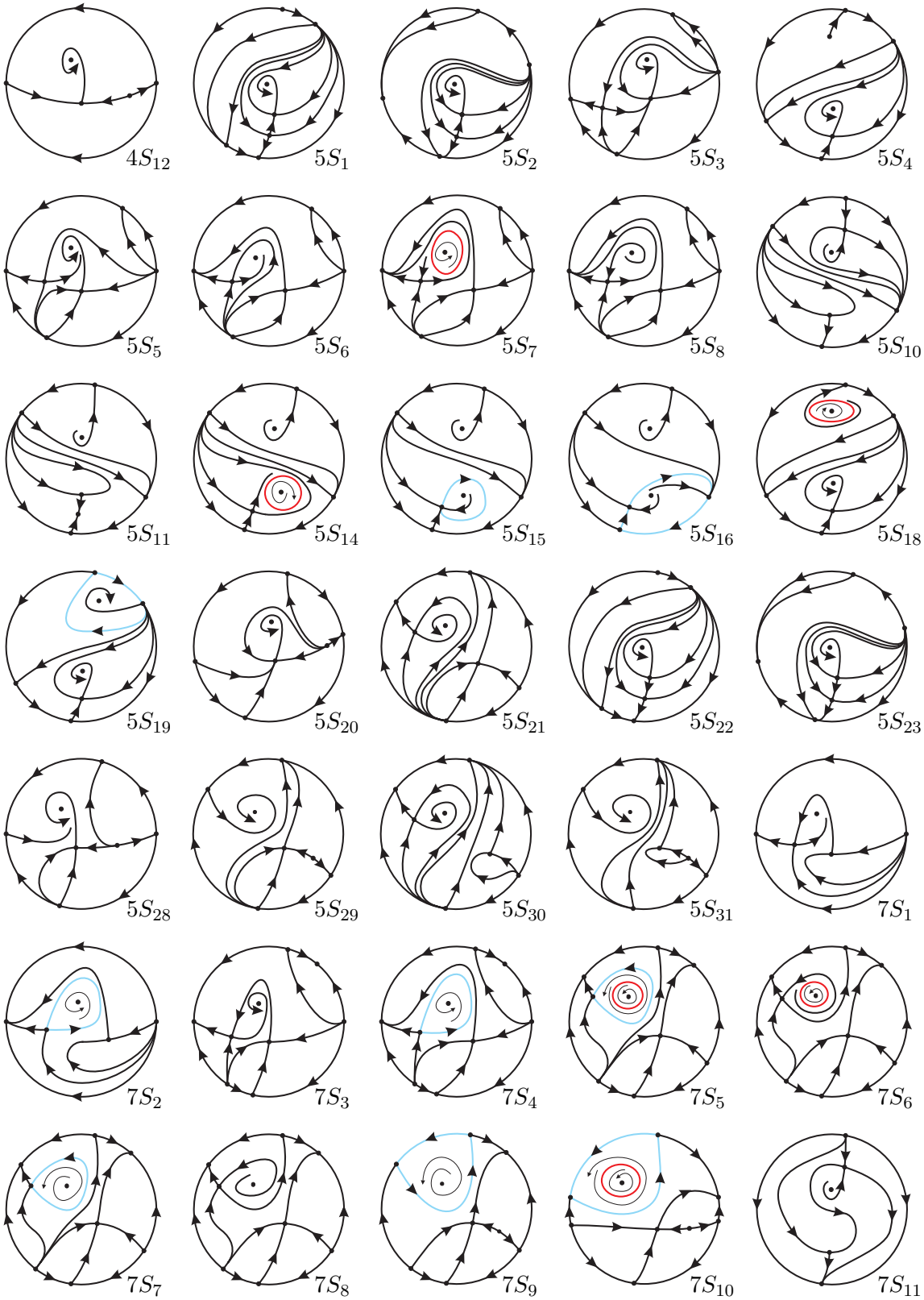

Fig. 2.3: Continuation of Figure 2.2.

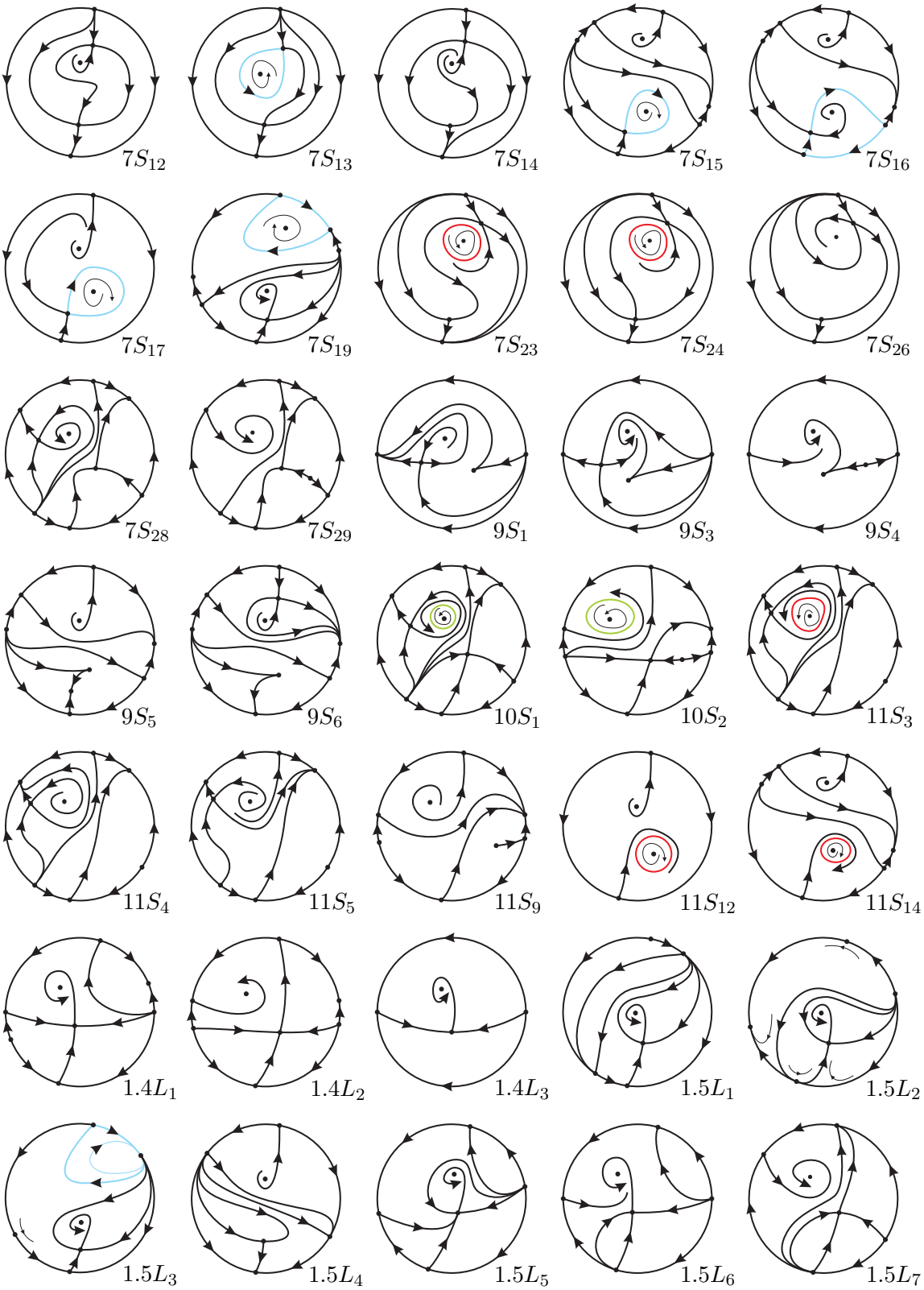

Fig. 2.4: Continuation of Figure 2.3.

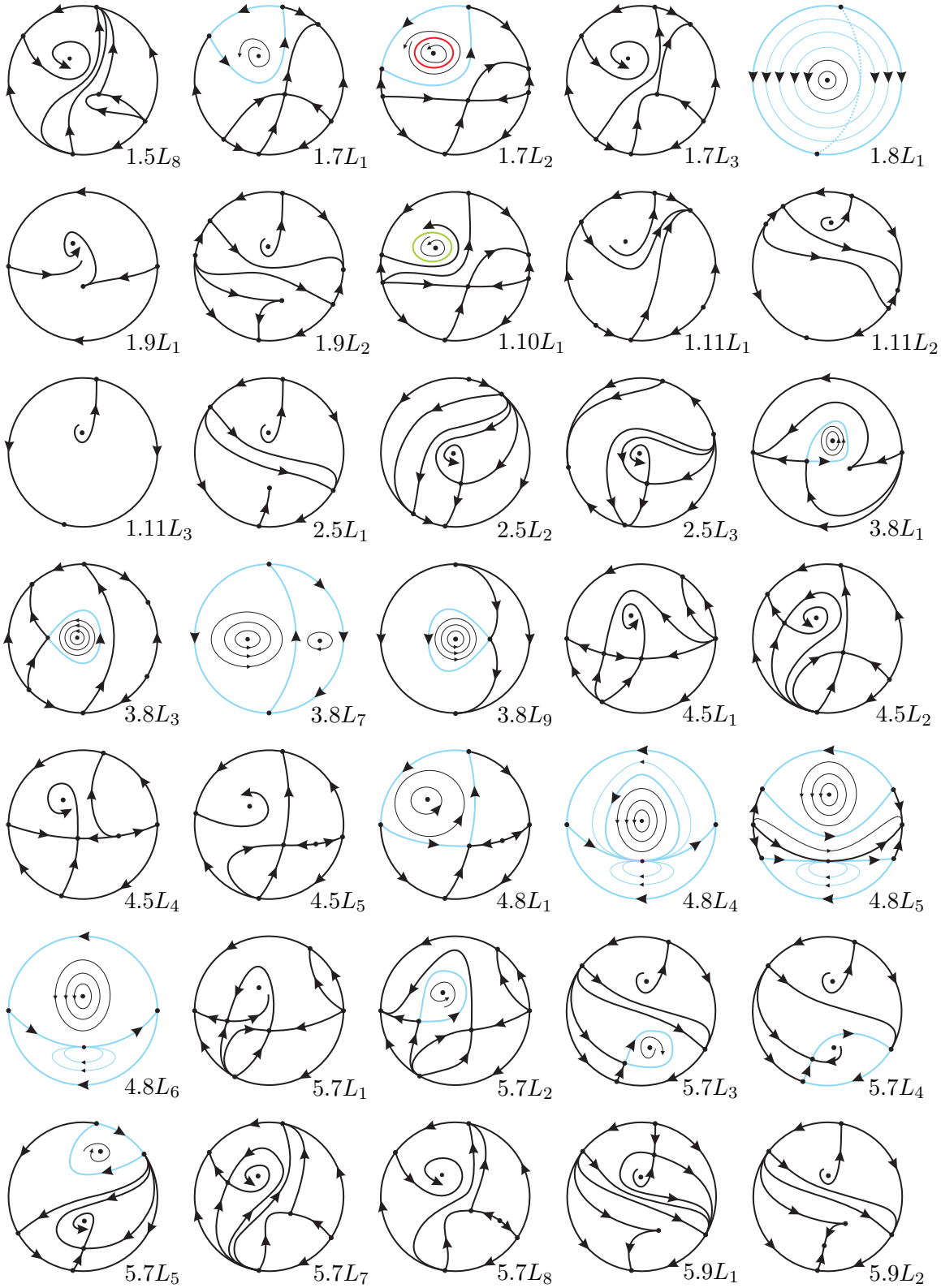

Fig. 2.5: Continuation of Figure 2.4.

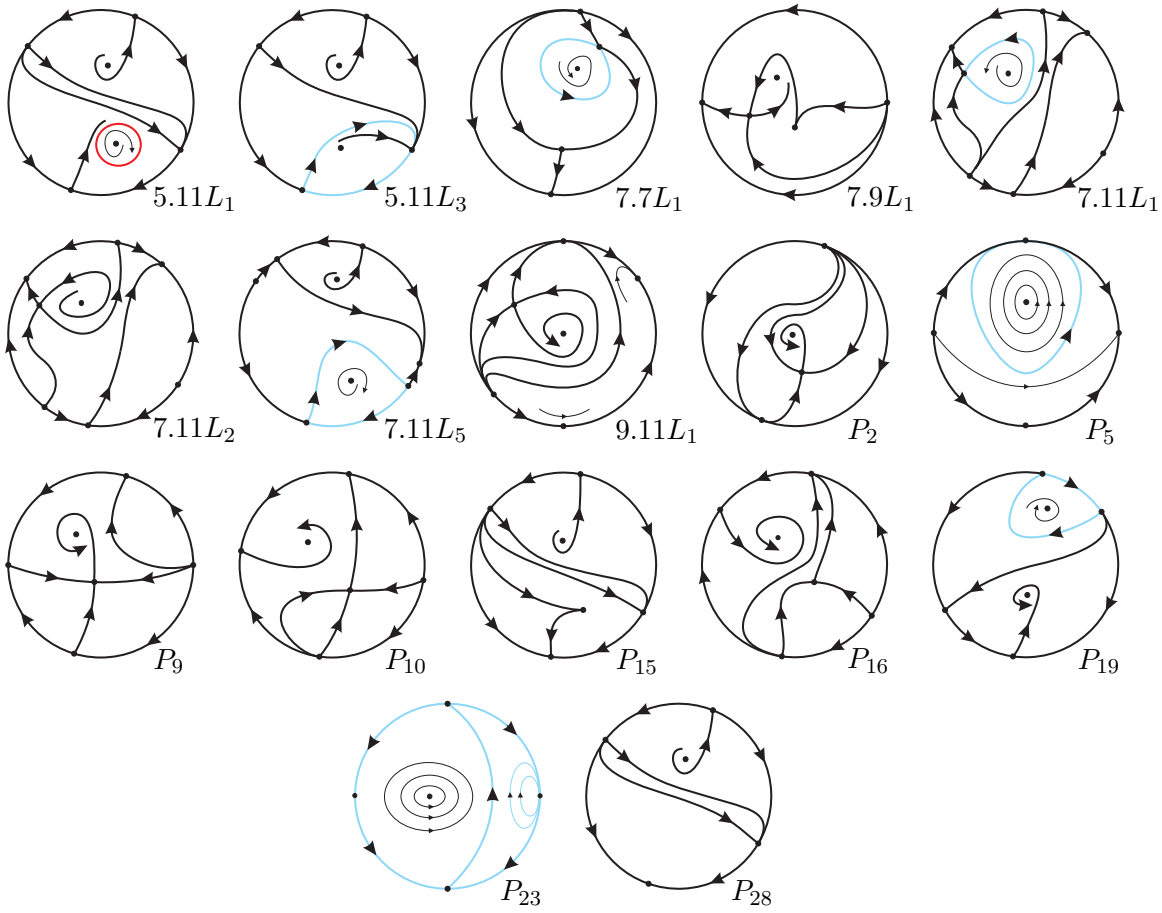

Fig. 2.6: Continuation of Figure 2.5.

3. QS with a finite saddle-node $\overline{sn}_{(2)}$ and a weak focus of first order $f^{(1)}$

The aim of this section is double. On the one hand, we construct the normal form for systems in $\overline{\mathbf{Qwf1sn}}$. On the other hand, we explain in detail how our parameter space will be treated. The procedures used are very similar to those given in [Artés *et al.*, 2006].

3.1. Constructing the normal form for the class $\overline{Qwf1sn}$

We start describing new definitions and designations for singular points which make part of a set of new definitions more deeply related to the geometry of the singular points, their multiplicities and, especially, their Jacobian matrices. We summarize here the definitions, but the entire new designation is completely explained in Chapter 3 of [Artés *et al.*, 2021a]. Let $X \in \mathbf{QS}$ and let $p \in \mathbb{R}^2$ a singular point of X. We denote by $DX(p)$ the Jacobian matrix of X at p. Let $\lambda_1, \lambda_2 \in \mathbb{C}$ the two eigenvalues of $DX(p)$. We denote the singular point p in one of the following four ways, depending on λ_1 and λ_2, as explained in the following diagram:

$$\begin{cases} \textbf{Elemental}: \ \lambda_1 \neq 0, \lambda_2 \neq 0 \\ \textbf{Semi-elemental}: \ \textit{Exactly one eigenvalue is } 0 \\ \textbf{Nilpotent}: \lambda_1 = \lambda_2 = 0 \ \textit{ but } \ DX(p) \neq 0 \\ \textbf{Intricate}: \lambda_1 = \lambda_2 = 0 \ \textit{ and } \ DX(p) = 0 \end{cases}$$

We also need to recall some additional notation: A singular point $p \in \mathbb{R}^2$ of $X \in \mathbf{QS}$ is said to be a *linear center* if the eigenvalues of its linear part, $DX(p)$, are pure imaginary numbers, i.e. $\pm i\beta$ with $\beta \in \mathbb{R} \setminus \{0\}$. We say that $p \in \mathbb{R}^2$ is a *center* of X if p is an isolated singularity such that there exists an open neighborhood U of p satisfying that p is the unique singular point contained in U and all orbits of X different from p contained in U are periodic. It is well known that a linear center p is either a center, or a focus. In this last case p is called a *weak focus*. We recall that $p \in \mathbb{R}^2$ is a *strong focus* if the eigenvalues of its linear part are of the form $\alpha \pm i\beta$ with $\alpha\beta \neq 0$. Finally, we say that $p \in \mathbb{R}^2$ is a *saddle-node* if there exists a small neighborhood of p formed by the union of two hyperbolic sectors and one parabolic sector (see [Dumortier *et al.*, 2006, Artés *et al.*, 2021a] for more details).

The next result is due to Shi (see [Shi, 1981, Shi, 1984]). We point out that this lemma is better stated in [Schlomiuk, 1993] where the rings involved are explicitly written, and where a sketch of the proof is also given. For the sake of completeness we give below the statement.

Lemma 3.1. *Consider the planar polynomial differential system of degree m:*

$$\begin{cases} \dot{x} = P(x,y) = -y + P_2(x,y) + \cdots + P_m(x,y) \\ \dot{y} = Q(x,y) = x + Q_2(x,y) + \cdots + Q_m(x,y) \end{cases} \tag{2}$$

where $m \geq 2$ and

$$P_i(x,y) = \sum_{j=0}^{i} a_{ij} x^{i-j} y^j, \quad Q_i(x,y) = \sum_{j=0}^{i} b_{ij} x^{i-j} y^j$$

$\forall\ i \in \{2, \ldots, m\}$. Then there exists a formal power series $F \in (\mathbb{Q}[a_{20}, \ldots, a_{mm}, b_{20}, \ldots, b_{mm}])[x,y]$,

$$F = \frac{1}{2}(x^2 + y^2) + F_3(x,y) + F_4(x,y) + \ldots$$

and there exists polynomials $V_1, V_2, V_3, \ldots$ belonging to the ring $\mathbb{Q}[a_{20}, \ldots, a_{mm}, b_{20}, \ldots, b_{mm}]$ and satisfying that

$$\frac{dF}{dt} = \frac{\partial F}{\partial x} P(x,y) + \frac{\partial F}{\partial y} Q(x,y) = \sum_{i=1}^{+\infty} V_i (x^2 + y^2)^{i+1}$$

The quantities V_i are called the *Poincaré-Lyapunov coefficients* and are not uniquely determined. In fact, for each $i \in \mathbb{N} \setminus \{0\}$ there is an infinite number of possibilities for a V_i. But according to a result also proven by Shi, all such $V_i's$ are in the same coset modulo the ideal generated by $V_1, ..., V_{i-1}$ in the ring $\mathbb{Q}[a_{20}, \ldots, a_{mm}, b_{20}, \ldots, b_{mm}]$. From the work of Poincaré (see [Poincaré, 1885]) it follows that system (2) has a center at the origin if and only if $V_i = 0$ for all i. By Hilbert's basis theorem, the ideal $I = \langle V_1, V_2, V_3, \ldots \rangle$ has a finite basis. It follows from the work of Bautin (see [Bautin, 1962]) that for quadratic systems ($m = 2$) this ideal is determined by the values of V_i with $i \leq 3$. The above result implies that $V_1 = V_2 = V_3 = 0$ if and only if $V_i = 0$ for all i and the origin is a center.

It is easy to see that any $S \in \mathbf{QS}$ having a linear center, say $p \in \mathbb{R}^2$, can be transformed by an affine change of variables (which sends p to the origin) and

a time rescaling into a quadratic differential system of the form (2), say S', for certain coefficients a_{ij}, b_{ij} and with $m = 2$. Taking this fact into account, we say that p is

(a) A *weak focus of first order* (and we denote it by $f^{(1)}$) if $V_1 \neq 0$.

(b) A *weak focus of second order* (and we denote it by $f^{(2)}$) if $V_1 = 0, V_2 \neq 0$.

(c) A *weak focus of third order* (and we denote it by $f^{(3)}$) if $V_1 = 0, V_2 = 0, V_3 \neq 0$.

where of course the values V_1, V_2 and V_3 corresponds to the ones introduced in Lemma 3.1 associated to the system S'.

Lemma 3.2. *Let $S \in$ **Qwf1sn**. Then S has a unique finite saddle-node. Moreover, it must be semi-elemental and must have multiplicity two.*

Proof. By assumption, S has at least one finite saddle-node, say sn. Since $S \in \mathbf{QS}$, it is known that sn must be nilpotent or semi-elemental (see Appendix A of [Artés *et al.*, 2021a]). If sn were nilpotent, then its multiplicity would be four (see again Appendix A of [Artés *et al.*, 2021a]) but since S has another finite singularity, which is a $f^{(1)}$, the total finite multiplicity of S would be at least five, which is impossible, and hence sn must be semi-elemental. Once again by Appendix A of [Artés *et al.*, 2021a], we know that a finite semi-elemental saddle-node must have multiplicity 2 or 4. If the multiplicity were four, then an analogous reasoning to the previous one leads us to contradiction. Hence, must be two. The uniqueness of the finite saddle-node sn is clear since otherwise S would have finite multiplicity at least five. ■

Finally, according to the notation introduced in [Artés *et al.*, 2021a], we denote a finite semi-elemental saddle-node of multiplicity 2 as $\overline{sn}_{(2)}$.

The next result is due to Ye Yanqian (see [Yanqian *et al.*, 1986]).

Lemma 3.3. *Any $S \in$ **QS** having a linear center at the origin can be transformed, by affine changes of variables and a time rescaling, into a system of the form*

$$\begin{cases} \dot{x} = -y + gx^2 + 2hxy + ky^2 \\ \dot{y} = x + lx^2 + 2mxy \end{cases} \tag{3}$$

for a certain values $(l, g, m, h, k) \in \mathbb{R}^5$. Furthermore, the transformation into the form (3) depends continuously on the parameters.

Proof. Since S has at least one linear center, say $p \in \mathbb{R}^2$, we know that S can be transformed by an affine change of variables (which sends p to the origin) and a time rescaling into a quadratic system of the form (2), say S', for certain coefficients a_{ij}, b_{ij} and with $m = 2$. Hence, we know that $\vec{0}$ is a linear center of S'. Now, we can consider the system S'' obtained from S' performing the following linear change (in fact, a rotation on angle θ)

$$\begin{pmatrix} X \\ Y \end{pmatrix} = \begin{pmatrix} \cos\theta & -\sin\theta \\ \sin\theta & \cos\theta \end{pmatrix} \begin{pmatrix} x \\ y \end{pmatrix}$$

It is easy to see that S'' is of the form

$$\begin{cases} \dot{X} = -Y + a'_{20}X^2 + a'_{11}XY + a'_{02}Y^2 \\ \dot{Y} = X + b'_{20}X^2 + b'_{11}XY + b'_{02}Y^2 \end{cases}$$

with $(a'_{20}, a'_{11}, a'_{02}, b'_{20}, b'_{11}, b'_{02}) \in \mathbb{R}^6 \setminus \vec{0}$. Moreover, the expression of b'_{02} is:

$$\begin{aligned} b'_{02} \;=\; & b_{02}\cos^3\theta + (a_{02} + b_{11})\cos^2\theta\sin\theta \\ & + (a_{11} + b_{20})\cos\theta\sin^2\theta + a_{20}\sin^3\theta \end{aligned}$$

Now, observe that the previous expression corresponds to a cubic trigonometric polynomial, and therefore it must have at least one real root (which depends continuously on the parameters). Thus, we can choose θ so that $b'_{02} = 0$. Finally, notice that all the transformations we have performed are continuous. The claim is proved. ■

The next calculations are due to Chengzhi Li (see [Li, 1983]). Suppose that we have a system (3). Then we have: $V_1 = L_1$, $V_2 = L_2 (mod\ V_1)$ and $V_3 = L_3 (mod\ V_1, V_2)$, where

$$\begin{aligned} L_1 &= 2h(g+k) - 2l(m+g) \\ L_2 &= 2hl(5l - 2h)\left[(g+k)^2(k+2m) - l^2(2m+2g+k)\right] \\ L_3 &= 2hl^2\left[2l^2 + k(g+2k)\right] \\ &\quad \left[(g+k)^2(k+2m) - l^2(2m+2g+k)\right] \end{aligned} \tag{4}$$

Finally, we get the following result:

Proposition 3.4. *Any $S \in$ **Qwf1sn** can be written, by a time rescaling and affine changes of variables, as*

$$\begin{cases} \dot{x} = -y + gx^2 + 2hxy - 2my^2 =: p(x,y) \\ \dot{y} = x + lx^2 + 2mxy =: q(x,y) \end{cases} \tag{5}$$

for a certain values $(l, g, m, h) \in \mathbb{R}^4$ satisfying that $m \neq 0$ and $L_1 = V_1 = 2h(g - 2m) - 2l(m + g) \neq 0$. Furthermore, the transformation into the form (5) depends continuously on the parameters.

Proof. Let $S \in$ **Qwf1sn**. By Lemma 3.3, we know that S is topologically equivalent to a system $S' \in$ **Qwf1sn** of the form (3) with $(l, g, m, h, k) \in \mathbb{R}^5$. Moreover, performing a rotation if necessary we can assume that $k \neq 0$ and that the unique finite saddle-node of S' is placed in $(0, 1/k)$. Furthermore, we have

$$DS'(0, 1/k) = \begin{pmatrix} 2h/k & 1 \\ 1 + 2m/k & 0 \end{pmatrix}$$

By Lemma 3.2 we know that the point $(0, 1/k)$ must be semi-elemental, and a necessary condition for this to happen is that $\det DS'(0, 1/k) = 0$. We observe that

$$\det DS'(0, 1/k) = 0 \iff k = -2m$$

The rest of the proof is straightforward. ∎

Remark 3.5. The reciprocal of Proposition 3.4 is not true, that is, not any system of the form (5) with $m \neq 0$ and $L_1 = V_1 \neq 0$ belongs to **Qwf1sn**. The reason is simple: Of course the condition $L_1 = V_1 \neq 0$ tells us that the origin is a $f^{(1)}$. Moreover, the condition $m \neq 0$ tells us that $(0, -1/2m)$ is a finite singularity (not necessarily isolated) and from the proof of Proposition 3.4 we know that at least one of its eigenvalues must be 0. Reasoning by multiplicities we deduce that it cannot be an intricate singularity, but it can be nilpotent and semi-elemental. However, generically it is a $\overline{sn}_{(2)}$, as will become clear in the subsequent sections.

3.2. Determination of the parameter space

As explained in Section 1, in order to study the closure of the family **Qwf1sn** with respect to the normal form (5), that is $\overline{\textbf{Qwf1sn}}$, we need to consider all the values of the parameters in (5), including those which satisfy $L_1 = V_1 = 0$ or $m = 0$.

We observe that systems (5) depend on the parameter $\lambda = (l, g, m, h) \in \mathbb{R}^4$. Then, the corresponding bifurcation diagram is actually in the four-dimensional Euclidean space $\mathbb{R}^4$, which is of course very difficult to study because we cannot plot it. In what follow we *reduce* the parameter space in order to be able to study it.

We start noticing that the case $\lambda = (l, g, m, h) = 0$ corresponds to a linear system and it does not belong to our family. Hence we consider systems (5) which are nonlinear, i.e. $\lambda = (l, g, m, h) \neq 0$. That is, here we exclude the linear center Vul_1 included in Vulpe's classification (see [Vulpe, 1983]). In this case a system (5) can be rescaled, with the transformation $(x, y, t) \to (\alpha x, \alpha y, t)$, $\alpha \neq 0$. In fact, applying this transformation we obtain:

$$\begin{cases} \dot{x} = -y + \alpha g x^2 + 2\alpha h xy - 2\alpha m y^2 \\ \dot{y} = x + \alpha l x^2 + 2\alpha m xy \end{cases} \tag{6}$$

Then, this transformation takes the systems with parameters (l, g, m, h) to systems with parameters $(\alpha l, \alpha g, \alpha m, \alpha h)$. We consider now the 3-dimensional projective space $\mathbb{RP}^3$, which can be viewed as the quotient space $(\mathbb{R}^4)^*/\sim$ of $(\mathbb{R}^4)^*$, $(\mathbb{R}^4)^* := \mathbb{R}^4 \setminus \vec{0}$, by the equivalence relation: (l, g, m, h) is equivalent to $(\alpha l, \alpha g, \alpha m, \alpha h)$ for any $\alpha \neq 0$. The elements of $\mathbb{RP}^3$ are $[\lambda] = [l : g : m : h]$ for $\lambda = (l, g, m, h) \in (\mathbb{R}^4)^*$, where by definition:

$$[\lambda] = [l : g : m : h] = \{\alpha(l, g, m, h) \mid \alpha \in \mathbb{R} \setminus 0\}$$

In view of the previous observations, we may consider $\mathbb{RP}^3$ as our parameter space in the sense that each element $\alpha(l, g, m, h)$, $\alpha \neq 0$, of the equivalence class $[\lambda] = [l : g : m : h] \in \mathbb{RP}^3 = (\mathbb{R}^4)^*/\sim$ leads us topological equivalent systems (5) by means of a simple rescaling, and hence all the elements of the class $[l : g : m : h]$ can be identified.

Remark 3.6. Due to the symmetry $(x, y, t) \to (-x, y, -t)$ we have $(l, g, m, h) \to (-l, g, m, -h)$. Indeed, after applying the symmetry $(x, y, t) \to (-x, y, -t)$ in (5) we obtain the following quadratic system

$$\begin{cases} \dot{x} = -y + g x^2 - 2h xy - 2m y^2 \\ \dot{y} = x - l x^2 + 2m xy \end{cases} \tag{7}$$

This fact implies that it suffices to consider only $h \geq 0$ or $l \geq 0$, and in fact we choose to consider only the case $h \geq 0$. In other words, we identify the classes $[l : g : m : h]$ and $[-l : g : m : -h]$ of $\mathbb{RP}^3$, which are different elements of $\mathbb{RP}^3$ if $h \neq 0$ or if $l \neq 0$.

Since our parameter space is $\mathbb{RP}^3$, is convenient to choose adequate representatives of each class $[l : g : m : h] \in \mathbb{RP}^3$ in order to *transform*

our parameter space into a compact set where the bifurcation diagram can be completely studied.

Parameter space as a half ball

First of all, notice that each class $[\lambda] \in \mathbb{RP}^3$ has one or two representatives in $(\mathbb{S}^3)^+ = \{\lambda = (l,g,m,h) \in \mathbb{R}^4 \mid \|\lambda\| = 1, m \geq 0\}$ depending on whether the coordinate m of λ is 0 or not. Since for points $(l,g,m,h) \in (\mathbb{S}^3)^+ \subset \mathbb{S}^3$ we have $l^2+g^2+m^2+h^2 = 1$ and we can assume $m \geq 0$, we can write $m = \sqrt{1-(l^2+g^2+h^2)}$ where $0 \leq l^2+g^2+h^2 \leq 1$. From the previous observations and taking into account the identification between classes explained in Remark 3.6, it follows directly that each $[\lambda] \in \mathbb{RP}^3$ corresponds to at least one point in the half-ball $\mathcal{B}_{1/2} = \{(l,g,h) \in \mathbb{R}^3 \mid l^2+g^2+h^2 \leq 1\ ,\ h \geq 0\}$. In this sense we can view $\mathbb{RP}^3$ as $\mathcal{B}_{1/2}$.

Definition 3.7. We call *equator* to the subspace $h = m = 0$ in $\mathbb{RP}^3$, i.e. the set of points of the form $[l : g : 0 : 0] \in \mathbb{RP}^3$. We call *base* to the subspace $h = 0$ of $\mathbb{RP}^3$, i.e. the set of points of the form $[l : g : m : 0] \in \mathbb{RP}^3$.

It is clear that we can identify the equator defined in Def. 3.7 with the equator of $\mathcal{B}_{1/2}$, that is, $\mathbb{S}^1 = \{(l,g) \in \mathbb{R}^2 \mid l^2+g^2 = 1\}$, where of course two opposite points of $\mathbb{S}^1$ are identified because they correspond to the same element in $\mathbb{RP}^3$. If we take a point in the base, say $[l : g : m : 0] \in \mathbb{RP}^3$, then can be identified with $[l : g : m] \in \mathbb{RP}^2$. So the base defined in Def. 3.7 can be identified to $\mathbb{RP}^2$ which in turn can be viewed as the base of $\mathcal{B}_{1/2}$, that is $\{(l,g,0) \in \mathbb{R}^3 \mid l^2+g^2 \leq 1\}$. See Fig. 3.1.

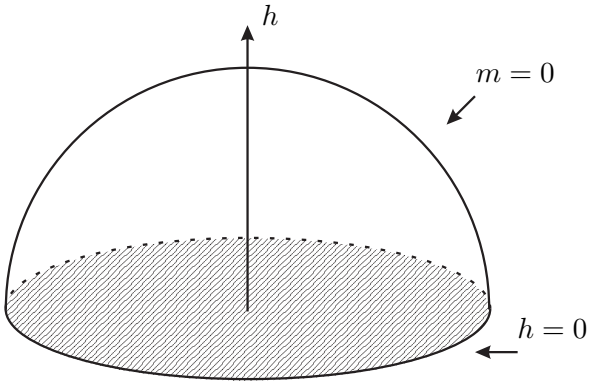

Fig. 3.1: The parameter space $\mathcal{B}_{1/2}$.

Definition 3.8. We call *affine part* of $\mathbb{RP}^3$ to the set of points of the form $[l : g : m : h] \in \mathbb{RP}^3$ with $m \neq 0$, and we call *infinite part* of $\mathbb{RP}^3$ to the subspace $m = 0$ of $\mathbb{RP}^3$, i.e. the set of points of the form $[l : g : 0 : h] \in \mathbb{RP}^3$.

Affine part of $\mathbb{RP}^3$ viewed as $(\mathbb{R}^3)^+$

By our previous considerations we can identify the infinite part of $\mathbb{RP}^3$ with $\mathbb{S}^2 \cap \mathcal{B}_{1/2}$, where $\mathbb{S}^2 = \{(l,g,h) \in \mathbb{R}^3 \mid l^2+g^2+h^2 = 1\}$. On the other hand, the affine part of $\mathbb{RP}^3$ can be identified with $B(\vec{0},1) \cap \mathcal{B}_{1/2}$, where $B(\vec{0},1) = \{(l,g,h) \in \mathbb{R}^3 \mid l^2+g^2+h^2 < 1\}$.

There is, however, another way to identify the affine part of $\mathbb{RP}^3$, which will be also essential in Sect. 4. Let a point $[\lambda] \in \mathbb{RP}^3 \setminus \{m = 0\}$. We can take as a representative of $[\lambda]$ the unique point of the form $\alpha\lambda$ with coordinate $m = 1$. More precisely, we have the affine chart:

$$\begin{aligned} &\mathbb{RP}^3 \setminus \{m = 0\} \leftrightarrow \mathbb{R}^3 \\ &\quad [l : g : m : h] \to \left(\frac{l}{m}, \frac{g}{m}, \frac{h}{m}\right) = (\overline{l}, \overline{g}, \overline{h}) \\ &\quad [\overline{l} : \overline{g} : 1 : \overline{h}] \leftarrow (\overline{l}, \overline{g}, \overline{h}) \end{aligned}$$

From the previous observations and taking into account the identification between classes explained in Remark 3.6, it follows directly that each $[\lambda] \in \mathbb{RP}^3 \setminus \{m = 0\}$ corresponds to at least one point in $(\mathbb{R}^3)^+ = \{(l,g,h) \in \mathbb{R}^3 \mid h \geq 0\}$. In this sense we can identify the affine part of $\mathbb{RP}^3$ with $(\mathbb{R}^3)^+$, which in fact justifies the terminology *affine*.

Relating the two points of view of the affine part of $\mathbb{RP}^3$

The two identifications of $\mathbb{RP}^3 \setminus \{m = 0\}$ can be transformed from one to another by means of the bijection defined as follows

$$\begin{aligned} (\mathbb{R}^3)^+ &\leftrightarrow B(\vec{0},1) \cap \mathcal{B}_{1/2} \\ (\overline{l}, \overline{g}, \overline{h}) &\leftrightarrow \left(\frac{\overline{l}}{k}, \frac{\overline{g}}{k}, \frac{\overline{h}}{k}\right) \end{aligned}$$

with $k = \sqrt{\overline{l}^2+\overline{g}^2+\overline{h}^2+1}$. More precisely, if $(\overline{l}, \overline{g}, \overline{h})$ is an identification in $(\mathbb{R}^3)^+$ of the class $[\lambda] \in \mathbb{RP}^3 \setminus \{m = 0\}$, then $\left(\frac{\overline{l}}{k}, \frac{\overline{g}}{k}, \frac{\overline{h}}{k}\right)$ is an identification in $B(\vec{0},1) \cap \mathcal{B}_{1/2}$ of $[\lambda]$, and vice versa.

How do we study the parameter space?

To study the bifurcation diagram (see Sect. 4), we will take $\mathcal{B}_{1/2}$ as a representative of our parameter space since is a compact set in which we can

check that the regions studied have a coherence as we approach to the boundary of $\mathcal{B}_{1/2}$.

First of all, in order to study the affine part of $\mathbb{RP}^3$, we note that we can pass from $B(\vec{0},1)\cap\mathcal{B}_{1/2}$ to $(\mathbb{R}^3)^+$ by means of the bijection previously given. Hence when studying the affine part of $\mathbb{RP}^3$ we can study its identification in $(\mathbb{R}^3)^+$ by taking $m=1$ in (5) and considering the parameters (l,g,h) with $h\geq 0$, and then the return to $B(\vec{0},1)\cap\mathcal{B}_{1/2}$. As we will explain in detail in Sect. 4, we do not have to study all $(\mathbb{R}^3)^+$ but only certain planes in $(\mathbb{R}^3)^+$ of the form $h=h_0$ (where h_0 is a non-negative constant), which will be called *slices*. It is clear that each plane of the form $h=h_0\geq 0$ in $(\mathbb{R}^3)^+$ corresponds to a certain set in $B(\vec{0},1)\cap\mathcal{B}_{1/2}$. From the bijection between $B(\vec{0},1)\cap\mathcal{B}_{1/2}$ and $(\mathbb{R}^3)^+$ given before it is easy to check that the plane $h=h_0>0$ corresponds to the half ellipsoid $\left\{h^2(1+h_0)^2/h_0^2+l^2+g^2=1\right\}\cap\{h>0\}$, and the plane $h=0$ corresponds to the interior of the base of $\mathcal{B}_{1/2}$, i.e. $\left\{(l,g)\in\mathbb{R}^2\mid l^2+g^2<1\right\}$ (see Fig. 3.2).

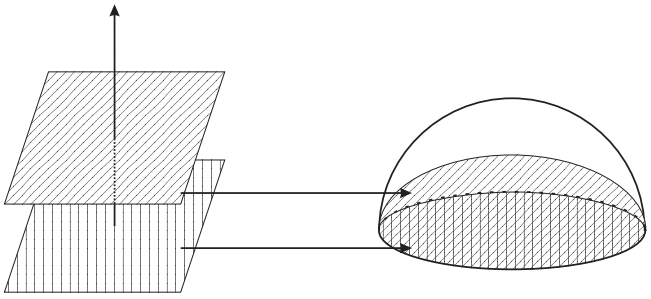

Fig. 3.2: Correspondence between planes and ellipsoides

In order to study the infinite part of $\mathbb{RP}^3$ we can consider separately the equator and the set points of the form $[l:g:0:h]$ with $h\neq 0$, called $\infty\setminus Eq$, where of course $\infty\setminus Eq\subset\mathbb{RP}^3\cap\{m=0\}$. By our previous considerations we know that $\infty\setminus Eq$ can be identified with $\mathbb{S}^2\cap\{h>0\}$. However, we can also identify it with $\mathbb{R}^2$ by means of taking as a representative of each $[\lambda]\in\infty\setminus Eq$ the unique element of the form $\alpha\lambda$ with coordinate $h=1$. Similarly to what have happened before, we can pass from one identification to another through the normalization:

$$\mathbb{R}^2\leftrightarrow\mathbb{S}^2\cap\{h>0\}$$
$$(\overline{l},\overline{g},1)\equiv(\overline{l},\overline{g})\leftrightarrow\left(\frac{\overline{l}}{k},\frac{\overline{g}}{k},\frac{1}{k}\right)$$

with $k=\sqrt{\overline{l}^2+\overline{g}^2+1}$. Hence we can perform the study of $\infty\setminus Eq$ when identified with $\mathbb{R}^2$ and then return to $\mathbb{S}^2\cap\{h>0\}$. We also note that $\infty\setminus Eq$ can also be interpreted as the slice $h=+\infty$.

Finally, we point out that in order to study the equator visualized into $\mathcal{B}_{1/2}$ we only need to study $\mathbb{S}^1$. As we will see in Sect. 4, the equator has a big importance since it allows us to check if the regions encountered in the considered slices are coherent when we go to infinity (see Fig. 3.2).

4. The bifurcation diagram of the systems in $\overline{\mathbf{Qwf1sn}}$

The objective of this thesis is to perform the study of the bifurcation diagram of $\overline{\mathbf{Qwf1sn}}$. This is a global work and as such it uses global methods. In particular it uses algebraic and topological invariants. The algebraic invariants make results independent of specific normal forms. They also distinguish the phase portraits as the topological invariants also do. In this section we use the concepts of algebraic invariant and comitant as formulated by the Sibirsky's School for differential equations. For a summary of the general theory of these polynomial invariants and their relevance in working with polynomial differential systems see Section 7 of [Artés *et al.*, 2006]. For a more detailed explanation see the Chapter 5 of the recently published book [Artés *et al.*, 2021a]. We start this section presenting the value of the algebraic invariants and comitants (with respect to normal form (5)) which are relevant in our study.

4.1. Algebraic bifurcation surfaces at the affine part of $\mathbb{RP}^3$

From book [Artés *et al.*, 2021a] we get the formulas which give the bifurcation surfaces of singularities in $\mathbb{R}^{12}$, produced by changes that may occur in the local nature of some or all the singular points, either finite or infinite. These bifurcation surfaces are all algebraic. Before describing them, we need an important observation:

Remark 4.1. We are considering systems of the form (5) and our parameter space is $\mathbb{RP}^3$. Hence, we are not considering the linear center $l=g=m=h=0$. Moreover, the following hold:

(*a*) The system (5) is degenerate (i.e. $\gcd(p,q) \neq$ constant) only for values of the parameters belonging to the set $\{[-2h:0:1:h] \mid h \in \mathbb{R}\}$ (contained in the affine part of $\mathbb{RP}^3$) plus the point $[-2:0:0:1]$ (in the infinite part of $\mathbb{RP}^3$). In such cases, the system (5) is of the form

$$\begin{cases} \dot{x} = -y(1 - 2\alpha hx + 2\alpha my) \\ \dot{y} = x(1 - 2\alpha hx + 2\alpha my) \end{cases} \tag{8}$$

with α being non-zero and taking $m = 1$ for the set in the affine part of $\mathbb{RP}^3$ and $m = 0$, $h = 1$ for the point in the infinite part of $\mathbb{RP}^3$. Hence, the phase portrait of (8) consists on a linear center with the line of singularities $(1-2\alpha hx+2\alpha my) = 0$, which does not contain the origin (see $1.8L_1$ in Thm. 2.3).

(*b*) The systems (5) do not have any degeneracy at infinity. Indeed, if we compute the comitant:

$$C_2 = -lx^3 - 2mx^2y + gx^2y + 2hxy^2 - 2my^3$$

which clearly is always different from the null polynomial if $(l, g, m, h) \neq 0$. Therefore, by Lemma 6.1 of [Artés *et al.*, 2021a] our claim is proved.

We start observing that by construction, systems (5) always have $(0, 0)$ as a finite isolated singular point, which could be a $f^{(1)}$, $f^{(2)}$, $f^{(3)}$ or a center. Hence, by Theorem 6.2 of [Artés *et al.*, 2021a] we know that the invariant polynomial $\mathcal{T}_4$ vanishes for all the values of the parameters for which the system (5) is quadratic and non-degenerate (i.e. $\gcd(p, q) =$ constant). We start constructing our bifurcation surfaces:

Bifurcation surface in $\mathbb{RP}^3$ due to the origin being a weak singularity of order > 1.

$(\mathcal{S}_8)$ This bifurcation surface will contain the points of the parameter space where the origin is a $f^{(i)}$ for $i = 2, 3$ or a center. A computation shows that $\sigma = 0$ implies $\mathcal{F}_1 = 0$ in (5). Hence, we deduce from Thm. 6.2 of [Artés *et al.*, 2021a] that a quadratic non-degenerate system of the form (5) has a weak singularity of order greater than one at the origin being either a $f^{(i)}$ for $i = 2, 3$ or a center if and only if the invariant polynomial $\mathcal{F}_1$ satisfy $\mathcal{F}_1 = 0$. In our normal form (5) we have:

$$\mathcal{F}_1 = -2(gh - gl - 2hm - lm)$$

Hence, according to our previous observations we define:

$$(\mathcal{S}_8) : gh - gl - 2hm - lm = 0$$

Remark 4.2. In the subspace $[l : g : 1 : 0]$ (placed in the affine part of $\mathbb{RP}^3$) we have that $\mathcal{T}_3 = 0$ and hence, according to Thm. 6.2 of [Artés *et al.*, 2021a] (and Remark 4.1), if the origin is a weak singularity of order greater than one in such subspace, then must be of infinite order (i.e. must be a center).

Bifurcation surface in $\mathbb{RP}^3$ due to the presence of a second weak singularity (generically a $f^{(1)}$ or a $s^{(1)}$).

$(\mathcal{S}_3)$ This bifurcation surface will contain the points of the parameter space for which there is a second finite weak singularity apart from the origin, which generically will be a $f^{(1)}$ or a $s^{(1)}$. According to Thm. 6.2 of [Artés *et al.*, 2021a], we know that a necessary condition for a quadratic non-degenerate system of the form (5) to have two finite weak singularities is that $\mathcal{T}_4 = \mathcal{T}_3 = 0$. Since in our case the origin is always a weak singularity (focus or center) the unique possibility of having two weak singularities with the origin being a focus is that the origin is a $f^{(1)}$ and there exists another finite singularity being either a $f^{(1)}$ or a $s^{(1)}$. In our normal form (5) we have:

$$\mathcal{T}_3 = -8h^2(gh + gl + 2hm + lm)$$

Hence, according to our previous observations we define:

$$(\mathcal{S}_3) : h(gh + gl + 2hm + lm) = 0$$

We observe that we get a weak singularity when the trace of a strong focus or a strong saddle becomes zero. We also highlight that this bifurcation can produce a topological change if the weak point is a focus (appearance of limit cycle due to Hopf bifurcation), but if the weak point is a saddle produce just a C^∞ change except in some situations, as for example when this bifurcation coincides with a loop bifurcation associated to the same saddle, in which case the change may be topological. In principle this last situation does not occur in our family (see Sect. 5.3), but occurs in [Artés *et al.*, 2021c], for instance.

Remark 4.3. In the subspace $[l : g : 1 : 0]$ (in the affine part of $\mathbb{RP}^3$) the surface $(\mathcal{S}_3)$ should be redefined. Indeed, for all values of this plane we have $\mathcal{T}_i = 0$ for $i = 2, 3, 4$. Moreover,

(a) If $l \neq 0$ and $g \neq 0$ system (5) is non-degenerate and satisfies $\mathcal{T}_1 \neq 0$. Hence, by Thm. 6.2 of [Artés *et al.*, 2021a] we have a unique weak singularity which is the origin being a $f^{(1)}$.

(b) We consider now the set $[0 : g : 1 : 0]$, $g \in \mathbb{R}$. If $g = 0$, see Remark 4.1. If $g \neq 0$ then system (5) is non-degenerate and satisfies $\mathcal{T}_1 = 0$. We have two options:

($b1$) If $g \neq -1$ then $\sigma \neq 0$ and $\mathcal{F}_1 = 0$. Hence we have a unique weak singularity (the origin being a center).

($b2$) If $g = -1$ then $\sigma = \mathbf{D} = \mathbf{T} = \mathbf{P} = 0$, $\mathbf{R} \neq 0$ and $\mu_0 > 0$. Hence we have a unique weak singularity which is the origin being a center.

(c) We consider now the set $[l : -1 : 1 : 0]$, $l \in \mathbb{R}$. If $l = 0$ see case (b). For all values of this set with $l \neq 0$ the system (5) is non-degenerate and satisfies $\sigma = 0$, $\mu_0 > 0$, $\mathbf{D} = 0$ and $\mathbf{T} \neq 0$. Hence we have two weak singularities: The origin (center) and a finite saddle.

In conclusion, in the subspace $[l : g : 1 : 0]$ the surface $(\mathcal{S}_3)$ must be redefined as $[l : -1 : 1 : 0]$ with $l \neq 0$.

In addition, if we are in the equator $[l : g : 0 : 0]$ (contained in the infinite part of $\mathbb{RP}^3$) the system (5) is non-degenerate and satisfies that $\mathcal{T}_i = 0$ for $i = 1, 2, 3, 4$. If $g \neq 0$ then $\sigma \neq 0$ and hence we have a unique weak singularity which is the origin being a $f^{(1)}$ if $l \neq 0$ (because $\mathcal{F}_1 \neq 0$ in this case) and being a center if $l = 0$ (because $\mathcal{F}_1 = 0$ in this case). If $g = 0$ then $\sigma = \mu_0 = \mathbf{D} = 0$ and hence we have two weak singularities: the origin (center) and a finite saddle.

Bifurcation surface in $\mathbb{RP}^3$ due to a at least one finite singularity has escaped to infinity.

$(\mathcal{S}_1)$ This is the bifurcation surface due to multiplicity of infinite singularities, which contains the values of the parameters for which at least one finite point collides with at least one infinite point. This phenomenon is detected by the invariant polynomial μ_0 (see Lemma 5.5 of [Artés *et al.*, 2021a]) whose expression with respect to our normal form (5) is given by:

$$\mu_0 = -4m^2(-2hl - l^2 + 2gm)$$

Hence, according to our previous observations we define:

$$(\mathcal{S}_1) : m(-2hl - l^2 + 2gm) = 0$$

Bifurcation surface in $\mathbb{RP}^3$ due to at least two infinite singularities have collided.

$(\mathcal{S}_5)$ This is the bifurcation surface due to multiplicity of infinite singularities, which contains the values for which at least two infinite singular points collide. This phenomenon is detected by the invariant polynomial η (see Lemma 5.5 of [Artés *et al.*, 2021a]) which in our normal form (5) is given by:

$$\begin{aligned}\eta = 4(&g^2h^2 + 8h^3l + 2g^3m - 4gh^2m \\ &+ 18ghlm - 12g^2m^2 + 4h^2m^2 \\ &- 36hlm^2 - 27l^2m^2 + 24gm^3 - 16m^4)\end{aligned}$$

Hence, we define the surface $(\mathcal{S}_5)$ by the equation:

$$\begin{aligned}(\mathcal{S}_5) : &g^2h^2 + 8h^3l + 2g^3m - 4gh^2m \\ &+ 18ghlm - 12g^2m^2 + 4h^2m^2 \\ &- 36hlm^2 - 27l^2m^2 + 24gm^3 - 16m^4 = 0\end{aligned}$$

Before introducing the next surface, we recall that a quadratic non-degenerate system of the form (5) with $m \neq 0$ satisfies that $\left(0, -\frac{1}{2m}\right)$ is a singularity of multiplicity at least 2 (see Appendix A of [Artés *et al.*, 2021a]). From the previous fact and noticing that we have also a simple singularity at the origin, we know by Prop. 6.1 of [Artés *et al.*, 2021a] that the invariant $\mathbf{D}$ vanishes.

Bifurcation surface in $\mathbb{RP}^3$ due to the existence of a triple finite collision.

$(\mathcal{S}_2)$ This bifurcation surface will contain the points of the parameter space for which at least three finite singularities have collided. If we consider now a quadratic non-degenerate system of the form (5), then Prop. 6.1 of [Artés *et al.*, 2021a] tells us that a necessary condition (and also sufficient if $\mu_0 \neq 0$, i.e. if we are outside $(\mathcal{S}_1)$) to have a triple finite collision is that the comitant $\mathbf{T}$ vanishes. In our normal form (5) we have:

$$\mathbf{T} = -48(2h + l)^2m^4x^2(gx + 2hy + ly)^2(lx + 2my)^2$$

Hence, according to our previous observations we define:

$$(\mathcal{S}_2) : (2h + l)m = 0$$

Remark 4.4. We note that we do not need to consider the possibility of having two finite singularities of multiplicity two. Indeed, since in (5) the origin is always a weak focus or a center (and hence it has multiplicity one), if we would have two finite singularities of multiplicity two then the total finite multiplicity would be at least five, which is impossible.

However, this is a situation that can happen if we use a normal form for **Qwf1sn** different from (5), in which we allow that the origin may be a double point. In fact, previous observation is a proof that we are not studying the whole set clousure of **Qwf1sn** in the whole parameter space.

Bifurcation surface in $\mathbb{RP}^3$ due to the possible existence of invariant straight lines.

$(\mathcal{S}_4)$ This surface will contain the points of the parameter space where invariant straight lines may appear. These straight lines may contain connections of separatrices from different singularities or not. So, in some cases, it may imply a topological bifurcation (the invariant line is a separatrix connection) and, in others, just a C^∞ bifurcation (the invariant line is not a separatrix connection). According to [Artés *et al.*, 2021a] the equation of this surface is given by the invariant polynomial B_1. It is worth mentioning that $B_1 = 0$ is only a necessary condition for the existence of an invariant straight line, but it is not sufficient, i.e. we may find some component of $B_1 = 0$ that does not represent an invariant straight line. For normal form (5) the invariant polynomial B_1 is:

$$B_1 = 2l^2(g^2 + 4h^2 + 4hl + l^2)(-gh + 2hm + lm)$$

We define the surface $(\mathcal{S}_4)$ by the equation:

$$(\mathcal{S}_4) : l(g^2 + 4h^2 + 4hl + l^2)(-gh + 2hm + lm) = 0$$

The bifurcation surfaces above are all algebraic and except surface $(\mathcal{S}_4)$, they are the bifurcation surfaces of finite and infinite singularities of systems (5) in the parameter space. We will detect other two bifurcation surfaces not necessarily algebraic. On one of them the systems have global connection of separatrices different from that given by $(\mathcal{S}_4)$ and on the other the systems possess a double limit cycle. The equations of these bifurcation surfaces can only be determined approximately by means of numerical tools. Using arguments of continuity in the phase portraits we can prove the existence of these components not necessarily algebraic in the part where they appear, and we can check them numerically. We shall name them surfaces $(\mathcal{S}_7)$ (connection of separatrices) and $(\mathcal{S}_{10})$ (double limit cycles).

The surface of C^∞ bifurcation due to a node ($\neq$ from the origin) becoming a focus

$(\mathcal{S}_6)$ This surface will contain the points of the parameter space where a finite node different from the origin turns into a focus. That is, in a neighborhood of $(\mathcal{S}_6)$, there is a singular point which changes in a continuous way from a node to a focus, or vice versa. This surface is a C^∞ but not a topological bifurcation surface. In fact, when we only cross the surface $(\mathcal{S}_6)$ in the bifurcation diagram, the topological phase portraits do not change. However, this surface is relevant to localize the regions where a limit cycle surrounding a finite antisaddle (different from the origin) cannot exist, as we will see later in detail. Using Thm. 6.1 of [Artés *et al.*, 2021a], we must consider the polynomial invariant W_4, whose expression is:

$$\begin{aligned} W_4 \ = & -256h^4(g^2h^2 + 2g^2hl + 8h^3l + g^2l^2 + 12h^2l^2 \\ & + 6hl^3 + l^4 - 4gh^2m - 2ghlm + 4h^2m^2 \\ & + 4hlm^2 + l^2m^2) \end{aligned}$$

Hence, we define $(\mathcal{S}_6)$ as:

$$\begin{aligned} (\mathcal{S}_6) : & h(g^2h^2 + 2g^2hl + 8h^3l + g^2l^2 + 12h^2l^2 \\ & + 6hl^3 + l^4 - 4gh^2m - 2ghlm + 4h^2m^2 \\ & + 4hlm^2 + l^2m^2) = 0 \end{aligned}$$

Remark 4.5. The whole subspace $[l : g : 1 : 0]$ (in the affine part of $\mathbb{RP}^3$) is contained in $(\mathcal{S}_6)$ since $W_4 = 0$ in such set. Using Theorem 6.1 of [Artés *et al.*, 2021a] we deduce that in such subspace cannot exist a focus different from the origin, or in other words, if exists an antisaddle (in this thesis, by an **antisaddle** we mean either a node or a focus) different from the origin, must be a node (and hence there are no limit cycles surrounding it).

In Appendix A.1 we present pictures of the algebraic surfaces $(\mathcal{S}_i)$ in the three-dimensional

affine space which is the hyperplane $m = 1$ in $\mathbb{R}^4$. If the reader prefers, the images are also available in the *Mathematica* file **surfaces.nb** at link `https://mat.uab.cat/~artes/articles/qwf1sn/qwf1sn.html`.

Remark 4.6. Systems corresponding to surface $(\mathcal{S}_{10})$ have at least one double limit cycle. Although this surface is obtained numerically, we know that must be placed near the points of the bifurcation diagram where the origin is a weak focus of order higher than one (i.e. the surface $(\mathcal{S}_8)$). As we will realize in soon, knowing which points of $(\mathcal{S}_8)$ correspond to $f^{(2)}$, $f^{(3)}$ and centers will help us incredibly to understand where and why limit cycles appear. According to Thm 6.2 of [Artés *et al.*, 2021a], if we have a quadratic non-degenerate system of the form (5) satisfying that $\mathcal{T}_4 = 0$ and $\mathcal{T}_3 \neq 0$ ($\mathcal{T}_3 \neq 0$ means we are outside $(\mathcal{S}_3)$) then we have a unique weak singularity (in our case the origin, being focus or center) which is:

- $f^{(1)} \iff \mathcal{F}_1 \neq 0$ (outside $(\mathcal{S}_8)$).
- $f^{(2)} \iff \mathcal{F}_1 = 0,\ \mathcal{F}_2 \neq 0$.
- $f^{(3)} \iff \mathcal{F}_1 = \mathcal{F}_2 = 0,\ \mathcal{F}_3\mathcal{F}_4 \neq 0$.
- center $\iff \mathcal{F}_1 = \mathcal{F}_2 = \mathcal{F}_3\mathcal{F}_4 = 0$.

Since the previous result is not valid when $\mathcal{T}_3 = \mathcal{T}_4 = 0$ and we always have $\mathcal{T}_4 = 0$, we should study the region defined as $\mathcal{F}_1 = \mathcal{T}_3 = 0$ (i.e. the region of $(\mathcal{S}_8)$ where the previous result is not valid, apart from the intersections of $(\mathcal{S}_8)$ with the degenerate regions studied in Remark 4.1). We get four lines and four points:

(a) The first line (placed in the affine part of $\mathbb{RP}^3$) is $[0 : g : 1 : 0]$, $g \in \mathbb{R}$, which arrives to infinity at $[0 : 1 : 0 : 0]$ (located in the equator). Both are studied in Remark 4.3.

(b) The second line (in the affine part of $\mathbb{RP}^3$) is defined as $[l : -1 : 1 : 0]$, $l \in \mathbb{R}$, which arrives to infinity at the point $[1 : 0 : 0 : 0]$ (located in the equator). Both regions are already studied in Remark 4.3.

(c) The third line (in the affine part of $\mathbb{RP}^3$) is defined as $[-2h : 0 : 1 : h]$, with $h \in \mathbb{R}$, which arrives to infinity at the point $[-2 : 0 : 0 : 1]$. Both regions correspond to degenerate regions studied in Remark 4.1.

(d) The fourth line (in the infinite part of $\mathbb{RP}^3$) is defined as $[l : 0 : 0 : 1]$, with $l \in \mathbb{R}$, which arrives to the equator at the point $[1 : 0 : 0 : 0]$. This last point is studied in Remark 4.3. Regarding to the infinite line, if $l = -2$ see Remark 4.1. If $l \neq -2$ the system (5) is non-degenerate and we have three options:

($d1$) If $l = 0$, $\mathcal{T}_i = 0$ for $i = 1, 2, 3, 4$, $\mathcal{F}_1 = 0$ and $\sigma \neq 0$. Hence, in this case the origin is the unique weak singularity being a center.

($d2$) If $l \in (-2, 0)$, $\mathcal{F} = \mathcal{T}_3 = 0$, $\mathcal{T}_2 < 0$, $\mathcal{F}_1 = 0$. Hence we have two weak singularities, both centers.

($d3$) If $l \in \mathbb{R} \setminus [-2, 0]$, $\mathcal{F} = \mathcal{T}_3 = 0$, $\mathcal{T}_2 > 0$, $\mathcal{F}_1 = 0$. Hence we have two weak singularities, one center (the origin) and one finite saddle.

If we compute the solutions of $\mathcal{F}_1 = \mathcal{F}_2 = 0$ we obtain two affine lines plus their corresponding intersection points with the infinite part of $\mathbb{RP}^3$ (plus the four previous lines and the four previous points, which also satisfy $\mathcal{F}_1 = \mathcal{F}_2 = 0$):

(e) The first line is $[0 : 2 : 1 : h]$, $h \in \mathbb{R}$. For $h = 0$ this line intersect the one described in (a) at $[0 : 2 : 1 : 0]$. For the rest of values the system is non-degenerate and satisfies $\mathcal{T}_3 \neq 0$, $\mathcal{F}_1 = \mathcal{F}_2 = \mathcal{F}_3\mathcal{F}_4 = 0$. Hence the unique weak singularity is the origin (which is a center). The previous line arrives at infinity at $[0 : 0 : 0 : 1]$, a value for which (5) is non-degenerate and satisfies: $\mathcal{T}_i = 0 = \mathcal{F}_1$ for $i = 1, 2, 3, 4$ and $\sigma \neq 0$. Hence, in this last point the system has a unique weak singulatity (which is a center).

(f) The second line is $[2h/5 : 4 : 1 : h]$, $h \in \mathbb{R}$. For values of this line with $h \neq 0$ the systems of family (5) are non-degenerate and satisfy $\mathcal{T}_3 \neq 0$, $\mathcal{F}_3\mathcal{F}_4 \neq 0$ and $\mathcal{F}_1 = \mathcal{F}_2 = 0$. Hence the unique weak singularity is the origin (which is a $f^{(3)}$). For $h = 0$ the line intersect the one described in (a) at the point $[0 : 4 : 1 : 0]$. The previous line arrives at infinity at $[2/5 : 0 : 0 : 1]$, for which (5) is non-degenerate and satisfies: $\mathcal{T}_3 = 0$, $\mathcal{T}_2 > 0$ and $\mathcal{F}_1 = 0$. Hence in this last point the system has two weak singularities: the origin (center) and a finite saddle.

We note that the previous facts grouped together tell us all the information regarding weak singularities in surface $(\mathcal{S}_8)$. We also remark that we have not named the previous lines and points in order not to be confused with the notation that we will establish in the study of the bifurcation diagram. In fact, some of the previous lines shall be separated in some parts due to our numeration rules, as we will explain soon. However, we will use the previous results later.

If the reader would like to check if the expressions of the surfaces we have given in this section are correct, she/he can do it by means of a program made by Joan C. Arthat allows to calculate the comitants and invariants described in [Artés *et al.*, 2021a] for a general quadratic system. The program is available at link `https://mat.uab.cat/~artes/articles/qwf1sn/qwf1sn.html` (inside a *Mathematica* file called **comitants.nb**). Moreover, in Appendix B of [Artés *et al.*, 2021a] you can find an usage tutorial.

Remark 4.7. Even though we can draw a two-dimensional picture of the algebraic bifurcation surfaces of singularities in the three-dimensional affine space (corresponding the hyperplane $m = 1$ in $\mathbb{R}^4$) as we did in Appendix A.1, it is pointless to see a single two-dimensional image of all these bifurcation surfaces because, as we shall see later, the partition of the parameter space obtained from these bifurcation surfaces has a large number of parts: Precisely 399.

Due to the last remark, in order to study the bifurcation diagram in the affine part of $\mathbb{RP}^3$ (which can be identified with $(\mathbb{R}^3)^+$ as explained in Sect. 3.2) we shall foliate $(\mathbb{R}^3)^+$ by the planes $h = \widetilde{h}$, with $\widetilde{h}$ being a non-negative constant, and we shall give pictures of the resulting bifurcation diagram on these planar sections or in the planar projection of the half elliposides contained in $B(\vec{0}, 1) \cap \mathcal{B}_{1/2}$ corresponding to the previous planes, as explained in Sect. 3.2. We recall that in the planes $h = \widetilde{h}$ contained in $(\mathbb{R}^3)^+$, the coordinates are (l, g) where the horizontal line is the l–axis. We also recall from Sect. 3.2 that in order to study the identification in $(\mathbb{R}^3)^+$ of the affine part of $\mathbb{RP}^3$ we must take take $m = 1$ in (5) and consider as a parameter (l, g, h) with $h \geq 0$.

As the final bifurcation diagram is quite complex, it is useful to introduce some colors which will be used to refer to the bifurcation surfaces:

(a) Surface $(\mathcal{S}_1)$ is drawn in dark blue (contains the points in which one finite singularity escapes to infinity).

(b) Surface $(\mathcal{S}_2)$ is drawn in green (contains the points in which there is a triple finite collision).

(c) Surface $(\mathcal{S}_3)$ is drawn in yellow (there is a second weak singularity). We draw it as a continuous curve if it implies a topological change or as a dashed curve otherwise.

(d) Surface $(\mathcal{S}_4)$ is drawn in purple (possible existence of an invariant straight line). We draw it as a continuous curve if it implies a topological change (the invariant line corresponds to a separatrix connection) or as a dashed curve otherwise (the invariant line does not correspond to a separatrix connection).

(e) Surface $(\mathcal{S}_5)$ is drawn in red (contains the points in which at least two infinite singularities coalesce).

(f) Surface $(\mathcal{S}_6)$ is drawn in black (an antisaddle is on the edge of turning from a node to a focus or vice versa). Despite it is crucial for isolating regions where a limit cycle surrounding the finite antisaddle different from the origin cannot exists, and it helps in the understanding of some other degeneracies when combined with other bifurcations, we draw it as a dashed curve since it does not imply a topological change.

(g) Surface $(\mathcal{S}_7)$ is also drawn in purple (contains the points in which there is a connection of separatrices).

(h) Surface $(\mathcal{S}_8)$ is drawn in cyan (origin is a weak focus of order > 1 or a center (i.e. a weak focus of infinite order)).

(i) Surface $(\mathcal{S}_{10})$ is drawn in gray (contains the points whose associated phase portrait has a double limit cycle).

We point out that we use the same color for $(\mathcal{S}_4)$ and $(\mathcal{S}_7)$ since both surfaces deal with connections of separatrices mostly.

At this point, we need some observations. First of all, if we want to study the slices $h = \widetilde{h}$ where $\widetilde{h}$

is a non-negative constant it is clear that we cannot study every value $\widetilde{h} \geq 0$. Hence, our first task must be to find all the values $h \geq 0$ in which there are topological changes of the bifurcation surfaces (we call them **singular slices**), that is, if $h_a > h_b$ are two consecutive singular slices then for each pair of values $h, h' \in (h_b, h_a)$ the slices h and h' are topologically identical but both topologically different from h_a and h_b. Once we find the singular slices, the study of the affine part of $\mathbb{RP}^3$ will be reduced to study in detail all the singular slices, plus one slice from each interval determined for two consecutive singular slices. Thus, it is clear that the singular slices correspond to those slices h in which the intersection among at least three surfaces or other equivalent phenomena happen. The problem is that we do not have an explicit expression for the surfaces $(\mathcal{S}_7)$ and $(\mathcal{S}_{10})$ and hence finding the singular slices in a systematic way it is not possible. Hence, in order to find all the singular slices in a feasible way we must start finding the values h in which at least three bifurcation surfaces intersect (or other equivalent phenomena) but only taking into account the algebraic surfaces. Such values are called **algebraic singular slices**, which of course are also singular slices. The rest of singular slices (those which involve changes related with $(\mathcal{S}_7)$ and $(\mathcal{S}_{10})$) are called **non-algebraic singular slices** and the non-singular slices are called **generic**.

Roughly speaking, to find the algebraic singular slices we must start by finding all possible intersections between two distinct algebraic surfaces and also the singularities of those surfaces. Once we have them, the next step is to determine the values h in which at least three distinct surfaces intersect. These values h determine the singular algebraic slices. In the first article of this typology (see [Artés *et al.*, 2006]), the above calculations were made by hand. However, Joan C. Artés and collaborators developed a systematical way of doing the calculations implemented in *Mathematica*. This general procedure is easily adaptable to the quadratic family which is being studied. In particular, we have adapted it to our family. Due to the very large extension of the previous computations, we have decided not to include here any of the calculations done with the previous program. Anyway, you can check all the calculations directly in the program, called **Qwf1sn.nb**, at `https://mat.uab.cat/~artes/articles/qwf1sn/qwf1sn.html`.

Lemma 4.8. *There are a total of* 10 *algebraic singular slices in the bifurcation diagram of the family* ***Qwf1sn****, which are:*

$$\begin{gathered} h_1 = +\infty,\ h_3 = 3\sqrt{3}, \\ h_5 = \tfrac{\sqrt{3}}{4\sqrt{2}}\sqrt{69 + \sqrt{302797 - 7696\sqrt{37}} + \sqrt{302797 + 7696\sqrt{37}}}, \\ h_{13} = 3,\ h_{17} = 5/\sqrt{3},\ h_{19} = 2\sqrt{2},\ h_{21} = \sqrt{\tfrac{243}{32}}, \\ h_{23} = 2,\quad h_{25} = 1,\quad h_{29} = 0 \end{gathered} \tag{9}$$

We have also detected some negative slices but they are not needed since we are working in $(\mathbb{R}^3)^+$*, as explained before.*

We observe that the numeration in (9) is not consecutive since we reserve numbers for generic and singular non-algebraic slices, as the reader can observe in (10).

Once we have found the algebraic singular slices, we must find the non-algebraic ones. In order to do it, we start considering a value $\widetilde{h}$ not corresponding to an algebraic singular slice. For this value $\widetilde{h}$ (in principle we do not know if this slice is generic or non-algebraic singular) we draw all the algebraic bifurcation surfaces. However, as it will be discussed later, the presence of non-algebraic bifurcations will be detected and hence the non-algebraic singular slices will be approximately determined. In addition, as we have explained before, we add to each interval of singular values of h an intermediate value (generic slice) for which we represent the bifurcation diagram. In (10) we present all the slices needed for the bifurcation diagram of the class $\overline{\mathbf{Qwf1sn}}$.

$$\begin{array}{ll} h_1 = +\infty & h_{16} = 3 - \epsilon_5 \\ h_2 = 6 & h_{17} = 5/\sqrt{3} \approx 2.88 \\ h_3 = 3\sqrt{3} \approx 5.19 & h_{18} = 2.85 \\ h_4 = 5 & h_{19} = 2\sqrt{2} \approx 2.82 \\ h_5 \approx 4.361 \ \text{(see (9))} & h_{20} = 2.8 \\ h_6 = 4.2 & h_{21} = \sqrt{\frac{243}{32}} \approx 2.75 \\ h_7 = 4.2 - \epsilon_1^* & h_{22} = 2.5 \\ h_8 = 4.2 - \epsilon_1 & h_{23} = 2 \\ h_9 = 4.2 - \epsilon_2^* & h_{24} = 1.5 \\ h_{10} = 4.2 - \epsilon_2 & h_{25} = 1 \\ h_{11} = 4.2 - \epsilon_3^* & h_{26} = 0.3 \\ h_{12} = 4.2 - \epsilon_3 & h_{27} = 0.3 - \epsilon_6^* \\ h_{13} = 3 & h_{28} = 0.3 - \epsilon_6 \\ h_{14} = 3 - \epsilon_4 & h_{29} = 0 \\ h_{15} = 3 - \epsilon_5^* & \end{array} \tag{10}$$

In fact, to be completely precise we must say that the above non-algebraic singular slices are sufficient for the transition from slice $h_1 = +\infty$ to $h_{29} = 0$ to be completely coherent, since there exists the theoretical possibility of having some infinitesimal topological changes regarding the non-algebraic surfaces (which would produce more singular non-algebraic slices). See Sect. 5.2.

On the other hand, we observe that the values indexed by positive even indices in (10) correspond to generic slices and those indexed by odd indices to singular slices, which are necessary to the coherence of the bifurcation diagram. In addition, due to the presence of many (and very close together) non-algebraic slices, sometimes it is difficult (and unnecessary) to predict the concrete value of h where the changes in the parameter space happen. Thus, with the purpose to set an order for these changes in the parameter space, we introduce the following notation. If the bifurcation happens between two concrete values of $h > h'$, then we subtract a sufficiently small positive value ϵ_i or ϵ_j^* from h (which is a reference value) thus obtaining non-concrete values $h - \epsilon_i, h - \epsilon_j^* \in (h', h)$. The representation ϵ_i means that the $h - \epsilon_i$ refers to a generic slice, whereas ϵ_j^* means that the $h - \epsilon_j^*$ refers to a singular slice. Moreover, considering the values ϵ_i^*, ϵ_i, ϵ_{i+1}^* and ϵ_{i+1} it means that $\epsilon_i^* < \epsilon_i < \epsilon_{i+1}^* < \epsilon_{i+1}$ meanwhile the slices corresponding to the previous values belong to the same interval determined by the two concrete values of h. In (10) we have used the previous notation.

4.2. Bifurcation surfaces due to connections (non-algebraic) at the affine part of $\mathbb{RP}^3$

We now begin the analysis of the bifurcation diagram by studying completely one generic slice and after by moving from slice to slice and explaining all the changes that occur. As an exact drawing of the curves produced by intersecting the surfaces with the slices gives us very small parts which are difficult to distinguish, and points of tangency are almost impossible to recognize, we have produced topologically equivalent figures where parts are enlarged and tangencies are easy to observe. The reader may find the exact pictures of the 10 algebraic singular slices (containing only the algebraic surfaces) described in (10) in a PDF file called **slices.pdf** available at `https://mat.uab.cat/~artes/articles/qwf1sn/qwf1sn.html`, or even better, you can use the plotter in the *Mathematica* file **Qwf1sn.nb** (also available in the previous link) in order to create your own pictures.

We now describe the labels used for each part of the bifurcation diagram. As we have mentioned in the previous sections, the subsets of dimensions 3, 2, 1 and 0 of the partition of the parameter space will be denoted respectively by V, S, L and P for Volume, Surface, Line and Point, respectively. The surfaces are named using a number which corresponds to each bifurcation surface which is placed on the left side of the letter S. To describe the portion of the surface we place an index. The curves that are intersection of surfaces are named by using their corresponding numbers on the left side of the letter L, separated by a point[1]. To describe the segment of the curve we place an index. Finally, Volumes and Points are simply indexed (since three or more surfaces may be involved in such an intersection). We consider an example: surface $(\mathcal{S}_2)$ splits into 4 different two–dimensional parts labeled as $2S_1$, $2S_2$, $2S_3$ and $2S_4$, plus some one–dimensional arcs labeled as $2.iL_j$ (where i denotes the other surface intersected by $(\mathcal{S}_2)$ and j is a number), and some zero–dimensional parts. In order to simplify the labels in all figures we see **V1** which stands for the TEX notation V_1. Analogously, **2S1** (resp. **2.5L1**) stands for $2S_1$ (resp. $2.5L_1$).

With the purpose to explain all the changes in the bifurcation diagram, we would have to present two versions of the picture of each slice: one of them without labels and the other with labels in each new part. However, as the number of slices is considerably large, we will do it only in the first studied slice ($h_2 = 6$) and in the others we will present only a labeled drawing containing the algebraic and non-algebraic bifurcation surfaces, but only of the slice's sub-regions in which a topological change of the position of the bifurcation surfaces w.r.t the neighborhood slices has occurred.

Remark 4.9. Wherever two parts of equal dimension d are separated only by a part of dimension $d - 1$ of the black bifurcation surface $(\mathcal{S}_6)$,

[1] When three or more surfaces intersect at the same line, we have chosen the numbers of the most geometrically representative surfaces.

their respective phase portraits are topologically equivalent since the only difference between them is that a finite node different from the origin has turned into a focus without change of stability and without appearance of limit cycles. We denote such parts with different labels, but in Thm. 2.3 we have drawn only one of the two versions of the phase portrait (the one associated to the corresponding region appearing in Thm. 2.3), which in some cases is the version with node and in some others the one with focus. Anyway, in the file **PhasePortraits.pdf** (which is available in `https://mat.uab.cat/~artes/articles/qwf1sn/qwf1sn.html`) you can find the phase portraits of all the 399 regions of the parameter space, including topological repetitions between distinct regions and making the distinction between the versions with node and focus previously mentioned.

We also recall that in Sect. 6 neither do we give specific invariant description distinguishing between these nodes and foci, even though we could easily introduce one.

Now we start studying the generic slice $h_2 = 6$, which is presented in Fig. 4.1 but only showing the algebraic bifurcation surfaces. We note that in Fig. 4.1 we have also shown the planar projection in the unit disk of the half ellipsoid in $B(\vec{0},1) \cap \mathcal{B}_{1/2}$ corresponding to the plane $h = h_2$ of $(\mathbb{R}^3)^+$ (see Sect. 3.2 for more details).

Remark 4.10. As we can appreciate in Figs. 4.1 and 4.9, the equator is colored in orange. In order to explain the notation used in the equator, we need an observation. Since the slice $h = +\infty$ (resp. $h = 0$) is a special slice, we will denote the generic parts in this slice as $11S_j$ (resp. $9S_j$), where j is a number. Therefore, since the equator is the intersection between the slices $h = 0$ and $h = +\infty$ (see Sect. 3.2), the lines in the equator will be denoted as $9.11L_j$, where j is a number (see Sects. 4.3 and 4.4). Finally, a point in the equator will be denoted as in the affine part, i.e. P_j where j is a number.

We recall that in this slice we will make a complete study of all its parts, whereas in the next slices we will only describe the changes. In addition, in this section we also study the equator. It is clear that the equator only must be studied once and, as explained in Sect. 3.2, it is crucial in order to check that the regions found in each slice (including those in the slices $h = +\infty$ and $h = 0$) are coherent when we go to infinity, fact that cannot be checked if we consider the finite slices in $(\mathbb{R}^3)^+$ and the slice $h = +\infty$ in $\mathbb{R}^2$ (see Sect. 3.2).

We also point out that the gray dots that appear in surface $(\mathcal{S}_8)$ indicate weak focus of third order or center (denoted respectively as $f^{(3)}$ and c), according to Remark 4.6.

We now place for each set of the partition on this slice the local behavior of the flow around the singular points. For a specific value of the parameters of each one of the sets in this partition we compute the global phase portrait with the numerical program P4 (see Chapters 9 and 10 of [Dumortier *et al.*, 2006]).

In this slice we have a partition in two–dimensional parts bordered by curved polygons, all of them bounded when viewed in $B(\vec{0},1) \cap \mathcal{B}_{1/2}$. From now on, we use lower?case letters provisionally to describe the sets found algebraically in order to do not interfere with the final partition described with capital letters.

For each two-dimensional part we obtain a phase portrait which is coherent with those of all their borders; except 17 parts, which are shown inside a small square in Fig. 4.1 and named as follows:

- v_{9a}: the topological triangle bordered by purple, cyan and red curves;
- v_{9b}: the topological triangle bordered by cyan, red and yellow curves;
- v_{12}: the topological pentagon bordered by purple, cyan, yellow and red curves;
- v_{15}: the topological pentagon bordered by cyan, purple and dark blue curves and infinity;
- v_{20}: the topological ellipse bordered by cyan and dark blue curves;
- v_{22a}: the topological triangle bordered by cyan, purple and dark blue curves;
- v_{23}: the topological quadrilateral bordered by cyan, dark blue and purple curves;
- v_{29}: the topological triangle bordered by cyan, red and dark blue curves;
- v_{34}: the topological ellipse bordered by yellow and cyan curves;

- v_{35}: the topological ellipse bordered by yellow and purple curves;
- v_{42}: the topological triangle bordered by yellow, red and black curves;
- v_{46}: the topological triangle bordered by yellow, red and purple curves;
- v_{49}: the topological triangle bordered by blue, purple and black curves;
- v_{53}: the topological triangle bordered by yellow, red and black curves;
- v_{61}: the topological ellipse bordered by blue and black curves;
- v_{63}: the topological triangle bordered by purple and red curves and infinity;
- v_{64}: the topological pentagon bordered by purple, yellow, red and dark blue curves;

The study of these parts is quite important for the coherence of the bifurcation diagram and hence we must carry out a very detailed study of all non-algebraic bifurcation surfaces.

Remark 4.11. Despite most of the diagrams in this section are drawn by simplicity in planar sections of $(\mathbb{R}^3)^+$, the previous definitions of the 17 previous parts and all the results regarding the surfaces that we give in this section are stated thinking $\mathcal{B}_{1/2}$ as our parameter space. This is because, as we have explained in Sect. 3.2, we take as a representative of our parameter space the half ball $\mathcal{B}_{1/2}$ since is a compact set in which we can fully study the bifurcation diagram and check the coherence when we approach to its borders. We only use the identification of the affine part of $\mathbb{RP}^3$ with $(\mathbb{R}^3)^+$ in order to simplify the study and the computations.

In Figures 2.1 to 2.6 in Section 2 the reader can find all the topological phase portraits that we have found. However, as mentioned before, in such pictures do not appear all the regions studied since there are different regions with topological equivalent phase portraits. All such equivalences are described in detail in Tables 7.1-7.9 of Section 7. Hence, we recommend the reader to print both the tables and the phase portraits in order to follow the explanation easily. You can also use the file **PhasePortraits.pdf** (available in `https://mat.uab.cat/~artes/articles/qwf1sn/qwf1sn.html`) which contains the phase portraits of all the 399 regions found, including topological repetitions between distinct regions.

Remark 4.12. Before starting, we recall that limit cycles in planar polynomial systems can only be generated from multiple limit cycles, graphics, Hopf bifurcations and centers.

Due to the great number of regions of the slice $h_2 = 6$, we must show the complete bifurcation diagram divided in five parts described in Figs. 4.2, 4.4, 4.5, 4.6 and 4.7, plus some extra pictures and diagrams that are very useful in order to emphasize bifurcations occurring in some specific regions.

Remark 4.13. We have added in the bifurcation diagram a label associated to each part of the bifurcation ($\mathcal{S}_7$) indicating the type of connection produced by this bifurcation. The possibilities are "($loop$)", "($f-f$)" (for a connection between different finite singularities), "($f-\infty$)" (for a connection between a finite singularity and an infinite one), and "($\infty-\infty$)" (for a connection between different infinite singularities). These labels are indicated only in the first time that the corresponding nonalgebraic bifurcation is detected.

We begin the analysis of parts v_{29}, v_{34} and v_{35}. We consider the segment $8s_9$ in Fig. 4.1. By Remark 4.6 we know that the origin is a weak focus of order two in this segment and, consequently, this branch of surface ($\mathcal{S}_8$) corresponds to a Hopf bifurcation. This means that either in v_{29} or in v_{34} we must have a simple limit cycle, and in fact it is in v_{34}.

If we take a point in $8s_9$, enough close to $1.8l_1$, the phase portrait is equivalent to the one in $8S_9$. Moreover, if we perturb it by entering to v_{29} (resp. v_{34}) we get a phase portrait equivalent to the one in V_{33} (resp. V_{34}).

If we keep moving away from $1.8l_1$ through $8s_9$, at some moment we get a phase portrait equivalent to the one in $8S_{13}$. Moreover, if we perturb it by entering to v_{29} (resp. v_{34}) we get a phase portrait equivalent to the one in V_{32} (resp. V_{72}).

Finally, if we keep moving away from $1.8l_1$ through $8s_9$ even more, at some moment we get a phase portrait equivalent to the one in $8S_{14}$. Moreover, if we perturb it by entering to v_{29} (resp. v_{34})

we get a phase portrait equivalent to the one in V_{29} (resp. V_{71}).

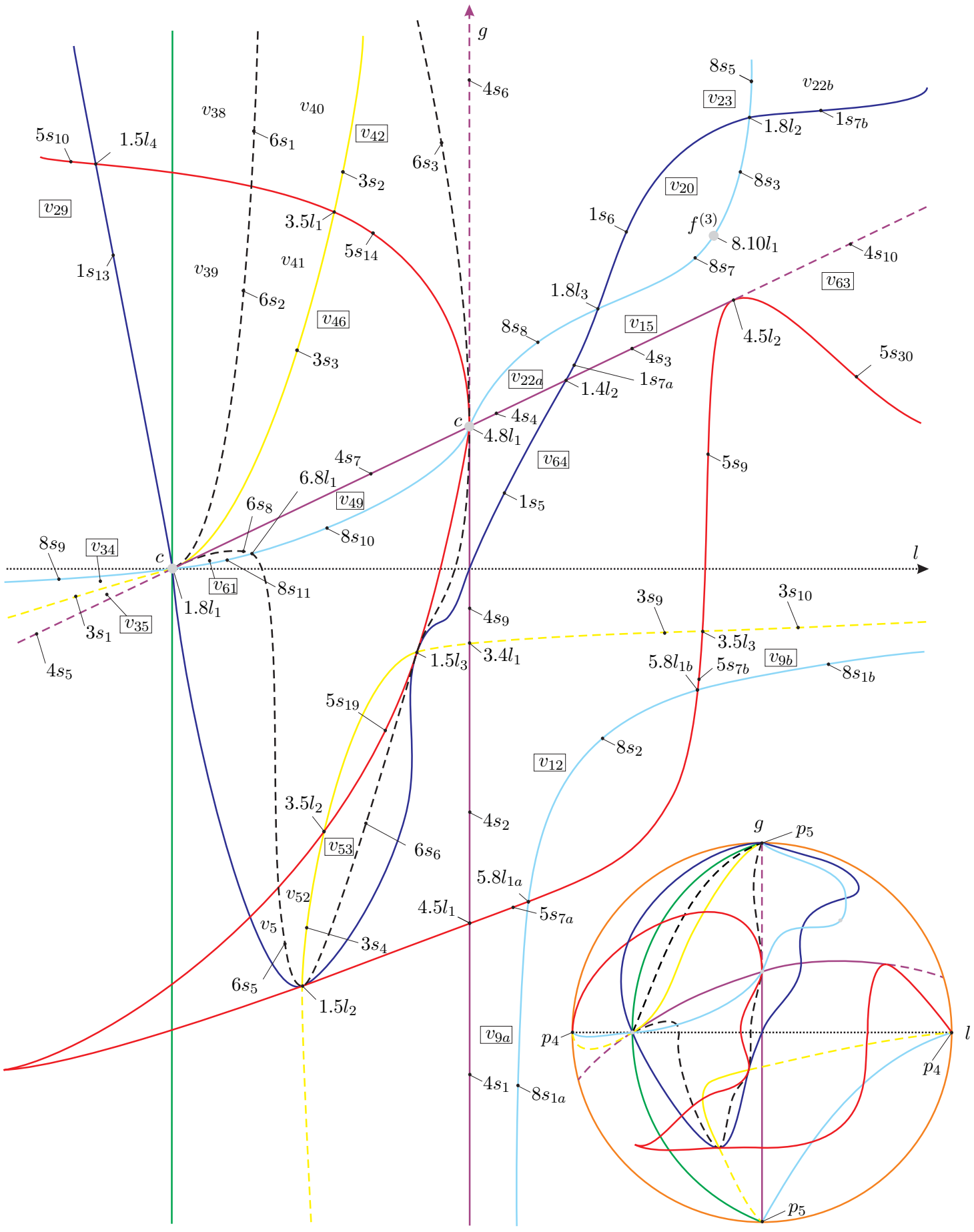

Fig. 4.1: Slice of parameter space when $h = 6$ (only algebraic surfaces). In the lower right corner we also show a small picture of the slice $h = 6$ (with only algebraic surfaces) in the unit disk, where the equator is drawn in orange.

Let's extract the consequences of the previous facts. On the one hand, clearly there must exist two elements $7S_{12}$ and $7S_{11}$ of surface $(\mathcal{S}_7)$ which split part v_{29} into three "new" parts: V_{29}, V_{32} and V_{33} (see Fig. 4.2). On the other hand, clearly there must exist two elements $7S_{23}$ and $7S_{24}$ of surface $(\mathcal{S}_7)$ which split part v_{34} into three "new" parts: V_{34}, V_{71} and V_{72} (see Fig. 4.2). Furthermore, the parts $7S_{11}$ and $7S_{23}$ (resp. $7S_{12}$ and $7S_{24}$) must have a common endpoint in $8s_9$, namely $7.8L_4$ (resp. $7.8L_5$). Notice also that all the previous portions of surface $(\mathcal{S}_7)$ correspond to a $(f-f)$ connection, as we have indicated in Fig. 4.2.

If we are in V_{71} (resp. V_{34}) and from there we approach to $3s_1$ the limit cycle has been lost in both cases, which implies (by Remark 4.12) the existence of at least one element $7S_{25}$ (resp. $7S_{13}$) of surface $(\mathcal{S}_7)$ separating part V_{71} (resp. V_{34}) from a "new" sub-region V_{73} (resp. V_{36}) of v_{34}, which represents a bifurcation due to existence of an homoclinic orbit (loop) connecting two separatrices of the finite saddle. See Fig. 4.2 for a graphical representation of the situation.

Lemma 4.14. *Parts $7S_{13}$, $7S_{25}$, $7S_{23}$ and $7S_{24}$ have a common endpoint, namely $7.7L_1$, as you can appreciate in Fig. 4.2.*

Proof. Notice that a system in region V_{72} cannot lose the limit cycle through a loop unless more than one connection occur at the same time, since one separatrix of the finite saddle-node is between the two separatrices of the finite saddle that must connect to form the loop in which the limit cycle must die. Therefore, since $7S_{23}$ and $7S_{24}$ are bordering V_{72}, we conclude that $7S_{23}$ and $7S_{24}$ must intersect at a point, say $7.7L_1$, and clearly the unique possible phase portrait is the one corresponding to region $7.7L_1$ in Fig. 2.6. Finally, just notice that by perturbing $7.7L_1$ we can obtain the phase portraits corresponding to regions $7S_{25}$, V_{71}, $7S_{23}$, V_{72}, $7S_{24}$, V_{34} and $7S_{13}$. This concludes the proof. ■

An important observation is the following:

Remark 4.15. In principle, $7S_{13}$ and $7S_{25}$ should be located between $8s_9$ and $3s_1$ without intersecting $3s_1$ (see Figs. 4.2 and 4.9), because we have parametrized the part $3s_1$ and "walked" on it and in all the cases we have obtained a phase portrait corresponding to $3S_1$, $3.7L_3$ and $3S_{12}$. However, there exists the theoretical possibility that $7S_{13}$ (resp. $7S_{25}$) crosses completely $3s_1$ in some small places that we have not detected numerically. In this case a second limit cycle will be generated due to the weakness of the finite saddle in $3s_1$, as discussed in detail in Sect. 5.3.

If we now take a point in $3s_1$, enough close to $1.8l_1$, the phase portrait is equivalent to the one in $3S_1$. Moreover, if we perturb it by entering to v_{34} (resp. v_{35}) we get a phase portrait equivalent to the one in V_{36} (resp. V_{35}).

If we keep moving away from $1.8l_1$ through $3s_1$, at some moment we get a phase portrait equivalent to the one in $3S_{12}$. Moreover, if we perturb it by entering to v_{34} (resp. v_{35}) we get a phase portrait equivalent to the one in V_{73} (resp. V_{74}).

Clearly, the previous facts imply that there must exist one element $7S_{26}$ (resp. $7S_{27}$) of surface $(\mathcal{S}_7)$ which splits part v_{34} (resp. v_{35}) into two "new" parts: V_{36} and V_{73} (resp. V_{35} and V_{74}). See Fig. 4.2. Furthermore, the parts $7S_{26}$ and $7S_{27}$ must have a common endpoint in $3s_1$, namely $3.7L_3$. Notice also that all the previous portions of surface $(\mathcal{S}_7)$ correspond to a $(f-f)$ connection, as we have indicated in Fig. 4.2.

Lemma 4.16. *Part $7S_{26}$ has $7.7L_1$ as endpoint. See Fig. 4.2.*

Proof. Just observe that the phase portrait in $7.7L_1$ is compatible with the ones in V_{73}, $7S_{26}$ and V_{36} under perturbations, that is, perturbing $7.7L_1$ we can get the ones in V_{73}, $7S_{26}$ and V_{36}. ■

Remark 4.17. In principle, $7S_{27}$ should be located between $3s_1$ and $4s_5$ without intersecting $4s_5$ (see Figs. 4.2 and 4.9), because we have parametrized the part $4s_5$ and "walked" on it and in all the cases we have obtained a phase portrait corresponding to $4S_5$. However, there exists the theoretical possibility that $7S_{27}$ crosses $4s_5$ in some small places that we have not detected numerically. Anyway, this hypothetical situation is irrelevant since it wouldn't produce any new phase portrait.

Remark 4.18. As explained in Remark 4.11, all the results given in this section regarding the bifurcation surfaces are stated thinking $\mathcal{B}_{1/2}$ as our param-

eter space. It is clear that in $\mathcal{B}_{1/2}$ all the considered regions are bounded, but it is not true when thinking the affine part of $\mathbb{RP}^3$ as $(\mathbb{R}^3)^+$; in this case it depends on the considered region. For example, $7S_{25}$ is not bounded if we think it in $(\mathbb{R}^3)^+$.

To proceed, we need the following definition.

Definition 4.19. By a *basin* we understand a region bordered by two separatrices of one same singularity which have the same limit-object, most commonly, they end at an infinite singularity and we call it an *infinite basin* or they end at a finite singularity and we call it a *finite basin*.

Now we can start performing the study of v_{29}. If we are sufficiently close to part $5s_{10}$, the respective phase portrait is topologically equivalent to the one in V_{29}, which has two disjoint infinite basins (one generated by the finite saddle and the other by finite saddle-node).

If we take a point of $1s_{13}$ and we perturb it by entering to v_{29} we get a phase portrait equivalent to the one in V_{37}, which has one finite basin and also an infinite one (and the finite one is inside the infinite one). If we keep moving to the left we get a phase portrait equivalent to V_{32}, which has no basin. This fact implies the existence of one element $7S_{14}$ of surface $(\mathcal{S}_7)$, which represents a connection between two finite singularities, separating V_{32} from a "new" sub-region of v_{29} called V_{37} (see Figs. 4.2 and 4.9).

Now we study how $7S_{11}$, $7S_{12}$ and $7S_{14}$ are positioned. We start giving an important observation.

Remark 4.20. Numerical analysis suggest that parts $7S_{12}$ and $7S_{14}$ do not intersect each other (see Figs. 4.2 and 4.9). However, there exists the theoretical possibility that they intersect in some small places that we have not detected numerically. Indeed, in such intersection we would have the following phase portrait

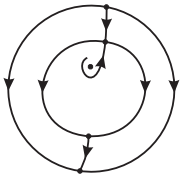

whose existence in our family cannot be ruled out in principle. Since after a careful numerical analysis we have no evidence about its existence and the bifurcation diagram doesn't need its existence in order to be coherent, we conjecture that $7S_{12}$ and $7S_{14}$ do not intersect.

Notice that this is not just a problem to check if in this slice they intersect or not. It may not happen in this slice, but it could happen in other slices forming a band as narrow as wished, and so, very difficult to detect numerically.

Lemma 4.21. *The parts $7S_{11}$ and $7S_{14}$ do not intersect each other and neither the parts $7S_{11}$ and $7S_{12}$. See Figs. 4.2, 4.9.*

Proof. Numerical analysis suggests our claims. In what follow we prove them. Firstly, we note that $7S_{11}$ and $7S_{14}$ cannot intersect since otherwise for values in such intersection the two stable separatrices of the finite saddle-node must coincide. Analogously, $7S_{11}$ and $7S_{12}$ cannot intersect since otherwise for values in such intersection the two unstable separatrices of the finite saddle must coincide. ■

Remark 4.22. Careful numerical analysis suggest two facts: (1) Parts $7S_{12}$ and $7S_{14}$ have $1.8l_1$ as a common endpoint; (2) Parts $7S_{11}$ and $7S_{14}$ have $1.5l_4$ as a common endpoint. If we assume both previous numerical evidences, then the situation is the one shown in Figs. 4.2 and 4.9. Despite the complete coherence of our numerical intuitions, it is theoretical possible that some of them are not true. For example, it could happen that $7S_{14}$ has an endpoint in $1s_{13}$ instead of in $1.5l_4$. Anyway, as one can realize very easily, none of the previous hypothetical situations would give us any new phase portrait that the ones we already have. Therefore, since the final objective is to get a complete coherent diagram, we work conjecturing our numerical evidences.

In Fig. 4.2 we have shown the complete bifurcation diagram of part 1 of the slice $h = 6$ (which contains the regions v_{29}, v_{34} and v_{35}). In Fig. 4.9 we have also illustrated the previous regions. We have also shown the sequence of phase portraits in region v_{29} in Fig. A.8 and we have shown in Fig. A.7 the sequence of phase portraits in v_{34} bifurcating from $1.8L_1$, both in Appendix A.2. The previous sequences are very useful in order to understand the transitions of phase portraits when we move from

one region to another because we can see step by step which changes are taking place.

Finally, in Fig. 4.3 we have shown the sequence of phase portraits around $7.7L_1$

Remark 4.23. In Figs. 4.2 and 4.4 we have labeled as $2S_1$ two apparently different parts of $(\mathcal{S}_2)$. This is not a mistake since in fact both regions are the same, as will become clear when we move from slice to slice in Sect. 4.4.

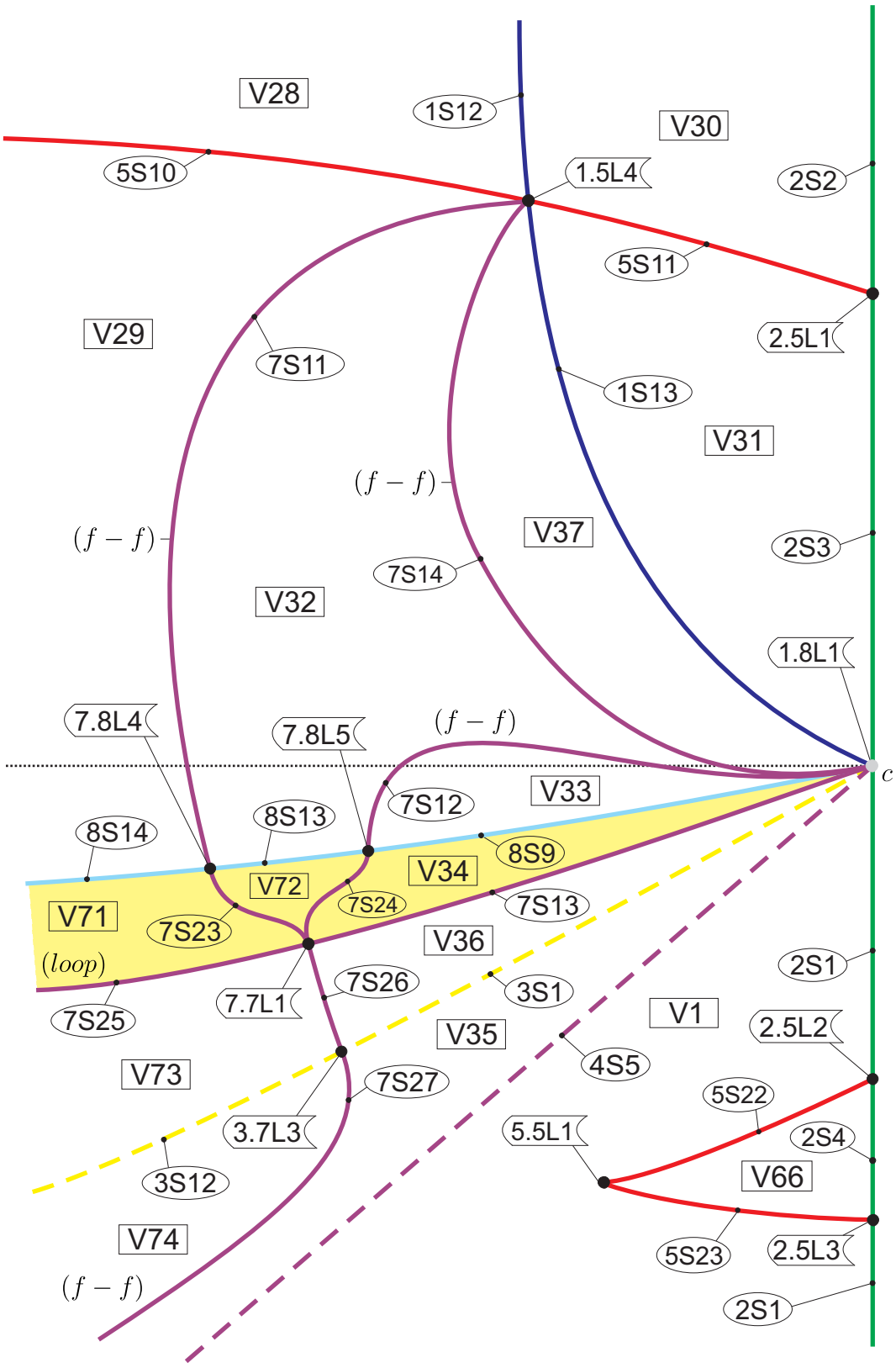

Fig. 4.2: Complete bifurcation diagram for slice $h = 6$ (Part 1, contained in second and third quadrant). When a two-dimensional region is colored in yellow means the existence of one simple limit cycle in such region.

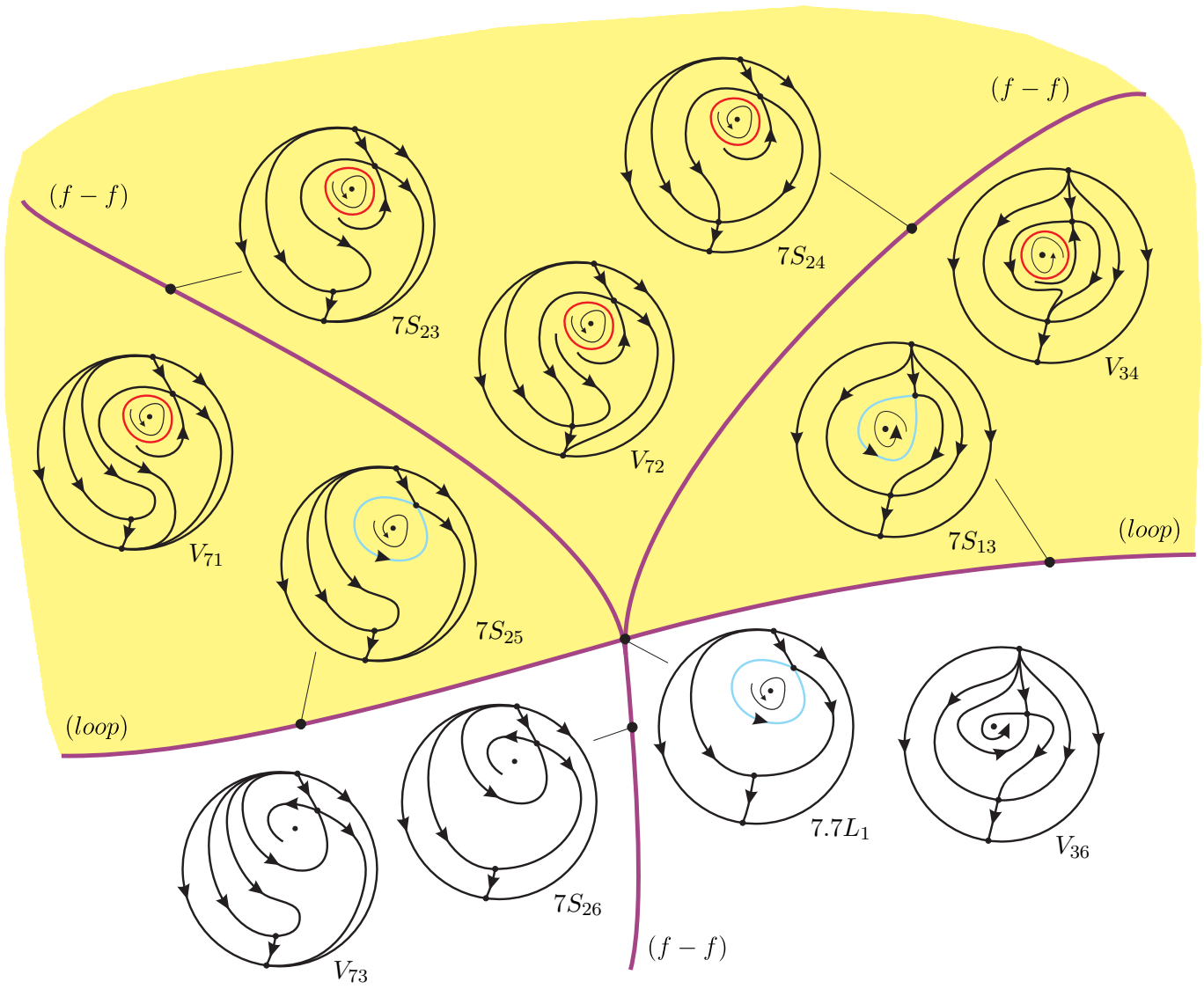

Fig. 4.3: Amplification of neighboring regions of part $7.7L_1$.

Now, we carry out the analysis of part v_{53} (see Figs. 4.1, 4.4 and 4.9). In part v_5 the phase portrait is equivalent to the one in V_5, which has two finite antisaddles (one is the origin, which is a $f^{(1)}$, and the other is an unstable node). As explained in Sect. 4.1, when we cross $6s_5$ the finite node turns into a focus, and hence the phase portrait in v_{52} is topologically equal than the one in v_5 but with the difference that in v_{52} the finite antisaddle different from the origin is an unstable strong focus instead of an unstable node. We recall that in $6s_5$ the finite antisaddle different from the origin must be a node which is "near" to be a focus, as for example a star node n^* or a one-direction node n^d (see Appendix A of [Artés *et al.*, 2021a]). In $3s_4$ the phase portrait is the same that the one in v_{52} but with the finite antisaddle different from the origin being an unstable $f^{(1)}$ instead of an unstable strong focus. In addition, in v_{53} the finite antisaddle different from the origin is a stable strong focus. Hence, this branch of surface $(\mathcal{S}_3)$ corresponds to a Hopf bifurcation and consequently in v_{53} we have a limit cycle. If we are sufficiently close to part $3s_4$ the respective phase portrait is topologically equivalent to the one in V_{53}. However, when we get close to $6s_6$ the limit cycle has been lost, which implies (by Remark 4.12) the existence of at least one element $7S_{19}$ of surface $(\mathcal{S}_7)$ dividing v_{53} into two "new" parts, V_{53} and V_{54}, which must represents a bifurcation surface due to the connection of two infinite separatrices.

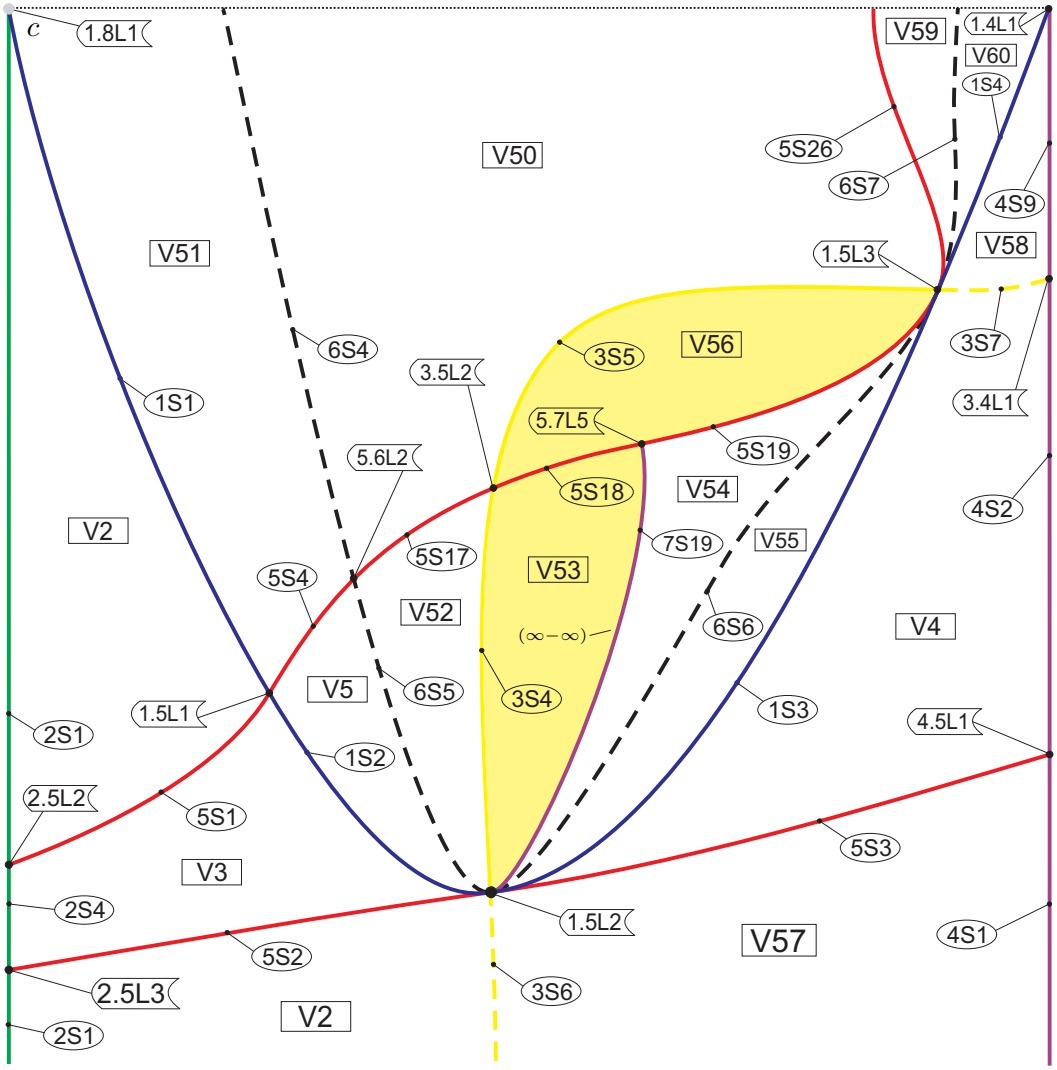

Fig. 4.4: Complete bifurcation diagram for slice $h = 6$ (Part 2, contained in third quadrant). When a two–dimensional region is colored in yellow means the existence of one simple limit cycle in such region.

Let's discuss how portion $7S_{19}$ is positioned.

Lemma 4.24. *The element $7S_{19}$ of surface $(\mathcal{S}_7)$ has $1.5l_2$ as endpoint. The other endpoint is in $5s_{19}$, namely $5.7L_5$ (see Figs. 4.1, 4.4 and 4.9).*

Proof. Numerical analysis suggests our claims. In what follow we prove them. Firstly, if an endpoint of $7S_{19}$ is any point of $3s_4$, then a portion of $3s_4$ must not refer to a Hopf bifurcation, which is a contradiction. Secondly, part $7S_{19}$ cannot intersect $6s_6$ since otherwise for the values in such intersection we must have a nondegenerate graphic surrounding a unique point being a node, which contradicts item **(vii)** in Appendix B.1. However, we can also give a direct argument: If the previous hypothetical situation were possible, then we would be able to generate a quadratic system with a limit cycle surrounding a node by breaking the graphic with quadratic perturbations, thus contradicting item **(ix)** in Appendix B.1. Thirdly, if we take a value of $5s_{19}$ near $3.5l_2$ and we perturb it by entering to v_{53} we get a phase portrait equivalent to one in V_{53}. However, if we do the same but taking a point in $5s_{19}$ near $1.5l_3$ we get a phase portrait equivalent to the one in V_{54}. The three previous observations prove our statements. ∎

In Fig. 4.4 we show the complete bifurcation diagram of part 2 of the slice $h = 6$, which contains the region v_{53} we have just studied. In Fig. 4.9 we have also illustrated the previous regions. In addition, in Fig. A.9 in Appendix A.2 we show the sequence of phase portraits along the planar region v_{53}.

Remark 4.25. We note that V_{56} (see Fig. 4.4) is a region completely bordered by algebraic surfaces whose associated phase portrait has a simple limit cycle. This fact is completely coherent with Remark 4.12. Indeed, the part $3S_5$ corresponds to a Hopf bifurcation and in the part $5S_{19}$ we have a phase portrait with a graphic, although it was not a necessary fact according to the definition of surface $(\mathcal{S}_5)$ given in Sect. 4.1.

We now perform the study of parts v_{49} and v_{61} (see Figs. 4.1, 4.5 and 4.9). We consider the segments $8s_{10}$ and $8s_{11}$ in Fig. 4.1. By Remark 4.6 we know that in both parts the origin is a weak focus of order two, and consequently both branches of surface $(\mathcal{S}_8)$ corresponds to a Hopf bifurcation. In fact, the unique difference between both previous regions is that the finite antissadle different from the origin is a strong focus in $8s_{10}$ and a node in $8s_{11}$ (see Remark 4.9). As a consequence, it is easy to check that in v_{49} and in v_{61} we have a simple limit cycle. If we are sufficiently close to part $8s_{10}$ (resp. $8s_{11}$) the respective phase portrait is topologically equivalent to the one in V_{49} (resp. V_{61}). However, when we get close to $4s_7$ the limit cycle has been lost, which implies (by Remark 4.12) the existence of at least two elements $7S_{18}$ and $7S_{20}$ of surface $(\mathcal{S}_7)$ such that $7S_{18}$ (resp. $7S_{20}$) divides v_{49} (resp. v_{61}) into two "new" parts, V_{48} and V_{49} (resp. V_{61} and V_{62}). In addition, both segments represent a bifurcation due to existence of an homoclinic orbit (loop) connecting two separatrices of the finite saddle-node. See Figs. 4.5 and 4.9.

Remark 4.26. There is a slight inaccuracy in the above argument that should be qualified. Despite the existence of $7S_{18}$ is clear, we cannot assure at all the existence of $7S_{20}$ (and therefore neither that of V_{62}). The difficulties that we have are the following ones: (1) As mentioned before, in Fig. 4.1 we have produced a topological equivalent version of the slice $h = 6$ (with only algebraic surfaces) since some regions are very small. This is the case of v_{61}, since it is so small that it is practically impossible for us to test numerical values of its interior. (2) The existence of $7S_{20}$ is not needed for the coherence of the bifurcation diagram. For example, it would be completely coherent that $7S_{18}$ did not intersect $6s_8$ and that it had as endpoints $1.8l_1$ and $4.8l_1$. However, certain arguments based on tangencies of surfaces make us conjecture the existence of $7S_{20}$ (fully contained in v_{61}, as explained before) and that one of its endpoints is $1.8l_1$. Anyway, notice that independently on which of the previous situations is the real one, the topological phase portraits we obtain are exactly the same. Therefore, since the objective is to obtain a coherent bifurcation diagram and previous facts are completely coherent, we work assuming our conjectures previously explained.

Lemma 4.27. *Part $7S_{18}$ has one of its two endpoints in $4.8l_1$. Moreover, $7S_{20}$ and $7S_{18}$ have an endpoint in common in part $6s_8$, namely $6.7L_1$ (see Figs. 4.1, 4.5 and 4.9).*

Proof. If the endpoint of $7S_{18}$ (resp. $7S_{20}$) is in $8s_{10}$ (resp. $8s_{11}$) then a portion of $8s_{10}$ (resp. $8s_{11}$) must not refer to a Hopf bifurcation, which contradicts Remark 4.6. Using the previous fact and taking into account the assumptions done in Remark 4.26, it is clear that $7S_{18}$ (resp. $7S_{20}$) must have an endpoint in $4.8l_1$ (resp. $1.8l_1$) and also that both must have the other endpoint in $6s_8$. In addition, the two previous endpoints in $6s_8$ must coincide since $7S_{18}$ is the continuation of $7S_{20}$ through $6s_8$. Hence, our claims are proved. ■

Now, we carry out the analysis of parts v_{42} and v_{46} (see Figs. 4.1, 4.5 and 4.9). In the part v_{38} (resp. v_{39}) the phase portrait is topologically equivalent to the one in V_{38} (resp. V_{39}), both possessing two finite antisaddles (one is the origin, which is a $f^{(1)}$, and the other is a stable node). As explained in Sect. 4.1, when we cross the part $6s_1$ (resp. $6s_2$) the finite node turns into a focus, and hence the phase portrait in v_{40} (resp. v_{41}) is topologically equivalent to the one in part v_{38} (resp. v_{39}) but with the difference that in v_{40} (resp. v_{41}) the finite antisaddle different from the origin is a stable strong focus instead of a stable node. We recall again that in $6s_1$ and in $6s_2$ the finite antisaddle different from the origin must be a node which is "near" to be a focus.

In part $3s_2$ (resp. $3s_3$) the phase portrait is the topologically equivalent to the one in v_{40} (resp. v_{41}) but with the finite antisaddle different from the origin being a stable $f^{(1)}$ instead of a stable strong focus. Moreover, in v_{42} and in v_{46} the finite

antisaddle different from the origin is an unstable strong focus. Therefore, the branches $3s_2$ and $3s_3$ of surface $(\mathcal{S}_3)$ corresponds to a Hopf bifurcation, and consequently, in v_{42} and in v_{46} we must have a simple limit cycle surrounding the finite antisaddle different from the origin.

If we are sufficiently close to part $3s_2$ (resp. $3s_3$) the respective phase portrait is topologically equivalent to the one in V_{42} (resp. V_{46}). However, when in v_{46} we get close to the part of $5s_{14}$ near $4.8l_1$, the limit cycle has been lost, which implies (by Remark 4.12) the existence of at least one element $7S_{17}$ of surface $(\mathcal{S}_7)$ dividing v_{46} into two "new" parts, V_{46} and V_{47}, which represent a bifurcation surface due to the connection of two separatrices of the finite saddle-node.

The situation in v_{42} is more complicated. If we trace a straight line from $3s_2$ to $6s_3$ (fully contained in v_{42}) and we walk on it we realize that if we are near $3s_2$ the phase portrait is equivalent to the one in V_{42}. If we move away from $3s_2$ we have a phase portrait equivalent to the one in V_{43}. Moreover, if we continue moving away from $3s_2$ and we go near $6s_3$ the phase portrait is equivalent to the one in V_{44}. The previous facts imply the existence of at least two elements $7S_{15}$ and $7S_{16}$ of surface $(\mathcal{S}_7)$ dividing v_{42} into three "new" parts, V_{42}, V_{43} and V_{44}. Moreover, $7S_{15}$ must represent a connection between two separatrices of the finite saddle-node (loop) and $7S_{16}$ must represent a bifurcation due to the connection of separatrices between a finite and an infinite singularity (see Figs. 4.1, 4.5 and 4.9).

In what follows we study how parts $7S_{15}$, $7S_{16}$ and $7S_{17}$ are positioned in regions v_{42} and v_{46}.

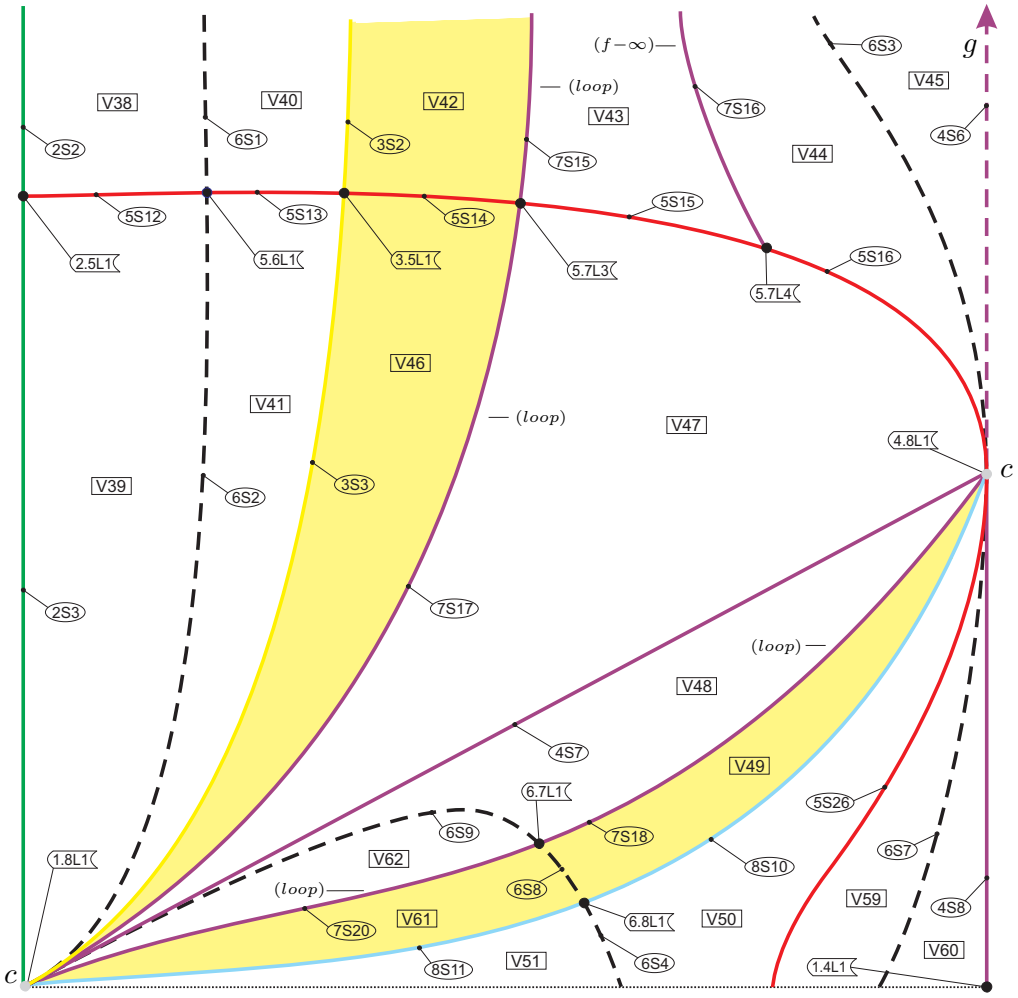

Fig. 4.5: Complete bifurcation diagram for slice $h = 6$ (Part 3, contained in the second quadrant). When a two–dimensional region is colored in yellow means the existence of one simple limit cycle in such region.

Lemma 4.28. *Part $7S_{17}$ has an endpoint in $1.8l_1$ and the other is in $5s_{14}$, namely $5.7L_3$. Part $7S_{15}$ has its endpoints in p_5 (placed in the equator) and in $5.7L_3$. Finally, part $7S_{16}$ has one of its endpoints in p_5 and the other is in $5s_{14}$, namely $5.7L_4$ (with $5.7L_4 \neq 5.7L_3$). See Figs. 4.1, 4.5 and 4.9.*

Proof. Numerical analysis suggests our statements. In what follow we prove them. Firstly, if $7S_{15}$ has an endpoint in $3s_2$ then a portion of $3s_2$ must not refer to a Hopf bifurcation, which is a contradiction. Secondly, $7S_{16}$ cannot intersect $6s_3$ since otherwise for values in such intersection we must have a phase portrait with a node inside a non-degenerate graphic, which contradicts item **(vii)** in Appendix B.1. Thirdly, if we take a value in $5s_{14}$ near $3.5l_1$ and we perturb it by entering to v_{42} we get a phase portrait equivalent to V_{42}. If we do the same but taking a point in $5s_{14}$ near $4.8l_1$ we get a phase portrait equivalent to V_{44}. In addition, there is a central region in $5s_{14}$ in which if we take a value in such region and we perturb it by entering to v_{42} we get a phase portrait equivalent to V_{43}. Previous facts prove that $7S_{15}$ and $7S_{16}$ have one of its endpoints in p_5 and the other in $5s_{14}$, namely $5.7L_3$ and $5.7L_4$ respectively, with $5.7L_3 \neq 5.7L_4$. Fourthly, if we take a value in $5s_{14}$ near $3.5l_1$ and we perturb it by entering to v_{46} we get a phase portrait equivalent to V_{46}, but if we do the same taking a point in $5s_{14}$ near $4.8l_1$ we get a phase portrait equivalent to V_{47}. Fifth, if $7S_{17}$ has an endpoint in $3s_3$ then a portion of $3s_3$ must not refer to a Hopf bifurcation, which is a contradiction. The two previous facts prove that $7S_{17}$ has one of its ends in $1.8l_1$ and the other in $5s_{14}$. Finally, we note that the endpoints in $5s_{14}$ of $7S_{17}$ and $7S_{15}$ must coincide since one part is the continuation of the other through $(\mathcal{S}_5)$. Hence, our claims are proved. ■

In Fig. 4.5 we show the complete bifurcation diagram of part 3 of the slice $h = 6$ (which contains the regions v_{49}, v_{61}, v_{42} and v_{46}). In Fig. 4.9 we have also illustrated the previous regions. We have also shown the sequence of phase portraits along regions v_{49} and v_{61} in Fig. A.10 and also along regions v_{42} and v_{46} in Fig. A.11, both in Appendix A.2.

We now perform the analysis of parts v_{9a}, v_{9b}, v_{12} and v_{64} (see Figs. 4.1, 4.6, 4.7 and 4.9). The meaning of the subscripts "a" and "b" is explained in Remark 4.33. We start by considering the segments $8s_2$, $8s_{1a}$ and $8s_{1b}$ in Fig. 4.1. By Remark 4.6 we know that in all three parts the origin is a weak focus of order two, and consequently all three branches of surface $(\mathcal{S}_8)$ corresponds to a Hopf bifurcation. As a consequence, one can easily verify that in v_{9a}, v_{9b} and v_{12} we must have a simple limit cycle.

If we are sufficiently close to part $8s_{1b}$ the respective phase portrait is topologically equivalent to the one in V_9. However, when we get close to $3s_{10}$ the limit cycle has been lost, which implies (by Remark 4.12) the existence of at least one element $7S_2$ of surface $(\mathcal{S}_7)$ dividing v_{9b} into two "new" parts, V_8 and V_9, which must represent a bifurcation due to existence of an homoclinic orbit (loop) connecting two separatrices of the finite saddle (see Figs. 4.6 and 4.9).

Remark 4.29. Similarly to what we have exposed in Remark 4.15, in principle $7S_2$ should be located between $8s_{1b}$ and $3s_{10}$ without intersecting $3s_{10}$ (see Figs. 4.6 and 4.9), because we have parametrized the yellow surface $3s_{10}$ and "walked" on it and in all the cases we have obtained a phase portrait corresponding to $3S_{10}$, which is topologically distinct to those in $7S_2$. However, there exists the theoretical possibility that $7S_2$ crosses completely $3s_{10}$ in some small places that we have not detected numerically. In this case a second limit cycle will be generated due to the weakness of the finite saddle in $3s_{10}$, as discussed in detail in Sect. 5.3.

If we assume that $7S_2$ and $3s_{10}$ do not intersect, the following result holds (otherwise we could adapt it):

Lemma 4.30. *The surface $7S_2$ has p_4 (placed in the equator) as endpoint. Moreover, its other endpoint in in part $5s_{7b}$, namely $5.7L_2$ (see Figs. 4.1, 4.6 and 4.9).*

Proof. Numerical analysis suggests our claims. In what follow we prove them. Firstly, if $7S_2$ has an endpoint in $8s_{1b}$, then a portion of $8s_{1b}$ must not refer to a Hopf bifurcation, which contradicts the fact that on $8s_{1b}$ the origin is a weak focus of order two (see Remark 4.6). Secondly, if we take a value on $5s_{7b}$ near $5.8l_{1b}$ and we perturb it by entering to v_{9b} we get a phase portrait equivalent to V_9. However, if we do the same but taking a value in $5s_{7b}$

near $3.5l_3$ we get a phase portrait equivalent to V_8. Using the previous two facts and that by assumption $7S_2$ does not intersect $3s_{10}$ (see Remark 4.29) our initial claims are proved. ■

Now we move to part v_{9a}. If we trace a straight line from $8s_{1a}$ to $4s_1$ (fully contained in v_{9a}) and we "walk" on it we realize that if we are near $8s_{1a}$ the phase portrait is equivalent to the one in V_9, which has a limit cycle. However, if we move away from $8s_{1a}$ we have a phase portrait equivalent to the one in V_8, in which the limit cycle has been lost. Moreover, if we keep moving away from $8s_{1a}$ and we go near $4s_1$ the phase portrait is equivalent to the one in V_7. The previous facts imply the existence of at least two elements $7S_1$ and $7S_2$ of surface $(\mathcal{S}_7)$ dividing v_{9a} into three "new" parts, V_9, V_8 and V_7. Moreover, $7S_1$ (resp. $7S_2$) must represent a connection between two separatrices of two different finite singularities (resp. of the same finite saddle, i.e. a loop). See Figs. 4.1, 4.6 and 4.9.

Remark 4.31. Notice that parts $7S_1$ and $4s_1$ do not intersect each other (see Figs. 4.6 and 4.9). Indeed, if both previous surfaces intersect, then the phase portrait for a point in such intersection must be

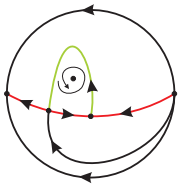

which has an invariant line colored in red and a $f^{(1)}$ in the origin. The previous system cannot exist in the family **QS** since otherwise using Hopf by means of adding the trace in (5) and breaking the green connection, we can produce an example of a quadratic system with two limit cycles and an invariant straight line, thus contradicting item **(xiv)** in Appendix B.1.

Lemma 4.32. *Parts $7S_1$ and $7S_2$ do no intersect each other. Part $7S_1$ has one of its endpoints in $5s_{7a}$, namely $5.7L_1$. Part $7S_2$ has one of its endpoints in $5s_{7a}$, namely $5.7L_2$, with $5.7L_1 \neq 5.7L_2$. The other endpoint of $7S_1$ and of $7S_2$ is p_5, which is placed in the equator. See Figs. 4.1, 4.6, 4.9.*

Proof. Numerical analysis suggests our previous claims. In what follow we prove them. Firstly, if $7S_1$ intersect $7S_2$ then for a point in such intersection we must have a phase portrait equivalent to the one shown in Remark 4.31. But by item **(v)** in Appendix B.1 the system in such intersection must have an invariant line (the line passing through the finite saddle and the finite saddle-node, which belongs to the graphic). But as we have reasoned in Remark 4.31, the previous situation is not possible. Therefore, $7S_1$ and $7S_2$ cannot intersect, as we wanted to show. Secondly, part $7S_2$ cannot end in $8s_{1a}$ since otherwise a part of $8s_{1a}$ must not refer to a Hopf bifurcation, which contradicts Remark 4.6. Thirdly, if we take a value in $5s_{7a}$ near $4.5l_1$ and we perturb it by entering to v_{9a} we get a phase portrait equivalent to V_7. If we do the same but taking a value in $5s_{7a}$ near $5.8l_{1a}$ we get a phase portrait equivalent to V_9. In addition, there is a central region in $5s_{7a}$ in which if we take a value in such region and we perturb it by entering to v_{9a} we get a phase portrait equivalent to V_8 (see Fig. 4.6). Using the three previous facts and taking into account that parts $7S_1$ and $4s_1$ do not intersect each other (see Remark 4.31), our claims are proved. ■

Remark 4.33. As the reader may have noticed, in Figs. 4.6, 4.7 and 4.9 there are some apparently different parts which are labeled with the same name. This is not a mistake since in fact they are the same regions, as will become clear in Sect. 4.4. As a consequence, we have used the notation v_{9a} and v_{9b} in order be coherent with the fact that region V_9 in v_{9a} and region V_9 in v_{9b} are exactly the same. The other cases in this section where we have used the subscripts "a" and "b" have identical justifications.

Finally, we move to parts v_{12} and v_{64}. We start by v_{12}. If we trace a straight line from $8s_2$ to $4s_2$ (not intersecting neither $3s_9$ nor $5s_{7a}$) and we "walk" on it we realize that if we are near $8s_2$ the phase portrait is equivalent to the one in V_{12}. However, if we move away from $8s_2$ we have a phase portrait equivalent to the one in V_{11}, in which the limit cycle has been lost. Moreover, if we keep moving away from $8s_2$ and we go near $4s_2$ the phase portrait is equivalent to the one in V_6. The previous facts imply the existence of at least two elements $7S_3$ and $7S_4$ of surface $(\mathcal{S}_7)$ dividing v_{12} into three "new" parts, V_6, V_{11} and V_{12}. Moreover, $7S_4$ must represent a connection between two finite separatrices of the

same finite saddle (loop) and $7S_3$ must represent a bifurcation due to the connection of separatrices between a finite saddle and a finite saddle-node (see Figs. 4.6 and 4.9).

Regarding to v_{64}, if we take a value near $1s_5$ or $4s_9$ we get a phase portrait equivalent to V_{64}. However, if we take a value in v_{64} near $5s_9$ we get a phase portrait equivalent to V_{65}. This fact imply the existence of at least one element $7S_{21}$ of surface $(\mathcal{S}_7)$ dividing v_{64} into two "new" parts, V_{64} and V_{65}, which must represent a connection of separatrices between two different finite singularities, as one can appreciate in Figs. 4.6, 4.7 and 4.9.

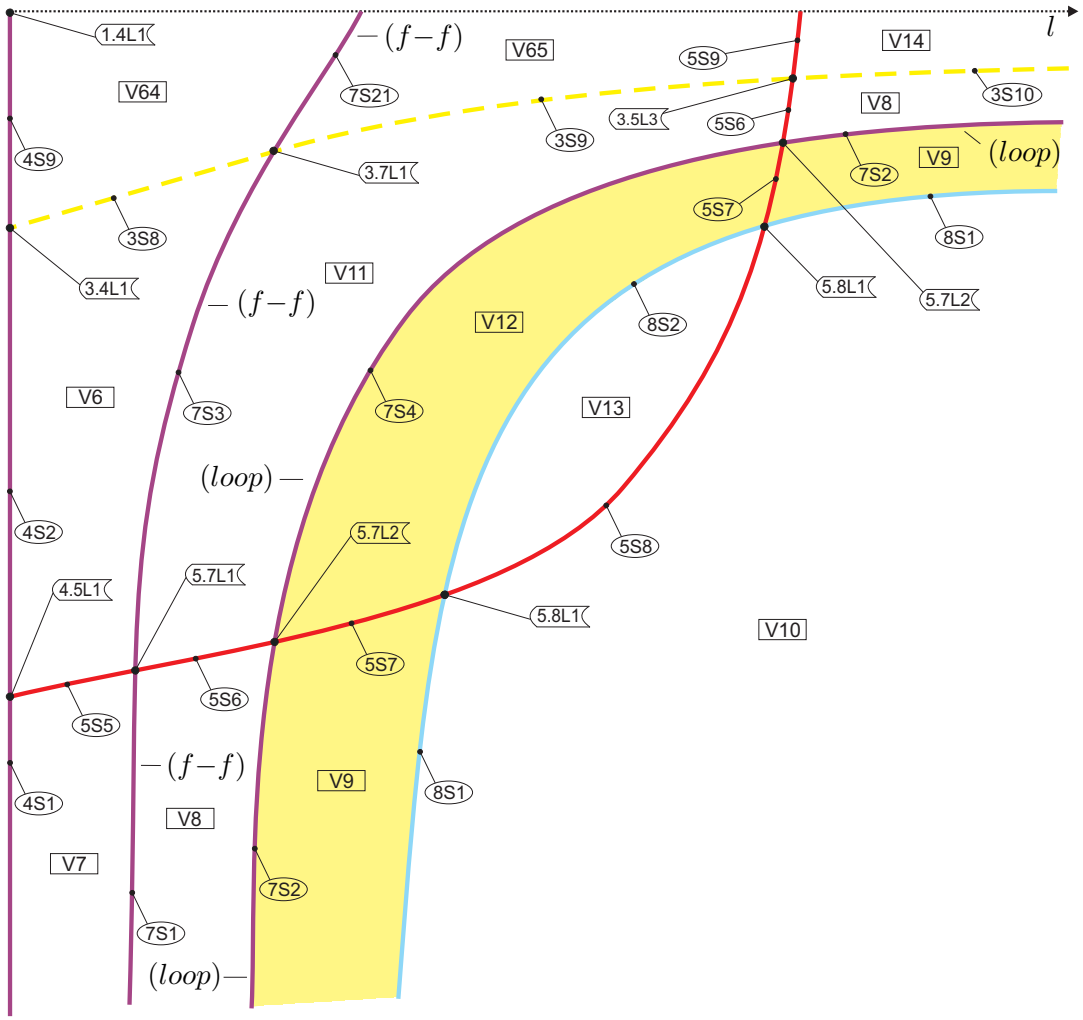

Fig. 4.6: Complete bifurcation diagram for slice $h = 6$ (Part 4, fourth quadrant complete). When a two–dimensional region is colored in yellow means the existence of one simple limit cycle in such region.

Remark 4.34. Analogously to Remark 4.31, we can assure that part $7S_3$ does not intersect $4s_2$ and that $7S_{21}$ does not intersect $4s_9$. Indeed, the phase portrait in such intersections would be

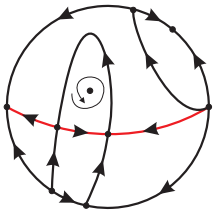

which has an invariant line colored in red and a $f^{(1)}$ placed in the origin. An analogous argument than the one in given in Remark 4.31 proves that previous system cannot exist in **QS**.

Lemma 4.35. *Parts $7S_3$ and $7S_4$ do not intersect each other. Part $7S_4$ has one endpoint in $5.7L_2$ of $5s_{7a}$ (see Lemma 4.32), and the other in part $5.7L_2$ in $5s_{7b}$ (see Lemma 4.30). We recall that $5.7L_2$ in $5s_{7a}$ and $5.7L_2$ in $5s_{7b}$ are in fact the same curve,*

see Remark 4.33. Part $7S_3$ *has* $5.7L_1$ *in* $5s_{7a}$ *as endpoint (see Lemma 4.32) and its other endpoint is in* $3s_9$*, namely* $3.7L_1$*. Part* $7S_{21}$ *has also* $3.7L_1$ *as endpoint and its other endpoint is in* $1.4l_2$*. See Figs. 4.1, 4.6, 4.7 and 4.9.*

Proof. Careful numerical analysis suggests our claims. In what follow we prove them. The argumentation follows in several steps: (1) If $7S_3$ and $7S_4$ intersect then for a point in such intersection we must have a phase portrait equivalent to the one shown in Remark 4.34. But by item **(v)** in Appendix B.1 the system in such intersection must have an invariant line (the line passing through the finite saddle and the finite saddle-node, which belongs to the graphic). But as we have reasoned in Remark 4.34, the previous situation is not possible. Therefore, $7S_3$ and $7S_4$ cannot intersect, as we wanted to show; (2) Part $7S_4$ cannot have an end in $8s_2$ since otherwise a part of $8s_2$ must not refer to a Hopf bifurcation, which contradicts Remark 4.6; (3) If we take a value in $5s_{7b}$ (resp. $3s_9$) near $3.5l_3$ and we perturb it by entering to v_{12} we get a phase portrait equivalent to V_{11}, but if we do the same taking a point in $5s_{7b}$ (resp. $3s_9$) near $5.8l_{1b}$ (resp. $3.4l_1$) we get a phase portrait equivalent to V_{12} (resp. V_6); (4) If we take a value in $5s_{7a}$ near $5.8l_{1a}$ and we perturb it by entering to v_{12} we get a phase portrait equivalent to V_{12}. If we do the same but taking a point in $5s_{7a}$ near $4.5l_1$ we get a phase portrait equivalent to V_6. In addition, there is a central region in $5s_{7a}$ in which if we take a value in such region and we perturb it by entering to v_{12} we get a phase portrait equivalent to V_{11}. The four previous facts plus the result given in Remark 4.34 prove that part $7S_4$ has one endpoint in $5s_{7a}$ and the other in $5s_{7b}$ and also that part $7S_3$ has an endpoint in $5s_{7a}$ (different from the corresponding to $7S_4$) and the other in $3s_9$.

(5) Part $7S_{21}$ cannot intersect $4s_3$ since otherwise for points in such intersection we must have a phase portrait in which a finite saddle's separatrix, a finite saddle-node's separatrix and an infinite separatrix must coincide, which is impossible; (6) If we take a value in $3s_9$ near $3.5l_3$ and we perturb it by entering to v_{64} we get a phase portrait equivalent to V_{65}, but if we do the same taking a point in $3s_9$ near $3.4l_1$ we get a phase portrait equivalent to V_{64}; (7) If we perturb the region $1.4l_2$ by entering to v_{64} we can get a phase portrait equivalent to the one in V_{64}, in V_{65} and in $7S_{21}$. Using the three previous facts and taking into account Remark 4.34 we conclude that $7S_{21}$ has one of its two endpoints in $3s_9$ and the other in $1.4l_2$.

Finally, the fact that all the endpoints of which we have demonstrated the existence in this proof are exactly the ones given in the statement of this lemma is clear because the branches $7S_{21}$, $7S_3$ and $7S_1$ of $(\mathcal{S}_7)$ are in fact a single branch which crosses through $(\mathcal{S}_3)$ and $(\mathcal{S}_5)$. Analogously, the branches $7S_4$ and $7S_2$ of $(\mathcal{S}_7)$ are in fact a single branch which crosses through $(\mathcal{S}_5)$. ■

In Figs. 4.6 and 4.7 we have shown the complete bifurcation diagram of parts 4 and 5 of the slice $h = 6$, which contains the regions v_{9a}, v_{9b}, v_{12} and v_{64}. In Fig. 4.9 we have also illustrated the previous regions. We have also shown the sequence of phase portraits along regions v_{9a} and v_{9b} in Fig. A.12, along region v_{64} in Fig. A.13 and along region v_{12} in Fig. A.14, all three in Appendix A.2.

We now perform the analysis of part v_{63} (see Figs. 4.1, 4.7 and 4.9). If we take a value in v_{63} near $4s_{10}$, we get a phase portrait equivalent to V_{63}, which has one infinite basin generated by the finite saddle. However, if we take a point in $5s_{30}$ enough far from $4.5l_2$ and we perturb it by entering to v_{63} we get a phase portrait equivalent to the one in V_{75}, which has two infinite basins (one generated by the finite saddle and the other by the finite saddle-node). The previous facts imply the existence of at least one branch of surface $(\mathcal{S}_7)$, denoted as $7S_{28}$, which splits v_{63} into two "new" parts: V_{63} and V_{75}. Moreover, $7S_{28}$ must correspond to a bifurcation surface due to the connection of separatrices between a finite singularity and an infinite one (precisely, the finite saddle-node and a infinite saddle). See Fig. 4.7.

Lemma 4.36. *Part* $7S_{28}$ *has an endpoint in* $5s_{30}$*, namely* $5.7L_7$*. See Figs. 4.1, 4.7 and 4.9.*

Proof. Just observe that if we take a point in $5s_{30}$ close enough to $4.5l_2$ and we perturb it by entering to v_{63} we get a phase portrait equivalent to the one in V_{63}. But if we do the same taking a point in $5s_{30}$ far enough from $4.5l_2$ we get a phase portrait equivalent to the one in V_{75}. ■

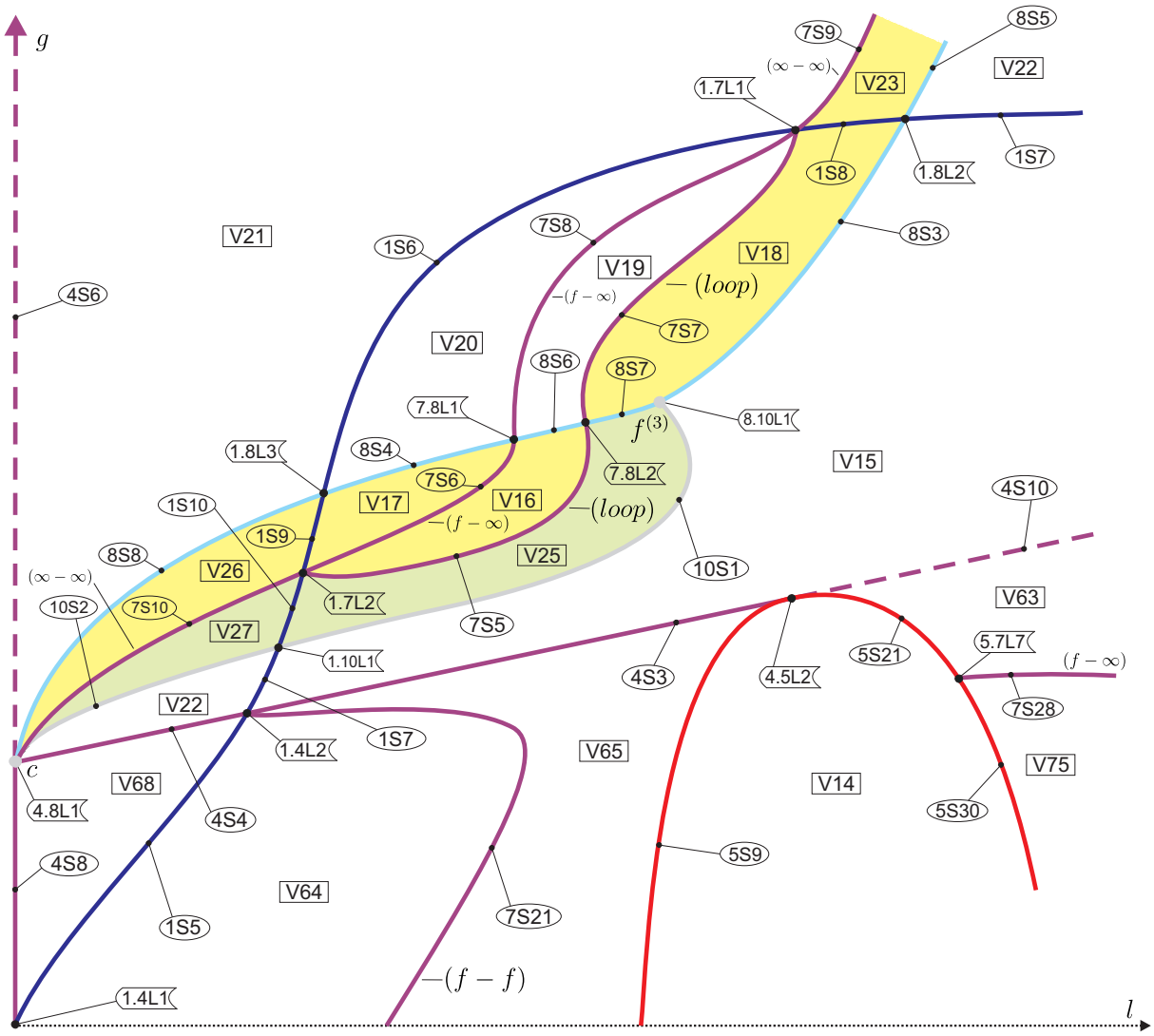

Fig. 4.7: Complete bifurcation diagram for slice $h = 6$ (Part 5, first quadrant complete). When a two–dimensional region is colored in yellow (resp. green) means the existence of one (resp. two) simple limit cycle in such region. We also recall that on the branches $10S_1$ and $10S_2$ of surface $(\mathcal{S}_{10})$ we have one double limit cycle.

We now perform the analysis of parts v_{15}, v_{22a}, v_{20} and v_{23} (see Figs. 4.1, 4.7 and 4.9). We start by considering the parts $8s_7$, $8.10l_1$ and $8s_3$. According to Remark 4.6, we know that the origin is a weak focus of third order $f^{(3)}$ (stable) in $8.10l_1$ and a weak focus of second order $f^{(2)}$ in $8s_7$ and in $8s_3$ (unstable in $8s_7$ and stable in $8s_3$). Hence, part $8.10l_1$ of $(\mathcal{S}_8)$ corresponds to a Hopf bifurcation inside $(\mathcal{S}_8)$. As a consequence, in $8s_7$ we must have a simple limit cycle.

On the other hand, by Remark 4.6 we know that in $8s_3$, $8s_5$, $8s_7$ and in $8s_8$ the origin is a weak focus of order two $f^{(2)}$, and hence all three branches of surface $(\mathcal{S}_8)$ correspond to a Hopf bifurcation. As a consequence, since in $8s_3 \cup 8.10l_1$ and in v_{15} (resp. in $8s_5$ and in v_{22b}) the origin is stable we know that in v_{20} (resp. v_{23}) we must have a simple limit cycle generated by Hopf when crossing from v_{15} (resp. v_{22b}) to v_{20} (resp. v_{23}) through $8s_3 \cup 8.10l_1$ (resp. $8s_5$). Analogously, since in $8s_8$ and in v_{23} (resp. in $8s_7$ and in v_{20}) the origin is unstable we know that in v_{22a} (resp. v_{15}) we must have a simple limit cycle generated by Hopf when crossing from v_{23} (resp. v_{20}) to v_{22a} (resp. v_{15}) through $8s_8$ (resp. $8s_7$). But that is not all, since we can assure the existence of two limit cycles (both simple) in a certain subset of v_{15}. Indeed, as explained before must exist a subset of $8s_7$ adjacent to $8.10l_1$, namely $8S_7$, in which we have a limit cycle (simple) generated as a consequence of the Hopf bifurcation in $(\mathcal{S}_8)$. Moreover,

according to our previous observations, if we cross from v_{20} to v_{15} through $8S_7$ then a second simple limit cycle must be generated, again by Hopf, thus giving birth to a subset of v_{15} possessing two simple limit cycles.

Once studied where the regions with limit cycles must appear (using only Hopf arguments), we must study how these regions are positioned and where and how they end. For example, as we will see soon, there exists a subset of v_{22a} with two simple limit cycles which is a "natural continuation" of the region with two limit cycles in v_{15} (see Figs. 4.7, 4.9).

If we are in v_{23} and sufficiently close to part $8s_5$ the respective phase portrait is topologically equivalent to the one in V_{23}, which has a limit cycle. However, when we move away from $8s_5$ the limit cycle has been lost, which implies (by Remark 4.12) the existence of at least one element $7S_9$ of surface $(\mathcal{S}_7)$ dividing v_{23} into two "new" parts, V_{21} and V_{23}, which represents a bifurcation due to the connection of separatrices between two infinite singularities (see Figs. 4.7,4.9).

Remark 4.37. Parts $7S_9$ and $4s_6$ do not intersect each other (see Figs. 4.7 and 4.9). The proof is very similar to the one given in Remark 4.31: If $7S_9$ and $4s_6$ would intersect, then the phase portrait corresponding to a point in such intersection would have an invariant straight line (not being a separatrix connection) joining two infinite nodes and also would have a graphic surrounding a $f^{(1)}$. Using Hopf by means of adding the trace in (5) and breaking the graphic, we can get a phase portrait with two limit cycles and an invariant straight line, thus contradicting item **(xiv)** in Appendix B.1.

Lemma 4.38. *Part $7S_9$ has p_5 as endpoint (placed in the equator). Its other endpoint is in $1s_6$, namely $1.7L_1$. See Figs. 4.1, 4.7 and 4.9.*

Proof. Numerical analysis suggests our claims. In what follow we prove them. Firstly, $7S_9$ cannot have an end in $8s_5$ since otherwise a portion of $8s_5$ must not refer to a Hopf bifurcation, which contradicts Remark 4.6. Secondly, if we take a value in $1s_6$ near $1.8l_2$ and we perturb it by entering to v_{23} we get a phase portrait equivalent to V_{23}, but if we do the same taking a point in $1s_6$ near $1.8l_3$ we get a phase portrait equivalent to V_{21}. Using the previous facts and taking into account the results we have given in Remark 4.37 the rest of the proof is straightforward. ■

If we are in v_{20} and we trace a straight line from $8s_3$ to $1s_6$ (fully contained in v_{20} and with its intersection with part $1s_6$ enough far from $1.8l_2$) and we "walk" on it we realize that if we are near $8s_3$ the phase portrait is equivalent to the one in V_{18}, which has a limit cycle. However, if we move away from $8s_3$ we have a phase portrait equivalent to the one in V_{19}, in which the limit cycle has been lost. Moreover, if we keep moving away from $8s_3$ and we go near $1s_6$ the phase portrait is equivalent to the one in V_{20}. The previous facts imply the existence of at least two elements $7S_8$ and $7S_7$ of surface $(\mathcal{S}_7)$ dividing v_{20} into three "new" parts, V_{18}, V_{19} and V_{20}. Moreover, $7S_7$ represents a bifurcation due to the connection between two separatrices of the finite saddle and $7S_8$ represents a bifurcation due to the connection of separatrices between a finite and an infinite singularity (see Fig. 4.7).

Lemma 4.39. *Parts $7S_7$ and $7S_8$ do not intersect each other and have $1.7L_1$ (see Lemma 4.38) as a common endpoint. The other endpoint of $7S_8$ (resp. $7S_7$) is in $8s_7$, namely $7.8L_1$ (resp. $7.8L_2$), with $7.8L_1 \neq 7.8L_2$. See Figs. 4.1, 4.7, 4.9.*

Proof. Careful numerical analysis suggests our claims. In what follow we prove them. Firstly, $7S_7$ cannot intersect $7S_8$ since otherwise in a point of such intersection we must have a phase portrait with two separatrices of the finite saddle coinciding with an infinite separatrix, which is impossible. Secondly, $7S_7$ cannot have an end in $8s_3$ since otherwise a portion of $8s_3$ must not refer to a Hopf bifurcation, which contradicts Remark 4.6. Thirdly, if we take a point in $8s_7$ near $1.8l_3$ and we perturb it by entering to v_{20} we get a phase portrait equivalent to V_{20}, but if we do the same taking a point in $8s_7$ near $8.10l_1$ we get a phase portrait equivalent to V_{18}. In addition, there is a central region in $8s_7$ in which if we take a value in such region and we perturb it by entering to v_{20} we get a phase portrait equivalent to V_{19}. Fourthly, if we take a value in $1s_6$ near $1.8l_2$ and we perturb it by entering to v_{20} we get a phase portrait equivalent to V_{18}, but if we do the same taking a point in $1s_6$ near $1.8l_3$ we get a

phase portrait equivalent to V_{20}. The previous four facts prove that: (1) $7S_7$ and $7S_8$ must have one of their two endpoints in different points of part $8s_7$. (2) $7S_7$ and $7S_8$ must have their other endpoint in $1s_6$. Of course both endpoints in $1s_6$ must coincide with $1.7L_1$ since otherwise we can easily arrive to some false topological equivalences when crossing from v_{20} to v_{23} through $1s_6$. Hence, our claims are proved. ■

If we are in v_{22a} and we trace a straight line from $8s_8$ to $4s_4$ (fully contained in v_{22a}) and we "walk" on it we realize that if we are near $8s_8$ the phase portrait is equivalent to the one in V_{26}, which has a limit cycle (simple). However, if we move away from $8s_8$ we have a phase portrait equivalent to the one in V_{27}, in which a second limit cycle has appeared (both simple). Moreover, if we keep moving away from $8s_8$ and we go near $4s_4$ the phase portrait is equivalent to the one in V_{22}, in which both limit cycles have been lost. The previous facts imply the existence of at least one element $7S_{10}$ of surface $(\mathcal{S}_7)$ and one element $10S_2$ of surface $(\mathcal{S}_{10})$ dividing v_{22a} into three "new" parts, V_{26}, V_{27} and V_{22}. Moreover, $7S_{10}$ must represent a bifurcation due to the connection between two separatrices of two different infinite singularities and $10S_2$ must represent a bifurcation due to the existence of a double limit cycle (see Figs. 4.1, 4.7 and 4.9).

Remark 4.40. In principle there exists the theoretical possibility that $10S_2$ intersects $7S_{10}$. However, it is very unlikely to happen. The reason is the following one: If $10S_2$ crosses $7S_{10}$ in some small places then we would have an example of a quadratic system with four limit cycles surrounding the same focus, as discussed in Sect. 5.4. Despite it is not proved that a quadratic system cannot have four limit cycles surrounding the same focus, nobody has found an example of such situation up to now. In fact, there exist a conjecture which says that: *A quadratic system can have at most four limit cycles, and in case of having four they must appear in configuration* $(3, 1)$. We note that S. Shi found an example of quadratic system with a configuration $(3, 1)$. See [Shi, 1980].

We must say that, after a careful numerical analysis, we have no evidences about the existence of the previous hypothetical intersection.

Lemma 4.41. *Parts $7S_{10}$ and $10S_2$ have $4.8l_1$ as a common endpoint. The other endpoint of $7S_{10}$ (resp. $10S_2$) is in $1s_{7a}$, namely $1.7L_2$ (resp. $1.10L_1$), $1.7L_2 \neq 1.10L_1$. See Figs. 4.1, 4.7, 4.9.*

Proof. Careful numerical analysis suggests our claims. In what follow we prove them. Firstly, $7S_{10}$ cannot have an end in $8s_8$ since otherwise a portion of $8s_8$ must not refer to a Hopf bifurcation, which contradicts Remark 4.6. Secondly, if we take a point in $1s_{7a}$ near $1.8l_3$ and we perturb it by entering to v_{22a} we get a phase portrait equivalent to V_{26}. If we do the same but taking a point in $1s_{7a}$ near $1.4l_2$ we get a phase portrait equivalent to V_{22}. In addition, there is a central region in $1s_{7a}$ from which if we take a point in such region and we perturb it by entering to v_{22a} we get a phase portrait equivalent to V_{27}. This last fact prove that $7S_{10}$ and $10S_2$ must have one of their two endpoints in different points of $1s_{7a}$. Finally, part $10S_2$ cannot intersect $4s_4$ since otherwise the phase portrait corresponding to a point in such intersection must have one double limit cycle and an invariant line, but this is impossible since contradicts item **(xiv)** in Appendix B.1. All previous facts grouped together prove our claims. ■

If we are in v_{15} and we trace a straight line from $8s_7$ to $4s_3$ (fully contained in v_{15} and with its intersection with part $8s_7$ enough close to $1.8l_3$) and we "walk" on it we realize that if we are near $8s_7$ the phase portrait is equivalent to the one in V_{17}, which has one simple limit cycle. However, if we move away from $8s_7$ we have a phase portrait equivalent to the one in V_{16}, in which the simple limit cycle is maintained. If we keep moving away from $8s_7$ we have a phase portrait equivalent to the one in V_{25}, in which a second limit cycle has appeared (both simple). Moreover, if continue moving away from $8s_7$ and we go near $4s_3$ the phase portrait is equivalent to the one in V_{15}, in which both limit cycles have been lost. The previous facts imply the existence of at least two elements $7S_5$ and $7S_6$ of surface $(\mathcal{S}_7)$ and an element $10S_1$ of surface $(\mathcal{S}_{10})$ dividing v_{15} into four "new" parts, V_{17}, V_{16}, V_{25} and V_{15}. Moreover, $7S_5$ must represent a bifurcation due to the connection between two separatrices of the finite saddle (loop), $7S_6$ must represent a bifurcation due to the connection of separatrices between a finite and an infinite singularity, and $10S_1$ must repre-

sent a bifurcation due to the existence of a double limit cycle (see Figs. 4.1, 4.7, 4.9).

Remark 4.42. Analogously to what we have exposed in Remark 4.40, it is also theoretical possible that $10S_1$ crosses $7S_5$ despite it is very unlikely to happen, since it would imply the existence of a phase portrait with four limit cycles surrounding the same focus, as discussed in Sect. 5.4. After a careful numerical analysis, we have no evidences about the existence of the previous hypothetical intersection.

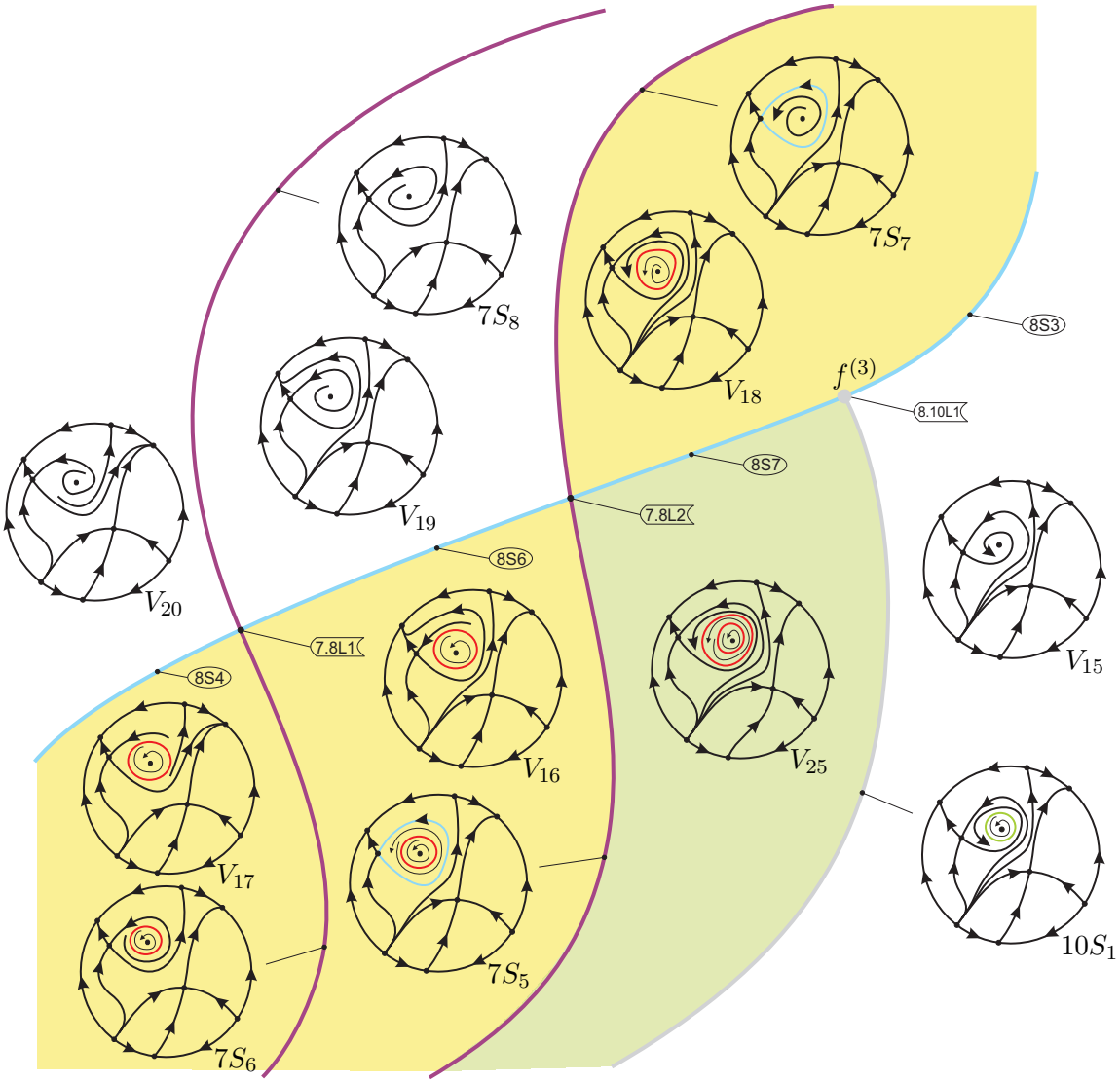

Fig. 4.8: Amplification of regions v_{15} and v_{20}. We recall that the phase portraits in $8S_3$ and in $8.10L_1$ are equivalent to the one in V_{15} (resp. $8S_7$ to V_{18}; $7.8L_2$ to $7S_7$; $8S_6$ to V_{19}; $7.8L_1$ to $7S_8$ and $8S_4$ to V_{20}.)

Lemma 4.43. *Parts $7S_5$ and $7S_6$ do not intersect each other and have $1.7L_2$ (see Lemma 4.41) as a common endpoint. The other endpoint of $7S_5$ (resp. $7S_6$) is in $8s_7$, namely $7.8L_2$ (resp. $7.8L_1$), with $7.8L_1 \neq 7.8L_2$ (see Lemma 4.39). Part $10S_1$ has its endpoints in $1.10L_1$ (see Lemma 4.41) and in $8.10l_1$. See Figs. 4.1, 4.7 and 4.9.*

Proof. Numerical analysis suggests our claims. In what follow we prove them. Firstly, $7S_6$ cannot intersect $7S_5$ since otherwise in a point of such intersection we must have a phase portrait in which two separatrices of the finite saddle must coincide with an infinite separatrix, which is impossible. Secondly, clearly part $10S_1$ must have $8.10l_1$ as endpoint since as a consequence of Remark 4.6 we know that in $8.10l_1$ the origin is a $f^{(3)}$, and the unfolding of a $f^{(3)}$ contains a surface in which a double limit

cycle exists. Thirdly, part $10S_1$ cannot intersect $4s_3$ since otherwise the phase portrait corresponding to a point in such intersection must have one double limit cycle and an invariant straight line, but this previous fact is impossible since contradicts item **(xiv)** in Appendix B.1. Fourthly, if we take a value in $1s_{7a}$ near $1.4l_2$ and we perturb it by entering to v_{15} we get a phase portrait equivalent to V_{15}. However, there is a central region in $1s_{7a}$ in which if we take a point in such region and we perturb it by entering to v_{15} we get a phase portrait equivalent to V_{25}. The previous facts prove that $10S_1$ has its other endpoint in $1s_{7a}$. Finally, we note that the endpoint of $7S_6$ (resp. $7S_5$) in $8s_7$ must coincide with the endpoint of $7S_8$ (resp. $7S_7$) in $8s_7$ since in fact $7S_6$ (resp. $7S_5$) is a continuation of $7S_8$ (resp. $7S_7$) trough $8s_7$. In a similar way we can conclude that the endpoint of $7S_6$ and $7S_5$ (resp. $10S_1$) in $1s_{7a}$ must coincide with the endpoint of $7S_{10}$ (resp. $10S_2$) in $1s_{7a}$. ■

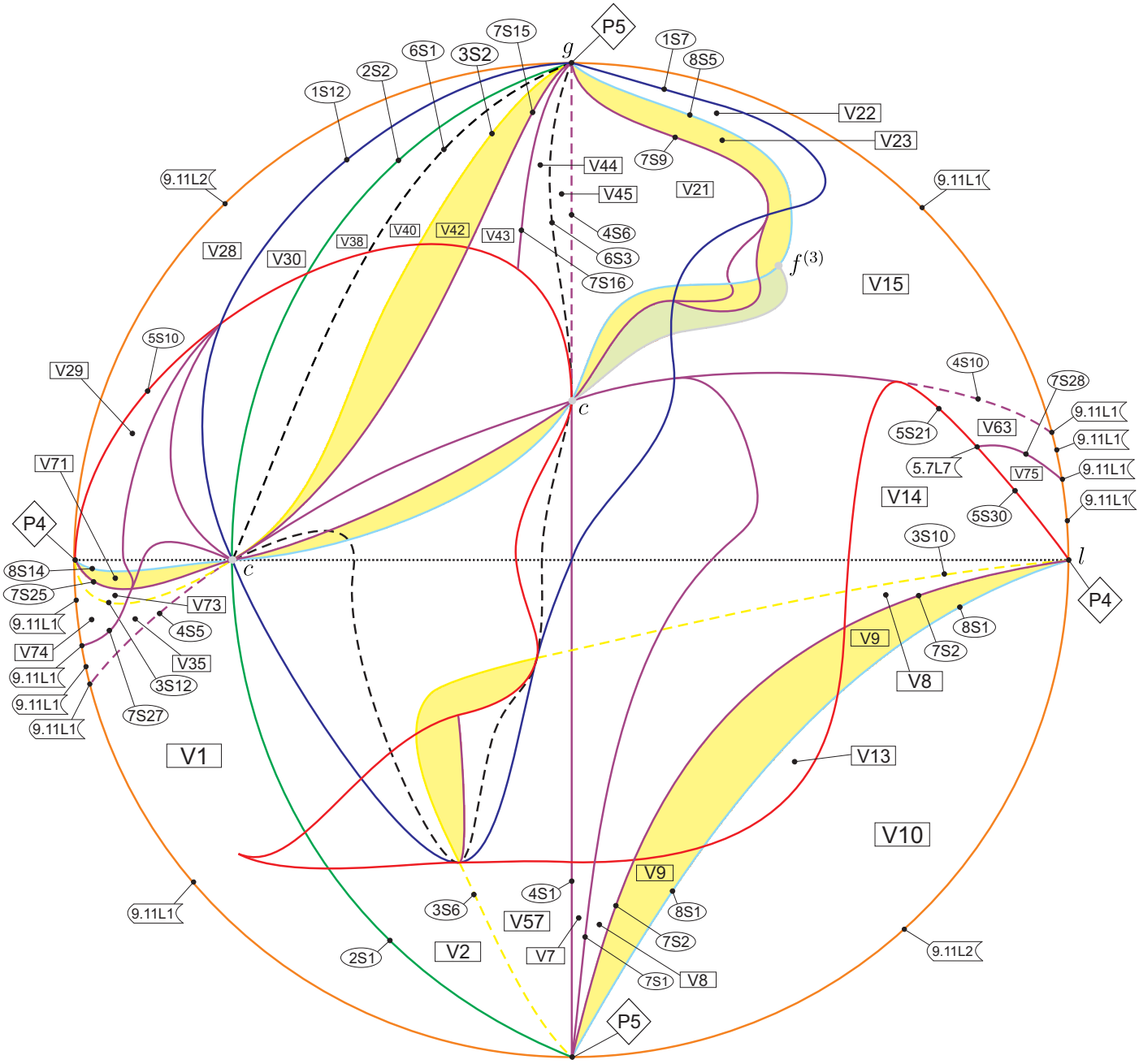

Fig. 4.9: Complete bifurcation diagram for slice $h = 6$ in the disc with labels only in a boundary of the equator.

In Fig. 4.7 we show the complete bifurcation diagram of part 5 of the slice $h = 6$, which contains the regions v_{15}, v_{20}, v_{22a} and v_{23}. In Fig. 4.9 we have also illustrated the previous regions. In Fig. 4.8 we show an amplification of regions v_{15} and v_{20} with the objective to clarify how the limit cycles behave in both previous regions.

In Fig. 4.9 we have drawn the complete bifurcation diagram of the slice $h = 6$ in the planar projection in the unit disk of the half ellipsoid in $B(\vec{0}, 1) \cap \mathcal{B}_{1/2}$ corresponding to the plane $h = 6$ of $(\mathbb{R}^3)^+$ (see Sect. 3.2 for more details). The boundary of the unit disk, which is $\mathbb{S}^1$, corresponds to the equator. We recall that in Fig. 4.9 we have only labeled the regions adjacent to the equator due to the great number of regions that we have encountered in the slice $h = 6$.

As we have explained in Sect. 3.2, two diametrically opposite points in $\mathbb{S}^1$ correspond to the same point in $\mathbb{RP}^3$ and hence also to the same region in our bifurcation diagram, as one can appreciate in Fig. 4.9. In fact, the differences between the phase portraits of two diametrically opposite points in $\mathbb{S}^1$ are principally symmetries and changes of time. Moreover, as we have mentioned in Sect. 3.2, the equator is the common boundary of all the slices (including the slice $h = +\infty$) when we compactify them in $\mathcal{B}_{1/2}$, and hence we only need to study it once. In addition, studying it is very important since it allows us to check if the bifurcation diagram of the corresponding slice we are studying is coherent when we approach to infinity. In order to do it, it is enough to check if the phase portraits corresponding to the regions adjacent to the equator are coherent with those in the equator. If this is the case, then we can assure that we have not left anything out, or at least, that no further region is necessary for the bifurcation diagram to make sense in the slice that we are considering.

We recall that by Remark 4.1 we know that all the phase portraits corresponding to the equator do not have any degeneracy (neither finite nor infinite). Moreover, the weak singularities of the systems in the equator have been completely studied in Remark 4.3 of Section 4.1.

We make a couple of observations regarding Figure 4.9: (1) From the point P_5 bifurcate 38 different regions and 19 from P_4; (2) There are 3 different regions with limit cycles which arrive to the point P_5 and two to P_4.

Remark 4.44. Notice that in Figure 4.9 we have labeled as $9.11L_1$ many apparently different parts of the equator. Let us justify that is fact they are the same part. Indeed, in the affine part (that is, we are taking $m = 1$) the surface $(\mathcal{S}_4)$ has two components: The plane $l = 0$ and the helicoid $-gh + 2h + l = 0$ (see Fig. A.3 in Appendix A.1). Of course the restriction of the previous helicoid to each slice h is a straight line. When $h = 0$, it corresponds to the line $l = 0$, and when $h = \pm\infty$ to the line $g = 0$. Therefore, for $h \in [-\infty, +\infty]$ the helicoid has rotated 180°. Of course, the previous fact implies that the intersection of $(\mathcal{S}_4)$ with the equator is the whole equator.

Similar arguments apply with parts $7S_{28}$ and $7S_{27}$ in Figure 4.9, as will become clear in the subsequent sections.

Having analyzed all the parts of the generic slice $h_2 = 6$ and explained the existence of the non-algebraic surfaces in such parts (modulo islands, see Sect. 5.1), we have finished the study of the generic slice $h_2 = 6$. However, we cannot assure that these are all the additional bifurcation surfaces in this slice, since there is the theoretical possibility of the existence of islands, i.e. there could exist closed non-algebraic surfaces placed in the three-dimensional parts of $\mathcal{B}_{1/2}$ and small enough to escape our numerical research (see Sect. 5.1). In addition, as we explain in Sect. 5, there are other phenomena implying more non-algebraic bifurcation surfaces that are also theoretical feasible.

For all other two-dimensional parts of the partition of the slice $h_2 = 6$ (different from those listed in pages 30 and 31), whenever we join two points which are close to different borders of the part, the two phase portraits are topologically equivalent. Hence, in such regions no non-algebraic surface is needed in order the bifurcation diagram to be coherent, despite the presence of islands and other phenomena is also theoretical feasible in such regions. In short, it is expected that the complete bifurcation diagram for the slice $h_2 = 6$ is the one shown in Fig. 4.9, or at least, no other non-algebraic bifurcation surface is needed in order for the bifurcation diagram in Fig. 4.9 to be completely coherent.

4.3. Studying the bifurcation surfaces at the infinite part of $\mathbb{RP}^3$

As explained before, see list (10), the highest finite slice needed is $h_2 = 6$. To justify the previous, we have to check that there are not more non-algebraic singular slices in the range $(h_2, +\infty)$. In order to do this we must study in detail the slice $h_1 = +\infty$, just as we have done with slice $h_2 = 6$. Once done, we must study if the slice $h_2 = 6$ is coherent (in terms of continuity) with the slice $h_1 = +\infty$. If so (as it will be the case), we will have proved that no other singular slice is needed in the range $(6, +\infty)$ for the bifurcation diagram to be coherent and hence the range $[6, +\infty]$ will be completely studied. If not (it will not be the case), then we will have proved the existence of non-algebraic singular slices in the range $(6, +\infty)$ and hence we must find them in order to complete the study of the whole range $[6, +\infty]$.

Remark 4.45. We recall that the slice $h = +\infty$ correspond to the infinite part of $\mathbb{RP}^3$ except the equator, as explained in Sect. 3.2. Just as the equator allows us to verify the coherence of the regions found in each slice as we take l and g to ∞, the slice $h = +\infty$ is also necessary in order to verify that the regions found in the affine part of $\mathbb{RP}^3$ are also coherent when we take $h \to +\infty$. We observe that, as mentioned in Sect. 3.2, the compactness of our parameter space $\mathcal{B}_{1/2}$ is essential in order to verify the coherence of its interior with its borders, since using a non bounded representative of our parameter space could not be verified.

So let's start the study of the slice $h_1 = +\infty$. First of all, notice that in the limit to infinity, the bifurcation diagram (of the algebraic surfaces) tends to be the one shown in Fig. 4.10.

The slice $h_1 = +\infty$ is an algebraic bifurcation surface which has, as we will see in a moment, some particularities.

For completeness, recall that the slice $h = +\infty$ is obtained by considering $h = 1$ and $m = 0$ in the normal form (5), which becomes:

$$\begin{cases} \dot{x} = -y + gx^2 + 2xy \\ \dot{y} = x + lx^2 \end{cases} \tag{11}$$

Lemma 4.46. *The change $(x, y, t) \to (x, -y, -t)$ transforms a system (11) with parameters (l, g) into a system (11) with parameters $(l, -g)$. Therefore, the bifurcation diagram in the slice $h_1 = +\infty$ is symmetric with respect to the l-axis.*

Proof. Direct computation. Left to the reader. ■

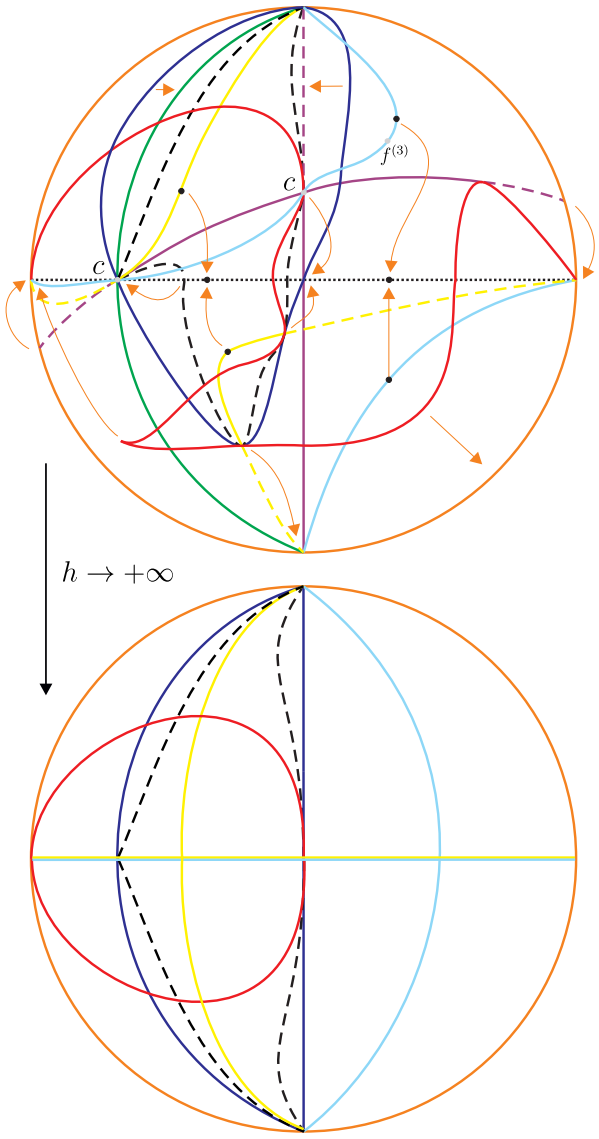

Fig. 4.10: Transition from $h \geq h_2 = 6$ to infinity. The orange arrows show the movement that the surfaces do as $h \to +\infty$.

Another crucial fact to take into account is that, when studying the slice $h_1 = +\infty$, some of the surfaces $(\mathcal{S}_i)$ defined in Sect. 4.1 must be redefined.

First of all, notice that if we are in $h_1 = +\infty$ (that is, we take $m = 0$ and $h = 1$), then we have $\mu_0 = \mu_1 = 0$. Therefore, by Lemma 5.5 and Prop. 6.3 of [Artés *et al.*, 2021a] we know that in

the slice $h_1 = +\infty$ a double singularity have escaped to infinity (precisely, the finite saddle-node). Consequently, the surface $(\mathcal{S}_1)$ must be redefined at $h_1 = +\infty$.

Bifurcation surface in $h_1 = +\infty$ due to a a second finite singularity has escaped to infinity

$(\mathcal{S}_1')$ This surface will contain the points of the slice $h_1 = +\infty$ in which a second finite singularity has escaped to infinity. Since the origin cannot escape to infinity and the saddle-node has already escaped to infinity, the unique possibility is that a second singularity different from the origin (with multiplicity one) escapes to infinity. Therefore, we can have two distinct situations:

- A second finite singularity escapes to infinity in a different direction that the finite saddle-node. According to Lemma 5.5 of [Artés *et al.*, 2021a], we must consider the comitant $\tilde{K}$, which has the following expression w.r.t the normal form (11):

$$\tilde{K} = -4l^2x^2 = 0 \iff l = 0$$

- A second finite singularity escapes to infinity but in the same direction that the finite saddle-node. Thus, by Prop. 6.3 in [Artés *et al.*, 2021a], we must consider the comitant μ_2, which has the following expression w.r.t normal form (11):

$$\mu_2 = l(2+l)x^2 = 0 \iff l(2+l) = 0$$

From Prop. 6.3 in [Artés *et al.*, 2021a] we see that in fact μ_2 also contains the cases in which a second finite singularity has escaped to infinity in a different direction as the finite saddle-node, that is, μ_2 also contains the information given by $\tilde{K}$.

Hence, in $h_1 = +\infty$ we must redefine the surface $(\mathcal{S}_1)$ as:

$$(\mathcal{S}_1') : l(2+l) = 0$$

Moreover, from the previous arguments we conclude that in the line $l = -2$ a second finite singularity has escaped to infinity in the same direction as the finite saddle-node and in the line $l = 0$ in a distinct direction.

Parts in slice $h_2 = 6$	Parts in slice $h_1 = +\infty$	Parts in slice $h_2 = 6$	Parts in slice $h_1 = +\infty$
V_1	$11S_{22}$	V_2	$1.11L_4$, P_5
V_3	$1.11L_5$	V_4	$1.11L_6$
V_5	$11S_{24}$	V_6	$11S_8$
V_7	P_5	V_8	P_4, P_5
V_9	P_4, P_5	V_{10}	$9.11L_2$
V_{11}	$11S_7$	V_{12}	$11S_6$
V_{13}	$11S_2$	V_{14}	P_4
V_{15}	$11S_1$	V_{16}	$3.8L_4$, $3.8L_6$
V_{17}	$3.8L_6$	V_{18}	$11S_3$
V_{19}	$11S_4$	V_{20}	$11S_5$
V_{21}	$1.11L_1$	V_{22}	P_5, P_{23}
V_{23}	P_5	V_{25}	$3.8L_4$, $3.8L_6$
V_{26}	P_{23}	V_{27}	P_{23}
V_{28}	$11S_{16}$	V_{29}	$5.11L_5$
V_{30}	$1.11L_2$	V_{31}	$1.11L_3$
V_{32}	$11S_{18}$	V_{33}	$3.8L_9$
V_{34}	$3.8L_9$	V_{35}	$3.8L_9$
V_{36}	$3.8L_9$	V_{37}	$1.11L_3$
V_{38}	$11S_{15}$	V_{39}	$11S_{17}$
V_{40}	$11S_{13}$	V_{41}	$11S_{11}$
V_{42}	$11S_{14}$	V_{43}	$7.11L_5$
V_{44}	$11S_{10}$	V_{45}	$11S_9$
V_{46}	$11S_{12}$	V_{47}	$3.8L_7$, $5.11L_3$, P_{23}
V_{48}	$3.8L_7$, $3.8L_8$	V_{49}	$3.8L_7$, $3.8L_8$
V_{50}	$11S_{20}$	V_{51}	$11S_{21}$
V_{52}	$11S_{25}$	V_{53}	$11S_{26}$
V_{54}	$11S_{27}$	V_{55}	$11S_{28}$
V_{56}	$11S_{19}$	V_{57}	P_5
V_{58}	P_{23}	V_{59}	P_{23}
V_{60}	P_{23}	V_{61}	P_{29}
V_{62}	P_{29}	V_{63}	P_4
V_{64}	$3.8L_6$	V_{65}	$3.8L_3$, $3.8L_4$, $3.8L_5$, $3.8L_6$
V_{66}	$11S_{23}$	V_{68}	P_{23}
V_{71}	P_4	V_{72}	P_4
V_{73}	P_4	V_{74}	P_4
V_{75}	P_4		

Table 4.1: Transition from slice $h_2 = 6$ to $h_1 = +\infty$. Here we present the correspondence between the volumetric regions from slice $h_2 = 6$ and the respective parts from slice $h_1 = +\infty$.

Remark 4.47. Notice that the surface $(\mathcal{S}_2)$ is irrelevant in the slice $h_1 = +\infty$. Indeed, since generically a finite saddle-node has escaped to infinity and the origin cannot collide with any finite singularity, we cannot have finite collisions in $h_1 = +\infty$ (and in particular neither triple collisions).

Remark 4.48. Notice that the l-axis of $h_1 = +\infty$ is a special region, since belongs to $(\mathcal{S}_3)$ and also to $(\mathcal{S}_8)$. However, it was already studied in detail in Remark 4.6, and in fact we concluded that it is a region with centers.

We now have finished describing the algebraic curves appearing in the slice $h_1 = +\infty$. In Fig. 4.11

we present this slice completely and properly labeled. We draw special attention to the fact that the nonalgebraic curves (numerically detected and which existence was proved before) still remain in this slice and they maintain the same relative positions with respect to the algebraic curves in the transition from slice $h_2 = 6$ to slice $h_1 = +\infty$; numerical tools support this claim.

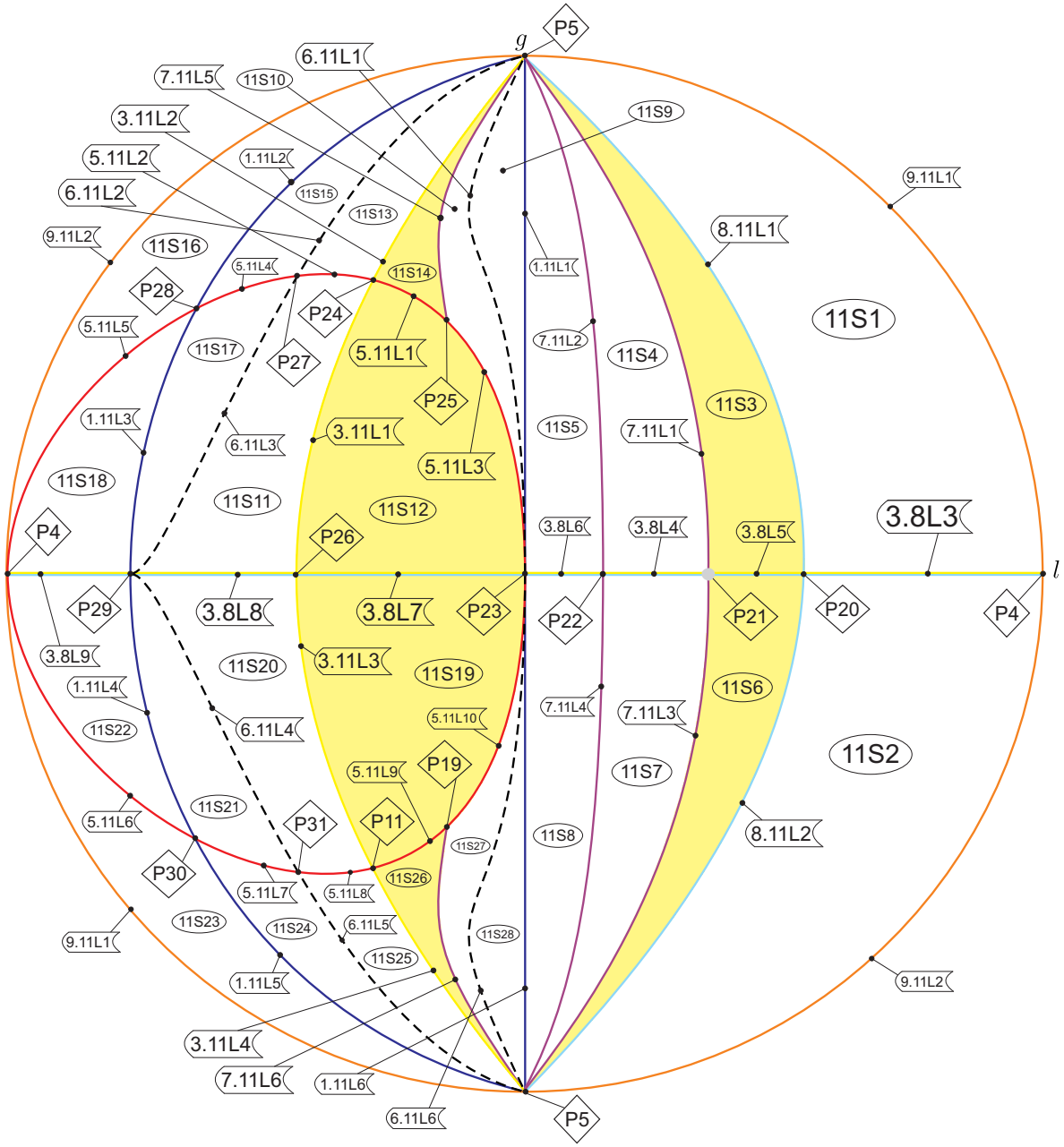

Fig. 4.11: Complete bifurcation diagram for slice $h_1 = +\infty$.

Remark 4.49. As explained in Remark 4.10, additional notation also will be used in the slice $h_1 = +\infty$. Precisely, as in slice $h_1 = +\infty$ we are in a surface, we point out that all the "generic" parts in this slice are labeled as $11S_j$ and the points as P_j. Regarding the lines, they are labeled as $i.11L_j$ except in one situation: The lines in the l-axis of $h_1 = +\infty$ are denoted as $3.8L_j$. The reason is the following: The l-axis is a special region with centers (see Remark 4.48), as mentioned before. Of course we could have denoted such regions as $3.11L_j$ or $8.11L_j$, but both previous notations are already

used in the slice $h_1 = +\infty$ for regions without centers. Finally, notice that we have used the orange color for the equator.

In Table 4.1 we indicate the "death" of all volumetric parts from slice $h_2 = 6$ to $h_1 = +\infty$. Then, we have established the correspondence between the phase portraits of the slices $h_2 = 6$ and $h_1 = +\infty$. Therefore, the convergence from slice $h_2 = 6$ to $h_1 = +\infty$ is completely coherent.

To finish this section, let us make a couple of comments on the complete bifurcation diagram presented in Fig. 4.11.

First of all, despite in Fig. 4.11 we have drawn the parts $7.11L_j$ as straight lines for simplicity, a careful numerical analysis confirms that they are not. We recall that, despite surface $(\mathcal{S}_7)$ is generically non-algebraic, it could contain some sub-parts which are algebraic, as for instance some curves. Of course, if in any slice one suspect that a curve might be algebraic, we have to use numerical methods to reinforce/disprove our suspicions. In case the numerical methods reinforce our theory, then we have to prove formally that the curve under consideration is indeed algebraic.

On the other hand, notice that the point P_{21} is colored in gray in Fig. 4.11. The reason of doing so is that the point P_{21} is where the line $8.10L_1$ (see Fig. 4.7) ends. In fact, we can give an explicit expression for P_{21}. According to Remark 4.6, the line $8.10L_1$ has the expression $[2h/5 : 4 : 1 : h]$, $h \in \mathbb{R}$, which of course arrives to infinity at $[2/5 : 0 : 0 : 1]$, that is, $(l, g) = (2/5, 0)$. However, since the previous point is an algebraic value and parts $7.11L_1$ and $7.11L_3$ are not algebraic, we cannot assure that the common endpoint of $7.11L_1$ and $7.11L_3$ in the l-axis is exactly $(l, g) = (2/5, 0)$ (notice that in the set $\{(l, 0) \mid l > 0\} \subset \{h = +\infty\}$ the phase portrait is always the same). However, a careful numerical analysis suggest that in fact the common endpoint of $7.11L_1$ and $7.11L_3$ in the l-axis is $(l, g) = (2/5, 0)$, denoted as P_{21} in Fig. 4.11.

4.4. Transition from slice to slice at the affine part of $\mathbb{RP}^3$

Since there is coherence (modulo islands, as discussed in Sec. 5) between the slices $h_1 = +\infty$ and $h_2 = 6$, no more slices $h > 6$ are needed. Therefore, the range $h \in [6, +\infty]$ is completely studied.

Having finished the complete study of slice $h = 6$ and having presented the transition from $h = 6$ to $h = +\infty$, the next step is to decrease the values of h, according to equation (10), and make an analogous study for each one of the slices that we need to consider and also search for changes when going from one slice to the next one.

Remark 4.50. As we have already mentioned in Sect. 4.2, in the slices listed in (10) different from $h_2 = 6$ we will present only a labeled drawing containing the algebraic and non-algebraic bifurcation surfaces, but only of the slice's sub-regions in which a topological change of the bifurcations surfaces' position w.r.t the neighborhood slices has occurred. Moreover, in pictures presented in this section the red labels correspond to parts which have appeared in previous slices and black labels correspond to the "new" parts.

We now start decreasing the values of the parameter h, according to the list of slices (10), in order to explain as much as we can the bifurcations in the parameter space.

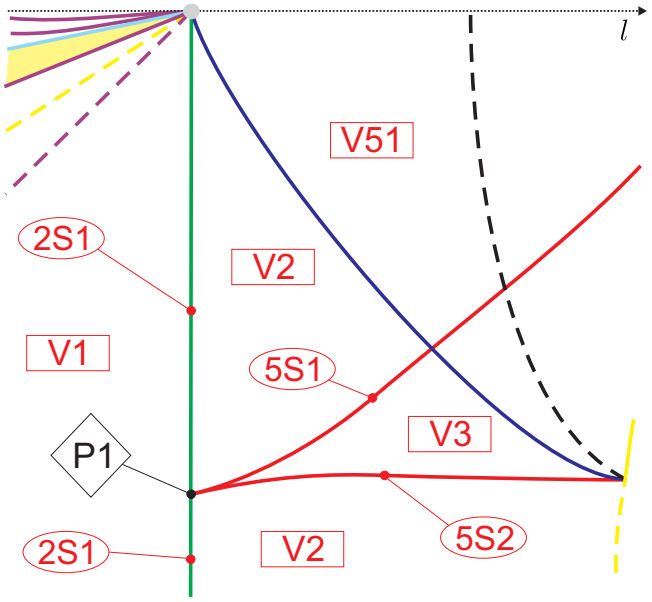

Fig. 4.12: Sub-region of the algebraic singular slice $h_3 = 3\sqrt{3}$ in which the topological changes have appeared.

We start considering the curved triangle V_{66} in the part 1 of slice $h_2 = 6$ (see Fig. 4.2), having $5.5L_1$, $2.5L_2$ and $2.5L_3$ as a vertexes. As we move down from $h_2 = 6$ to $h_3 = 3\sqrt{3}$ (which is an alg.

sing. slice), this triangle collapses to a single point in slice $h_3 = 3\sqrt{3}$, denoted by P_1 in Fig. 4.12.

The remaining sub-regions of the slice $h_3 = 3\sqrt{3}$ remain topologically unchanged w.r.t the generic slice $h_2 = 6$. We also point out that the phase portrait in P_1 is equivalent to those in $2S_1$, and hence the slice $h_3 = 3\sqrt{3}$ does not bring us any new topological phase portrait.

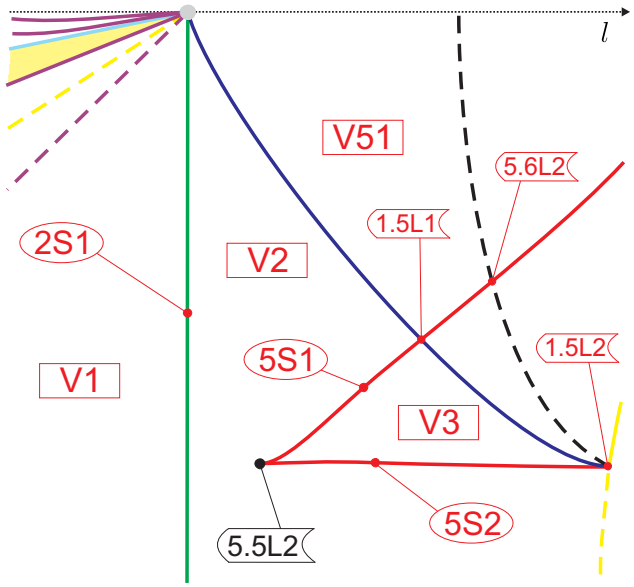

Fig. 4.13: Sub-region of the generic slice $h_4 = 5$ in which the topological changes have appeared.

When we go to the next slice in (10), which is the generic slice $h_4 = 5$, we observe that the point P_1 has detached from the green surface $(\mathcal{S}_2)$, giving rise to the birth of a "new" line denoted as $5.5L_2$, as we can appreciate in Fig. 4.13. The rest of the slice $h_4 = 5$ remains topologically unchanged respect the slice $h_3 = 3\sqrt{3}$. In addition, we note that the phase portrait corresponding to the "new" part $5.5L_2$ is topologically equivalent to the one in V_2. Therefore, the slice $h_4 = 5$ does not bring us any new topological phase portrait.

Remark 4.51. As mentioned in Remark 4.23, in Figs. 4.2, 4.4 and 4.12 we have labeled as $2S_1$ two apparently different parts of $(\mathcal{S}_2)$. We observe that Fig. 4.13 justifies that both regions are the same. Indeed, the restriction of the surface $2S_1$ in the slice $h_4 = 5$ consists in a half straight line (see Fig. 4.13). However, when we move from slice $h_4 = 5$ to $h_2 = 6$, a portion of the curved triangle V_3 (in Fig. 4.13) crosses the green surface $(\mathcal{S}_2)$, thus causing that the restriction of the surface $2S_1$ in the slice $h_2 = 6$ consist in two disconnected segments (see Figures 4.2 and 4.4).

We move now to the next slice listed in (10), which corresponds to the algebraic singular slice $h_5 \approx 4.361$ (see Fig. 4.14). For the algebraic expression of the value h_5, see (9).

We start noticing that the topological changes in the slice $h_5 \approx 4.361$ appear in a distinct region from the one in which have appeared in the two previous slices (see Fig. 4.14).

In order to describe the topological changes occurred in the slice h_5, we consider the curved ellipse V_{13} in the part 4 of the slice $h_2 = 6$ (see Figs. 4.6 and 4.9), which also exists in the slices $h_3 = 3\sqrt{3}$ and $h_4 = 5$. As we move down from $h_2 = 6$ to h_5, the previous ellipse collapses to a single point, say b, in the slice h_5, which belongs to curve $5.8L_1$ as explained in the following remark:

Remark 4.52. In Fig. 4.6 we have labeled as $5.8L_1$ two apparently different curves. The existence of the point b justifies that both previous curves labeled as $5.8L_1$ are in fact the same curve (see Remark 4.33), and of course the point b belongs to the curve $5.8L_1$. See Fig. 4.14.

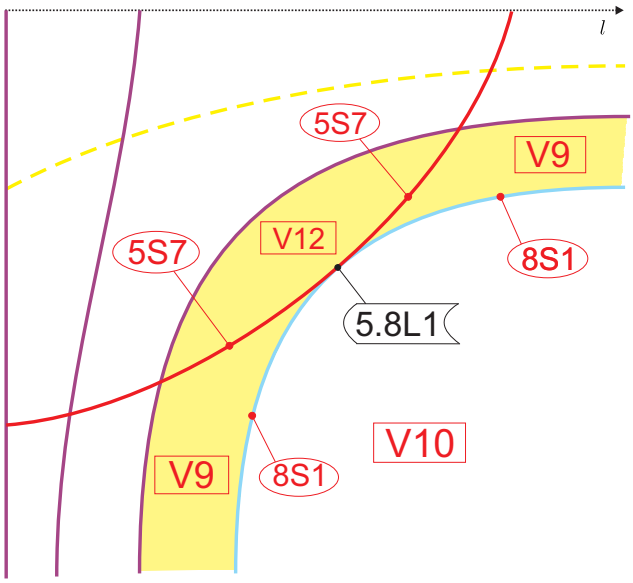

Fig. 4.14: Sub-region of the algebraic singular slice $h_5 \approx 4.361$ in which the topological changes have appeared.

The remaining sub-regions of the slice $h_5 \approx 4.361$ remain topologically unchanged with respect to the slice $h_4 = 5$. In addition, we point out that

the slice $h_5 \approx 4.361$ does not bring us any new topological phase portrait.

We now move to the next slice in (10), which is the generic slice $h_6 = 4.2$ (see Fig. 4.15). As we can appreciate in Fig. 4.15, the curve $5.8L_1$ does not appear in such slice. Consequently, the surface $8S_1$ do not intersect any other surface in the slice $h_6 = 4.2$. The remaining sub-regions of the slice remain topologically unchanged with respect to the slice $h_5 \approx 4.361$. In addition, we point out that the slice $h_6 = 4.2$ does not bring us any new topological phase portrait.

Remark 4.53. We recall that in Figs. 4.6 and 4.9 we have labeled two apparently different parts as V_9 (resp. $5S_7$; and $8S_1$). It is clear that Fig. 4.15 justifies that both parts labeled as V_9 (resp. $5S_7$; and $8S_1$) are the same (see Remark 4.33).

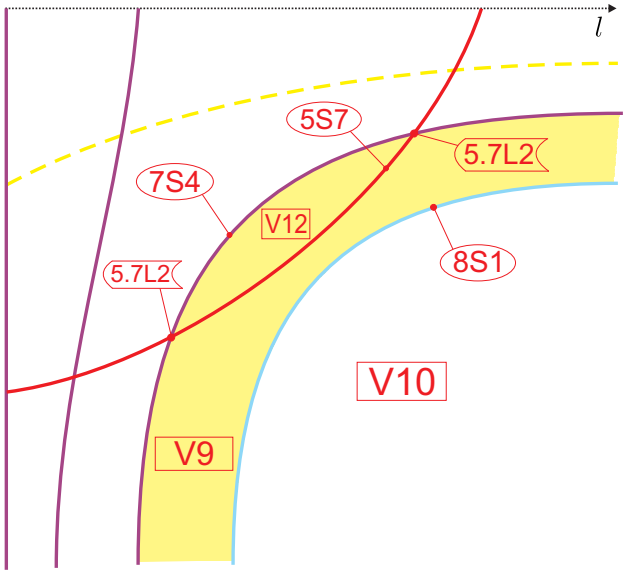

Fig. 4.15: Sub-region of the generic slice $h_6 = 4.2$ in which the topological changes have appeared.

The next slice in list (10) corresponds to the singular non-algebraic slice $h_7 = 4.2 - \epsilon_1^*$, where ϵ_1^* is a certain positive value (see Fig. 4.16). We recommend the reader to consult the notation for slices that we have introduced in detail in Section 4.1 (page 29).

In order to describe the topological changes that have occurred in slice $h_7 = 4.2 - \epsilon_1^*$, we consider the curved ellipse V_{12} in Fig. 4.15. As we move down from slice $h_6 = 4.2$ to $h_7 = 4.2 - \epsilon_1^*$, the previous ellipse collapses to a single point, say c, in the slice $h_7 = 4.2 - \epsilon_1^*$, which belongs to curve $5.7L_2$ as explained in the following remark:

Remark 4.54. In Fig. 4.6 we have labeled as $5.7L_2$ two apparently different curves. The existence of the point c justifies that both previous branches labeled as $5.7L_2$ are in fact the same curve (see Remark 4.33), and of course the point c belongs to the curve $5.7L_2$. See Fig. 4.16.

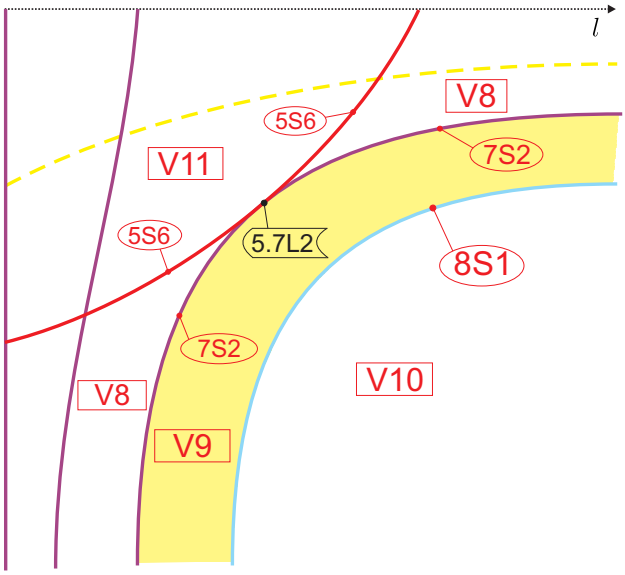

Fig. 4.16: Sub-region of the non-algebraic singular slice $h_7 = 4.2 - \epsilon_1^*$ in which the topological changes have appeared.

The remaining sub-regions of the slice $h_7 = 4.2 - \epsilon_1^*$ remain topologically unchanged with respect to the slice $h_6 = 4.2$. In addition, we point out that the slice $h_7 = 4.2 - \epsilon_1^*$ does not bring us any new topological phase portrait.

We now move to the next slice in (10), which corresponds to the generic slice $h_8 = 4.2 - \epsilon_1$ (see Fig. 4.17), where ϵ_1 is a certain positive value satisfying that $0 < \epsilon_1^* < \epsilon_1$. As we can appreciate in Fig. 4.17, the curve $5.7L_2$ does not appear in such slice. Consequently, the surface $7S_2$ do not intersect any other surface in the slice $h_8 = 4.2 - \epsilon_1$. The remaining sub-regions of the slice remain topologically unchanged with respect to the slice $h_7 = 4.2 - \epsilon_1^*$. In addition, we point out that the slice $h_8 = 4.2 - \epsilon_1$ does not bring us any new topological phase portrait.

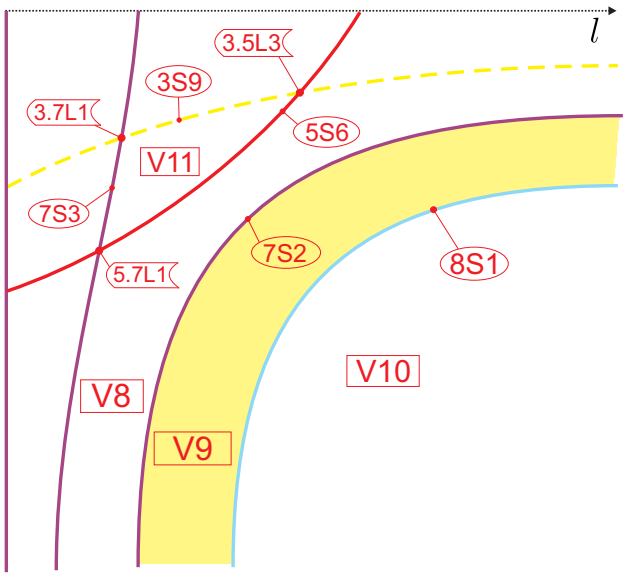

Fig. 4.17: Sub-region of the generic slice $h_8 = 4.2 - \epsilon_1$ in which the topological changes have appeared.

Remark 4.55. We recall that in Fig. 4.6 we have labeled two apparently different parts as V_8 (resp. $5S_6$; and $7S_2$). It is clear that Fig. 4.17 justifies that both parts labeled as V_8 (resp. $5S_6$; and $7S_2$) are the same (see Remark 4.33).

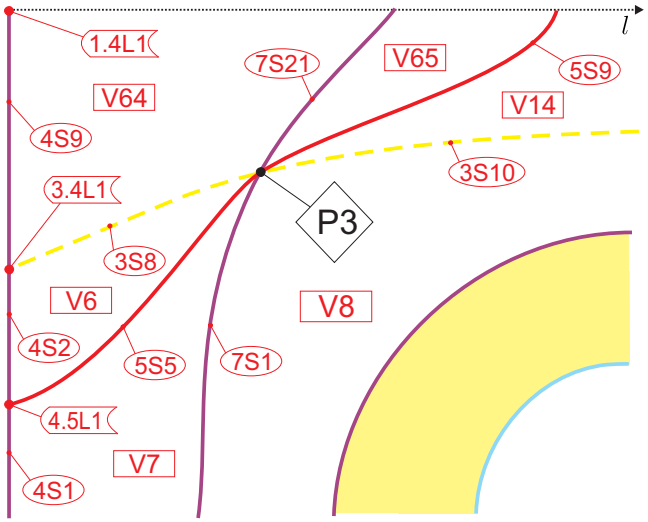

Fig. 4.18: Sub-region of the non-algebraic singular slice $h_9 = 4.2 - \epsilon_2^*$ in which the topological changes have appeared.

The next slice in list (10) corresponds to the singular non-algebraic slice $h_9 = 4.2 - \epsilon_2^*$, where $0 < \epsilon_1^* < \epsilon_1 < \epsilon_2^*$ (see Fig. 4.18). We now consider the curved triangle V_{11} in Fig. 4.17, having $3.5L_3$, $3.7L_1$ and $5.7L_1$ as a vertexes. As we move down from $h_8 = 4.2 - \epsilon_1$ to $h_9 = 4.2 - \epsilon_2^*$, this triangle collapses to a single point called P_3 in the slice $h_9 = 4.2 - \epsilon_2^*$ (see Fig. 4.18). The rest of slice $h_9 = 4.2 - \epsilon_2^*$ remains topologically unchanged with respect to the slice $h_8 = 4.2 - \epsilon_1$. We also point out that the phase portrait in P_3 is equivalent to those in $5.7L_1$, and hence the slice $h_9 = 4.2 - \epsilon_2^*$ does not bring us any new topological phase portrait.

When we go to the next slice in (10), which is the generic slice $h_{10} = 4.2 - \epsilon_2$ (where $0 < \epsilon_1^* < \epsilon_1 < \epsilon_2^* < \epsilon_2$), we observe that the triple intersection of surfaces $(\mathcal{S}_7)$, $(\mathcal{S}_3)$ and $(\mathcal{S}_5)$ at point P_3 (see Fig. 4.18) has disappeared in the slice $h_{10} = 4.2 - \epsilon_2$, giving rise to the birth of a new curved triangle denoted as V_{67} (see Fig. 4.19). As we can appreciate in Fig. 4.19, seven "new" regions have appeared. However, it is direct to verify that none of them give us new topological phase portraits (see Tables 7.1-7.9 in Sect. 7). In addition, the rest of the slice $h_{10} = 4.2 - \epsilon_2$ remains topological unchanged w.r.t the slice $h_9 = 4.2 - \epsilon_2^*$, and therefore the slice $h_{10} = 4.2 - \epsilon_2$ does not bring us any new phase portrait.

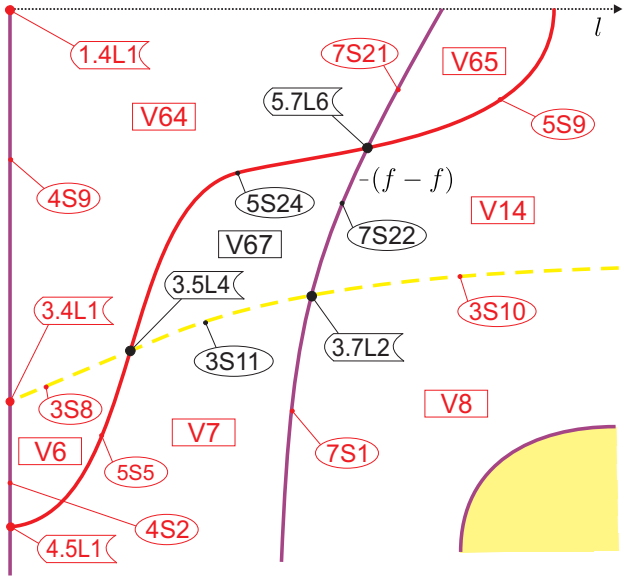

Fig. 4.19: Sub-region of the generic slice $h_{10} = 4.2 - \epsilon_2$ in which the topological changes have appeared.

The next slice in list (10) corresponds to the singular non-algebraic slice $h_{11} = 4.2 - \epsilon_3^*$, where ϵ_3^* satisfies that $0 < \epsilon_1^* < \epsilon_1 < \epsilon_2^* < \epsilon_2 < \epsilon_3^*$ (see Figure 4.20). We now consider the curved triangles V_{16} and V_{17} in Fig. 4.7, which of course still existing in the slice h_{10}. As we move down from h_{10} to h_{11}, both triangles collapse to a single point called P_7 in the slice $h_{11} = 4.2 - \epsilon_3^*$ (see Fig. 4.20),

which of course is a "new" region. The rest of slice h_{11} remains topologically unchanged with respect to the slice h_{10}. We also point out that the phase portrait in P_7 is equivalent to those in $1.7L_1$, and hence the slice $h_{11} = 4.2 - \epsilon_3^*$ does not bring us any new topological phase portrait.

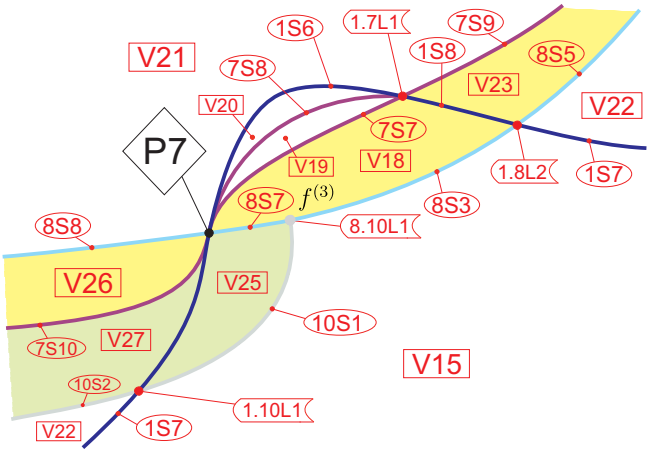

Fig. 4.20: Sub-region of the non-algebraic singular slice $h_{11} = 4.2 - \epsilon_3^*$ in which the topological changes have appeared.

The next slice in list (10) corresponds to the generic slice $h_{12} = 4.2 - \epsilon_3$, where the value ϵ_3 satisfies that $0 < \epsilon_1^* < \epsilon_1 < \epsilon_2^* < \epsilon_2 < \epsilon_3^* < \epsilon_3$ (see Figure 4.21). Notice that seven apparently new regions have appeared (the topological triangle V_{23} and its six bordering regions: $7.8L_3$, $8S_{12}$, $1.8L_4$, $1S_8$, $1.7L_1$, $7S_9$ and $7.8L_3$). However, despite all the previous regions are marked in black and all of them seem to be new, some of them are not new (precisely, V_{23}, $1S_8$, $1.7L_1$ and $7S_9$). Indeed, notice that in Figure 4.21 there are exactly two regions labeled as V_{23} (resp. $1S_8$, $1.7L_1$ and $7S_9$), one of them marked in red and the other in black, which seem to correspond to different regions. The fact that they are the same region will become clear later as we keep decreasing the value of h. Finally, the apparently new regions $7.8L_3$, $8S_{12}$ and $1.8L_4$ are truly new regions, which did not existed in the previous slices in (10). The rest of slice h_{12} remains topologically unchanged with respect to the slice h_{11}. Finally, the phase portrait in part $1.8L_4$ (resp. $8S_{12}$; $7.8L_3$) is topologically equivalent to the one in part $1S_8$ (resp. V_{23}; $7S_9$). Therefore, the slice h_{12} does not bring us any new topological phase portrait.

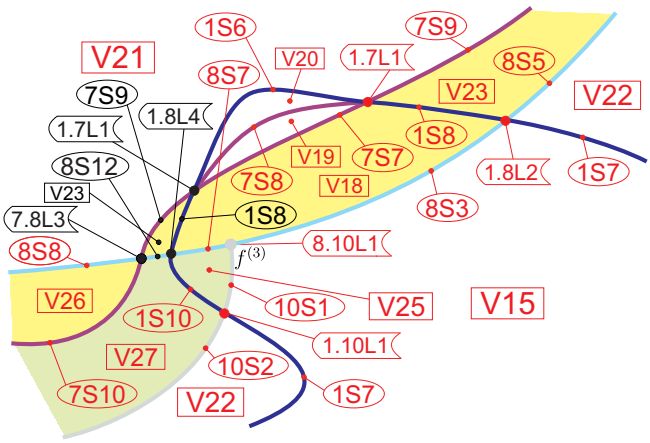

Fig. 4.21: Sub-region of the generic slice $h_{12} = 4.2 - \epsilon_3$ in which the topological changes have appeared.

We move now to the next slice in list (10), which corresponds to the singular algebraic slice $h_{13} = 3$ (see Fig. 4.22).

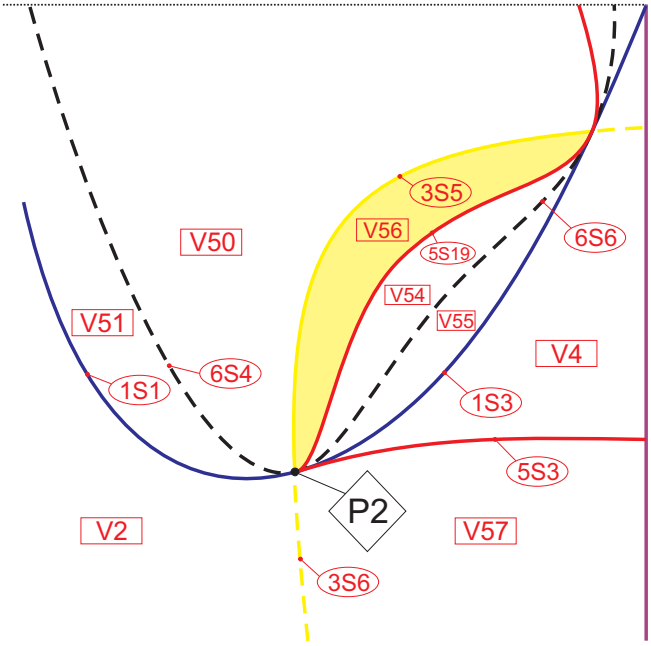

Fig. 4.22: Sub-region of the algebraic singular slice $h_{13} = 3$ in which the topological changes have appeared.

We note first that the topological changes in slice $h_{13} = 3$ appear in a different region than in the previous slices, as we can appreciate in Fig. 4.22. We now describe such changes: We consider the lines $5.5L_2$, $1.5L_1$, $1.5L_2$, $5.6L_2$ and $3.5L_2$ (see Figs. 4.4 and 4.13). As we move down from h_{12} to $h_{13} = 3$ the five previous lines become closer and closer until they collapse to a single point in slice $h_{13} = 3$, called P_2 (see Fig. 4.22). Consequently, the regions V_3, V_5, V_{52} (see Figs. 4.4 and 4.13) have

also collapsed to P_2 in slice $h_{13} = 3$. The question is: What happen with V_{53} and $7S_{19}$ (see Fig. 4.4)? Since the surface $7S_{19}$ is not algebraic, we need additional considerations to know whether $7S_{19}$ has also collapsed to P_2, or in case it has not, to know how it is positioned on the slice $h_{13} = 3$. There are four possible situations:

(a) Parts $5.7L_5$ and $7S_{19}$ have collapsed at point P_2 in slice $h_{13} = 3$ (this is the situation represented in Figure 4.22). We observe that, in this case, parts $5S_{18}$ and V_{53} must collapse at point P_2 in slice $h_{13} = 3$.

(b) Parts $5.7L_5$ and $5S_{18}$ have collapsed at point P_2 in slice $h_{13} = 3$, but part V_{53} continues existing (and hence also $7S_{19}$) is slice $h_{13} = 3$ as a small bubble attached to P_2.

(c) The lines $5.7L_5$ and $1.5L_3$ (see Fig. 4.4) become closer and closer until they collapse in the slice h_{13}. In this case, in the slice h_{13} the parts V_{53} and $7S_{19}$ are maintained and $5S_{19}$ disappears.

(d) Parts $5S_{19}$ and $5S_{18}$ continue existing in the slice h_{13}, and hence also V_{53} and $7S_{19}$.

Numerical analysis allows us to assure that the situation (c) is not possible because we can easily check that part $5S_{19}$ continues existing in slice h_{13}. On the other hand, trying to determine in which situation (a), (b) or (d) we are is very difficult since the regions considered are so small and hence numerical analysis becomes a difficult task. Moreover, the phase portrait in point P_2 (see Fig. 4.22) in slice h_{13} (that is, the point in slice h_{13} where intersect the lines $3.5L_2$ and $1.5L_2$) is compatible with the situations (a), (b) and (d), fact that makes even more difficult to know in which situation we are. However, very careful numerical analysis suggest that we are in situation (a), which is represented in Figure 4.22. Hence, since the final objective is to get a coherent bifurcation diagram and the situation (a) is coherent and the one suggested by our numerical research, we assume it is the real situation. Anyway, the situations (a), (b) and (d) give us the same topological phase portraits so the previous uncertainty is not a big problem in terms of phase portraits.

Finally, we must say that the phase portrait corresponding to part P_2 is new, that is, it has not been found in any of the previously studied slices. Therefore, slice h_{13} gives us a new phase portrait.

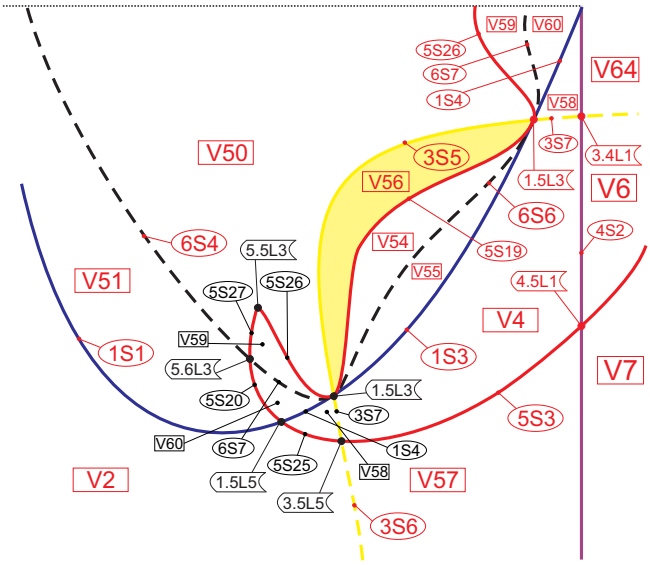

Fig. 4.23: Sub-region of the generic slice $h_{14} = 3 - \epsilon_4$ in which the topological changes have appeared.

We now move to the next slice in list (10), which corresponds to the generic slice $h_{14} = 3 - \epsilon_4$ (see Fig. 4.23), where ϵ_1 is a certain positive value. As we can appreciate in Fig. 4.23, the difference with the slice h_{13} (see Fig. 4.22) is that the pointed part of $(\mathcal{S}_5)$ has broken through $(\mathcal{S}_1)$ and $(\mathcal{S}_6)$ in the slice h_{14}, thus giving rise to 15 apparently new regions marked in black in Fig. 4.23. We point out that despite all the 15 previous regions seem to be new, eight of them are not (precisely, $1.5L_3$, $3S_7$, V_{58}, $5S_{26}$, V_{59}, V_{60}, $6S_7$ and $1S_4$). Indeed, notice that in Figure 4.23 there are exactly two regions labeled as $1.5L_3$ (resp. $3S_7$, V_{58}, $5S_{26}$, V_{59}, V_{60}, $6S_7$ and $1S_4$), one of them marked in red and the other in black, which seem to correspond to different regions. The fact that they are the same region will become clear later as we keep decreasing the value of h. The remaining sub-regions of the slice h_{14} remain topologically unchanged with respect to the slice h_{13}. Moreover, slice h_{14} brings two new topological phase portraits: The one corresponding to part $5S_{20}$ (which is topologically the same as the ones in parts $5S_{27}$ and $5.6L_3$) and the one corresponding to part $1.5L_5$. See Tables 7.1-7.9 in Section 7.

The next slice listed in (10) is the non-algebraic singular slice $h_{15} = 3 - \epsilon_5^*$ (see Fig. 4.24), where the value ϵ_5^* satisfies that $0 < \epsilon_4 < \epsilon_5^*$. Consider the two topological ellipses V_{19} and V_{20} in Fig. 4.21. As we move from h_{12} to h_{15} these two ellipses collapse to single point, say d, in the slice h_{15}, which belongs to

curve $1.7L_1$. This justifies that the two apparently distinct parts labeled as $1.7L_1$ in Fig. 4.21 are the same part, as we have commented before.

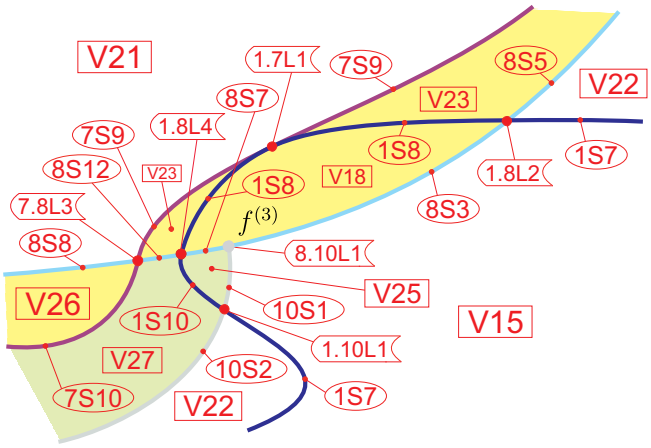

Fig. 4.24: Sub-region of the non-algebraic singular slice $h_{15} = 3 - \epsilon_5^*$ in which the topological changes have appeared.

The remaining sub-regions of the slice h_{15} remain topologically unchanged with respect to the slice h_{14}. In addition, the slice h_{15} does not bring us any new topological phase portrait.

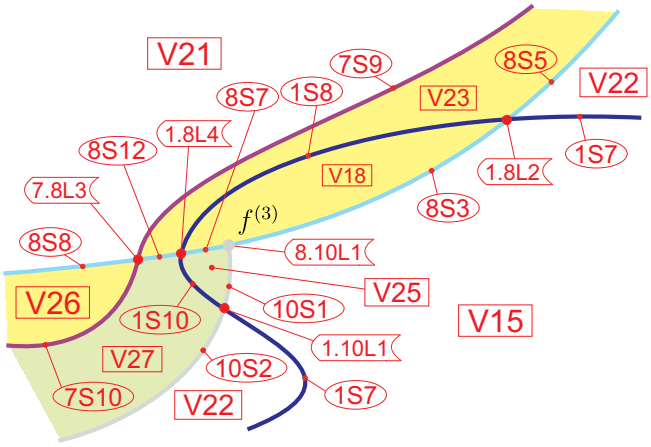

Fig. 4.25: Sub-region of the generic slice $h_{16} = 3 - \epsilon_5$ in which the topological changes have appeared.

We move now to the next slice listed in (10), which is the generic slice $h_{16} = 3 - \epsilon_5$ (see Fig. 4.25), where the value ϵ_5 satisfies that $0 < \epsilon_4 < \epsilon_5^* < \epsilon_5$. As we can appreciate in Fig. 4.25, the curve $1.7L_1$ has detached from the surface $(\mathcal{S}_7)$ (see Fig. 4.24). This proves that the two apparently different parts labeled as $7S_9$, V_{23} and $1S_8$ in Fig. 4.21 are indeed the same part, as mentioned before. The remaining sub-regions of the slice h_{16} remain topologically unchanged with respect to the slice h_{15}. In addition, we point out that the slice h_{16} does not bring us any new topological phase portrait.

In the next slice listed in (10), which is the algebraic singular slice $h_{17} = 5/\sqrt{3}$ (see Fig. 4.26), the surface $(\mathcal{S}_1)$ coincides with the region with $f^{(3)}$. Consequently, part $8S_7$ in Fig. 4.25 disappears and a new point called P_6 appears (see Fig. 4.26). The remaining sub-regions of the slice h_{17} remain topologically unchanged with respect to the slice h_{16}. Moreover, since the phase portrait in P_6 is equivalent to the one in $1S_8$, we conclude that the slice h_{17} does not bring us any new topological phase portrait.

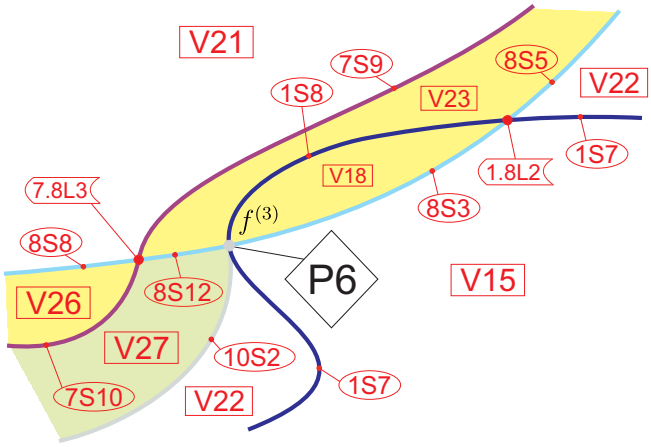

Fig. 4.26: Sub-region of the algebraic singular slice $h_{17} = 5/\sqrt{3}$ in which the topological changes have appeared.

In the next slice listed in (10), which is the generic slice $h_{18} = 2.85$ (see Fig. 4.27), the blue surface $(\mathcal{S}_1)$ has detached from the region with $f^{(3)}$, thus making disappear the point P_6 in Fig. 4.26 and also giving rise to 3 apparently new regions marked in black in Fig. 4.27. However, despite the three previous regions seem to be new, two of them are not new (precisely, $8S_5$ and $1.8L_2$). Indeed, notice that in Figure 4.27 there are exactly two regions labeled as $8S_5$ (resp. $1.8L_2$), one of them marked in red and the other in black, which seem to correspond to different regions. The fact that they are the same region will become clear later as we keep decreasing the value of h. Finally, the apparently new curve $8.10L_2$ is a truly new region, which did not existed in the previous slices in (10). The remaining sub-regions of the slice h_{18} remain topologically unchanged with respect to the slice h_{17}. In addition, we point out that the slice h_{18} does not bring us any new topological phase portrait be-

cause the phase portrait in part $8.10L_2$ is equivalent to the one in part $8S_5$.

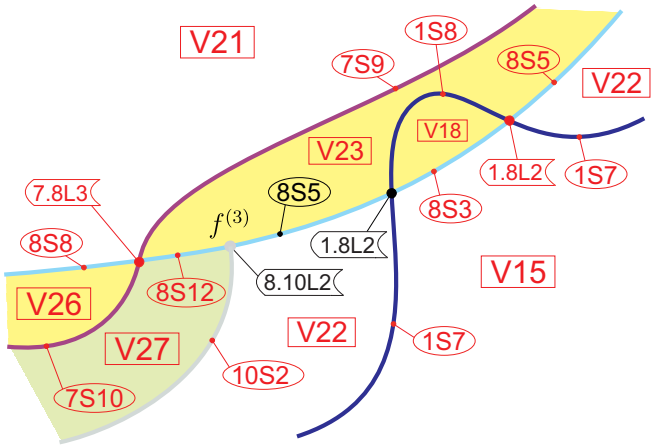

Fig. 4.27: Sub-region of the generic slice $h_{18} = 2.85$ in which the topological changes have appeared.

In the next slice listed in (10), which is the algebraic singular slice $h_{19} = 2\sqrt{2}$, the changes appear in two separated regions (see Fig. 4.28). On the one hand, the topological ellipse V_{18} in Fig. 4.27 collapses to a single point in slice h_{19}, say e, which of course belongs to curve $1.8L_2$ (see Fig. 4.28). The existence of e proves that the two apparently distinct parts labeled as $1.8L_2$ in Fig. 4.27 are indeed the same curve, as we have commented before.

On the other hand, the three topological ellipses V_{56}, V_{54} and V_{55} in Fig. 4.23 collapse to a single point as we move from h_{14} to h_{19}, say f, which of course belongs to the curve $1.5L_3$ (see Fig. 4.28). The existence of f proves that the two apparently distinct parts labeled as $1.5L_3$ in Fig. 4.23 are indeed the same curve, as we have commented before.

Finally, notice that as we move from h_{14} to h_{19} the lines $4.5L_1$ and $3.4L_1$ in Fig. 4.23 become closer and closer until they collapse in the slice h_{19}, thus generating a new point called P_8 (see Fig. 4.28), whose phase portrait is the same as the one in $4.5L_1$ (see Fig. 4.23). Notice also that regions $4S_2$ and V_6 in Fig. 4.23 collapse in P_8 in the slice h_{19}.

The remaining sub-regions of the slice h_{19} remain topologically unchanged with respect to the slice h_{18}. Moreover, slice h_{19} does not bring us any new phase portrait.

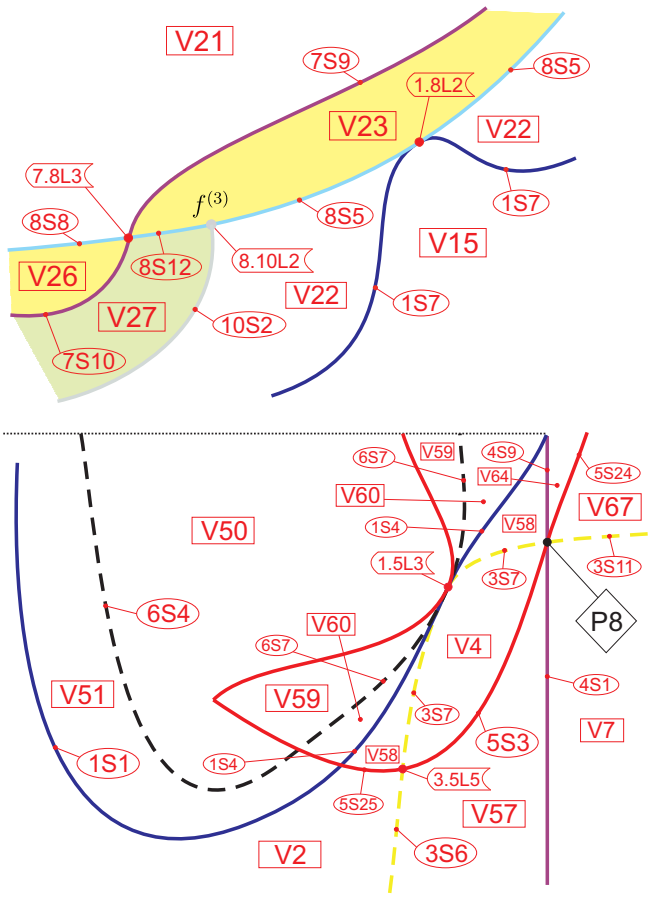

Fig. 4.28: The two disconnected sub-regions of the singular algebraic slice $h_{19} = 2\sqrt{2}$ in which the topological changes have appeared.

The next slice listed in (10) is the generic slice $h_{20} = 2.8$. In this slice, the changes appear in two separated regions (see Fig. 4.29). On the one hand, the contact between $(\mathcal{S}_1)$ and $(\mathcal{S}_8)$ in Fig. 4.28 has disappeared in slice h_{20} (see Fig. 4.29). In particular, this proves that the two apparently distinct regions labeled as V_{22}, $1S_7$ and $8S_5$ in Fig. 4.27 are indeed the same region, as commented before (see also Remark 4.33).

On the other hand, as we can appreciate in Fig. 4.29, the red surface $(\mathcal{S}_5)$ has crossed the intersection between $(\mathcal{S}_3)$ and $(\mathcal{S}_4)$, thus giving rise to 7 apparently new regions marked in black in Fig. 4.29 (the topological triangle V_2 and its six bordering regions). We point out that despite all the 7 previous regions seem to be new, four of them are not (precisely, V_2, $5S_{25}$, $3.5L_5$ and $3S_6$). Indeed, notice that in Figure 4.29 there are exactly two regions labeled as V_2 (resp. $5S_{25}$, $3.5L_5$ and $3S_6$), one of them marked in red and the other in black, which seem to correspond to different regions. However,

the fact that they are indeed the same region will become clear later as we keep decreasing the value of h.

The remaining sub-regions of the slice h_{20} remain topologically unchanged with respect to the slice h_{19}. Moreover, clearly slice h_{20} does not bring us any new phase portrait.

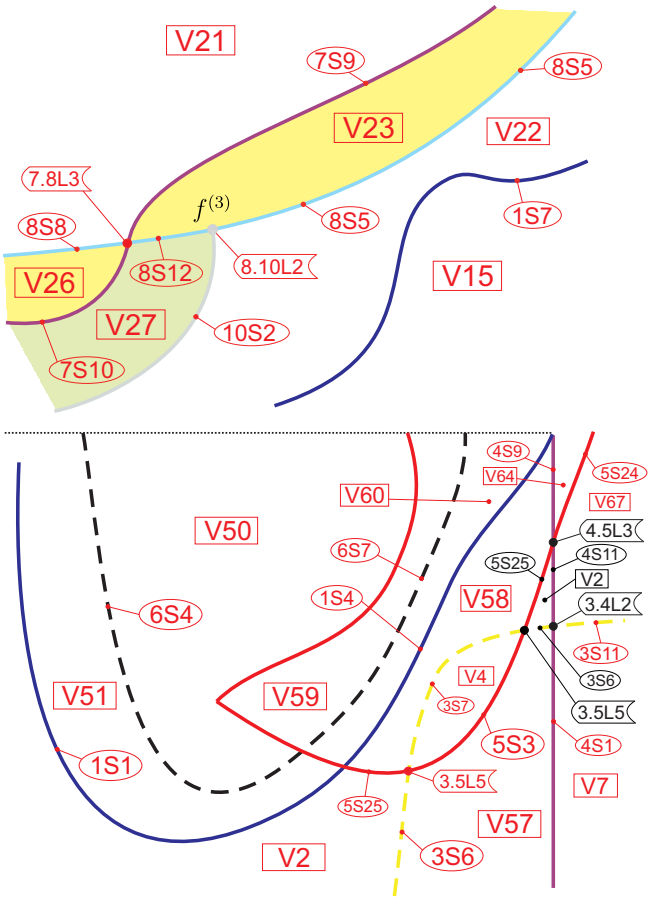

Fig. 4.29: The two disconnected sub-regions of the generic slice $h_{20} = 2.8$ in which the topological changes have appeared.

In the next slice listed in (10), which is the algebraic singular slice $h_{21} = \sqrt{243/32}$, the topological ellipse V_4 in Fig. 4.29 collapse to a single point in h_{21}, say g, which of course belongs to curve $3.5L_5$ (see Fig. 4.30). The existence of g proves that the two apparently distinct parts labeled as $3.5L_5$ in Fig. 4.29 are indeed the same curve, as we have commented before. The remaining sub-regions of the slice h_{21} remain topologically unchanged with respect to the slice h_{20}, and slice h_{21} does not bring us any new phase portrait.

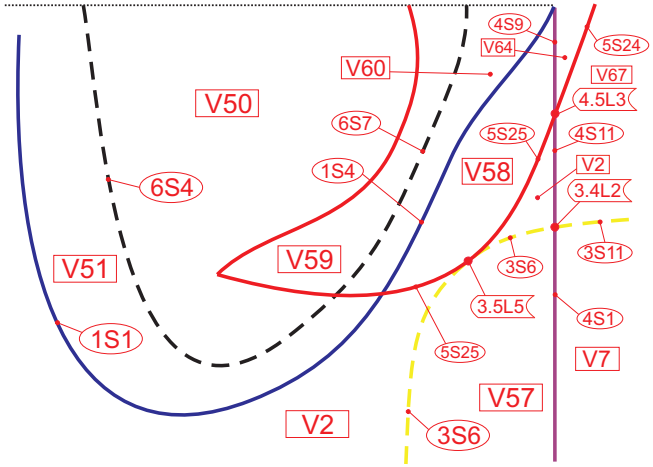

Fig. 4.30: Sub-region of the algebraic singular slice $h_{21} = \sqrt{243/32}$ in which the topological changes have appeared.

The next slice listed in (10) is the generic slice $h_{22} = 2.5$. Notice that the contact between $(\mathcal{S}_5)$ and $(\mathcal{S}_3)$ in Fig. 4.30 has disappeared in slice h_{22} (see Fig. 4.31). In particular, this proves that the two apparently distinct regions labeled as V_2, $3S_6$ and $5S_{25}$ in Fig. 4.29 are indeed the same region, as commented before. The other sub-regions of the slice h_{22} remain topologically unchanged with respect to the slice h_{21}, and clearly slice h_{22} does not bring us any new phase portrait.

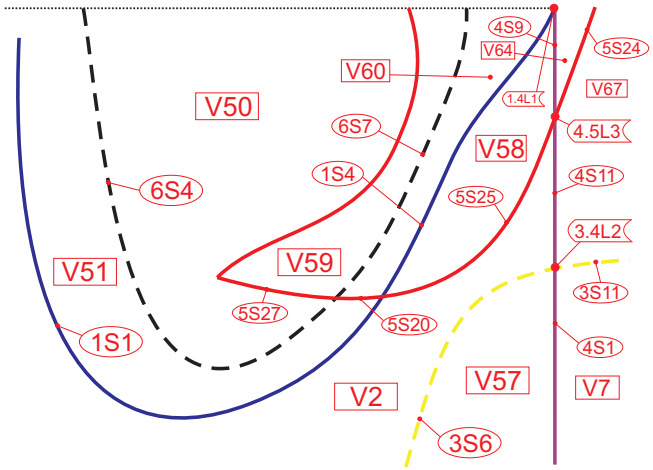

Fig. 4.31: Sub-region of the generic slice $h_{22} = 2.5$ in which the topological changes have appeared.

If we now move to the next slice listed in (10), which is the singular algebraic slice $h_{23} = 2$, we observe that the topological triangle V_{58} in Fig. 4.31 has collapsed to a single point P_9, which of course is a new region (see Fig. 4.32).

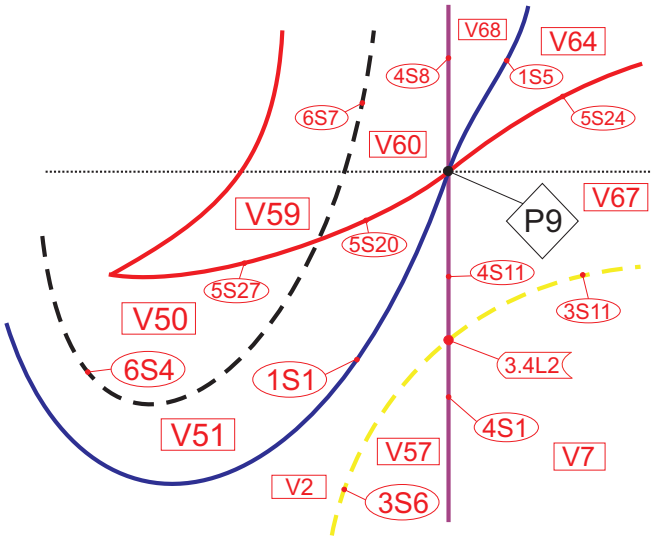

Fig. 4.32: Sub-region of the singular algebraic slice $h_{23} = 2$ in which the topological changes have appeared.

We point out that the phase portrait corresponding to the point P_9 is new, that is, it has not been found in the previously studied slices. The other sub-regions of the slice h_{23} remain topologically unchanged with respect to the slice h_{22}.

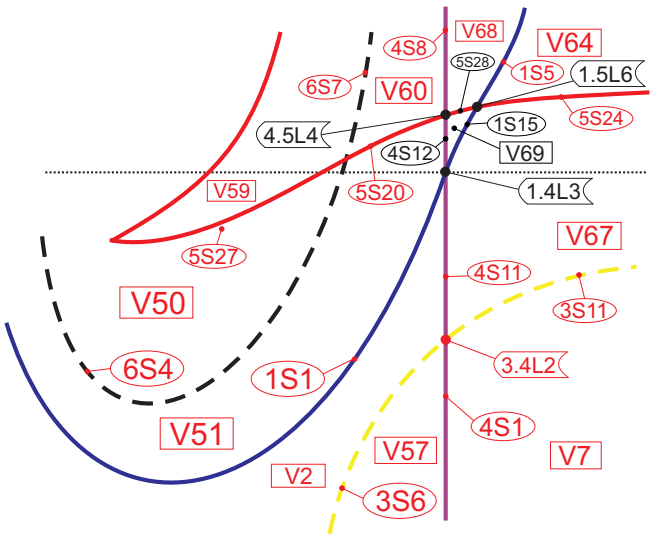

Fig. 4.33: Sub-region of the generic slice $h_{24} = 1.5$ in which the topological changes have appeared.

The next slice listed in (10) is the generic slice $h_{24} = 1.5$. As we can appreciate in Fig. 4.33, the difference with Fig. 4.32 is that the red surface $(\mathcal{S}_5)$ has crossed the intersection between $(\mathcal{S}_4)$ and $(\mathcal{S}_1)$, thus giving rise to 7 new regions marked in black in Fig. 4.33 (the topological triangle V_{69} and its six bordering regions). Moreover, six out of the seven previous regions (all of them except V_{69}) give us new topological phase portraits (see Tables 7.1-7.9 in Section 7). Let us emphasize that the previous fact is very curious, since all the phase portraits in the boundary of V_{69} are new but the phase portrait in V_{69} has already appeared.

The topological changes in the four following slices happen in a distinct regions than in all the previous slices. The next slice listed in (10) is the singular algebraic slice $h_{25} = 1$.

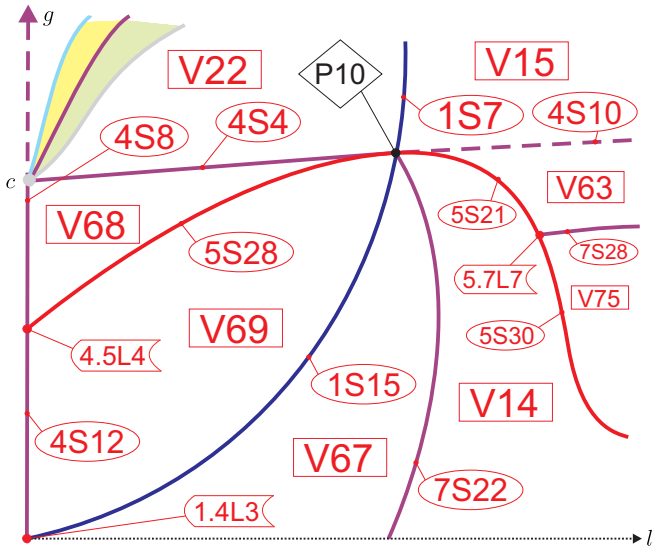

Fig. 4.34: Sub-region of the singular algebraic slice $h_{25} = 1$ in which the topological changes have appeared.

Consider the lines $4.5L_2$ and $1.4L_2$ in Fig. 4.7, which of course still existing in slice h_{24}. As we move down from h_2 to h_{25} the lines $4.5L_2$ and $1.4L_2$ become closer and closer until they collapse to a single point called P_{10} in slice h_{25} (see Fig. 4.34). Notice that parts V_{64}, V_{65}, $7S_{21}$, $1S_5$ and $4S_3$ (see Fig. 4.7) also "collapse" at P_{10} in slice h_{25}. Moreover, the phase portrait corresponding to part P_{10} is new.

The next slice listed in (10) is the generic slice $h_{26} = 0.3$, which is represented in Fig. 4.35. As we can see in Fig. 4.35, the difference with Fig. 4.34 is that the red surface $(\mathcal{S}_5)$ has crossed the intersection between $(\mathcal{S}_4)$ and $(\mathcal{S}_1)$, thus giving rise to 7 new regions marked in black in Fig. 4.35 (the topological triangle V_{70} and its six bordering regions). Moreover, three out of the seven previous regions (which are $5S_{29}$, $1.5L_7$ and $4.5L_5$) give us new topological phase portraits (see Tables 7.1-7.9 in Section 7).

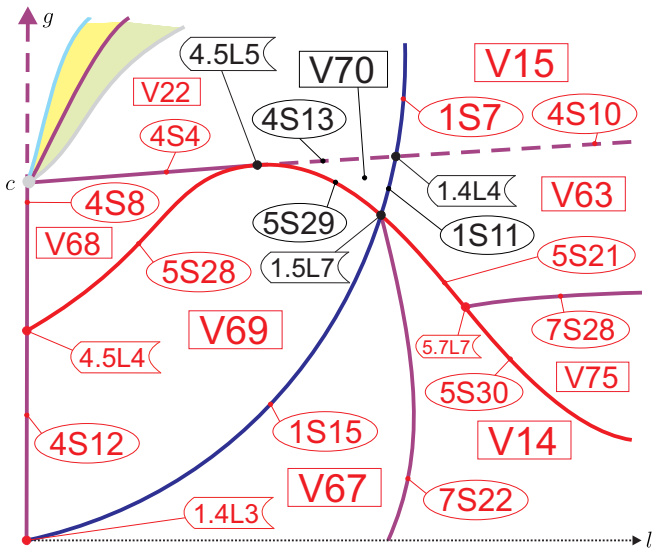

Fig. 4.35: Sub-region of the generic slice $h_{26} = 0.3$ in which the topological changes have appeared.

The next slice listed in (10) is the singular non-algebraic slice $h_{27} = 0.3 - \epsilon_6^*$, where ϵ_6^* is a certain positive value (see Fig. 4.36). When we move from h_{26} to h_{27}, the curves $5.7L_7$ and $1.5L_7$ (see Fig. 4.35) become closer and closer until they collapse at a single point called P_{16} in slice h_{27} (see Fig. 4.36). Of course, P_{16} is a new region and its associated topological phase portrait is also new, as one can check looking at Tables 7.1-7.9 in Sect. 7.

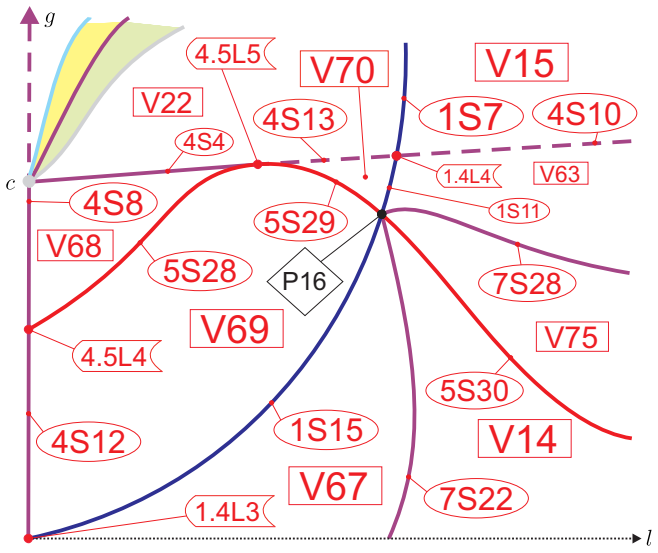

Fig. 4.36: Sub-region of the singular non-algebraic slice $h_{27} = 0.3 - \epsilon_6^*$ in which the topological changes have appeared.

The penultimate slice listed in (10) is the generic slice $h_{28} = 0.3 - \epsilon_6$ where ϵ_6 satisfies that $0 < \epsilon_6^* < \epsilon_6$ (see Fig. 4.37). The difference with the slice h_{27} (see Fig. 4.36) is that the purple surface $(\mathcal{S}_7)$ has crossed the intersection of $(\mathcal{S}_5)$ and $(\mathcal{S}_1)$, thus giving rise to seven new regions colored in black in Fig. 4.37, which are the topological triangle V_{24} and its six bordering regions. We point out that the phase portraits corresponding to the seven previous regions are new, as the reader can check in Tables 7.1-7.9 in Section 7.

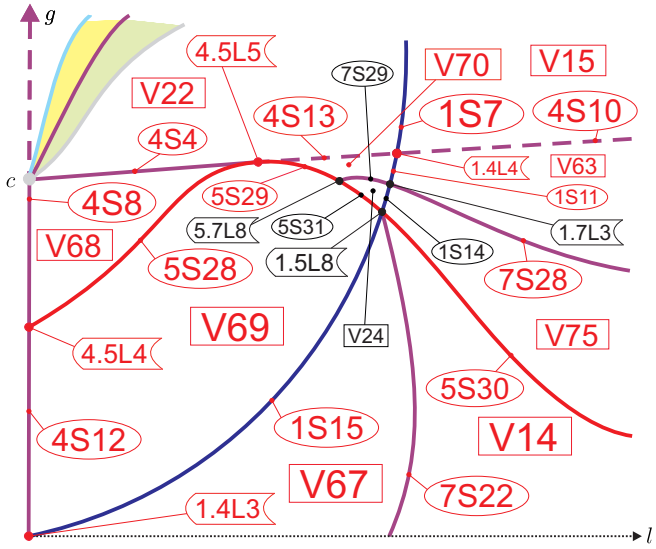

Fig. 4.37: Sub-region of the generic slice $h_{28} = 0.3 - \epsilon_6$ in which the topological changes have appeared.

Since the slice h_{28} is the penultimate slice listed in (10), in Fig. 4.38 we have shown the complete bifurcation diagram in slice h_{28}. This will allow us to understand better the transition from h_{28} to $h_{29} = 0$ that we are going to study next.

So let's perform the study of the slice $h_{29} = 0$ and show that the transition from h_{28} to h_{29} is coherent in terms of continuity. First of all, notice that in the limit $h \to 0$, the bifurcation diagram (of the algebraic surfaces) tends to be the one shown in Fig. 4.39.

The slice $h_{29} = 0$ is an algebraic bifurcation surface which has, as we will see in a moment, some particularities.

For completeness, recall that the slice $h = 0$ is obtained by considering $h = 0$ and $m = 1$ in the normal form (5), which becomes:

$$\begin{cases} \dot{x} = -y + gx^2 - 2y^2 \\ \dot{y} = x + lx^2 + 2xy \end{cases} \tag{12}$$

Lemma 4.56. *The change $(x, y, t) \to (-x, y, -t)$ transforms a system (12) with parameters (l, g) into a system (12) with parameters $(-l, g)$. Therefore,*

the bifurcation diagram in the slice $h_{29} = 0$ is symmetric with respect to the g-axis.

Proof. Direct computation. Left to the reader. ■

Another crucial fact to take into account is that, when studying the slice $h_{29} = 0$, the surface $(\mathcal{S}_3)$ must be redefined, which has been already done in Remark 4.3. Precisely, in the previous remark we have concluded that in the slice $h = 0$ the surface $(\mathcal{S}_3)$ must be redefined as the set $(l, -1)$ with $l \neq 0$. In the previous set, we have exactly two weak singularities: the origin, which is a center, and a finite saddle (see Remark 4.3 for more details).

Notice also that in $h_{29} = 0$, surface $(\mathcal{S}_6)$ does not make sense as a consequence of Remark 4.5.

Remark 4.57. Despite in the slice $h = 0$ the surface $(\mathcal{S}_8)$ must not be redefined, it is interesting to mention that it has the following expression in the slice $h = 0$: $l(g + 1) = 0$ (see Sect. 4.1). Moreover, as we have explained in Remark 4.2, if the origin is a weak focus of order greater than one in the slice $h = 0$ (fact that happens if we are in $(\mathcal{S}_8)$), then it must be of infinite order, that is, a center. Furthermore, recall that the weak singularities in the surface $(\mathcal{S}_8)$ have been studied in detail in Remark 4.6.

Finally, an interesting property of the slice $h = 0$ is that, generically, the finite saddle-node has been transformed into a cusp, as stated in the following lemma.

Lemma 4.58. *Assume that $l \neq 0$. Then, the singular point $(0, -1/2)$ of system (12) is a nilpotent cusp of multiplicity two, denoted as $\widehat{cp}_{(2)}$ (see Appendix A of [Artés* et al.*, 2021a]).*

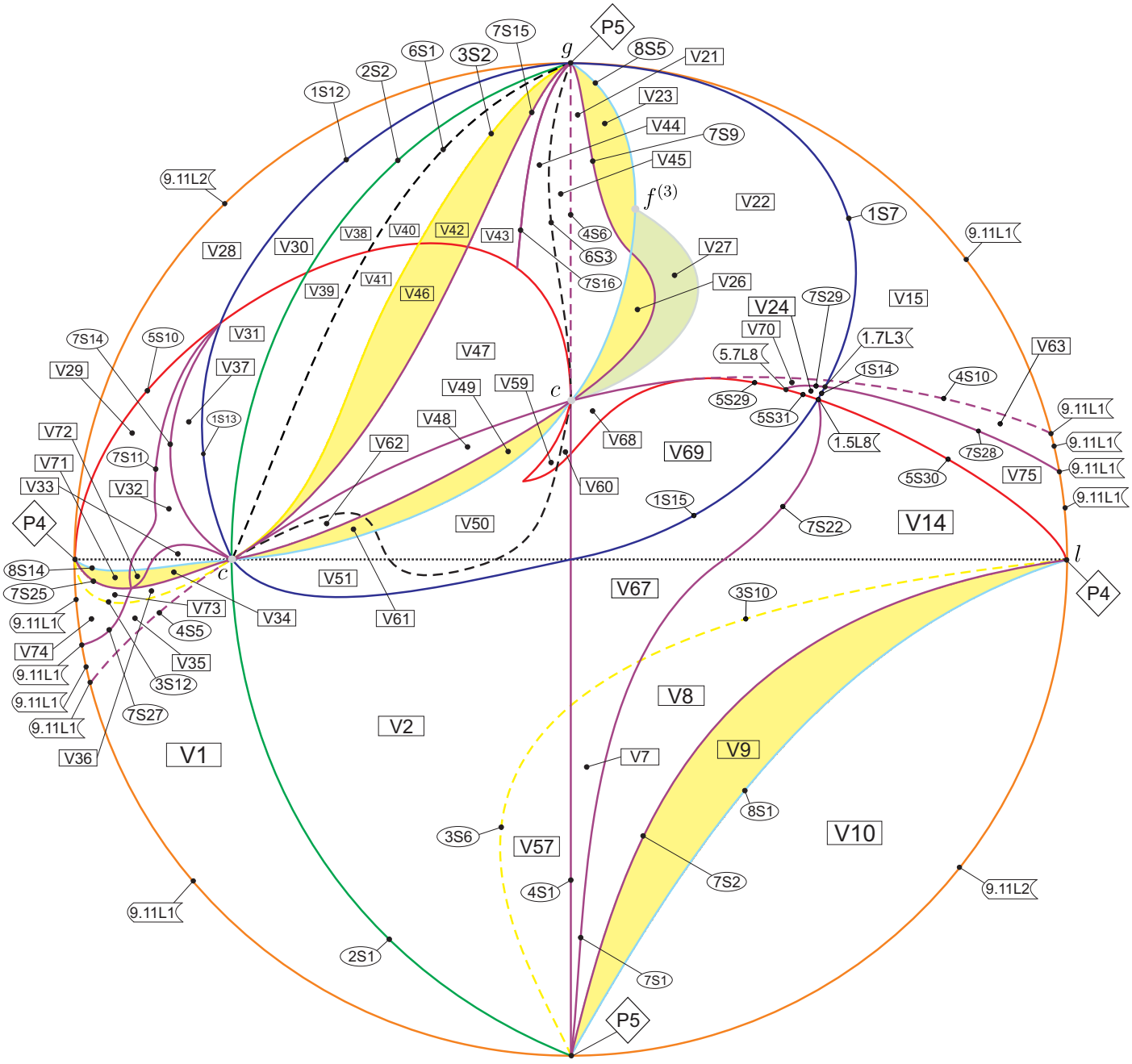

Fig. 4.38: Complete bifurcation diagram for slice $h_{28} = 0.3 - \epsilon_6$ in the disc with labels only in some parts.

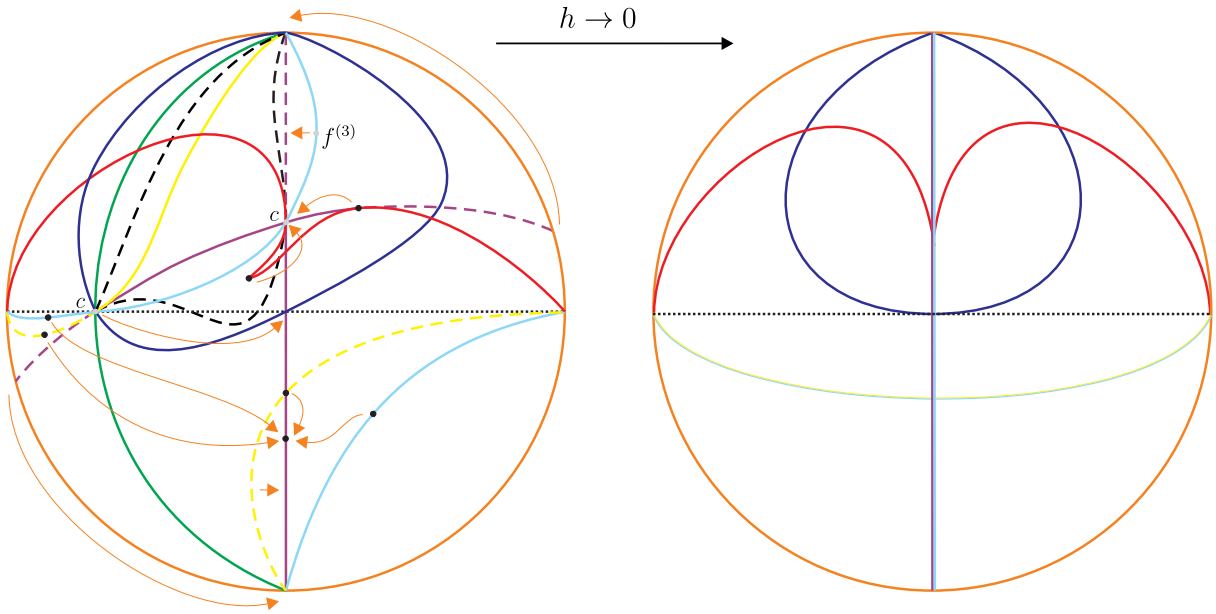

Fig. 4.39: Transition from $h \leq h_{28}$ to $h_{29} = 0$. The orange arrows show the movement that the surfaces do as $h \to 0$.

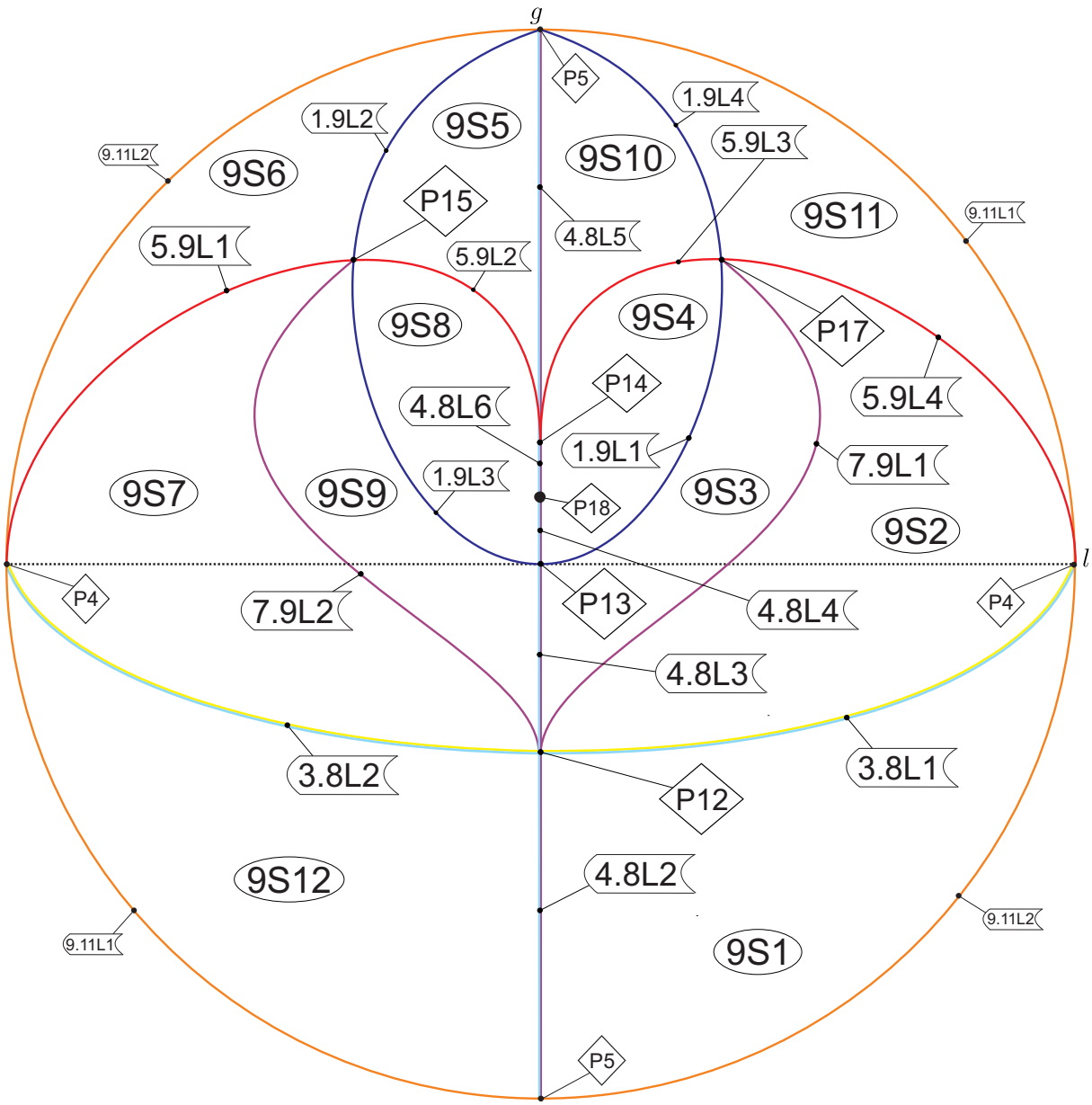

Fig. 4.40: Complete bifurcation diagram for slice $h_{29} = 0$.

Proof of Lemma 4.58. First, notice that in the slice $h = 0$ the singularity $(0, -1/2)$ is nilpotent. Indeed, if we compute the Jacobian matrix of system (12) at $(0, -1/2)$ we get

$$\begin{pmatrix} 0 & 1 \\ 0 & 0 \end{pmatrix}$$

Said that, notice that since we are assuming $l \neq 0$ and in $h = 0$ surface $(\mathcal{S}_2)$ is given by $l = 0$ (see Remark 4.60), we deduce that in $h = 0$, $l \neq 0$ we can have two and only two distinct situations: (1) If we are outside $(\mathcal{S}_1)$, then we have two finite singularities of multiplicity one (one of them is the origin), and another of multiplicity two, which is $(0, -1/2)$; (2) If we are in $(\mathcal{S}_1)$, then we have one finite singularity of multiplicity one (the origin) and one finite singularity of multiplicity two, which is $(0, -1/2)$. In both situations, $(0, -1/2)$ is a singularity of multiplicity two. But recall that $(0, -1/2)$ is nilpotent, and therefore, since system (12) is quadratic, according to Appendix A in [Artés *et al.*, 2021a] we deduce that $(0, -1/2)$ must be a cusp of multiplicity two, as we wanted to prove. ■

We now have finished describing the algebraic curves appearing in the slice $h_{29} = 0$. In Fig. 4.40 we present this slice completely and properly la-

beled. We draw special attention to the fact that some of the nonalgebraic curves (numerically detected and which existence was proved before) still remain in this slice and they maintain the same relative positions with respect to the algebraic curves in the transition from slice h_{28} to slice $h_{29} = 0$; numerical tools support this claim.

Parts in slice h_{28}	Parts in slice $h_{29} = 0$	Parts in slice h_{28}	Parts in slice $h_{29} = 0$
V_1	$4.8L_2$, $4.8L_3$	V_2	$4.8L_2$, $4.8L_3$
V_7	$4.8L_2$	V_8	$3.8L_1$, $4.8L_2$
V_9	$3.8L_1$, $4.8L_2$	V_{10}	$9S_1$
V_{14}	$9S_2$	V_{15}	P_5
V_{21}	$4.8L_5$	V_{22}	$4.8L_5$
V_{23}	$4.8L_5$	V_{24}	$9S_{10}$
V_{26}	$4.8L_5$	V_{27}	$4.8L_5$
V_{28}	$9S_6$	V_{29}	$9S_7$
V_{30}	$9S_5$	V_{31}	$9S_8$
V_{32}	$7.9L_2$	V_{33}	$4.8L_3$
V_{34}	$4.8L_3$	V_{35}	$4.8L_2$, $4.8L_3$
V_{36}	$4.8L_3$	V_{37}	$9S_9$
V_{38}	$4.8L_5$	V_{39}	$4.8L_4$, $4.8L_6$
V_{40}	$4.8L_5$	V_{41}	$4.8L_4$, $4.8L_6$
V_{42}	$4.8L_5$	V_{43}	$4.8L_5$
V_{44}	$4.8L_5$	V_{45}	$4.8L_5$
V_{46}	$4.8L_4$, $4.8L_6$	V_{47}	$4.8L_4$, $4.8L_6$
V_{48}	$4.8L_4$, $4.8L_6$	V_{49}	$4.8L_4$, $4.8L_6$
V_{50}	$4.8L_4$, $4.8L_6$	V_{51}	$4.8L_4$, $4.8L_6$
V_{57}	$4.8L_2$	V_{59}	P_{14}
V_{60}	P_{14}	V_{61}	P_{13}
V_{62}	P_{13}	V_{63}	P_5
V_{67}	$9S_3$	V_{68}	P_{14}
V_{69}	$9S_4$	V_{70}	$4.8L_5$
V_{71}	$3.8L_2$	V_{72}	P_{12}
V_{73}	$3.8L_2$	V_{74}	$9S_{12}$
V_{75}	$9S_{11}$		

Table 4.2: Transition from slice h_{28} to $h_{29} = 0$. Here we present the correspondence between the volumetric regions from slice h_{28} and the respective parts from slice $h_{29} = 0$.

Remark 4.59. As explained in Remark 4.10, additional notation also will be used in the slice $h_{29} = 0$. Precisely, as in slice $h_{29} = 0$ we are in a surface, we point out that all the "generic" parts in this slice are labeled as $9S_j$ and the points as P_j. Regarding the lines, they are labeled as $i.9L_j$ except in two situations: the lines $g = -1$ and $l = 0$ (see Fig. 4.40). The one dimensional parts in the line $g = -1$ of $h_{29} = 0$ are denoted as $3.8L_j$. The reason is that, as we have mentioned before, the line $g = -1$ belongs to $(\mathcal{S}_8)$ in $h_{29} = 0$, and moreover we have already commented that in $h_{29} = 0$ the surface $(\mathcal{S}_3)$ must be redefined as the set of points of the form $(l, -1)$, $l \neq 0$. The one dimensional parts in the line $l = 0$ of $h_{29} = 0$ are denoted as $4.8L_j$. The reason is the following: Notice that when $h \to 0$ many surfaces "die" at $l = 0$ (see Fig. 4.39), so in order to denote the one dimensional parts in $l = 0$ of $h_{29} = 0$ we have chosen the two surfaces which are most representative, that is, surface $(\mathcal{S}_8)$ (because in $l = 0$ the origin is a weak focus of infinite order, i.e. a center. See Remark 4.57) and surface $(\mathcal{S}_4)$ (because in $l = 0$ of $h_{29} = 0$ the associated phase portrait has an invariant straight line corresponding to a connection of separatrices).

Remark 4.60. Notice that in the slice $h = 0$, the surface (S_2) has the following expression: $l = 0$ (see Sect. 4.1). We point out the previous fact because in Fig. 4.40 seems as if (S_2) does not appear, but this is not true. What happens is that in order to denote the lines in the axis $l = 0$ we have chosen the notation $4.8L_j$, as explained in Remark 4.59. However, in the line $l = 0$ a triple finite collision occurs.

In Table 4.2 we indicate the "death" of all volumetric parts from slice h_{28} to $h_{29} = 0$. Then, we have established the correspondence between the phase portraits of the slices h_{28} and $h_{29} = 0$. Therefore, the convergence from slice h_{28} to $h_{29} = 0$ is completely coherent.

To finish this section, let us make a couple of comments on the complete bifurcation diagram presented in Fig. 4.40.

First of all, consider the line $8.10L_2$ in Fig. 4.29. According to Remark 4.6, we know that $8.10L_2$ is a region in which the origin is a $f^{(3)}$. Moreover, as we have studied in detail in Remark 4.6, we know that the line $8.10L_2$ has the expression $[2h/5 : 4 : 1 : h]$, $h \in \mathbb{R}$, which of course arrives at slice $h = 0$ at $[0 : 4 : 1 : 0]$, that is, $(l, g) = (0, 4)$. The previous point is placed in part $4.8L_5$ in Fig. 4.40, and therefore the origin is a center in $(l, g) = (0, 4)$.

Secondly, notice that in the line $l = 0$ in

Fig. 4.40 there is a point colored in black called P_{18}, whose expression is $(l, g) = (0, 1)$. The phase portraits of regions $4.8L_4$, P_{18} and $4.8L_6$ is given in Fig. 4.41.

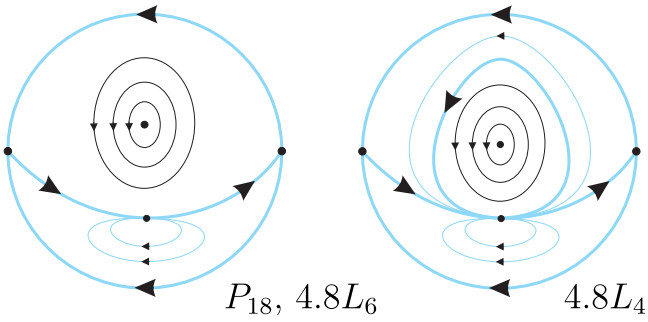

Fig. 4.41: Phase portraits of regions $4.8L_4$, P_{18} and $4.8L_6$.

Since the transition from $h_1 = +\infty$ to $h_{29} = 0$ that we have explained in detail is completely coherent, no more slices are needed for the complete coherence of the bifurcation diagram. So, all the values of h in (10) are sufficient for the coherence of the bifurcation diagram. Thus, we can affirm that we have described a complete bifurcation diagram for class $\overline{\textbf{Qwf1sn}}$, modulo islands and some other phenomena as we describe in detail in Section 5.

In `https://mat.uab.cat/~artes/articles/qwf1sn/qwf1sn.html` the reader can find a folder called **PhasePortraitsP4.zip** which contains the numerical examples (P4 files) that we have used to study the bifurcation diagram.

Moreover, as we have already commented throughout the previous sections, in the previous website you can find all the additional tools that we have used to perform our study, as for example all the programs needed to perform the computations and to obtain the plots, or additional pictures which are useful to understand better the bifurcation diagram.

5. Other relevant facts about the bifurcation diagram of $\overline{\mathbf{Qwf1sn}}$

In the previous section we have studied in full detail the bifurcation diagram for the class $\overline{\mathbf{Qwf1sn}}$. The bifurcation diagram we have obtained is completely coherent, i.e. in family (5), by taking any two points in the parameter space and joining them by a continuous curve, along this curve the changes in phase portraits that occur when crossing the different bifurcation surfaces can be completely explained. Nevertheless, we cannot be sure that this bifurcation diagram is the complete bifurcation diagram for $\overline{\mathbf{Qwf1sn}}$ due to the possibility of certain phenomena which we describe below:

5.1. Possible existence of "islands"

The first phenomenon we must take into account is the possible existence of "islands" inside a certain region R belonging to the partition of our parameter space given in Sect. 4, i.e. a subset of R which has escaped from our numerical research and which has associated a different phase portrait from the rest of the region R. In case of existence, these "islands" would not mean any modification of the nature of the singular points. So, on the border of these "islands" we could only have bifurcations due to connections of separatrices or multiple limit cycles, since all the surfaces corresponding to the nature of singular points are algebraic and we already have them completely located and controlled.

In case of existence of an "island" surrounded by a non-algebraic bifurcation surface S, we should still be able to join two representatives of any two parts of the parameter space with a continuous curve either without crossing such bifurcation surface, or in case the curve crosses it, it must do so an even number of times without tangencies, otherwise one must take into account the multiplicity of the tangency, so the total number must be even. This is why we call these potential regions "islands".

An example of a potential "island" could be a topological three-dimensional ball B placed inside a three-dimensional part of our bifurcation diagram, satisfying that in ∂B appears a double limit cycle (i.e. ∂B is a part of $(\mathcal{S}_{10})$) and in $Int(B)$ the double limit cycle splits in two simple limit cycles.

We recall that in none of the studies of this typology (see Sect. 1) has been detected an "island".

We also point out that in case of existence, these "islands" could be infinitesimally small and hence they become practically impossible to detect.

5.2. Possible existence of more non-algebraic singular slices

The second phenomenon we must take into account is the possible existence of more non-algebraic singular slices.

In Remarks 4.15, 4.17, 4.20, 4.22, 4.26, 4.29, 4.40 and 4.42 (and also in some other parts in Sect. 4) we have exposed some theoretical feasible intersections between surfaces and other potential situations. Despite a careful numerical analysis suggests that previous situations do not happen, there exists the theoretical possibility that some of them happen in small regions that we have not detected numerically.

It is clear that the potential situations mentioned in previous remarks could generate more singular non-algebraic slices that the ones we have listed in (10). However, as explained in the previous section, since the final objective is to get a complete bifurcation diagram in terms of coherence and the one we have obtained is, then we can assume that our study is finished, despite we always have to take into account that we cannot be sure that we have not left out any non-algebraic singular slice.

5.3. Possible intersection of a loop branch of surface $(\mathcal{S}_7)$ with a weak saddle branch of surface $(\mathcal{S}_3)$

A potential situation of particular interest is the one described in Remarks 4.15 and 4.29. These remarks warn us about the possible existence of intersections between a loop branch of $(\mathcal{S}_7)$ and a weak saddle branch of $(\mathcal{S}_3)$. In what follow we describe this previous situation in detail: We consider an elemental saddle (see Sect. 3.1) of a quadratic system X, say p. We define the *hyperbolicity ratio* of p as the value $r = -\lambda_1/\lambda_2$, where $\lambda_1 < 0 < \lambda_2$ are the two eigenvalues of $DX(p)$. In addition, the elemental saddle p is called *strong* if $\lambda_1 + \lambda_2 \neq 0$ and *weak* if $\lambda_1 + \lambda_2 = 0$ (see [Artés *et al.*, 2021a] for more details). If now we consider a loop associated to p (which must have a unique singular point in

its interior, being a focus or a center; see item **(vii)** in Appendix B.1), it is well known that if $|r| > 1$ then the loop is internally attractor and if $|r| < 1$ the loop is internally repellor (see [Perko, 2000], for example). If $r = 1$ (i.e. p is weak), the loop can be either internally attractor/repellor (if p is a $s^{(i)}$ for $i = 1, 2, 3$) or only internally stable (if p is a weak saddle of infinite order). In our particular case, if a loop branch of $(\mathcal{S}_7)$ associated to a finite saddle crosses a weak saddle branch of $(\mathcal{S}_3)$ at a certain point, say A, then in A the loop must be internally attractor or repellor since it is surrounding the origin being a $f^{(1)}$ (and hence, the saddle p must be a $s^{(1)}$. See Thm. 6.2 in [Artés *et al.*, 2021a]). As a consequence, in one of the two parts of the loop branch of $(\mathcal{S}_7)$ delimited by A, a simple limit cycle surrounding the origin must appear bifurcating from the loop.

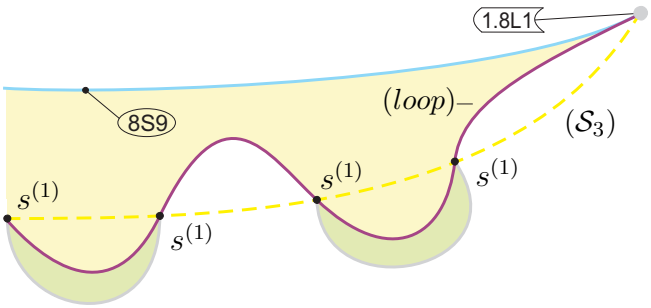

Fig. 5.1: Possible situation in case that a loop branch of $(\mathcal{S}_7)$ intersects a weak saddle branch of $(\mathcal{S}_3)$ many times.

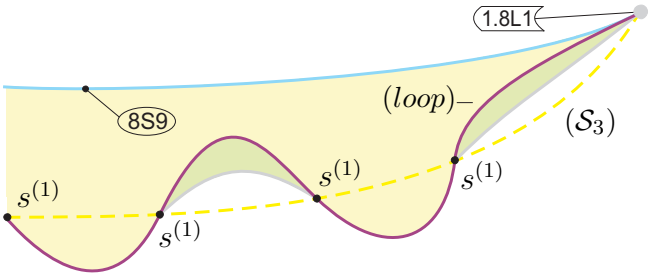

Fig. 5.2: Possible situation in case that a loop branch of $(\mathcal{S}_7)$ intersects a weak saddle branch of $(\mathcal{S}_3)$ many times and with the limit cycle in $(\mathcal{S}_7)$ appearing at the other side of $(\mathcal{S}_3)$.

A potential intersection between $(\mathcal{S}_7)$ and $(\mathcal{S}_3)$ near $8S_9$ is described in Fig. 5.4 (see Remark 4.15), in which a second simple limit cycle must also be generated. However, it could also happen that $(\mathcal{S}_7)$ intersects many times $(\mathcal{S}_3)$ or that the limit cycle in the loop branch of $(\mathcal{S}_7)$ appears in the other side of $(\mathcal{S}_3)$. In Figs. 5.1 and 5.2 we have presented the two previous general situations near $8S_9$.

Remark 5.1. In Figs. 5.1, 5.2 and 5.4 we have colored the regions with one simple limit cycle with a softer yellow color than the one used in Sect. 4, in order to be able to visualize the dashed branches of surface $(\mathcal{S}_3)$ contained in the regions with one simple limit cycle.

The possible intersections regarding loop branches of surface $(\mathcal{S}_7)$ and weak saddle branches of surface $(\mathcal{S}_3)$ near $8S_1$ (see Remarks 4.29) can be described analogously.

Remark 5.2. The phenomenon we have just illustrated is a way to generate limit cycles from a graphic without breaking it, and of course can be generalized to more complicated graphics (see [Perko, 2000], for instance).

Finally, we point out that despite the previous potential situations are theoretical feasible in our family, after a careful numerical analysis we have no evidences of their existence, despite they could exist in some small places which have escaped from our numerical research.

5.4. A potentially impossible situation of four limit cycles surrounding the same focus

In Remarks 4.40 and 4.42 we have warned of the possible situation in which $10S_1$ (resp. $10S_2$) crosses completely $7S_5$ (resp. $7S_{10}$) in some small places we have not detected. However, we conjecture that previous situation does not happen since it will imply the existence of a quadratic system with four limit cycles surrounding the same focus, which is firmly believed to be false as explained in Remark 4.40, despite it is not proved yet.

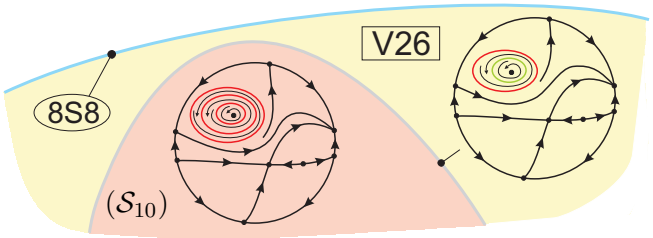

Fig. 5.3: Situation in case $10S_2$ crosses $7S_{10}$.

Let us explain how the four limit cycles would be generated in case that previous intersections occur. If $10S_2$ crosses $7S_{10}$, then we must have the situation described in Fig. 5.3. Since the phase portrait in the red region has three limit cycles surrounding the origin (which is a $f^{(1)}$), adding the trace in (5) we can generate a fourth limit cycle surrounding the origin by Hopf. The situation regarding $10S_1$ and $7S_5$ is analogous.

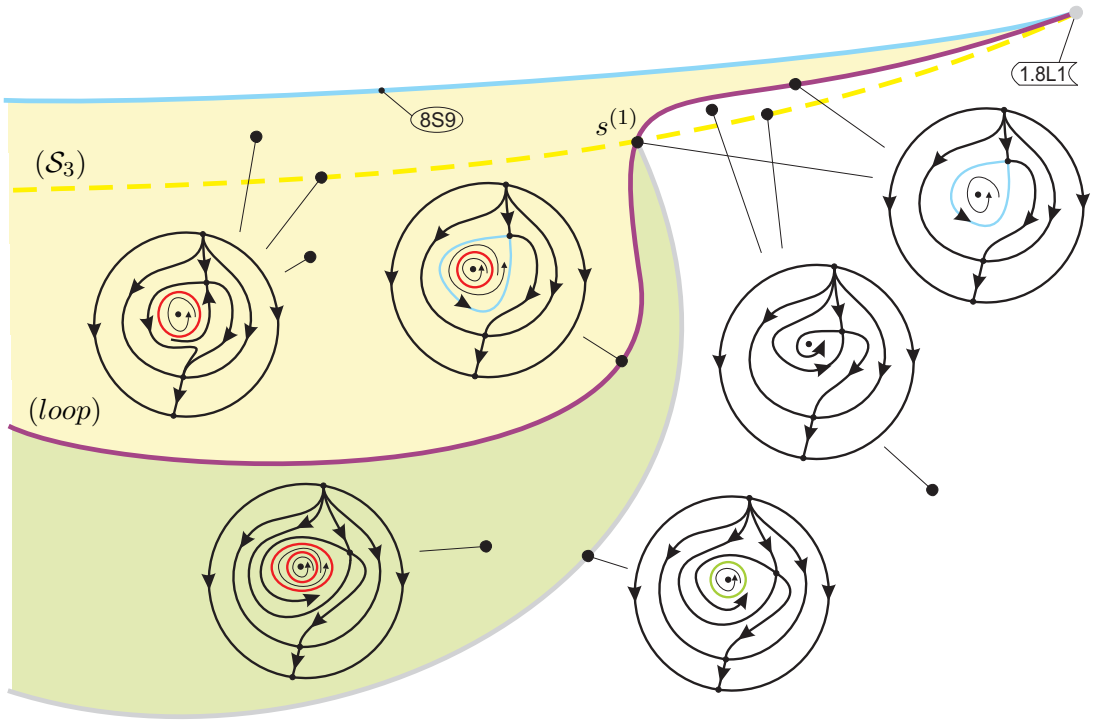

Fig. 5.4: Possible situation in case that a loop branch of $(\mathcal{S}_7)$ associated to a finite saddle intersects a weak saddle branch of $(\mathcal{S}_3)$.

6. Completion of the proof of the main theorem

In a bifurcation diagram we may have topologically equivalent phase portraits belonging to distinct regions of the parameter space. As here we have many parts of the parameter space, to help us identify or to distinguish phase portraits, we need to introduce some invariants and we actually choose integer-valued invariants (see Chapt. 4 of [Artés *et al.*, 2021a] for a general introduction to *invariants* in mathematical classification problems). These integer-valued invariants yield a classification which is easier to grasp. To complete our classification we need twelve invariants, which will be defined in order of their importance in the classification problem. In the following definitions, S denote an arbitrary quadratic differential system.

Definition 6.1. If S is not a center, let $I_1(S)$ be the number of real finite singularities of S. If S is a center, then $I_1(S)$ is a symbol Vul_i with $i \in \{1, \ldots, 32\}$ depending on the global topological phase portrait of the center (remember that, the global phase portraits of the quadratic systems with centers are completely studied. See [Vulpe, 1983]).

Definition 6.2. Let $I_2(S)$ the sum of the indices of the isolated real finite singular points.

Definition 6.3. Assume that S has a finite number of real infinite singularities and let $I_3(S)$ denote the sequence of digits such that each digit describes the total number of local or global separatrices[2] (different from the line of infinity) ending (or starting) at an infinite singular point. The number of digits in the sequences is 2, 4 or 6 according to the number of infinite singular points. We start the sequence at the infinite singular point which receives (or sends) the greatest number of separatrices and take the direction which yields the greatest absolute value, e.g. the values 2110 and 2011 for this invariant are symmetrical (and, therefore, they are the same), so we consider 2110.

Definition 6.4. If the system S has a unique finite saddle-node then $I_4(S)$ denotes the number of local separatrices of the finite sadddle-node going to (or coming from) the finite antisaddles (or to the most external of their limit cycles). We recall that by an **antisaddle** we mean either a focus or node. Moreover, if the system S has a cusp instead of a saddle-node, then the value of $I_4(S)$ is $\widehat{cp}_{(2)}$.

Definition 6.5. Let $I_5(S)$ denote the number of global separatrices going to (or comming from) the finite antisaddles (or to the most external of their limit cycles).

Definition 6.6. Let $I_6(S)$ denote a sequence of two digits such that the first digit corresponds to the number of simple limit cycles of S and the second digit corresponds to the number of double limit cycles of S.

Definition 6.7. Assume that S has exactly two finite antisaddles and let $I_7(S)$ denote a letter chosen from the set $\{S, D\}$ (S for same and D for different) according to the stability of the two finite antisaddles (or the stability of the most external of their limit cycles).

Definition 6.8. Assume that S has exactly one finite antisaddle and one finite saddle-node, and let $I_8(S)$ denote a word chosen from the set $\{Yes, No\}$ according to the answer to the following question: *"Has the nodal part of the finite saddle-node the same stability than the finite antissadle (or the stability of the most external of their limit cycles)?"*

Definition 6.9. Assume that the system S has a unique finite saddle-node and that S possesses limit cycles but surrounding only one of its two finite antisaddles. Let $I_9(S)$ the number of local separatrices of the finite saddle-node going to (or coming from) the most external limit cycle.

Definition 6.10. Assume that S has limit cycles but surrounding only one of its two finite antisaddles and that his eye of limit cycles receive a unique global separatrix called γ. Let $I_{10}(S)$ denote a letter chosen from the set $\{F, I\}$ (I if γ starts or finish at infinity and F in any other case).

[2] Let p a singular point of $S \in$ **QS**. If p has own separatrices then they are called **local separatrices** (e.g. a saddle has 4 local separatrices and a saddle-node 3). However, if p has an attractor (resp. repellor) sector, exists the possibility that p receives (resp. sends) local separatrices of another singular point p' of S which are not local separatrices of p. These separatrices are called **global separatrices** of p.

Definition 6.11. If S has a graphic, then $I_{11}(S)$ denotes the type of graphic. We only need to distinguish between a $f-\infty$ graphic (contains an orbit connecting a finite and an infinite singular point), a $\infty-\infty$ graphic (contains an orbit, different from the line of infinity, that begins and ends at two different infinite singularities) and a *loop*. If S does not possess any graphic, then $I_{11}(S)$ is $\emptyset$.

Definition 6.12. Assume that S has exactly one finite saddle-node, and let $I_{12}(S)$ denote a word chosen from the set $\{Yes, No\}$ according to the answer to the following question: *"Do the two separatrices with the same stability of the finite saddle-node end (or start) at the same point?"*

Theorem 6.13. *Consider the class* $\overline{\boldsymbol{Qwf1sn}}$ *and all the phase portraits that we have obtained for this class. The values of the affine invariant* $\mathcal{I} = (I_1, I_2, I_3, I_4, I_5, I_6, I_7, I_8, I_9, I_{10}, I_{11}, I_{12})$ *given in the diagram from Tables 6.1 to 6.3 yield a partition of these phase portraits of the class* $\overline{\boldsymbol{Qwf1sn}}$*. Furthermore for each value of* $\mathcal{I}$ *in this diagram there corresponds a single phase portrait; i.e.* S *and* S' *are such that* $\mathcal{I}(S) = \mathcal{I}(S')$*, if and only if* S *and* S' *are topologically equivalent.*

Proof of Theorem 6.13. The above result follows from the results in the previous sections and a careful analysis of the bifurcation diagrams given in Sect. 4, the definition of the invariants I_j and their explicit values for the corresponding phase portraits. ■

We have detected 399 parts in the bifurcation diagram for $\overline{\mathbf{Qwf1sn}}$ which produce 192 topologically distinct phase portraits as described in Tables 6.1 to 6.3. The remaining 207 parts do not produce any new phase portrait which was not included in the 192 previous ones. The differences are basically the presence of a strong focus instead of a node and vice versa, weak points, invariant lines (which are not separatrix connections) and symmetries/changes of time.

The phase portraits having neither limit cycle nor graphic have been denoted surrounded by parenthesis, for example (V_1); the phase portraits having one or two simple limit cycles have been denoted surrounded by one or two brackets respectively, for example $[V_{46}]$ or $[[V_{25}]]$; the phase portraits having one graphic have been denoted surrounded by $\{*\}$ and those ones having two or more graphics have been denoted surrounded by $\{\{*\}\}$, for example $\{4.8L_1\}$ and $\{\{4S_7\}\}$. Consequently, phase portraits having a simple limit cycle and a graphic have been denoted surrounded by $[\{*\}]$, for example $[\{7S_{10}\}]$. Finally, the phase portraits possessing a double limit cycle have been denoted surrounded by $[*]^2$, for instance $[1.10L_1]^2$.

As we have noted in Remark 4.9, we do not distinguish between phase portraits whose only difference is that in one we have a finite node and in the other a focus. Both phase portraits are topologically equivalent and they can only be distinguished within the C^∞ class (see [Dumortier *et al.*, 2006]). Anyway, in case we may want to distinguish between them, a new invariant may easily be introduced.

$$
I_1 = \left\{ \begin{array}{l}
1 \ \& \ I_3 = \left\{ \begin{array}{l} 10 \ (1.11L_3) \\ 2120 \ (P_{28}) \\ 111110 \ (1.11L_2) \\ 211010 \ (1.11L_1) \end{array} \right. \\
2 \ \& \ I_2 = \left\{ \begin{array}{l}
0 \ \& \ I_3 = \left\{ \begin{array}{l} 21 \ (2S_1) \\ 3200 \ (9.11L_1) \\ 3211 \ (2.5L_3) \\ 4120 \ (2.5L_2) \\ 111110 \ (7.11L_2) \\ 211101 \ \{7.11L_1\} \\ 211110 \ (11S_5) \\ 221101 \ (11S_4) \\ 311101 \ \& \ I_6 = \left\{ \begin{array}{l} 00 \ (2S_4) \\ 10 \ [11S_3] \end{array} \right. \end{array} \right. \\
1 \ \& \ I_3 = \left\{ \begin{array}{l} 11 \ \& \ I_5 = \left\{ \begin{array}{l} 1 \ (1.4L_3) \\ 2 \ (1.9L_1) \\ 3 \ (1S_{13}) \end{array} \right. \\ 21 \ \& \ I_5 = \left\{ \begin{array}{l} 1 \ (1S_1) \\ 2 \ (1S_{15}) \end{array} \right. \\ 32 \ (P_2) \\ 2111 \ \& \ I_4 = \left\{ \begin{array}{l} 0 \ (P_{10}) \\ 1 \ (P_9) \end{array} \right. \\ 2121 \ (P_{16}) \\ 2211 \ (1.5L_6) \\ 3101 \ \{\{1.5L_3\}\} \\ 3111 \ (1.5L_5) \\ 3121 \ \& \ I_4 = \left\{ \begin{array}{l} 0 \ (1.5L_7) \\ \widehat{cp}_{(2)} \ (P_{15}) \end{array} \right. \\ 3200 \ (1.5L_2) \\ 3221 \ (1.5L_8) \\ 4120 \ (1.5L_1) \\ 4121 \ (1.5L_4) \\ 111110 \ (1.4L_2) \\ 111111 \ \& \ I_5 = \left\{ \begin{array}{l} 0 \ \& \ I_6 = \left\{ \begin{array}{l} 00 \ \{1.7L_1\} \\ 10 \ [\{1.7L_2\}] \end{array} \right. \\ 1 \ (1.7L_3) \end{array} \right. \\ 210110 \ (1.4L_1) \\ 211110 \ (1S_5) \\ 211111 \ \& \ I_4 = \left\{ \begin{array}{l} 0 \ \& \ I_6 = \left\{ \begin{array}{l} 00 \ \& \ I_8 = \left\{ \begin{array}{l} No \ (1S_6) \\ Yes \ (1S_7) \end{array} \right. \\ 10 \ \& \ I_8 = \left\{ \begin{array}{l} No \ [1S_9] \\ Yes \ [1S_8] \end{array} \right. \\ 20 \ [[1S_{10}]] \\ 01 \ [1.10L_1]^2 \end{array} \right. \\ \widehat{cp}_{(2)} \ (1.9L_2) \end{array} \right. \\ 221111 \ (1S_{14}) \\ 310110 \ (1S_4) \\ 311101 \ (1S_2) \\ 311111 \ (1S_{12}) \\ 411010 \ (1S_3) \end{array} \right. \\
2 \ \& \ I_3 = \left\{ \begin{array}{l} 11 \ \& \ I_6 = \left\{ \begin{array}{l} 00 \ (2S_3) \\ 10 \ [11S_{12}] \end{array} \right. \\ 2111 \ \{P_{19}\} \\ 2121 \ \& \ I_6 = \left\{ \begin{array}{l} 00 \ (2.5L_1) \\ 10 \ [5.11L_1] \end{array} \right. \\ 3111 \ \{5.11L_3\} \\ 111110 \ \{7.11L_5\} \\ 111111 \ \& \ I_6 = \left\{ \begin{array}{l} 00 \ (2S_2) \\ 10 \ [11S_{14}] \end{array} \right. \\ 211011 \ (11S_9) \end{array} \right.
\end{array} \right. \\
3 \text{ and } Vul_i \text{ follow on the next pages}
\end{array} \right.
$$

Table 6.1: Geometric classification for the family **Qwf1sn**.

$$
I_1 = \left\{ \begin{array}{l}
\text{1 and 2 listed on the previous page} \\
3\ \&\ I_2 = \left\{ \begin{array}{ll}
0\ \&\ I_3 = \left\{ \begin{array}{l}
21\ \&\ I_4 = \left\{ \begin{array}{l} 0\ \&\ I_5 = \left\{ \begin{array}{l} 0\ \{7.7L_1\} \\ 1\ \&\ I_6 = \left\{ \begin{array}{l} 00\ (7S_{12}) \\ 10\ [7S_{24}] \end{array} \right. \end{array} \right. \\ 1\ (7S_{14}) \\ \widehat{cp}_{(2)}\ (7.9L_1) \end{array} \right. \\
22\ \&\ I_4 = \left\{ \begin{array}{l} 0\ \&\ I_6 = \left\{ \begin{array}{l} 00\ (7S_{11}) \\ 10\ [7S_{23}] \end{array} \right. \\ 1\ \&\ I_6 = \left\{ \begin{array}{l} 00\ (V_{32}) \\ 10\ [V_{72}] \end{array} \right. \end{array} \right. \\
31\ \&\ I_4 = \left\{ \begin{array}{l} 0\ \&\ I_5 = \left\{ \begin{array}{l} 0\ \{7S_{13}\} \\ 1\ \&\ I_6 = \left\{ \begin{array}{l} 00\ \&\ I_8 = \left\{ \begin{array}{l} No\ (V_{33}) \\ Yes\ \&\ I_{12} = \left\{ \begin{array}{l} No\ (7S_{26}) \\ Yes\ (7S_1) \end{array} \right. \end{array} \right. \\ 10\ [V_{34}] \end{array} \right. \end{array} \right. \\ 1\ (4S_1) \\ 2\ (V_{37}) \\ \widehat{cp}_{(2)}\ (9S_3) \end{array} \right. \\
32\ \&\ I_{11} = \left\{ \begin{array}{l} loop\ \{7S_2\} \\ \emptyset\ (9S_1) \end{array} \right. \\
33\ \&\ I_6 = \left\{ \begin{array}{l} 00\ (V_{10}) \\ 10\ [V_9] \end{array} \right. \\
41\ \&\ I_4 = \left\{ \begin{array}{l} 0\ (V_1) \\ 1\ \&\ I_5 = \left\{ \begin{array}{l} 1\ (V_2) \\ 2\ (V_7) \end{array} \right. \end{array} \right. \\
42\ (V_8) \\
3211\ \&\ I_4 = \left\{ \begin{array}{l} 0\ (5.7L_1) \\ 1\ (4.5L_1) \end{array} \right. \\
3212\ \{5.7L_2\} \\
3311\ (5S_5) \\
3321\ \&\ I_6 = \left\{ \begin{array}{l} 00\ (5S_8) \\ 10\ [5S_7] \end{array} \right. \\
4111\ (4.5L_2) \\
4121\ (5.7L_7) \\
4131\ (5.9L_1) \\
4141\ (5S_{10}) \\
4211\ (5S_3) \\
4212\ (5S_6) \\
4231\ (5S_{30}) \\
5121\ (5S_{21}) \\
5211\ \&\ I_4 = \left\{ \begin{array}{l} 0\ (5S_{23}) \\ 1\ (5S_2) \end{array} \right. \\
6120\ \&\ I_4 = \left\{ \begin{array}{l} 0\ (5S_{22}) \\ 1\ (5S_1) \end{array} \right. \\
211111\ \&\ I_6 = \left\{ \begin{array}{l} 00\ (7S_8) \\ 10\ [7S_6] \end{array} \right. \\
211211\ \&\ I_6 = \left\{ \begin{array}{l} 00\ (V_{20}) \\ 10\ [V_{17}] \end{array} \right. \\
212110\ (7S_3) \\
221201\ \{7S_4\} \\
311011\ (4S_3) \\
311110\ (4S_2) \\
311111\ \&\ I_5 = \left\{ \begin{array}{l} 0\ \&\ I_6 = \left\{ \begin{array}{l} 00\ \{7S_7\} \\ 10\ [\{7S_5\}] \end{array} \right. \\ 1\ (7S_{28}) \end{array} \right. \\
311211\ (9S_6) \\
311311\ (V_{28}) \\
312110\ (V_6) \\
312211\ (V_{75}) \\
321021\ (V_{11}) \\
321111\ \&\ I_6 = \left\{ \begin{array}{l} 00\ (V_{19}) \\ 10\ [V_{16}] \end{array} \right. \\
321201\ \&\ I_6 = \left\{ \begin{array}{l} 00\ (V_{13}) \\ 10\ [V_{12}] \end{array} \right. \\
411110\ (V_4) \\
411111\ \&\ I_6 = \left\{ \begin{array}{l} 00\ (V_{15}) \\ 10\ [V_{18}] \\ 20\ [[V_{25}]] \\ 01\ [10S_1]^2 \end{array} \right. \\
511101\ \&\ I_4 = \left\{ \begin{array}{l} 0\ (V_{66}) \\ 1\ (V_3) \end{array} \right.
\end{array} \right. \\
\text{2 follows on the next page}
\end{array} \right. \\
Vul_i \text{ follow on the next page}
\end{array} \right.
$$

Table 6.2: Geometric classification for the family $\overline{\textbf{Qwf1sn}}$ *(cont.).*

$$
I_1 = \left\{
\begin{array}{l}
\text{1 and 2 listed in the previous pages} \\
3\ \&\ I_2 = \left\{
\begin{array}{l}
\text{0 listed in the previous page} \\
2\ \&\ I_3 = \left\{
\begin{array}{l}
11\ \&\ I_4 = \left\{
\begin{array}{l}
1\ \{7S_{17}\} \\
2\ \&\ I_5 = \left\{
\begin{array}{l}
2\ \{\{4S_7\}\} \\
3\ \&\ I_7 = \left\{
\begin{array}{l}
S\ \{V_{47}\} \\
D\ (4S_{12})
\end{array}
\right.
\end{array}
\right. \\
3\ \&\ I_5 = \left\{
\begin{array}{l}
4\ \&\ I_6 = \left\{
\begin{array}{l}
00\ (V_{39}) \\
10\ \&\ I_9 = \left\{
\begin{array}{l}
1\ [V_{46}] \\
2\ [V_{56}]
\end{array}
\right.
\end{array}
\right. \\
5\ (V_{31})
\end{array}
\right. \\
\widehat{cp}_{(2)}\ (9S_4)
\end{array}
\right. \\
1111\ \&\ I_4 = \left\{
\begin{array}{l}
2\ (4.5L_4) \\
3\ (5S_{20})
\end{array}
\right. \\
2111\ \&\ I_4 = \left\{
\begin{array}{l}
1\ (4.5L_5) \\
2\ (5S_{28})
\end{array}
\right. \\
2121\ \&\ I_7 = \left\{
\begin{array}{l}
D\ (5.7L_8) \\
S\ \{5.7L_4\}
\end{array}
\right. \\
3121\ \&\ I_4 = \left\{
\begin{array}{l}
0\ \{5.7L_3\} \\
1\ \&\ I_5 = \left\{
\begin{array}{l}
2\ \{5S_{15}\} \\
3\ \&\ I_7 = \left\{
\begin{array}{l}
D\ (5S_{29}) \\
S\ \{5S_{16}\}
\end{array}
\right.
\end{array}
\right. \\
2\ (5S_{31}) \\
\widehat{cp}_{(2)}\ (5.9L_2)
\end{array}
\right. \\
4111\ \{5.7L_5\} \\
4121\ \&\ I_5 = \left\{
\begin{array}{l}
2\ \&\ I_6 = \left\{
\begin{array}{l}
00\ (5S_4) \\
10\ \&\ I_{10} = \left\{
\begin{array}{l}
F\ [5S_{14}] \\
I\ [5S_{18}]
\end{array}
\right.
\end{array}
\right. \\
3\ (5S_{11})
\end{array}
\right. \\
5111\ \{5S_{19}\} \\
110110\ \&\ I_4 = \left\{
\begin{array}{l}
2\ (4S_8) \\
3\ (V_{59})
\end{array}
\right. \\
111110\ \&\ I_4 = \left\{
\begin{array}{l}
1\ (4S_4) \\
2\ (V_{68})
\end{array}
\right. \\
111111\ \&\ I_5 = \left\{
\begin{array}{l}
2\ \&\ I_6 = \left\{
\begin{array}{l}
00\ \&\ I_{11} = \left\{
\begin{array}{l}
f-\infty\ \{7S_{16}\} \\
\infty-\infty\ \{7S_9\}
\end{array}
\right. \\
10\ [\{7S_{10}\}]
\end{array}
\right. \\
3\ (7S_{29})
\end{array}
\right. \\
211111\ \&\ I_4 = \left\{
\begin{array}{l}
0\ \{7S_{15}\} \\
1\ \&\ I_5 = \left\{
\begin{array}{l}
2\ \{V_{43}\} \\
3\ \&\ I_6 = \left\{
\begin{array}{l}
00\ \&\ I_7 = \left\{
\begin{array}{l}
D\ (V_{22}) \\
S\ (V_{21})
\end{array}
\right. \\
10\ \&\ I_7 = \left\{
\begin{array}{l}
D\ [V_{23}] \\
S\ [V_{26}]
\end{array}
\right. \\
20\ [[V_{27}]] \\
01\ [10S_2]^2
\end{array}
\right.
\end{array}
\right. \\
2\ (V_{24}) \\
\widehat{cp}_{(2)}\ (9S_5)
\end{array}
\right. \\
311011\ \{7S_{19}\} \\
311111\ \&\ I_5 = \left\{
\begin{array}{l}
2\ \&\ I_6 = \left\{
\begin{array}{l}
00\ (V_5) \\
10\ \&\ I_{10} = \left\{
\begin{array}{l}
F\ [V_{42}] \\
I\ [V_{53}]
\end{array}
\right.
\end{array}
\right. \\
3\ (V_{30})
\end{array}
\right. \\
411011\ (V_{54})
\end{array}
\right.
\end{array}
\right. \\
Vul_2\ \{3.8L_9\} \\
Vul_7\ \{3.8L_1\} \\
Vul_{13}\ \{P_5\} \\
Vul_{14}\ \{\{P_{23}\}\} \\
Vul_{19}\ \{3.8L_3\} \\
Vul_{20}\ \{3.8L_7\} \\
Vul_{22}\ \{\{4.8L_4\}\} \\
Vul_{23}\ \{\{4.8L_6\}\} \\
Vul_{24}\ \{\{4.8L_5\}\} \\
Vul_{29}\ \{\{1.8L_1\}\} \\
Vul_{31}\ \{4.8L_1\}
\end{array}
\right.
$$

Table 6.3: Geometric classification for the family **$\overline{\text{Qwf1sn}}$** *(cont.).*

7. Tables of topological equivalences for the class $\overline{\text{Qwf1sn}}$

The purpose of this section is simple: We want to group all the regions that present the same topological phase portrait. In Tables 7.1 to 7.9 we list in the first column 192 parts with all the distinct phase portraits of Figs. 2.1 to 2.6. Corresponding to each part listed in column one we have in each row all parts whose phase portraits are topologically equivalent to the phase portrait appearing in column 1 of the same row. The contents of the other columns are described below:

In the eight column, called **Origin's role has changed**, we set all the parts whose systems yield topologically equivalent phase portraits to those in the first column but with the difference described as follows: Let S_2 a system corresponding to the eight column and let S_1 a system corresponding to the same row as S_2 but in the first column. Then, S_1 and S_2 have exactly two finite antisaddles, one of which is the origin in both cases, which is a $f^{(1)}$ in S_1 and also in S_2. We denote as $f_1^{(1)}$ the origin of S_1 and as p_1 the other finite antisaddle of S_1; Analogously, we denote as $f_2^{(1)}$ the origin of S_2 and as p_2 the other finite antisaddle of S_2. If we call h the homeomorphism (the topological equivalence) between the systems S_1 and S_2, we have that $h(f_1^{(1)}) = p_2$ and $h(p_1) = f_2^{(1)}$. In conclusion, the global topological role of the origin, which is a $f^{(1)}$ in both cases, have changed.

For example, the phase portraits corresponding to regions V_{46} and V_{49} are topologically equivalent (see Fig. 7.1). In V_{49} the origin (yellow point) is a $f^{(1)}$ and the green point is a strong focus; in V_{46} the origin (yellow point) is a $f^{(1)}$ and the green point is a strong focus.

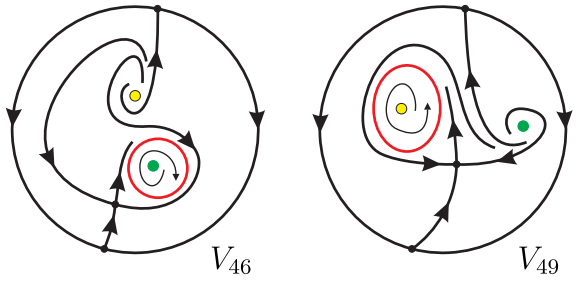

Fig. 7.1: Origin's global topological role has changed.

However, observing the position of the limit cycle in V_{46} and in V_{49} it is clear that the global topological role of the origin in V_{49} is the same as that of the finite antisaddle different from the origin in V_{46}. Moreover, notice that even they are topologically equivalent, the difference is very relevant since they are not geometrically equivalent. That is, by perturbing the weak focus and producing a limit cycle, we can get a $(2,0)$ configuration or a $(1,1)$.

Another example appears when considering the phase portraits corresponding to the regions V_{39} and V_{50}, which are topologically equivalent (see Fig. 7.2). In V_{39} the origin (yellow point) is a $f^{(1)}$ and the green point is a node; in V_{50} the origin (yellow point) is a $f^{(1)}$ and the green point is a strong focus.

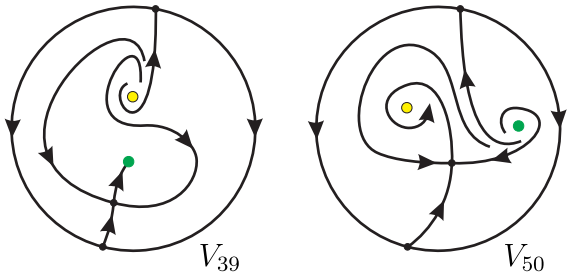

Fig. 7.2: Origin's global topological role has changed.

However, noticing where the separatrices of the finite saddle-node come from, it is clear that the global topological role of the origin in V_{39} is the same as that of the finite antisaddle different from the origin in V_{50}.

In the ninth column, called **Origin's role and its order have changed**, we set all the parts whose systems yield topologically equivalent phase portraits to those in the first column but with the difference described as follows: Let S_2 a system corresponding to the ninth column and let S_1 a system corresponding to the same row as S_2 but in the first column. Then, S_1 and S_2 have exactly two finite antisaddles, one of which is the origin in both cases, which is a $f^{(1)}$ in S_1 and a $f^{(2)}$ in S_2. We denote as $f_1^{(1)}$ the origin of S_1 and as p_1 the other finite antisaddle of S_1; Analogously, we denote as $f_2^{(2)}$ the origin of S_2 and as p_2 the other finite antisaddle of S_2. If we call h the homeomorphism (the topological equivalence) between the systems S_1 and S_2, we have that $h(f_1^{(1)}) = p_2$ and $h(p_1) = f_2^{(2)}$. In conclusion, the global topological role of the origin and its weakness order have changed.

For example, the phase portraits corresponding to regions V_{39} and $8S_{10}$ are equivalent (see Fig. 7.3). However, the origin in $8S_{10}$ (yellow point) is a $f^{(2)}$ and has the same global topological role than the

node in V_{39} (green point).

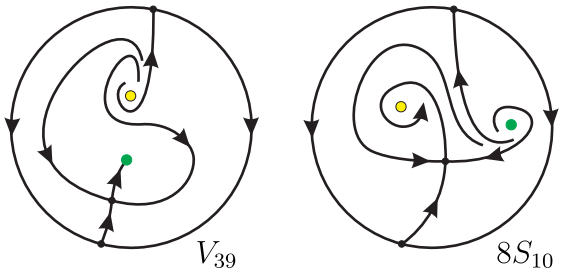

Fig. 7.3: Origin's global topological role and its weakness order have changed.

In the third column, called **Weak focus order 2 or 3**, we set all the parts whose systems yield topologically equivalent phase portraits to those in the first column, but with the difference that despite the origin has the same global topological role in both phase portraits, in the system of the third column is a $f^{(2)}$ or a $f^{(3)}$ instead of a $f^{(1)}$ as in the first column. In addition, in the Tables 7.1-7.9 we have highlighted in parentheses whether it is a weak focus of second or third order.

For example, the phase portraits corresponding to regions V_{10} and $8S_1$ are topologically equivalent (see Fig. 7.4). However, despite clearly the origin has the same global topological role in both regions, in V_{10} is a $f^{(1)}$ and in $8S_1$ is a $f^{(2)}$.

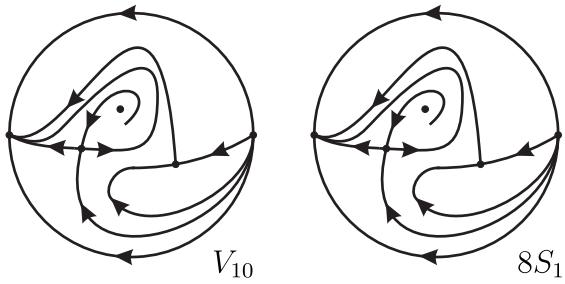

Fig. 7.4: The weakness order of the origin has increased.

In the fourth column, called **Finite antisaddle strong focus**, we set all the parts whose systems yield topologically equivalent phase portraits to those in the first column, but with the difference that despite the finite antissadle different from the origin has the same global topological role in both columns, it is a node in the system of the first column and a strong focus in the system of the fourth column.

For example, the phase portraits corresponding to regions V_5 and V_{52} are topologically equivalent (see Fig. 7.5). However, despite the antisaddle different from the origin (green point in both cases) has the same global topological role in both phase portraits, it is a node in region V_5 and a strong focus in region V_{52}.

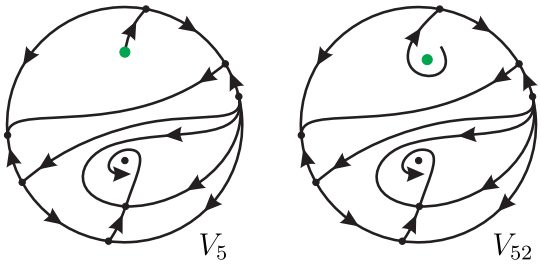

Fig. 7.5: Finite antisaddle different from the origin changing from node to strong focus.

In the fifth column, called **Finite antisaddle node-focus**, we set all the parts of the bifurcation diagram whose systems yield topologically equivalent phase portraits to those in the first column, but with the difference that despite the finite antissadle different from the origin has the same global topological role in both columns, it is a node-focus (that is, a node generated due to the fact that we are in the surface (S_6)) in the system of the fifth column.

In the sixth column, called **Singularity becoming weak**, we set all the parts whose systems yield topologically equivalent phase portraits to those in the first column, but with the difference that the system in the first column has a finite non-weak singularity $p \neq 0$ which has the same global topological role than a finite order weak singularity $\widetilde{p} \neq 0$ in the system in the sixth column. Hence, the system of the sixth column has two weak singularities (both of first order). One is the origin, which is a $f^{(1)}$, and the other is $\widetilde{p}$, which could be another $f^{(1)}$ or a $s^{(1)}$ (it is indicated in the Tables 7.1-7.9).

For example, the phase portraits corresponding to regions V_4 and $3S_7$ are topologically equivalent (see Fig. 7.6). However, the finite saddle is weak only in $3S_7$.

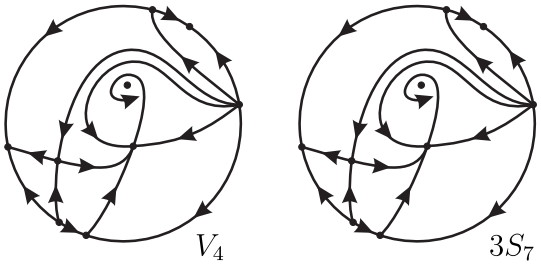

Fig. 7.6: Second weak singularity appears.

In the seventh column, called **Possessing invariant curve (no separatrix connection)**, we

set all the parts contained in $(\mathcal{S}_4)$ whose systems yield topologically equivalent phase portraits to those in the first column but with the possible existence of an invariant curve not yielding a connection of separatrices in seventh column's phase portraits.

In the second column, called **Algebro-geometric features**, we set all the parts whose systems yield topologically equivalent phase portraits to those in the first column but cannot be placed in any of the other columns because they do not meet the requirements.

Whenever phase portraits appear in a row in a specific column, the listing is done according to the decreasing dimension of the parts where they appear, always placing the lower dimensions on lower lines.

Presented Phase Portrait	Algebro-geometric features	Weak focus order 2 or 3	Finite antisaddle strong focus	Finite antisaddle node–focus	Singularity becoming weak	Possessing invariant curve (no sep. connect.)	Origin's role has changed	Origin's role and its order have changed
V_1	V_{35},V_{36} $5.5L_1$				$3S_1$ $(s^{(1)})$	$4S_5$		
V_2	V_{57} $5.5L_2$				$3S_6$ $(s^{(1)})$			
V_3								
V_4	V_{58}				$3S_7$ $(s^{(1)})$			
V_5			V_{52}	$6S_5$	$3S_4$ $(f^{(1)})$		V_{38},V_{40} $3S_2$,$6S_1$	
V_6	V_{64}				$3S_8$ $(s^{(1)})$			
V_7	V_{67}				$3S_{11}$ $(s^{(1)})$			
V_8	V_{14}, V_{73}, V_{74}				$3S_{10}$ $(s^{(1)})$, $3S_{12}$ $(s^{(1)})$			
V_9	V_{71}							
V_{10}	V_{29}	$8S_1$ $(f^{(2)})$, $8S_{14}$ $(f^{(2)})$						
V_{11}	V_{65}				$3S_9$ $(s^{(1)})$			
V_{12}								
V_{13}		$8S_2$ $(f^{(2)})$						
V_{15}	V_{63}	$8S_3$ $(f^{(2)})$ $8.10L_1$ $(f^{(3)})$				$4S_{10}$		
V_{16}								
V_{17}								
V_{18}		$8S_7$ $(f^{(2)})$						

Table 7.1: Topological equivalences for the family $\overline{\mathbf{Qwf1sn}}$.

Table 7.2: Topological equivalences for the family $\overline{\mathbf{Qwflsn}}$ (*cont.*).

Presented Phase Portrait	Algebro-geometric features	Weak focus order 2 or 3	Finite antisaddle strong focus	Finite antisaddle node–focus	Singularity becoming weak	Possessing invariant curve (no sep. connect.)	Origin's role has changed	Origin's role and its order have changed
V_{19}		$8S_6$ $(f^{(2)})$						
V_{20}		$8S_4$ $(f^{(2)})$						
V_{21}	V_{45}	$8S_8$ $(f^{(2)})$	V_{44}	$6S_3$		$4S_6$		
V_{22}	V_{70}	$8S_5$ $(f^{(2)})$ $8.10L_2$ $(f^{(3)})$				$4S_{13}$		
V_{23}		$8S_{12}$ $(f^{(2)})$						
V_{24}								
V_{25}								
V_{26}								
V_{27}								
V_{28}								
V_{30}								
V_{31}							V_{69}	
V_{32}		$8S_{13}$ $(f^{(2)})$						
V_{33}		$8S_9$ $(f^{(2)})$						
V_{34}								
V_{37}								
V_{39}			V_{41}	$6S_2$	$3S_3$ $(f^{(1)})$		V_{50}, V_{51} $3S_5$,$6S_4$ $5.5L_3$	$8S_{10}$, $8S_{11}$ $6.8L_1$
V_{42}								

Table 7.3: Topological equivalences for the family $\overline{\mathbf{Qwflsn}}$ (*cont.*).

Presented Phase Portrait	Algebro-geometric features	Weak focus order 2 or 3	Finite antisaddle strong focus	Finite antisaddle node–focus	Singularity becoming weak	Possessing invariant curve (no sep. connect.)	Origin's role has changed	Origin's role and its order have changed
V_{43}								
V_{46}							V_{49}, V_{61} $6S_8$	
V_{47}							V_{48}, V_{62} $6S_9$	
V_{53}								
V_{54}	V_{55}			$6S_6$				
V_{56}								
V_{59}	V_{60}			$6S_7$				
V_{66}								
V_{68}								
V_{72}								
V_{75}								
$1S_1$								
$1S_2$								
$1S_3$								
$1S_4$								
$1S_5$								
$1S_6$		$1.8L_3$ $(f^{(2)})$						
$1S_7$	$1S_{11}$	$1.8L_2$ $(f^{(2)})$ P_6 $(f^{(3)})$				$1.4L_4$		
$1S_8$		$1.8L_4$ $(f^{(2)})$						

Table 7.4: Topological equivalences for the family $\overline{\mathbf{Qwflsn}}$ (*cont.*).

Presented Phase Portrait	Algebro-geometric features	Weak focus order 2 or 3	Finite antisaddle strong focus	Finite antisaddle node–focus	Singularity becoming weak	Possessing invariant curve (no sep. connect.)	Origin's role has changed	Origin's role and its order have changed
$1S_9$								
$1S_{10}$								
$1S_{12}$								
$1S_{13}$								
$1S_{14}$								
$1S_{15}$								
$2S_1$	$11S_{18}$, $11S_{22}$ P_1							
$2S_2$	$11S_{15}$, $11S_{24}$		$11S_{13}$, $11S_{25}$	$6.11L_2$, $6.11L_5$	$3.11L_2$ $(f^{(1)})$, $3.11L_4$ $(f^{(1)})$			
$2S_3$	$11S_{17}$, $11S_{21}$		$11S_{11}$, $11S_{20}$	$6.11L_3$, $6.11L_4$	$3.11L_1$ $(f^{(1)})$, $3.11L_3$ $(f^{(1)})$			
$2S_4$	$11S_1$, $11S_2$, $11S_{16}$, $11S_{23}$	$8.11L_1$ $(f^{(2)})$, $8.11L_2$ $(f^{(2)})$						
$4S_1$	$4S_{11}$				$3.4L_2$ $(s^{(1)})$			
$4S_2$	$4S_9$				$3.4L_1$ $(s^{(1)})$			
$4S_3$								
$4S_4$								
$4S_7$								
$4S_8$								
$4S_{12}$								
$5S_1$								
$5S_2$								
$5S_3$	$5S_{25}$				$3.5L_5$ $(s^{(1)})$			
$5S_4$			$5S_{17}$	$5.6L_2$	$3.5L_2$ $(f^{(1)})$		$5S_{12}$, $5S_{13}$ $3.5L_1$,$5.6L_1$	
$5S_5$	$5S_{24}$				$3.5L_4$ $(s^{(1)})$			
$5S_6$	$5S_9$				$3.5L_3$ $(s^{(1)})$			
$5S_7$								
$5S_8$		$5.8L_1$ $(f^{(2)})$						
$5S_{10}$								
$5S_{11}$								
$5S_{14}$								
$5S_{15}$								

Presented Phase Portrait	Algebro-geometric features	Weak focus order 2 or 3	Finite antisaddle strong focus	Finite antisaddle node–focus	Singularity becoming weak	Possessing invariant curve (no sep. connect.)	Origin's role has changed	Origin's role and its order have changed
$5S_{16}$								
$5S_{18}$								
$5S_{19}$								
$5S_{20}$			$5S_{26}$, $5S_{27}$	$5.6L_3$				
$5S_{21}$								
$5S_{22}$								
$5S_{23}$								
$5S_{28}$								
$5S_{29}$								
$5S_{30}$								
$5S_{31}$								
$7S_1$	$7S_{22}$				$3.7L_2$ $(s^{(1)})$			
$7S_2$	$7S_{25}$							
$7S_3$	$7S_{21}$				$3.7L_1$ $(s^{(1)})$			
$7S_4$								
$7S_5$								
$7S_6$								
$7S_7$		$7.8L_2$ $(f^{(2)})$						
$7S_8$		$7.8L_1$ $(f^{(2)})$						
$7S_9$		$7.8L_3$ $(f^{(2)})$						
$7S_{10}$								

Table 7.5: Topological equivalences for the family $\overline{\mathbf{Qwflsn}}$ (*cont.*).

Presented Phase Portrait	Algebro-geometric features	Weak focus order 2 or 3	Finite antisaddle strong focus	Finite antisaddle node–focus	Singularity becoming weak	Possessing invariant curve (no sep. connect.)	Origin's role has changed	Origin's role and its order have changed
$7S_{11}$		$7.8L_4$ $(f^{(2)})$						
$7S_{12}$		$7.8L_5$ $(f^{(2)})$						
$7S_{13}$								
$7S_{14}$								
$7S_{15}$								
$7S_{16}$								
$7S_{17}$							$7S_{18}$, $7S_{20}$ $6.7L_1$	
$7S_{19}$								
$7S_{23}$								
$7S_{24}$								
$7S_{26}$	$7S_{27}$				$3.7L_3$ $(s^{(1)})$			
$7S_{28}$								
$7S_{29}$								
$9S_1$	$9S_2$, $9S_7$, $9S_{12}$							
$9S_3$	$9S_9$							
$9S_4$	$9S_8$							
$9S_5$	$9S_{10}$							
$9S_6$	$9S_{11}$							
$10S_1$								
$10S_2$								
$11S_3$	$11S_6$							
$11S_4$	$11S_7$							
$11S_5$	$11S_8$							
$11S_9$	$11S_{28}$		$11S_{10}$, $11S_{27}$	$6.11L_1$, $6.11L_6$				
$11S_{12}$	$11S_{19}$							
$11S_{14}$	$11S_{26}$							

Table 7.6: Topological equivalences for the family $\overline{\mathbf{Qwflsn}}$ (*cont.*).

Table 7.7: Topological equivalences for the family $\overline{\mathbf{Qwf1sn}}$ (*cont.*).

Presented Phase Portrait	Algebro-geometric features	Weak focus order 2 or 3	Finite antisaddle strong focus	Finite antisaddle node–focus	Singularity becoming weak	Possessing invariant curve (no sep. connect.)	Origin's role has changed	Origin's role and its order have changed
$1.4L_1$								
$1.4L_2$								
$1.4L_3$								
$1.5L_1$								
$1.5L_2$								
$1.5L_3$								
$1.5L_4$								
$1.5L_5$								
$1.5L_6$								
$1.5L_7$								
$1.5L_8$								
$1.7L_1$		P_7 ($f^{(2)}$)						
$1.7L_2$								
$1.7L_3$								
$1.8L_1$	P_{13}, P_{29}							
$1.9L_1$	$1.9L_3$							
$1.9L_2$	$1.9L_4$							
$1.10L_1$								
$1.11L_1$	$1.11L_6$							
$1.11L_2$	$1.11L_5$							
$1.11L_3$	$1.11L_4$							
$2.5L_1$	$5.11L_4$, $5.11L_7$		$5.11L_2$, $5.11L_8$	P_{27}, P_{31}	P_{11} ($f^{(1)}$), P_{24} ($f^{(1)}$)			
$2.5L_2$	$5.11L_5$, $5.11L_6$							
$2.5L_3$								
$3.8L_1$	$3.8L_2$							
$3.8L_3$	$3.8L_4$, $3.8L_5$, $3.8L_6$ P_{20}, P_{21}, P_{22}							
$3.8L_7$	$3.8L_8$ P_{26}							
$3.8L_9$	$4.8L_2$, $4.8L_3$ P_4, P_{12}							

Table 7.8: Topological equivalences for the family $\overline{\mathbf{Qwf1sn}}$ (*cont.*).

Presented Phase Portrait	Algebro-geometric features	Weak focus order 2 or 3	Finite antisaddle strong focus	Finite antisaddle node–focus	Singularity becoming weak	Possessing invariant curve (no sep. connect.)	Origin's role has changed	Origin's role and its order have changed
$4.5L_1$	$4.5L_3$				P_8 $(s^{(1)})$			
$4.5L_2$								
$4.5L_4$								
$4.5L_5$								
$4.8L_1$								
$4.8L_4$								
$4.8L_5$								
$4.8L_6$	P_{14}, P_{18}							
$5.7L_1$	$5.7L_6$				P_3 $(s^{(1)})$			
$5.7L_2$								
$5.7L_3$								
$5.7L_4$								
$5.7L_5$								
$5.7L_7$								
$5.7L_8$								
$5.9L_1$	$5.9L_4$							
$5.9L_2$	$5.9L_3$							
$5.11L_1$	$5.11L_9$							
$5.11L_3$	$5.11L_{10}$							
$7.7L_1$								
$7.9L_1$	$7.9L_2$							
$7.11L_1$	$7.11L_3$							
$7.11L_2$	$7.11L_4$							
$7.11L_5$	$7.11L_6$							
$9.11L_1$	$9.11L_2$							

Presented Phase Portrait	Algebro-geometric features	Weak focus order 2 or 3	Finite antisaddle strong focus	Finite antisaddle node–focus	Singularity becoming weak	Possessing invariant curve (no sep. connect.)	Origin's role has changed	Origin's role and its order have changed
P_2								
P_5								
P_9								
P_{10}								
P_{15}	P_{17}							
P_{16}								
P_{19}	P_{25}							
P_{23}								
P_{28}	P_{30}							

Table 7.9: Topological equivalences for the family $\overline{\mathbf{Qwf1sn}}$ (*cont.*).

A. Some complements for the study of the bifurcation diagram

The aim of this appendix is to group some images which are useful in Section 4.

A.1. Images of the surfaces $(\mathcal{S}_i)$ *in the hyperplane* $m = 1$ *in* $\mathbb{R}^4$

In this section we present a picture of the algebraic surfaces $(\mathcal{S}_i)$ in the three dimensional affine space which is the hyperplane $m = 1$. The surfaces $(\mathcal{S}_i)$ have been introduced in Section 4.1. We have not added the picture of $(\mathcal{S}_2)$ since it is simply a plane. Anyway, you can find all the pictures in the *Mathematica* file **surfaces.nb** at `https://mat.uab.cat/~artes/articles/qwf1sn/qwf1sn.html`. We recommend the visit of the page since in a paper we can only show a static image of the surface while in the *Mathematica* file, the reader can play with it and see it from different perspectives.

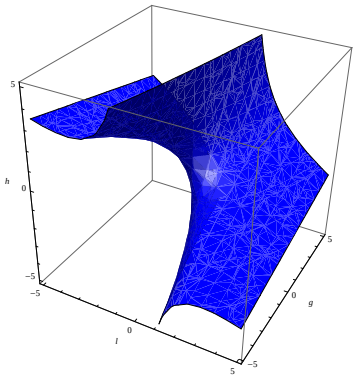

Fig. A.1: Suface $(\mathcal{S}_1)$ for $m = 1$.

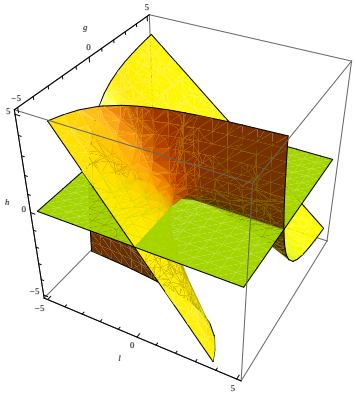

Fig. A.2: Suface $(\mathcal{S}_3)$ for $m = 1$.

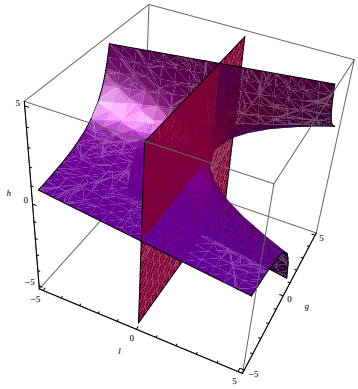

Fig. A.3: Suface $(\mathcal{S}_4)$ for $m = 1$.

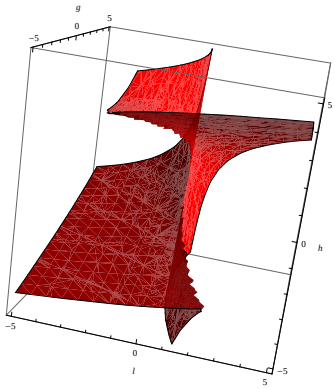

Fig. A.4: Suface $(\mathcal{S}_5)$ for $m = 1$.

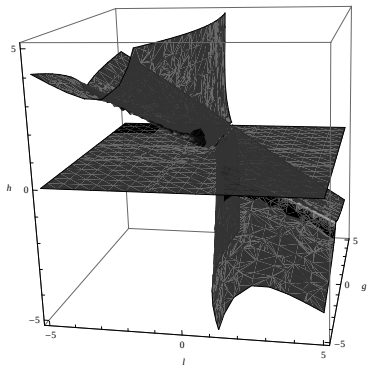

Fig. A.5: Suface $(\mathcal{S}_6)$ for $m = 1$.

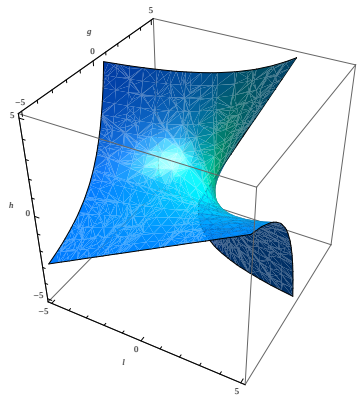

Fig. A.6: Suface ($\mathcal{S}_8$) for $m = 1$.

A.2. Sequences of phase portraits

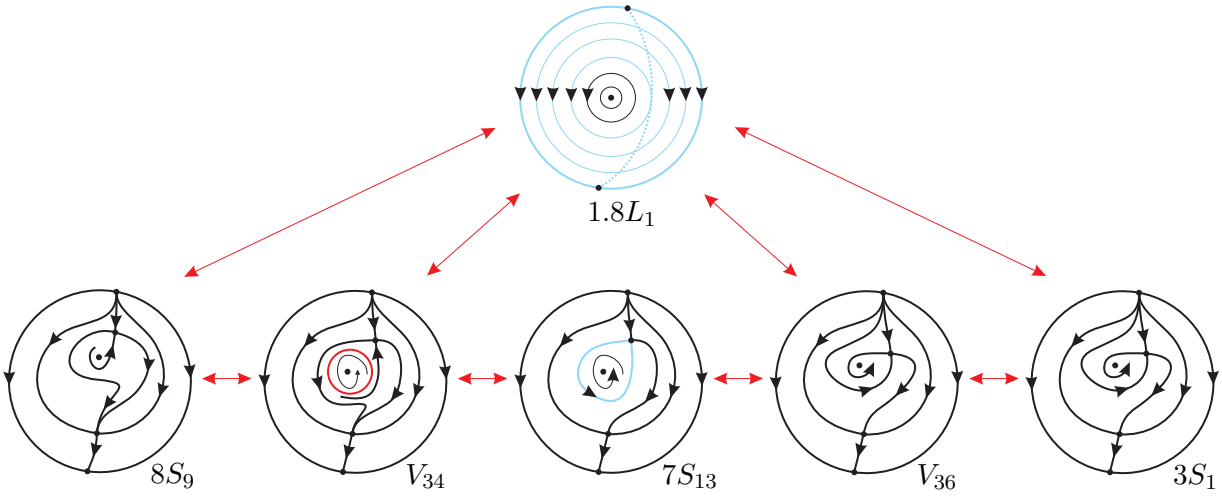

Fig. A.7: Sequence of phase portraits in part v_{34} of slice $h = 6$ bifurcating from $1.8L_1$ (the labels according to Fig. 4.2). The double arrow $\longleftrightarrow$ means that two regions are adjacent.

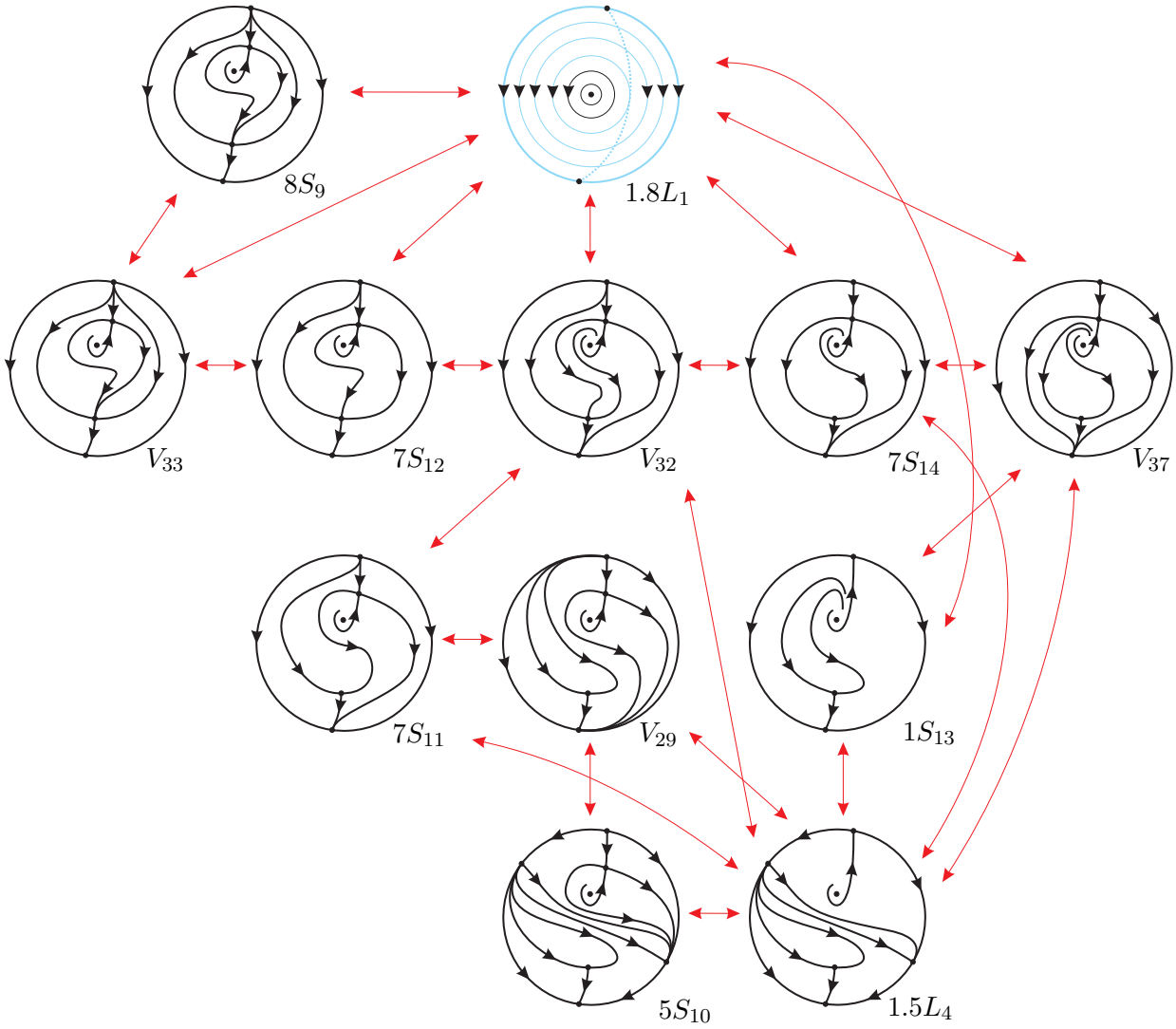

Fig. A.8: Sequence of phase portraits in part v_{29} of slice $h = 6$ (the labels according to Fig. 4.2). The double arrow $\longleftrightarrow$ means that two regions are adjacent.

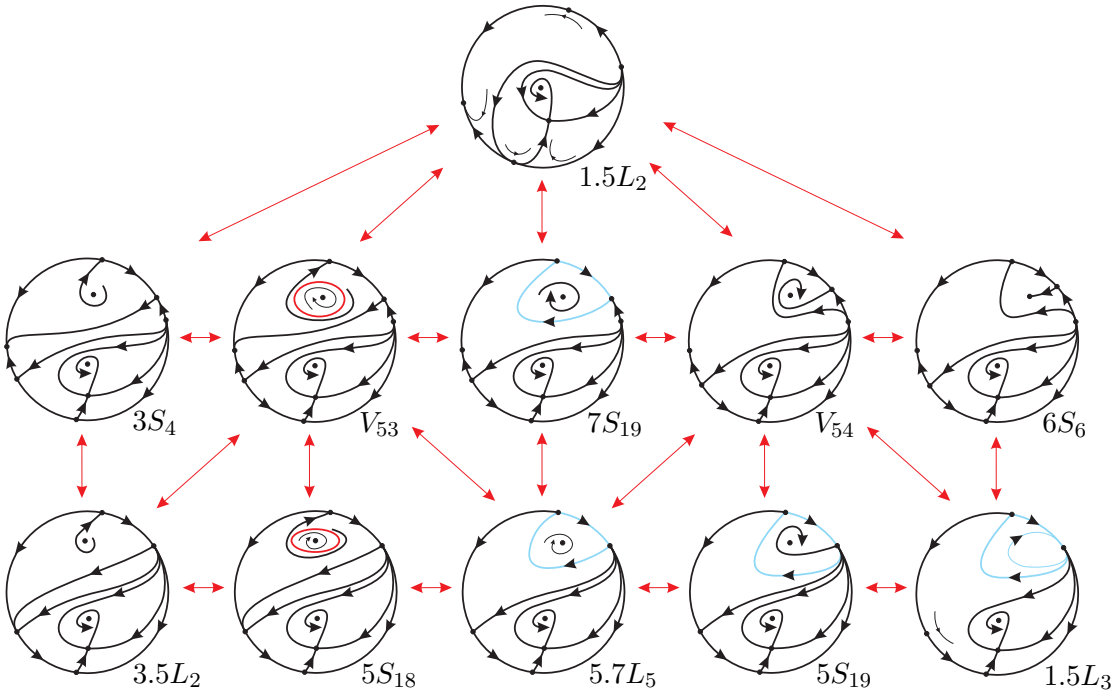

Fig. A.9: Sequence of phase portraits in part v_{53} of slice $h = 6$ (the labels according to Fig. 4.4). The double arrow $\longleftrightarrow$ means that two regions are adjacent. Moreover, we have drawn all possible adjacencies in the planar region v_{53} including its boundary.

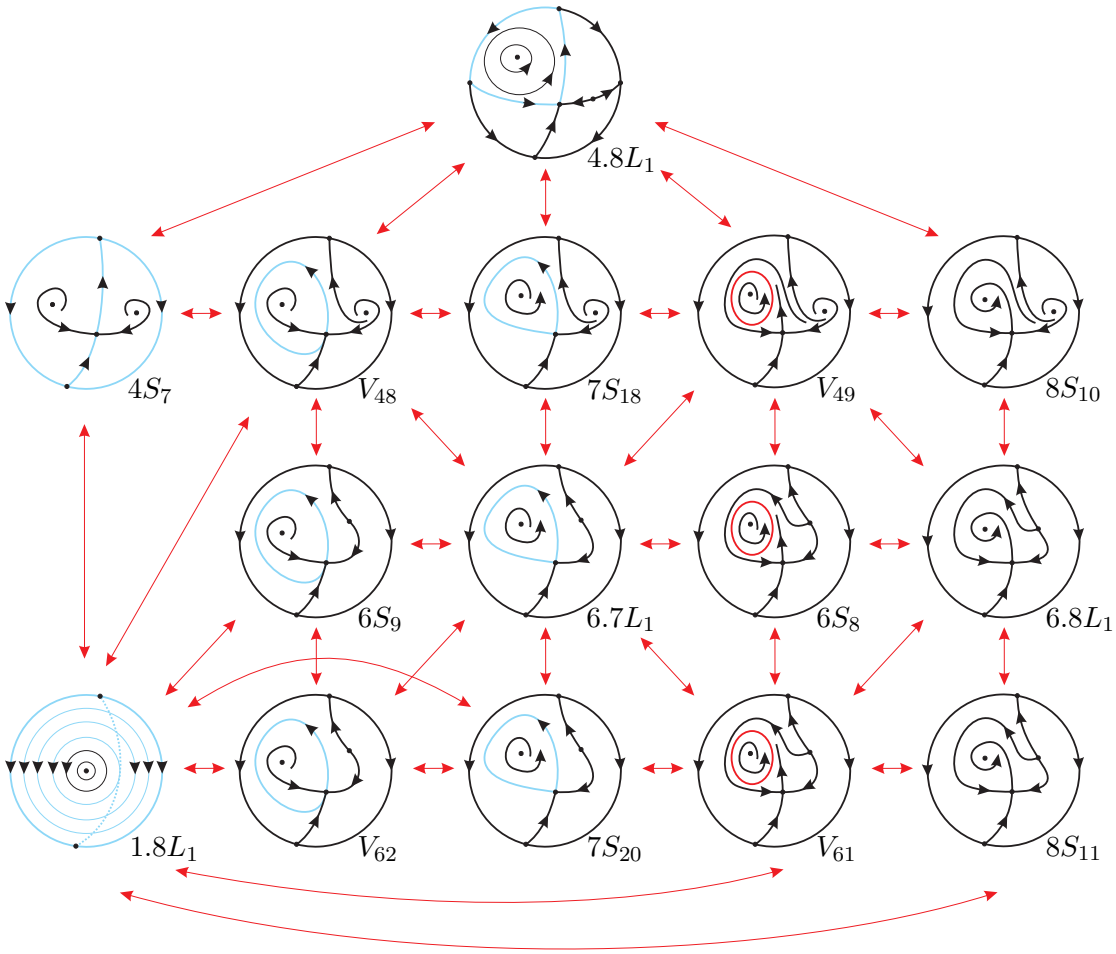

Fig. A.10: Sequence of phase portraits in parts v_{49} and v_{61} of slice $h = 6$ (the labels according to Fig. 4.5). The double arrow $\longleftrightarrow$ means that two regions are adjacent. Moreover, we have drawn all possible adjacencies in the planar regions v_{49} and v_{61} including its boundaries.

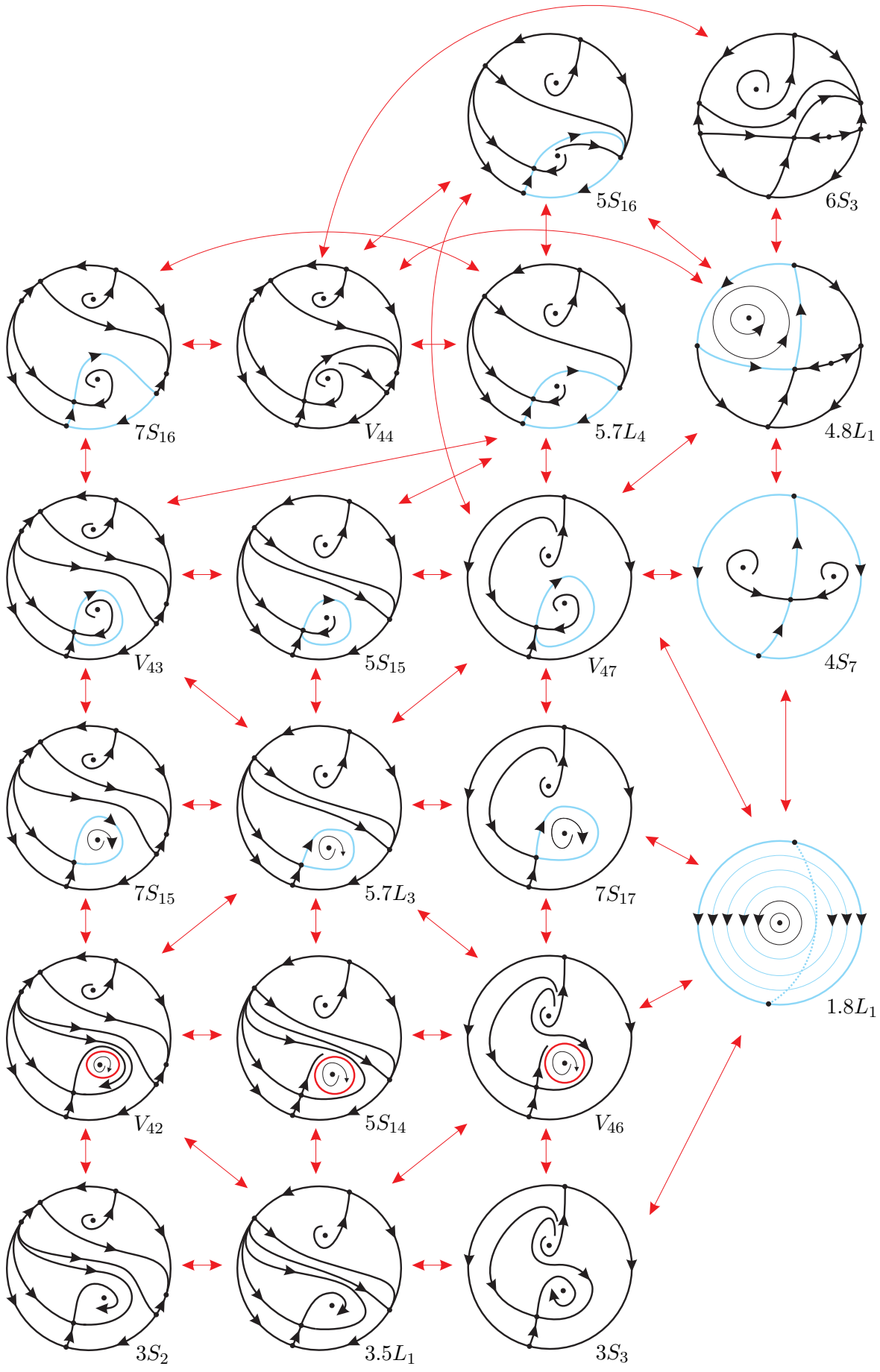

Fig. A.11: Sequence of phase portraits in parts v_{42} and v_{46} of slice $h = 6$ (the labels according to Fig. 4.5). The double arrow $\longleftrightarrow$ means that two regions are adjacent. Moreover, we have drawn all possible adjacencies in the planar regions v_{42} and v_{46} including its boundaries (except the equator).

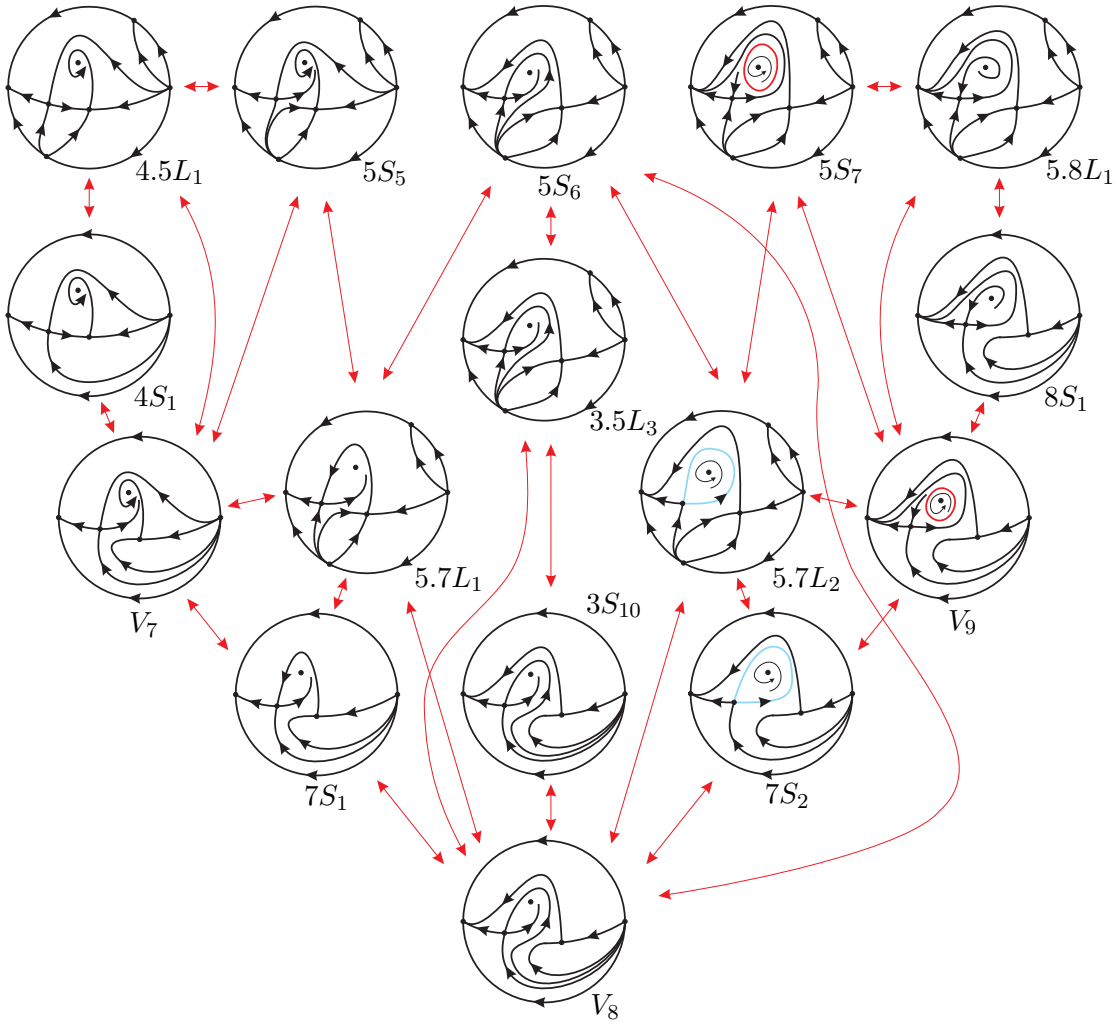

Fig. A.12: Sequence of phase portraits in parts v_{9a} and v_{9b} of slice $h = 6$ (the labels according to Fig. 4.6). The double arrow $\longleftrightarrow$ means that two regions are adjacent. Moreover, we have drawn all possible adjacencies in the planar regions v_{9a} and v_{9b} including its boundaries (except the equator).

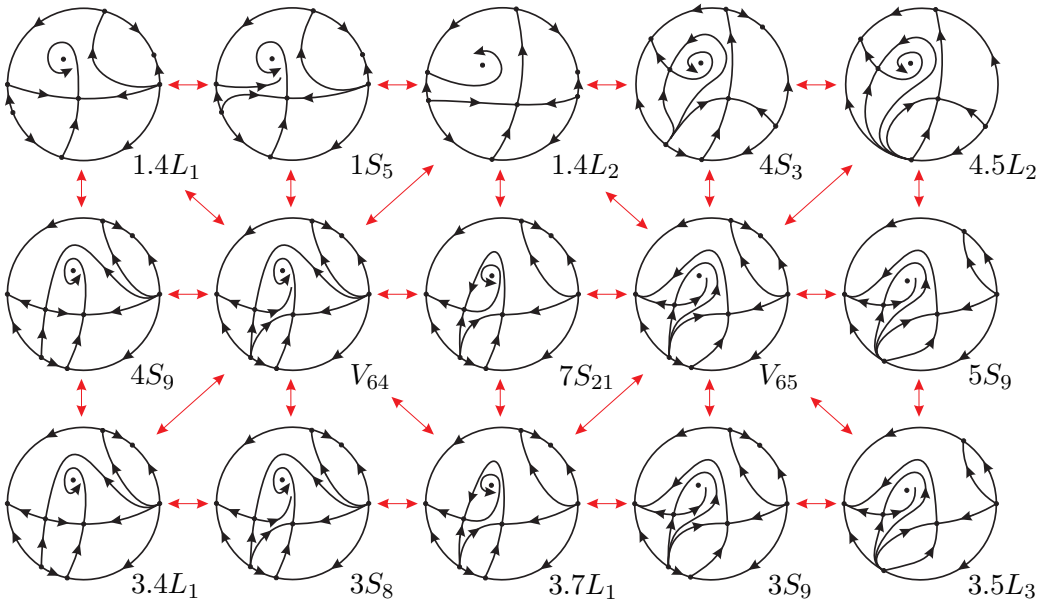

Fig. A.13: Sequence of phase portraits in part v_{64} (the labels according to Figs. 4.6 and 4.7). The double arrow $\longleftrightarrow$ means that two regions are adjacent. Moreover, we have drawn all possible adjacencies in the planar region v_{64} including its boundary.

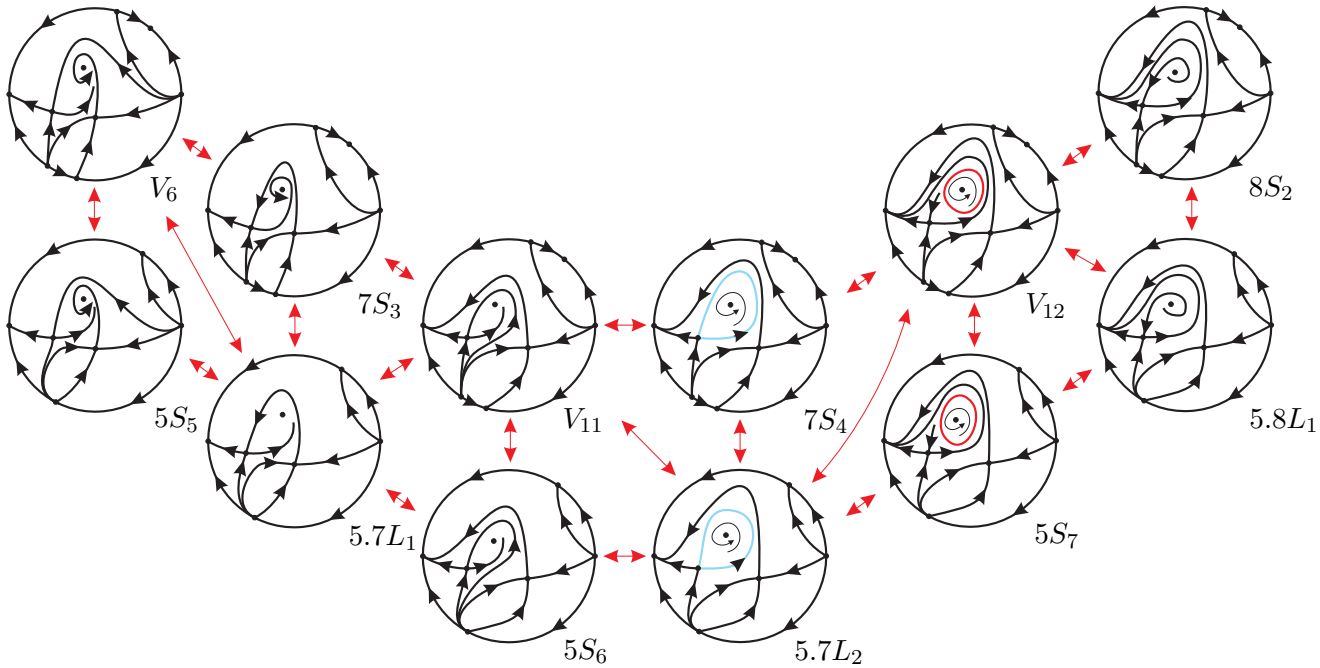

Fig. A.14: Sequence of phase portraits in part v_{12} (the labels according to Fig. 4.6). The double arrow $\longleftrightarrow$ means that two regions are adjacent. Moreover, we have drawn all possible adjacencies in the planar region v_{12} including the parts of its boundary which are not contained in $(\mathcal{S}_4)$ nor in $(\mathcal{S}_3)$.

B. Some results in qualitative theory relevant for our study

The aim of this Appendix is to group some notions that we have used during our research.

B.1. Basic properties of quadratic differential systems

We start listing some basic results on quadratic systems that will be useful for our study. We have subdivided them by topics and we have also indicated where the reader can find the corresponding proofs. We follow [Artés *et al.*, 2021a].

Contact points and line's structure

(i) A straight line either has at most two (finite) contact points (which may include the singular points) with a quadratic system, or it is formed by trajectories of the system. We recall that by definition a **contact point** of a straight line L is a point of L where the vector field has the same direction as L, or its is zero. See [Yanqian *et al.*, 1986] for a proof.

(ii) If a straight line passing through two real finite singular points q_1 and q_2 of a quadratic system is not formed by trajectories, then it is divided by these two singular points in three segments $\overline{\infty q_1}$, $\overline{q_1 q_2}$ and $\overline{q_2 \infty}$ such that the trajectories cross $\overline{\infty q_1}$ and $\overline{q_2 \infty}$ in one direction, and they cross $\overline{q_1 q_2}$ in the opposite direction. See [Yanqian *et al.*, 1986].

(iii) If a finite singular point is situated on the straight line joining two opposite infinite singular points on the Poincaré disc (see Appendix B.2) of a quadratic system, then this line is formed by trajectories, or it is a straight line without (finite) contact points except at that finite singular point. See [Yanqian *et al.*, 1986].

(iv) If in a quadratic system the separatrix of an infinite saddle connects with the separatrix of the diametrically opposite infinite saddle, then this separatrix is an invariant straight line. You can find the proof in [Sotomayor & Paterlini, 1983].

Structure of graphics and periodic orbits

(v) The interior of a closed curve is a convex region. Here a **closed curve** means either a periodic orbit, or a **finite** degenerate/non-degenerate graphic (See Definitions 2.1 and 2.2) that separates the plane into two regions (the interior and the exterior limited by the graphic). See [Coppel, 1966]. Moreover, a graphic which admits a return map must contain the line segment joining any two adjacent finite singularities belonging to the graphic, which must be an invariant line for the system. It follows straightforwardly from **(i)**.

(vi) There exists a unique singular point in the interior region limited by a periodic orbit, and this point is either a focus or a center. You can find the proof in [Coppel, 1966].

(vii) Any graphic (see Defs. 2.1, 2.2) in a real planar polynomial differential system must satisfy at least one of the following four situations: (1) It surrounds at least a singular point of index greater or equal than +1; (2) It contains a singular point having an elliptic sector situated in the region delimited by the graphic; (3) It is degenerate; (4) It contains an infinite number of singular points in its interior. If the considered system is quadratic, (1) can be replaced by: "It surrounds a unique singular point being a strong focus, a $f^{(1)}$, a $f^{(2)}$ or a center". The proof of this result can be found in [Artés *et al.*, 1998].

(viii) Two periodic orbits in a quadratic system are oppositely oriented if the bounded regions that they limit have no common points, and they have the same orientation if the bounded regions that they limit have a common point. See [Coppel, 1966].

Weak foci and limit cycles

(ix) Any individual quadratic system has a finite number of limit cycles. See [Bamon, 1986]. Moreover, if a quadratic system has a limit cycle, then it surrounds a unique singular point, and this point is a focus. See [Coppel, 1966].

(x) If a quadratic system has a center, then it is integrable; i.e. there exists a non-constant analytic first integral defined in the whole real plane except perhaps in some invariant algebraic curves. See [Schlomiuk *et al.*, 1990].

(xi) A quadratic system may have at most two foci and at most two centers. The proof is trivial using item **(ii)**.

(xii) There are no limit cycles in a quadratic system surrounding a weak focus of third order or a center. See [Li, 1986] for a proof. Moreover, there

is at most one limit cycle surrounding a weak focus of second order, and when it exists is hyperbolic. See [Pinguang, 2002] for a proof.

(xiii) Quadratic systems with a weak focus of second order can have at most two limit cycles, and they must occur in configuration $(1,1)$. See [Artés *et al.*, 2006, Pinguang, 2001].

(xiv) If a quadratic system has two real invariant straight lines, then it has no limit cycles, and if it has one real invariant straight line, then it has at most one limit cycle and in case of having one must be hyperbolic. See [Bautin, 1939, Coppel, 1989].

(xv) Any limit cycle of a quadratic system can be collapsed to its inner focus by means of a rotated family vector field, producing its death in a Hopf bifurcation. A proof of the previous result can be found in [Cherkas, 1982].

For more detailed information about specific properties of quadratic differential systems we invite the reader to see [Artés *et al.*, 2021a].

B.2. Compactification on the Poincaré sphere and Poincaré disc

In Section 2 we have drawn the phase portraits in the *Poincaré disc*. The main goal of this section is to present this technique, which enables us to join all the local behavior at each finite singular point with the behavior at infinity of a quadratic differential system by compactifying the whole plane $\mathbb{R}^2$ (in a "special" way), leading us to its global behavior (or global phase portrait). I am following [Dumortier *et al.*, 2006]. In this subsection we will use (x_1, x_2) as coordinates on the plane instead of (x, y). Let us assume that we have a differential system X defined as:

$$\begin{cases} \dot{x_1} = P(x_1, x_2) \\ \dot{x_2} = Q(x_1, x_2) \end{cases} \tag{13}$$

where P and Q are **polynomials** in the variables x_1 and x_2. Poincaré compactification works as follows. First we consider $\mathbb{R}^2$ as the plane in $\mathbb{R}^3$ defined by $(y_1, y_2, y_3) = (x_1, x_2, 1)$. We consider the sphere $\mathbb{S}^2 = \{y \in \mathbb{R}^3 \mid y_1^2 + y_2^2 + y_3^2 = 1\}$ (called *Poicaré Sphere*), which is tangent to $\mathbb{R}^2$ at the point $(0,0,1)$. Now we divide the Poincaré sphere into $H^+ = \{y \in \mathbb{S}^2 \mid y_3 > 0\}$ and $H^- = \{y \in \mathbb{S}^2 \mid y_3 < 0\}$ (which are called northern and southern hemispheres respectively) plus $\mathbb{S}^1 = \{y \in \mathbb{S}^2 \mid y_3 = 0\}$ (the equator). Now we consider the projection of the vector field X from $\mathbb{R}^2$ to $\mathbb{S}^2$ given by the central projections $f^+ : \mathbb{R}^2 \to \mathbb{S}^2$ and $f^- : \mathbb{R}^2 \to \mathbb{S}^2$. Precisely, denoting $x = (x_1, x_2)$ then $f^+(x)$ (resp. $f^-(x)$) is the intersection of the straight line passing through the point x and the origin with the northern (resp. southern) hemisphere of $\mathbb{S}^2$. The precise expressions are:

$$f^+(x) = \left(\frac{x_1}{\Delta(x)}, \frac{x_2}{\Delta(x)}, \frac{1}{\Delta(x)}\right)$$

$$f^-(x) = \left(-\frac{x_1}{\Delta(x)}, -\frac{x_2}{\Delta(x)}, -\frac{1}{\Delta(x)}\right)$$

where $\Delta(x) = \sqrt{x_1^2 + x_2^2 + 1}$. In Figure B.1b the situation is represented graphically. In this way, we obtain induced vector fields in each hemisphere. Of course, every induced vector field is analytically conjugate to X. The induced vector field on H^+ is $\overline{X}(y) = Df^+(x)X(x)$, where $y = f^+(x)$, and the one in H_- is $\overline{X}(y) = Df^-(x)X(x)$ where $y = f^-(x)$. We also remark that $\overline{X}$ is a vector field on $\mathbb{S}^2 \setminus \mathbb{S}^1$ that is everywhere tangent to $\mathbb{S}^2$. Now we would like to extend the induced vector field $\overline{X}$ from $\mathbb{S}^2 \setminus \mathbb{S}^1$ to $\mathbb{S}^2$. Unfortunately it does not in general stay bounded as we get close to $\mathbb{S}^1$, obstructing the extension. However, if we multiply the vector field by the factor $\rho(x) = y_3^{d-1}$, where $d = \max(\deg(P), \deg(Q))$, the extension becomes possible. The extended vector field on $\mathbb{S}^2$ is called the *Poincaré compactification* of the vector field X on $\mathbb{R}^2$, and it is denoted by $\rho(X)$. On each hemisphere H^+ and H^- it is no longer $C^\omega-$conjugate to X, but it remains $C^\omega-$equivalent. As it is usual when we are working with surfaces, we will use some charts to get explicit expressions of $\rho(X)$. This will allow us to make explicit calculations involving the singular points at infinity. For $\mathbb{S}^2$, we use the six local charts given by $U_k = \{y \in \mathbb{S}^2 \mid y_k > 0\}$, $V_k = \{y \in \mathbb{S}^2 \mid y_k < 0\}$ for $k = 1, 2, 3$. The corresponding local maps $\phi_k : U_k \to \mathbb{R}^2$ and $\psi_k : V_k \to \mathbb{R}^2$ are defined as $\phi_k(y) = (y_m/y_k, y_n/y_k)$ for $m < n$ and $m, n \neq k$, $y_k > 0$ and $\psi_k(y) = -(y_m/y_k, y_n/y_k)$ for $m < n$ and $m, n \neq k$, $y_k < 0$. We denote by $z = (u, v)$ the value of $\phi_k(y)$ or $\psi_k(y)$ for any k, such that (u, v) will play different roles depending on the local chart we are considering. Geometrically, the coordinates (u, v) can be expressed as in

Figure B.1a. The points of $\mathbb{S}^1$ in any chart have $v = 0$.

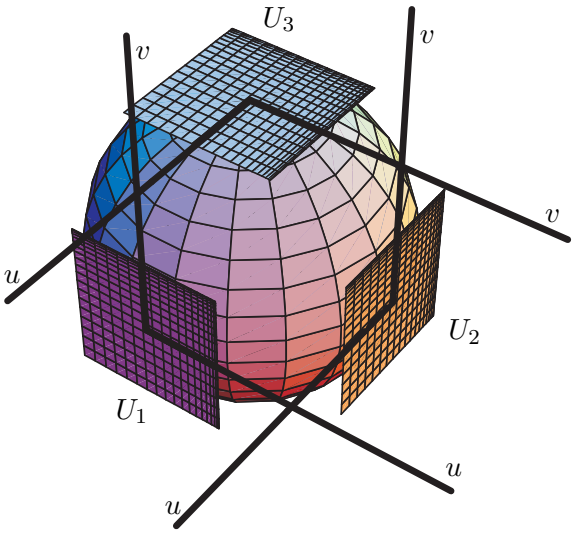

(a) Local charts (U_k, ϕ_k) for $k = 1, 2, 3$ on the Poincaré Sphere.

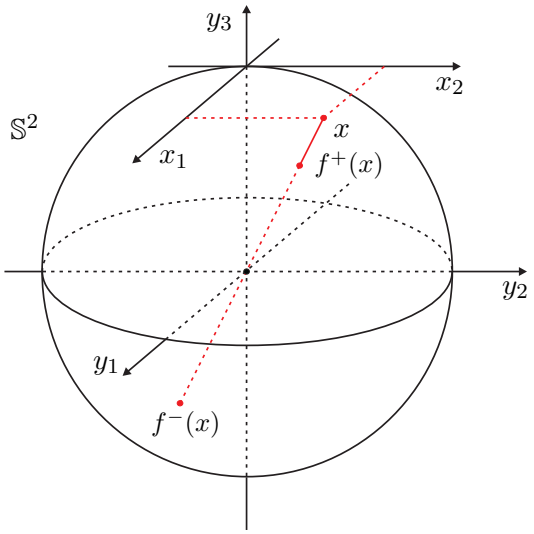

(b) Central projections f^+ and f^- onto the northern and southern hemispheres respectively.

Fig. B.1: Poincaré Sphere.

Now we can easily compute the expression for $\rho(X)$ in the previous local charts (see [Dumortier *et al.*, 2006]). The expression for $\rho(X)$ in the local chart (U_1, ϕ_1) is given by

$$\begin{cases} \dot{u} = v^d \left[-uP\left(\frac{1}{v}, \frac{u}{v}\right) + Q\left(\frac{1}{v}, \frac{u}{v}\right) \right] \\ \dot{v} = -v^{d+1} P\left(\frac{1}{v}, \frac{u}{v}\right) \end{cases} \tag{14}$$

The expression for (U_2, ϕ_2) is

$$\begin{cases} \dot{u} = v^d \left[P\left(\frac{u}{v}, \frac{1}{v}\right) - uQ\left(\frac{u}{v}, \frac{1}{v}\right) \right] \\ \dot{v} = -v^{d+1} Q\left(\frac{u}{v}, \frac{1}{v}\right) \end{cases} \tag{15}$$

The expression for (U_3, ϕ_3) is

$$\begin{cases} \dot{u} = P(u, v) \\ \dot{v} = Q(u, v) \end{cases} \tag{16}$$

The expression for $\rho(X)$ in the chart (V_k, ψ_k) is the same as for (U_k, ϕ_k) multiplied by $(-1)^{d-1}$, for $k = 1, 2, 3$. To study X in the complete plane $\mathbb{R}^2$, including its behavior near infinity, it clear suffices to work on $H_+ \cup \mathbb{S}^1$, which we call *Poincaré Disk*. All the calculation can be done in the three charts (U_k, ϕ_k) for $k = 1, 2, 3$ in which case the expressions are given by the formulas (14), (15) and (16). We remark that in each local chart the local representative of $\rho(X)$ is a polynomial vector field.

Definition B.1. We call **finite** (resp. **infinite**) singular points of X or $\rho(X)$ the singular points of $\rho(X)$ which lie in $\mathbb{S}^2 \setminus \mathbb{S}^1$ (resp. $\mathbb{S}^1$).

We note that if $y \in \mathbb{S}^1$ is a singular point then $-y \in \mathbb{S}^1$ is also a singular point. Since the local behavior near $-y$ is the local behavior near y multiplied by $(-1)^{d-1}$ it follows that the orientation of the orbits changes when de degree is even. Due to the fact that infinite singular points appear in pairs of diametrically opposite points, it is enough to study half of them, and using the degree of the vector field, we can determine the other half (and this explains why it suffices to study only the local charts (U_k, ϕ_k) for $k = 1, 2, 3$ previously mentioned).

Finally, we observe that the integral curves of $\mathbb{S}^2$ are symmetric with respect to the origin. In this sense, it is sufficient to represent the flow of $\rho(X)$ only in the closed northern hemisphere (the so called Poincaré disk). For practical purposes, in order to draw this as a disk in the plane, we can project the points of the closed northern hemisphere onto the disk $\left\{(y_1, y_2, y_3) \in \mathbb{R}^3 \mid y_1^2 + y_2^2 \leq 1, y_3 = 0\right\}$. This could be done by projecting each point of the sphere onto the disk using a straight line parallel to the y_3-axis; however, we can project using a family of straight lines passing through a point $(0, 0, y_3)$ with $y_3 < 0$. If y_3 is a value close to $-\infty$, we shall get the same result, but if y_3 is close to zero, then we might get a better representation of what is happening near infinity. In doing this we lose resolution in the regions close to the origin in the

(x_1, x_2)-plane. We recall that this technique is applied in the numerical program P4 (see Chaps. 9,10 of [Dumortier *et al.*, 2006]) that we have used to draw the phase portraits presented in Sect. 2.

B.3. Separatrix skeleton

Strictly speaking, in Section 2 we have not listed the phase portraits since these would be impossible to draw, containing *all* oriented phase curves. Instead we have listed the *completed separatrix skeleton*, concept which will define below. We will also see that the completed separatrix skeleton suffices. I am following [Dumortier *et al.*, 2006].

Definition B.2. We consider a differential equation $x' = X(x)$, where X is a C^1 function in $\mathbb{R}^2$. Let $\phi(s,t)$ the flow defined by the differential equation. We denote it by $(\mathbb{R}^2, \phi)$. We say that a flow $(\mathbb{R}^2, \phi)$ is **parallel** if it is topologically equivalent to one of the following flows.

(a) The flow defined on $\mathbb{R}^2$ by the differential system $x' = 1$, $y' = 0$, which we denote by **strip flow**.

(b) The flow defined in $\mathbb{R}^2 \setminus \{0\}$ by the differential system given in polar coordinates $r' = 0$, $\theta' = 1$, which we denote by **annulus flow**.

(c) The flow defined in $\mathbb{R}^2 \setminus \{0\}$ by the differential system given in polar coordinates $r' = r$, $\theta' = 0$, which we denote by **spiral** or **nodal flow**.

Given a maximal open region on $\mathbb{R}^2$ on which the flow is parallel, it is interesting to know the orbit structure of its boundary. Clearly the following types of orbits can be present:

(1) A singular point.

(2) A periodic orbit for which there does not exist a neighborhood entirely consisting of periodic orbits.

(3) A **separatrix**, i.e. an orbit $\gamma(p)$, homeomorphic to $\mathbb{R}$ for which there does not exist a neighborhood N of $\gamma(p)$ such that: (a) For all $q \in N$ $\alpha(q) = \alpha(p)$ and $\omega(q) = \omega(p)$; (b) The boundary ∂N of N, that is, $\partial N = \overline{N} \setminus N$, is formed by $\alpha(p), \omega(p)$ and two orbits $\gamma(q_1)$ and $\gamma(q_2)$ such that $\alpha(p) = \alpha(q_1) = \alpha(q_2)$ and $\omega(p) = \omega(q_1) = \omega(q_2)$.

The set of orbits satisfying either (1) or (3) is called the **separatrix skeleton**. If we also add the orbits satisfying (2) then we speak about the **extended separatrix skeleton**. It is easy to see that the extended separatrix skeleton S is closed and invariant under the flow. Let be a (maximal) connected component of $\mathbb{R}^2 \setminus S$ (we call it a **canonical region**). It can be proved that a canonical region is invariant under the flow and that the flow restricted to every canonical region must be parallel.

Given a flow $(\mathbb{R}^2, \phi)$, by the **completed separatrix skeleton** we mean the union of the extended separatrix skeleton of the flow together with one orbit from each one of the canonical regions. Let C_1 and C_2 be the completed separatrix skeletons of the flows $(\mathbb{R}^2, \phi_1)$ and $(\mathbb{R}^2, \phi_2)$ respectively. We say that C_1 and C_2 are *topologically equivalent* if there exist a homeomorphism form $\mathbb{R}^2$ to $\mathbb{R}^2$ that maps the orbits of C_1 to the orbits of C_2 preserving or reversing (globally) the orientations. The following result justify that our reduced phase portraits draws are enough.

Theorem B.3. ***(Markus-Neumann-Peixoto)*** *Assume that $(\mathbb{R}^2, \phi_1)$ and $(\mathbb{R}^2, \phi_2)$ are two continuous flows with only isolated singular points. Then these flows are topologically equivalent if and only if their completed separatrix skeletons are topologically equivalent.*

To conclude, we remark that the completed separatrix skeleton is an invariant under topological equivalence relation. However, a complete separatrix skeleton could contain many curves, which very often makes very difficult to decide if they are homeomorphic or not (fact that has become clear in Section 6, where we have had to define 12 invariants to distinguish the completed separatrix skeletons of our phase portraits).

Acknowledgements. The first author is partially supported by the Ministerio de Economia, Industria y Competitividad, Agencia Estatal de Investigación grants MTM2016-77278-P (FEDER) and MDM-2014-0445, the Agència de Gestió d'Ajuts Universitaris i de Recerca grant 2017SGR1617, and the H2020 European Research Council grant MSCA-

RISE-2017-777911. The second author is partially supported by the Centre de Recerca Matemàtica.

Comment. This paper is the article version of the Master's Thesis of Carles Trullàs at the Universitat Politècnica de Catalunya, whose realization received financial support from *Centre de Recerca Matemàtica (CRM).*

References

Artés, J.C. [2023] "Structurally unstable quadratic vector fields of codimension two: family possessing a finite saddle-node and a connection of separatrices," *preprint* , 93pp.

Artés, J.C., Kooij, R. & Llibre, J. [1998] "Structurally stable quadratic vector fields," *Memoires Amer. Math. Soc.* **134 (639)**, 108pp.

Artés, J.C., Llibre, J. & Rezende, A.C. [2018] "Structurally unstable quadratic vector fields of codimension one." 1. ed. *Birkhäuser*. v.1. 267p.

Artés, J.C., Llibre, J. & Schlomiuk, D. [2006] "The geometry of quadratic differential systems with a weak focus of second order," *Internat. J. Bifur. Chaos Appl. Sci. Engrg.* **16**, 3127–3194.

Artés, J.C., Llibre, J., Schlomiuk, D. & Vulpe, N. [2021a] "Geometric configurations of singularities of planar polynomial differential systems - A global classification in the quadratic case". *Birkhäuser.*

Artés, J.C., Llibre, J., Schlomiuk, D. & Vulpe, N. [2023] "Codimension in planar polynomial differential systems," *preprint* , 32pp.

Artés, J.C., Mota, M.C. & Rezende, A.C. [2021b] "Quadratic differential systems with a finite saddle-node and an infinite saddle-node (1, 1) SN-(A)," *International Journal of Bifurcation and Chaos* **31(02)**, 2150026.

Artés, J.C., Mota, M.C. & Rezende, A.C. [2021c] "Quadratic differential systems with a finite saddle-node and an infinite saddle-node (1, 1) SN-(B)," *International Journal of Bifurcation and Chaos* **31(09)**, 2130026.

Artés, J.C., Mota, M.C. & Rezende, A.C. [2021d] "Structurally unstable quadratic vector fields of codimension two: families possessing a finite saddle-node and an infinite saddle-node," *Electronic Journal of Qualitative Theory of Differential Equations* **35**, 1–89.

Artés, J.C., Oliveira, R.D.S. & Rezende, A.C. [2021e] "Structurally unstable quadratic vector fields of codimension two: families possessing either a cusp point or two finite saddle–nodes," *Journal of Dynamics and Differential Equations* **33(4)**, 1779-1821.

Bamon, R. [1986] "Quadratic vector fields in the plane have a finite number of limit cycles," *Publications Mathématiques de l'IHÉS* **64**, 111–142.

Bautin, N. [1939] "Du nombre de cycles limites naissant en cas de variation des coefficients d'un etat d'équilibre du type foyer ou centre," *Comptes Rendus (Doklady) de l'Académie des Sciences de l'URSS, Nouvelle Série* **24**, 669–672.

Bautin, N. [1962] "On the number of limit cycles which appear with the variation of the coefficients from an equilibrium point of focus or center type," *Transl. Amer. Math. Soc.* **1**, 396–413.

Cherkas, L. [1982] "Bifurcation of Limit Cycles of a Quadratic System With Variation of the Parameter Rotating the Field," *Differential Equations* **17(11)**, 1265–1276.

Chicone, C. [2006] "Ordinary Differential Equations with Applications". *Texts in Applied Mathematics, 34, Springer, 2 ed.*

Coppel, W.A. [1966] "A survey of quadratic systems," *J. Differential Equations* **2**, 293–304.

Coppel, W.A. [1989] "Some quadratic systems with at most one limit cycle", *Dynamics reported, Springer, 61–88.*

Dumortier, F., Llibre, J. & Artés, J.C. [2006] "Qualitative Theory of Planar Differential Systems," *Universitext, Springer–Verlag, New York–Berlin.*

Ecalle, J. [1990] "Finitude des cycles-limites et accéléro-sommation de l'application de retour", *Bifurcations of planar vector fields, Springer, 74–159.*

Ilyashenko, Y. [1991] "Finiteness theorems for limit cycles," *Monographs Amer. Math. Soc., Providence RI* **94**, 1259–1269.

Li, C. [1983] "Two problems of planar quadratic systems," *Science in China Series A-Math., Physics, Astronomy and Technological Science* **26(5)**, 471–481.

Li, C. [1986] "Non-existence of limit cycle around a weak focus of order three for any quadratic system," *Chinese Annals of Mathematics,* **2**.

Perko, L. [2000] "Differential Equations and Dynamical Systems," *Texts in Applied Mathematics, 7, Springer, 3ed.*

Pinguang, Z. [2001] "Quadratic systems with a 3rd–order (or 2nd–order) weak focus," *Ann. Differential Equations* **17**, 287–294.

Pinguang, Z. [2002] "On the distribution and number of limit cycles for quadratic systems with two foci," *Qualitative Theory of Dynamical Systems* **3**, 437–463.

Poincaré, H. [1885] "Mémoire sur les courbes définies par les équations différentielles," *J. Math. Pures Appl.* **1**, 167–244.

Schlomiuk, D. [1993] "Algebraic and geometric aspects of the theory of polynomial vector fields," *Bifurcations and periodic orbits of vector fields, Springer*, 429–467.

Schlomiuk, D., Guckenheimer, J. & Rand, R. [1990] "Integrability of plane quadratic vector fields," *Exposition. Math*, **8**, 3–25.

Shi, S. [1980] "A concrete example of the existence of four limit cycles for plane quadratic systems," *Scientia Sinica* **23(2)**, 153–158.

Shi, S. [1981] "A method of constructing cycles without contact around a weak focus," *Journal of Differential Equations* **41(3)**, 301–312.

Shi, S. [1984] "On the structure of Poincaré-Lyapunov constants for the weak focus of polynomial vector fields," *Journal of differential equations* **52(1)**, 52–57.

Sotomayor, J. & Paterlini, R. [1983] "Quadratic vector fields with finitely many periodic orbits," *Geometric dynamics, Springer, 753–766.*

Vulpe, N. [1983] "Affine-invariant conditions for the topological discrimination of quadratic systems with a center," *Differential Equations* **19(3)**, 273–280.

Yanqian, Ye & others [1986] "Theory of Limit Cycles." *Trans. of Mathematical Monographs, Second Edition, Vol. 66 (Amer. Math. Soc., Providence, RI).*